SOME EXPERIMENTAL STUDIES AND MODELING OF ROTARY TOOL MILLING WHILE MACHINING INCONEL - 625 ALLOY

Submitted in partial fulfillment of the requirements

for the award of the degree of

Doctor of Philosophy

by

GOPALA RAO THELLAPUTTA

Roll No: 701420

Department of Mechanical Engineering
NATIONAL INSTITUTE OF TECHNOLOGY
WARANGAL – 506004
Telangana State, INDIA.
September– 2018

SOME EXPERIMENTAL STUDIES AND MODELING OF ROTARY TOOL MILLING WHILE MACHINING INCONEL - 625 ALLOY

Submitted in partial fulfillment of the requirements
for the award of the degree of

Doctor of Philosophy

by

GOPALA RAO THELLAPUTTA

Roll No: 701420

Supervisor

Dr. P. Subhash Chandra Bose

Associate Professor

Department of Mechanical Engineering
NATIONAL INSTITUTE OF TECHNOLOGY
WARANGAL – 506004
Telangana State, INDIA.
September– 2018

THESIS APPROVAL FOR Ph. D.

This thesis entitled **"Some Experimental Studies and Modeling of Rotary tool Milling while Machining Inconel - 625 alloy"** by **Mr. Gopala Rao Thellaputta** is approved for the degree of Doctor of Philosophy.

Examiners

_____

_____

_____

Supervisor

Dr. P. Subhash Chandra Bose
Associate Professor, Mechanical Engineering Department, NIT Warangal

Chairman

Prof. P. Bangaru Babu
Head, Mechanical Engineering Department, NIT Warangal

NATIONAL INSTITUTE OF TECHNOLOGY

WARANGAL – 506 004, Telangana State, INDIA

CERTIFICATE

This is to certify the thesis entitled **"Some Experimental Studies and Modeling of Rotary tool Milling while Machining Inconel - 625 alloy"** submitted by **Mr. Gopala Rao Thellaputta** for, Roll No. 701420, to **National Institute of Technology, Warangal** in partial fulfillment of the requirements for the award of the degree of **Doctor of Philosophy in Mechanical Engineering** is a record of bonafide research work carried out by him under my supervision and guidance. This work has not been submitted elsewhere for the award of any degree.

Place: Warangal.
Date: 14-09-2018

Dr. P. Subhash Chandra Bose
(Supervisor)
Department of Mechanical Engineering,
National Institute of Technology,
Warangal, Telangana State.

NATIONAL INSTITUTE OF TECHNOLOGY

WARANGAL – 506 004, Telangana State, INDIA

DECLARATION

This is to certify that the work presented in the thesis entitled "**Some Experimental Studies and Modeling of Rotary tool Milling while Machining Inconel - 625 alloy**", is a bonafide work done by me under the supervision of Dr**. P. Subhash Chandra Bose**, Associate Professor, Department of Mechanical Engineering, NIT Warangal, India and has not been submitted for the award of any degree to any other University or Institute.

I declare that this written submission represents my ideas in my own words and where ever others ideas or words are included have been adequately cited and referenced with the original sources. I also declare that I have adhered to all principles of academic honesty and integrity and have not misrepresented or fabricated or falsified any idea/data/fact/source in my submission. I understand that any violation of the above will cause for disciplinary action by the institute and can also evoke penal action from the sources which have thus not been properly cited or from whom proper permission has not been taken when needed.

Place: Warangal.
Date: 14-09-2018

Gopala Rao Thellaputta
Roll No: 701420

Dedicated to

My Parents, My Wife and my lovely kids

Natya Krishna Navaneetha &

Geya Krishna Nishitha

ACKNOWLEDGEMENTS

I would like to express my sincere gratitude and profound indebtedness to **Dr. P. Subhash Chandra Bose**, Associate Professor of Mechanical Engineering, National Institute of Technology, Warangal for giving me an opportunity to carry out doctoral work under his esteemed supervision. This work is a reflection of his thoughts, ideas and concepts. Dr. P. Subhash Chandra Bose looks at things in the right perspective, and it has truly been a learning experience working with him. I owe a lot to him for making me a part of the continuity of the profession.

I extend my sincere gratitude to **Prof. N. V. Ramana Rao** Director, National Institute of Technology Warangal and also to **Prof. G. R. C Reddy, Prof. R. V. Chalam**, I/c Directors and **Prof. T. Srinivasa Rao**, former Director, National Institute of Technology, Warangal, India for providing the necessary facilities and encouragement throughout my work.

I am thankful to **Prof. P. Bangaru Babu**, Head, Department of Mechanical Engineering, and NIT Warangal and other faculty members for their encouragement and support extended during this period.

It's my great opportunity to express my deepest gratitude to the Doctoral Scrutiny Committee members, **Dr. C. S. P. Rao**, Professor, Dr**. N. Selvaraj**, Professor, Department of Mechanical Engineering, and **Dr. N. Narasaiah**, Professor, Department of Metallurgical and Materials Engineering for their adeptness and many discussions during the research period.

I am grateful to **Dr. C. S. Raju,** SC "G"**, Shri. Theenathyalan** SC "E", **Dr. B. Hari Prasd**, SC "G"**,** Director DOE**, Vinod Tiwari,** SC "E"**, Dr. Kiran** SC "G", **Bonam Ramesh,**

T.O "A" and all other technicians and operators of DRDL Hyderabad for their continuous support during the experimentation period.

I express my sincere thanks to my co -scholars **Kishore Kumar Kandi, T. Nagaveni, P. Gurabvaiah, C, Naresh, P Madhukar, Siva Prasad Nandhyala, Nikhil Toppil** and **Sangamesh,** NIT Warangal for their support and help in completion of this thesis. I would like to extend my heartfelt thanks to **Dr. V. Vasu,** Associate Professor-MED, NITW and **Dr. Shirish Sonawane**, Associate Professor, Dept. of Chemical Engineering NIT Warangal for their constant help and encouragement. Special thanks to my friend **Mr. K. Suresh Kumar** and family for hospitality.

I thank my wife **Mrs. K. Vidya Sagari**, for her patience, personal sacrifices and moral support throughout research period. I express my love to my Daughters **Natya Krishna Navaneetha and Geya Krishna Nishitha** for giving me wonderful smile and the joyful moments. I would like to express my love to my brother **T. Ravindra Babu** for his continues help financially. A special debt of deep gratitude to my parents and family members for their unceasing sacrifices, endeavors and encouragement.

Finally, I would also like to acknowledge the help given by all the persons who have directly or indirectly supported the work.

GOPALA RAO THELLAPUTTA

ABSTRACT

Nickel based superalloys are generally known as difficult to machine materials because of their toughness, high heat resistance, high operating temperatures, hardness and chemical property to react with tool materials, low thermal conductivity and creep resistance. Although these awesome properties are necessary design requirements, they cause a greater challenge to the manufacturing engineers due to the high temperatures and stresses generated during machining. The tool materials with better hardness like carbides, ceramics and CBN are regularly used for machining of Nickel based Super alloys. Betterments in machining productivity can be attaining with the advanced machining techniques such as rotary machining. The Nickel based superalloys mainly used in aerospace applications due to their excellent properties at high temperature. In the recent past, there is a rapid development in advanced aerospace materials resulting in the developments of Nickel, Titanium and structural composite materials with improved properties such as strength to weight ratio, corrosion resistance, etc. The difficulties in machining of these materials economically and effectively are limiting their applications. As the development of new cutting tool materials are reaching an optimum level, the attention of manufacturers all over the world is focused on novel tool designs. One such development is the rotary tool machining operations i.e. self-propelled rotary tool turning and self-propelled rotary tool milling operations in which the tool life increases enormously and aerospace materials can be machined at a faster rate at lesser tool cost than that of conventional machining operations.

Inconel 625 is nickel based superalloys with high temperature mechanical properties and outstanding oxidation resistance whose applications include gas turbine engines and Aerospace engines. Along with these properties they also exhibit very high hardness at high temperature which causes problems during machining. Defense organizations have been working with Inconel 625 for their scramjet engines. It is found that the machinability data of Inconel 625 is not available with rotary tools. Knowledge of interaction of machining process variables on surface finish, cutting force, and temperature and models for prediction of output variables are

scarcely available. Generation of such rotary machining data, response and models are very much required for the user industries such as aerospace and defense.

In this work, an attempt is made to design and fabricate a rotary face milling cutter with a provision for insert inclination angles 20°, 30°, 40° and 50° and testing of this cutter under varied machining conditions. The performance of the developed cutter has been evaluated while machining some of the difficult-to-cut aerospace materials like Nickel based super alloy namely Inconel 625 and SUS 304. Cutting forces in three directions (F_X, F_Y & F_Z), surface roughness (R_a) and tool chip interfacial cutting temperature have been considered for evaluation. Detailed investigations have been carried out based on Full-Factorial Experimentation for evaluating the performance of rotary face-milling cutter with the selected process parameters.

For cutting force, surface roughness and cutting temperature investigations, experiments have been conducted according to the Full-Factorial and Response Surface Methodology (RSM) techniques. Design Expert 7.0.0 software has been used for implementing the RSM .Analysis of experimental results using Analysis of Variance (ANOVA) has been employed to study the performance characteristics of the cutters. In addition to this work, experiments are conducted using MQL and MQL with nano coolants for three higher, medium and minimum values of output variables. Also, in this work, models for predicting the cutting forces, surface roughness and cutting temperature generated during the rotary face milling operation have been developed using RSM and same were validated. Also, soft computing model using Multi Gene Genetic Programming (MGGP) technique has been developed and validated for predicting the cutting forces, surface roughness and cutting temperature. A multi objective problem is formulated using Non-dominated Sorting Genetic Algorithm-II (NSGA-II) for an optimal combination of settings to minimize the cutting force, surface roughness and cutting temperature to obtain multiple sets of optimal solutions to choose a specific optimal set of input variables based on the particular requirements.

It can be noticed that the machining with lower inclination angles exhibits lower thrust forces and it is almost 30% of the total thrust force generated in the case of conventional face milling cutters. Hence, rotary milling cutters are recommended for mass production in machining of difficult to machine materials such as Nickel based super alloys and Titanium Alloys for

aerospace applications. According to the surface roughness variation graphs, cutting speed and feed rate show a greater influence on surface finish having less surface roughness at low feed rates and high surface roughness at high feed rates. In the case of insert inclination angle, there exists an optimum angle between 30^0 and 40^0 at which the surface roughness is found low. According to the cutting temperature variation graphs, cutting speed and feed rate show a greater influence on cutting temperature. The optimum inclination angles are in between 30^0 and 40^0 to get minimum cutting temperature.

The developed rotary face milling cutter can be used for machining of components made of high strength and difficult-to-cut alloys for aerospace and Defence applications. The validated models developed in this work can be ready to use by any industry to predict the cutting forces, surface roughness and cutting temperature for rotary milling operations.

CONTENTS

LIST OF FIGURES

LIST OF TABLES

NOTATIONS

A_c	Chip cross-sectional area, in mm^2
a_{cmax}	Maximum chip thickness, in mm = $C_t \sin\psi$
a_w	Width of the chip
C_t	Uncut chip thickness, in mm
f	Feed rate of the work piece, in mm/min
f_t	Feed rate in mm/rev
F_X	Main cutting force, i.e. Force component in X-direction
F_Y	Feed force, i.e. Force component in Y-direction, in N
F_Z	Thrust force, i.e. Force component in Z-direction, in N
F_T	Tangential force, in N
F_R	Radial force, in N
F_A	Axial force, in N
h	Depth of cut, in mm
i	Inclination angle, in deg
K_T	Specific cutting pressure, in N/mm^2
K_R	Empirical constant relating tangential force to radial force
K_A	Empirical constant relating tangential force to axial force
l_c	Length of the chip, in mm
R	Radius of the insert, in mm
R_a	Surface Roughness, in µm
R_t	Surface Roughness, peak to valley height in µm

S	Speed of the spindle, in RPM
v	Cutting velocity, in m/min
V_w	Absolute work piece velocity,
V_c	Absolute chip velocity
V_{cr}	Relative chip velocity
V_t, V_r	Rotary tool cutting velocity
τ	Shear stress, N/mm^2
σ	Standard deviation
η_c	Chip flow angle in the rake face in oblique cutting, in deg
η_{cr}	Relative chip flow angle, in deg
ψ	Absolute chip flow angle in milling, in deg
ϕ_n	Normal shear angle, in deg
θ	Cutter rotation angle, in deg
μ	Coefficient of friction

ABBREVIATIONS

RSM	Response Surface Methodology
MGGP	Multi gene genetic programming
NSGA-II	Non-dominated sorting genetic algorithm - II
ANOVA	Analysis of Variance
CMM	Coordinate Measuring Machine
Dof	Degrees of Freedom
DRT	Driven Rotary Tool
SPRT	Self-Propelled Rotary Tool

CHAPTER 1

INTRODUCTION

1.1 Introduction

One of the most difficulties facing the aerospace industry is to introduce high strength superalloys while continual adapting manufacturing processes to allow the creation of high-integrity components at low manufacturing costs, lower scrap rates and greater production rates. Safety critical components, such as turbine discs, are manufactured under strict quality standards set by aerospace manufacturers, in this regard surface integrity issues are of critical importance especially when new superalloys are adopted **[J. Kwong, D. A. Axinte P.J.Withers, M.C.Hardy*et al.*, 2009]**. Most about 50% wt. of materials used inaerospace engine, mainly in the gas turbine are Nickel based superalloys **[E.O. Ezugwu, J. Bonney, Y. Yamane*et al.*, 2003]**. The main strength of the Nickel based superalloys are being heat resistant, having high melting temperatures, retaining their mechanical and chemical properties at high temperatures, high

corrosion resistance as well as thermal fatigue, creep, erosion and thermal shock **[Durul Ulutan, Tugrul Ozel*et al.*, 2011]**.

These properties are required for the efficient and effective service performance of the domains in which the superalloys are used. The Nickel based superalloys can be strengthening and hardening through inter metallic compound precipitation in FCC matrix **[A. E. I. Elshwain, Norizah Redzuan*et al.*, 2013]**. Nickel based superalloys play an important role in gas turbine engines. In addition to their use in marine, aircraft, industrial and vehicular gas turbines. Nickel based superalloys are now also used in rocket engines, space vehicles, nuclear reactors, submarines, experimental aircrafts, petrochemical equipment, steam power plants and other high temperature applications. Nickel based super alloys are known as most difficult to machine materials in order to satisfy quality and production requirements **[E.O.Ezugwu a, Z.M.Wang, A.R.Machado, 1999].** The superalloys work hardened rapidly. High pressures that accompany machining causes a hardening effect that slow down further machining and may also cause warping in small components **[Victor M. Cassidy, 2008]**.

These alloys have been developed for high temperature service and include iron, cobalt and nickel based materials, although at present they are principally nickel based. These materials mostly used in air craft and power generation turbines, rocket engines, and other challenging environments, including chemical processing and nuclear power plants. The aero gas turbine was the impetus for the development of superalloys in the early 1940s, when conventional materials available at that time were insufficient for the demanding environment of the turbine. Therefore it can be said that "the development of super alloys made the modern gas turbine possible". A major application of superalloys is in jet engines, turbine materials, both disc and blades **[Melih Cemal Kushan, 2012]**. The use of superalloys can allow the operating temperature to be increased from 1200o F to 1300o F. Besides increasing efficiency and power output, higher temperatures results in reduced emissions because the combustion cycle is more complete. Nickel superalloys can play an important role in improving energy efficiency in steam turbines used to generate electricity **[INSG, 2013]**.

A large amount of the mechanical energy is converted into heat energy during the machining process. This heat energy is generated due to friction and shearing action between the cutting tool and the work- piece. The heat energy gets dissipated by conduction into the tool, work piece and the chip. The temperature increase in the tool tends to increase thermal softening of the cutting

tool and successive tool failure. To lower the tool temperature and to enhance the tool life, several methods were investigated [**V. Dessoly *et al.,* 2004**]. Particularly the application of cutting fluids that worked like transport mechanism of heat and acts as lubricant at the cutting tool and chip interface has been studied broadly and cutting fluids for many applications involving various types of materials and tools have been suggested by researchers and practicing engineers. However, in some cases, its effectiveness is limited by its lack of ability to penetrate the tool-chip interface. Furthermore, these days, the use of cutting fluids is less advantageous because of its undesirable effect on the environment. In some of the experimental investigations mentioned that the expose to particles produced by evaporation of cutting fluids can create breathing difficulties and skin problems. One technique of dropping the cutting tool temperatures and tool wear is to continuously change the active portion of the cutting tool edge in contact with the chip during machining [**Armarego *et al.,* 1994a**]. This can be achieved by having a round profiled tool which rotates about its own axis as the tool is penetrate into the moving work piece.

In this rotary machining process the cutting edge of rotary insert continuously changing and allows each part of the tool will cool and rest between contacts to the workpiece. Hence minimize the cutting tool temperature at cutting zone and tool wear which will be affected by the cutting tool temperature. Such tools referred as rotary tools and the related machining process is called as "Rotary tool machining processes. It has been used for facing, face milling, shaping, boring and turning. In this rotary tool cutting process the cutting edge of a rotary insert rotates about its own axis and continuously fed into the workpiece. Compared to a non – rotating circular tool or traditional stationary tool, rotary tool permits each point on circumference of cutting edge of rotary insert to be cooled between contacts to the work piece and the entire circumference of the cutting edge will be used, which has a positive effect on diminishing the total temperature [**S. Lei *et al.,* 2002**].

1.2 Self propelled Tools

"The self propelled tool is defined as a cutting tool whose cutting edge has a motion along its axis in addition to the motions of cutting speed and feed relative to the work piece."

Round inserts which are freely rotate about their own axis is used in the rotary tools. By providing cutting edge of the round insert in contact with the work piece at an angle with respect to the cutting velocity vector (V), self-rotation of the cutting edge can be achieved. This angle is

called inclination angle (*i*). The friction between tool cutting edge and the work piece causes tool rotation. The direction of insert rotation depends upon the orientation of work piece velocity (V_w) whereas rotational speed depends upon the magnitude of the work piece velocity and the inclination angle. The schematic illustration of self-propelled rotary cutting process is shown in Fig.1.1.

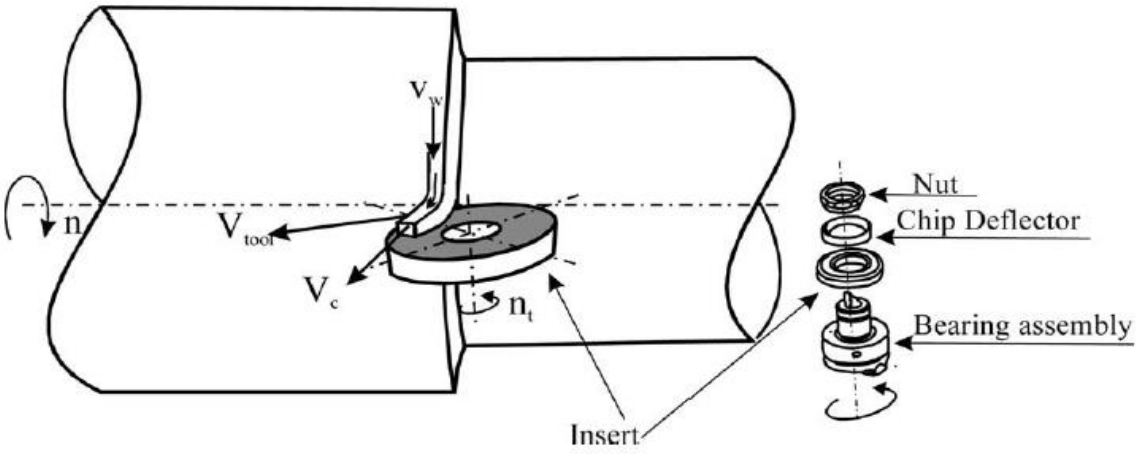

Fig.1.1. Self-propelled rotary tool process **[H.A.Kishawy, J.Wilcox, 2003]**

An uninterrupted cutting process can be achieved by these tools by providing a continuous cutting edge penetrated into the workpiece. The continuously rotating cutting edge dispenses the cutting temperature along the entire cutting edge and hence reduces the tool wear and in turn tool life. The temperature distribution avoids the chip impingement on the cutting edge for maximum possible extent which is a serious problem in achieving good surface finish. Thus it provides an additional advantage to its application. In rotary tool machining process, another way to explain the decrease of temperature could be given. Indeed, in metal removal process, the temperature generated at the tool-chip interface depends on the balance between the production and the dissipation of heat. In traditional cutting process, the consumed power is mainly converted into heat. In rotary tool machining, some energy is necessary to drive the tool and is turned into kinetic energy there by reducing the friction. Thus, the heat generated during the process is reduced.

Using Rotary tools are being used in various machining operations like milling, turning, boring, etc. These rotary tools can be used at higher feeds and speed rates comparatively traditional cutting tools without major undesirable effect on the working performance of the

cutting tool and machine tool. The commercially available rotary cutting tools are as shown in Fig. 1.2-1.4. (Make: Rotary Technologies Corporation)

Fig.1.2. Rotary turning tool (*Courtesy:*Rotary Technologies Corp., USA)

Fig.1.3. Rotary milling tool (*Courtesy:*Rotary Technologies Corp., USA)

Fig.1.4. Rotary boring tool (*Courtesy:*Rotary Technologies Corp., USA)

1.3 Round insert

Since around more than fifty years the rotary tool inserts have been used. The inserts are allowed to rotate freely which are fixed on thrust and radial bearings (Fig.1.5). This spinning creates a slicing action that, combined with the continuously change of the cutting edge zone showing to the material removal process. It cause to low temperature, increased tool life occurs from distribution of tool wear around the entire insert edge, low power requirements low cutting forces and better surface finish. Limitations of the tooling have been reliability difficulties occurs from extreme size of the insert holding cartridges, more initial cost of the cutter and inserts, system of the bearing, and a lack of effective systematic tools for cutting tool design. In the bearing system design the most important consideration for the rotary insert is that should bare higher radial thrust loads and higher running speeds with reasonably minimum eccentricity and less friction under dynamic situations.

Fig.1.5. Round insert

A compact cartridge system developed by Rotary Technologies Corporation for accommodating the bearings consisting of a stator enclosed by a needle roller bearing and thrust bearing. Under the action of machining forces the bearings permitted the rotor to rotate. The rotary inserts are mounted on the rotor and locked in place using a lock nut. A dovetail on the bottom of the stator enables the cartridge to be guided in the tool and locked in place using a clamping mechanism. Cartridges are sealed using O-rings that prevent contamination of the bearings by cutting fluids or chips. The major advantage of Rotary insert tools is depends on rotation of insert during the machining process, propelled by the cutting forces generated while the machining operation. The design of Rotary cutter is very critical because of the cutting forces causes the torque of the cutting insert are a difficult function and need to be lot of variables to overcome the friction inherent at the cartridge bearings.

1.3.1 Importance of round inserts

The geometry of an insert used in the rotary milling has a greater effect on the impact resistance of the insert material. The nose tip or cutting edge corner is the weakest portion of any milling insert, as it is resolved to continuous disrupted loads and excessive temperature changes. Due to the absence of corners round insert is safer than other shape. As the insert engages with the work material during cutting, it is exposed to high compressive loads. The primary contact between the insert cutting edge and the work material may be very poor depending on the arrangement of the cutter in relation to the workpiece. As the insert moves through the cut, the chip thickness continuously changes, varying the axial and radial machining forces. At last, the insert disengage the workpiece, it is experienced to tensile stresses that fail the carbide. One most important reason for the achievement of the circular insert in many applications is that the radial and axial cutting forces can be adjusted by changing the axial depth of cut. A high radial cutting force can cause vibration and chatter. On the other hand, a high axial force can cause trouble to the fixturing of the work material and resulting in fewer tolerances. With the use of conventional milling cutters, the lead angle controls the kind of cutting force achieved. Another cause for the wide usage of rotary cutter is that the high table feeds that can be provided. This is mainly due to the chip thinning effect of the round cutting edge. The chip thinning obtained due to the increasing of lead angle of the tool. The higher the lead angle, the thinner will be the chip as it is shared over a greater length of the cutting edge. Hence, for higher metal removal rates and feed per tooth, the load of the insert will decreased. In no lead angle tools, the chip thickness is equal to the feed per tooth. When feed per tooth is changed, the round insert cutters have changes the chip thickness. But different other lead angle cutter, the chip thickness for a round insert is also affected by a change in depth of cut. High velocity milling cutters are made for repeatability and protection at milling speeds of ceramic.**[Hossam A. Kishawy, Ali Hosseini et.al., 2019]**

Whisker reinforced ceramics work superior than the melting temperature of carbide inserts. Modern whisker reinforced ceramics contain a melting point of greater than 2000°C, it stated that ceramic inserts can work at higher speeds where as carbide tools fail. Coolants are not suggested for hard and solid milling applications with ceramic cutting inserts. Ceramic cutting inserts are withstood of machining hardened steel at much greater speeds than traditional carbide tools. Combination of the higher operating speeds with the suitable feed rates and a healthy step-

over and the shop can get some significant metal removal rates (MRR). Another important factor in increased production rates when cutter teeth density is more in milling. Every other tooth in a cutter increases the cross feed rate. More feed and higher speed ads up to lesser cycle times. The surface integrity generated by rough milling with ceramics leaves less work for a finishing operation, and decreases total production time. Milling at relatively low feed rates in hard steel with carbide cutting insert usually generate a good surface finish, but many times with ceramic inserts the rough finish is even improved than the desired finish. In some cases, grinding, finish milling and polishing can be eliminated [**J. Paulo Davim**, **et.al. 2011].**

1.3.2 Different types of Rotary Cutting Tools

The rotary cutting tools can be classified according to the angle between the tool axis and the plane of the machined surface. The classification is as shown in Fig.1.6.

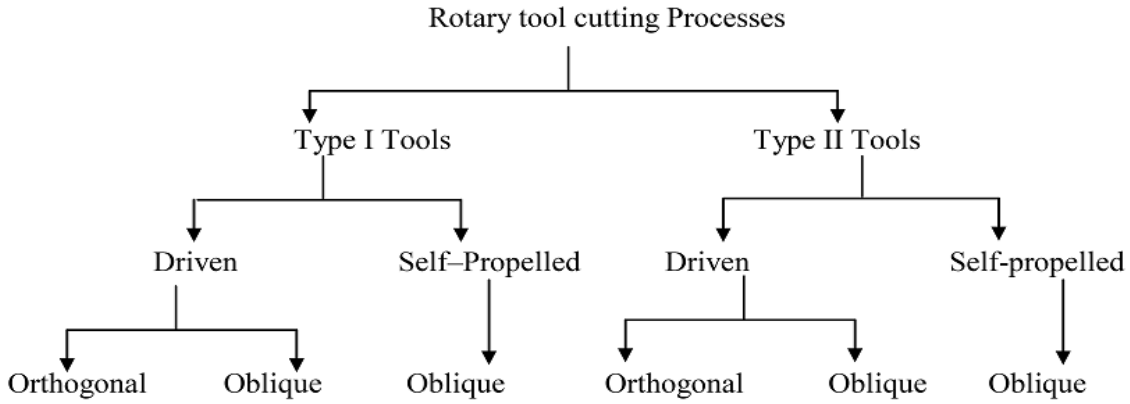

Fig.1.6. Classification of rotary cutting processes

The rotary tool can be considered as analogous to shape of frustum of a cone during operation with its axis normally oriented in two different ways relative to the work piece. The orientations are illustrated in Fig.1.7. (a) and (b). In first setting called Type-I setting, the tool axis is parallel to the machined surface and makes an angle *i* with the work piece velocity vector V_w. Angle *i*, the setting parameter of the tool, is equal to the nominal angle of obliquity (i_F) of the cutting edge. Whereas in second case called Type-II setting, the tool axis makes angle θ_H and θ_V to the normal to the machined surface as shown in Fig.1.7. (b). According to Venuvinod *et al.*, the normal angle of obliquity in this case is given by:

$$\tan\ i_F = \frac{\sin\theta_H}{\tan\theta_V} \qquad (1.1)$$

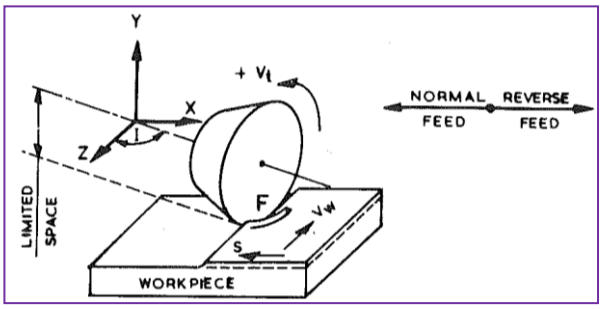

Fig.1.7 (a) Type-I rotary cutting tool **[Venuvinod *et al*., 1981]**

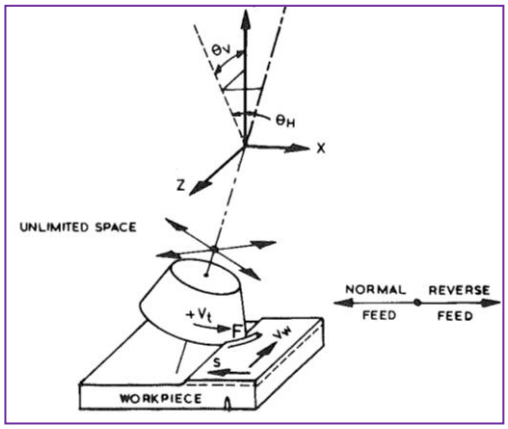

Fig.1.7 (b) Type-II rotary cutting tool **[Venuvinod*et al*., 1981]**.

From the literature there are two types of rotary tools are found in spite of their setting namely self-propelled and driven rotary tools. In the driven rotary tool, the rotary action of the insert is created by an external source during action of the flow of chip over the tool rake face rotates the insert for self-propelled tools. An oblique angle is necessary to bring the rotary movement in the latter type. The insert cutting edge movement may be given from an external source leading to a driven rotary tool (DRT). Alternatively, the tool may be held in a spindle, freely floating in bearings, with its axis inclined to the work piece such that the tool rotates freely about its axis when it comes into contact with the work piece. Such tool is called as self-propelled rotary tool (SPRT) **[Janardhan *et al*., 1979]**. The main advantage of the self-propelled rotary tool over the driven rotary tool is that it does not need an external drive.

There are two versions of mounting the tool. The 'Orthogonal' rotary tool cutting process is defined as process where the absolute work piece velocity (V_w)is perpendicular tothe tool

cutting edge. The 'Oblique' rotary tool cutting process is defined as process where the absolute work piece velocity (V_w) is inclined at an active inclination angle *i* to the normal to the cutting edge. It has been well recognized that while driven rotary tool cutting process can operate for both oblique and orthogonal cutting configurations. The self-propelled tool cutting process is only possible for oblique cutting process where the inclination angle *i* is non-zero. The orientation of *i* determines the direction of rotation of the self-propelled tools. The inclination angle of the tool in SPRT must be larger than 10° in order to have steady state tool rotation **[Radwan *et al.*, 1979]**.

The Conventional orthogonal cutting process which is equivalent to driven rotary tool cutting as shown in Fig.1.8 (a) & (b) and oblique cutting process which is equivalent to Self-propelled rotary tool cutting as shown below Fig.1.9 (a) & (b).

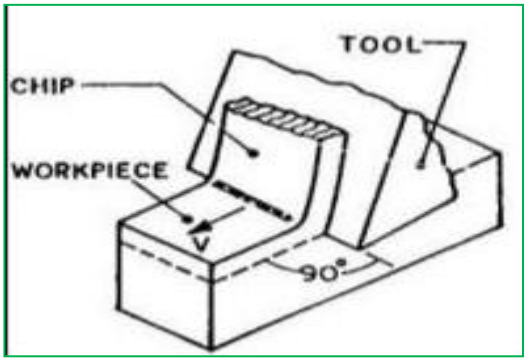

Fig.1.8 (a) Conventional Orthogonal Cutting

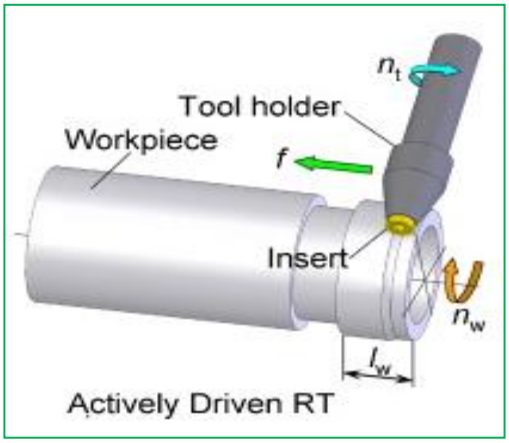

Fig.1.8 (b) Driven Rotary Tool **[Hosokawa *et al.*, 2010]**

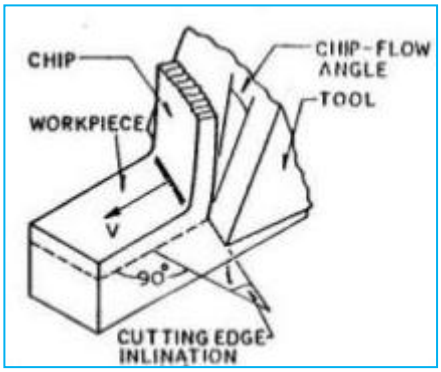

Fig.1.9 (a) Conventional oblique cutting process

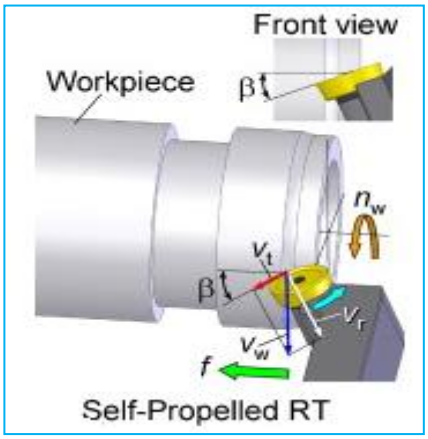

Fig.1.9 (b) Self-propelled rotary tool **[Hosokawa *et al.*, 2010]**

The applications stated by James Napier, rotary tools have received many researchers' attention. Shaw *et al.* (1952) carried out the early study of rotary tool machining and quantified velocity relations for rotary cutting. [**Ramaswamy *et al.* 1968]** carried out the early experimentation with the rotary tools. [**Venkatesh *et al.* 1972]** investigated the effects of different cutting parameters on surface finish, tool life and the chip generated during a face milling operation performed with a self-propelled round cutting insert face-milling cutter. It was known that the cutting temperature in rotary cutting operation is lesser than that of while machining with conventional tools and also there is a significant increase in tool life with rotary tools. Since then many authors have focused their attention on rotary cutting tools. [**Wang*et al.* 1998]** compared the wear of self-propelled rotary inserts with rhomboid and round stationary inserts when machining of difficult-to-cut material IMI318 and found that tool life of self-propelled rotary inserts is three and four times more than the conventional ones (Fig.1.10 (a) & (b)).

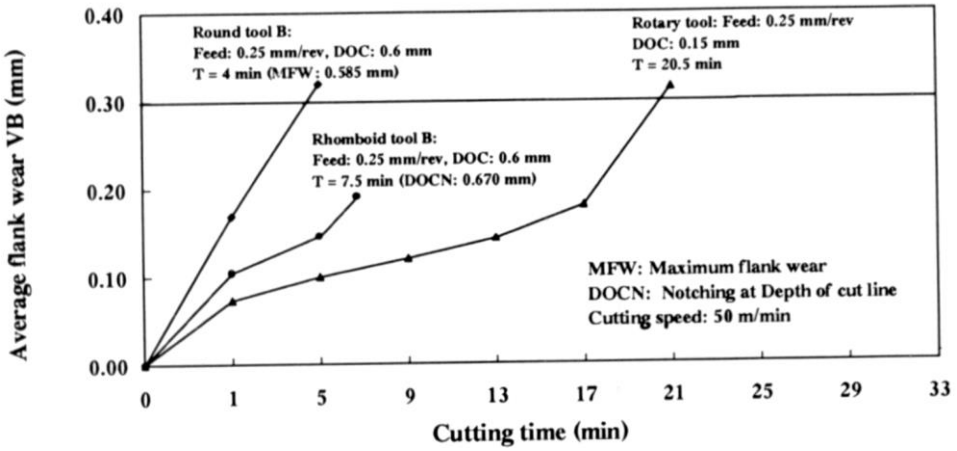

Fig.1.10 (a)Wears characteristics comparison when machining Inconel 718 with different cutting tools [**Wang *et al.*, 1998]**

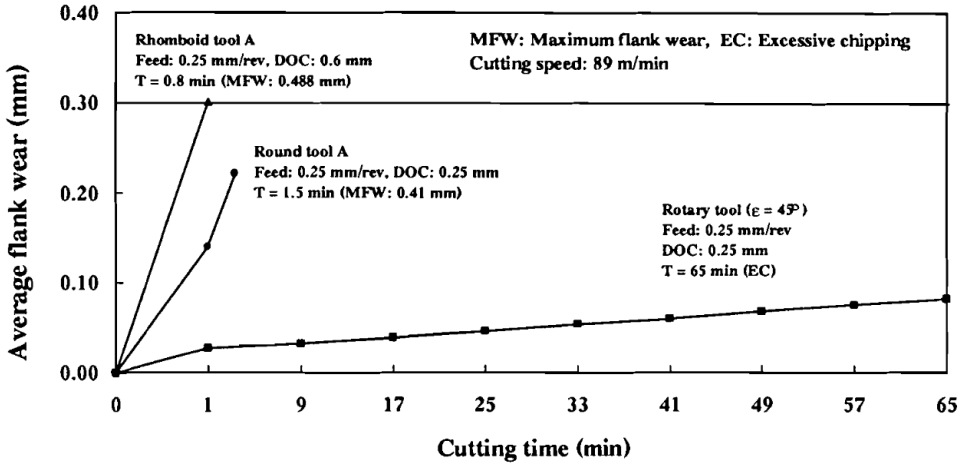

Fig.1.10 (b)Wears characteristics comparison when machining IMI 318 with different cutting tools [**Wang *et al.*, 1998]**

The rapid development in usage of advanced aerospace materials like titanium and titanium alloys, nickel alloys, nimonic alloys, etc. in aerospace industries are posing a major problem when machining such materials. Conventional machining tools worn out more quickly, while machining aerospace materials with compared to machining of conventional work materials. Hence, the machining time increases. Of all, Nickel alloy is the most commonly used aerospace material. The usage of the Nickel alloy has tremendously increased in the recent past particularly in aerospace industry, due to its excellent property of high strength to weight ratio **[Ezugwu *et al.*, 1997]**.

But unfortunately Nickel alloys are difficult to machine as compared to other conventional materials due to their exceptional machining properties.

The following characteristics of Inconel 625 affect machining procedures:

1. Inconel 625 reacts rapidly at high temperature with oxygen, nitrogen and constituents in cutting tools. In machining, this chemical activity contributes to seizing, galling and abrasion, and to the pyrophoric behavior of small particles of Inconel 625.

2. Chips of Inconel 625 ordinarily exhibit less shear deformation than those of other metals. The thinner chips cause higher sliding velocities and smaller tool-chip contact areas. These conditions, along with the relatively high strength of Nickel, produce high contact pressures and cutting forces.

3. Inconel 625 has relatively poor thermal conductivity than conventional steels (about $1/6^{th}$). This contributes to high temperatures at tool tip and subsequent tool wear **[Norman *et al.*, 1973]**.

Hence, there is potential for employing the rotary tools in machining of such exotic, difficult to machine and hardened materials in order to achieve increased tool life and higher material removal rates **[Danilov *et al.*, 1979]**.

1.4 Design of Experiments (DOE)

At least one process parameter or factors are deliberately changed in an experiment in order to study result of changes on at least one response of variable. The Design of Experiment (DOE) is an efficient methodology for scheduling tests, with the goal that the information got can be analyzed to yield legitimate as well as objective conclusions. **[Dong-Woo Kim, 2008]**

DOE starts with finding the objectives of an experimental trail and selecting the operational factors for the experimental study. It will explain a complete experimental procedure in advance for conducting the experiments. Appropriate experimental designs minimize the measure of data that can be acquired for a given measure of experimental attempt. **[Jacqueline K. Telford, 2007]**

Methods for design of Experiments

- Complete randomized design
- Designs Randomized blocks
- Design of full factorial
- Design of fractional factorial
- Design Response surface method

1.4.1Choosing a DOE

The decision of a test configuration relies upon the reactions of the investigation and the quantity of factors to be examined. The experimental design objectives are explained below.

Comparative Method: If one or more variables to be studied, but the primary objective of an experiment is to find one prior factor, then the question arises that whether factor is significant or not i.e. a comparative problem, thus solution of comparative design is required.

Screening Method: The experiment primary purpose is to choose otherwise screening out some significant effects from the experiment which are less significant. These selected designs are also termed as major effects of designs. **[Mark J. Anderson, 2004]**

Response Surface (method: Using RSM the experiments were planned to estimate the quadratic effects and interaction, and therefore get an idea about of the shape of the response surface that were investigating. For this cause, they are referred as response surface method (RSM) designs. RSM designs are used to:

- Estimate optimal or enhanced procedure settings
- Troubleshoot weak points and practice problems
- To create a more robust process or products (insensible to these influences) against the peripheral and uncontrollable influences.

Method of Regression model: With a specific end goal to demonstrate a reaction as a numerical function (either known or experimental) of a couple of persistent variables which requires great model parameter estimates (i.e., unbiased as well as minimum variance), at that point regression

design is required. Summary for choosing an investigational design for proportional, selecting and response surface designs is shown in Table 1.9.

Table 1.1 Summary for selecting an experimental design for screening, comparative, and response surface designs

No. of Factor	Comparative Method	Screening Method	Response Surface Method
1	complete randomized design for 1-factor	-	-
2-4	Design of Randomized block	fractional factorial or Full factorial	Box-Behnken or Central composite or
5 or more	Design of Randomized block	Plackett - Burman or Fractional factorial	Screen first to reduce number of factors

1.4.2 DOE Terminology

In higher order effects the estimation of an impact likewise effects the at least one different impacts are said to be associated. For instance, if in a four factor test the estimation of impact D really assesses (D + ABC) at that point the principle impact D is associated with the 3-way connection ABC, which reason to no trouble when the higher request communication is either non-present or immaterial.

Analysis of Variance (ANOVA): It is a numerical strategy for dealing with the changeability of a gathering of experimentations into convertible reasons and setting up different criticalness tests.

Balanced Design: It is an experimental plan, where all treatment mixes have a similar number of perceptions.

Blocking: it is a scheduled, for conducting treatment blends in an exploratory investigation to such an extent that any consequences for the trial comes about because of a known change in raw materials, operators, machines, etc, become concentrated in the levels of the blocking variable. The purpose for blocking is to isolate a efficient impact and keep it from obscuring the principle effects. Blocking is accomplished by limiting randomization.

Center Points: All factor ranges, Points at the inside estimation.

Comparative Designs: It is a design, which is aimed at making determinations about a significant factor, conceivably within the sight of at least one other irritation factors.

Confounding: A jumbling configuration is one where some treatment impacts (primary or interactions) are evaluated by indistinguishable liner combinations of the exploratory perceptions from some blocking impacts. For this situation, the treatment impact and the blocking effects are said to be confounded. It is also called as a general term to represent to that the estimation of a principle impact appraise originates from both the primary cause itself and furthermore infectivity or bias from higher order interactions. Confounding design clearly emerge when full factorial design outlines must be kept running in blocks and the block size is lesser than the quantity of various treatment combinations. They likewise happen at whatever point a fragmentary factorial design is picked rather than a full factorial plan **[Mary Natrelia, 1963].**

Design: An arrangement of trial information that grants to fit a specific model and locate the desired impacts.

Design Matrix: A matrix clarification of a test that is helpful for arranging and analyze experimental runs and unexplained variety in a group of observations. DOE's regularly require comprehension of both irregular mistake and absence of fit error.

Factors: Process inputs control to premise an adjustment in the result. The experimenter can't be controlled a few factors yet may influence the results. In the event that their impact is huge, at that point these uncontrolled elements ought to be estimated and utilized as a part of the information examination. The information sources might be consistent or discrete.

Crossed Factors: Two components are crossed, if each level of one happens with each level of the other in the test

Nested Factors: A factor "A" is settled inside another factor "B" if the levels or estimations of "A" are diverse for each level or estimation of "B". Nested factors or impacts have a progressive relationship. **[Sand wick Coromant, 2009]**

Fixed Effect: An impact related with an information variable that has a predetermined number of levels or in which just a set number of levels are important to the experimenter.

Interactions: Generated when the impact of one factor on a reaction relies upon the level of another factor(s).

Lack of Fit Error: Error that happens when the investigation discards at least one vital terms or factors from the procedure display. Counting replication in a DOE permits detachment of trial mistake into its segments: Lack of fit and arbitrary (pure) error.

Model: Mathematical relationship which relates changes in an offered reaction to changes in at least one variable.

Orthogonality: Two vectors of a similar length are symmetrical if the whole of the results of their relating components is 0. An exploratory design is symmetrical if the impacts of any factor offset (sum to zero) over the impacts of alternate elements.

Random Effect: An impact related with input factors picked indiscriminately from a populace having a vast or infinite number of conceivable values.

Random error: Error that happens because of regular variety all the while. Note: Random mistake is commonly thought to be typically dispersed with zero mean and a consistent difference. Random error is additionally called experimental error.

Randomization: A calendar for allotting treatment material and for directing treatment mixes in a DOE with the end goal that the conditions in a single run neither rely upon the states of the past run nor anticipate the conditions in the ensuing runs. Note: The significance of randomization can't be over pushed. Randomization is essential for conclusions attracted from the analysis to be right, unambiguous and faultless.

Replication: Performing a similar treatment blend more than once. Note: Including replication permits a gauge of the random error free of any lack of fit mistake. **[Mary Natrelia, 1963]**

Resolution: A term which portrays how much evaluated principle impacts are associated (or frustrated) with assessed 2-level relations, 3-level relations, and so forth. In general, the determination of a design plan is one more than the smallest order relations that some primary impact is perplexed (associated) with. In the event that some primary impacts are perplexed with some 2-level relations, the determination is 3. Full factorial design has no frustrating and are said to have determination endlessness. For most pragmatic purposes, a determination 5 design is superb and determination 4 designs might be sufficient. Determination 3 designs are helpful as economical screening design.

Reactions: The output(s) of a procedure. At times called dependent variable (s).

Response Surface Designs: A DOE that completely investigates the procedure window and models the reactions. These designs are the best when there are under 5 factors. Quadratic models are utilized for RSM and no less than three levels of each factor are required in the design.

Variance Components: The Overall variation partitioning into convertible components. **[Mary natrelia, 1963]**

1.4.3 Response Surface Methodology (RSM)

Reaction surface procedure (RSM) is a gathering of scientific and measurable systems for exact model building. The goal is to improve a reaction (output variable) which is impacted by a few autonomous variables (input variable). An investigation is successions of tests, called runs, in which changes are made in the factors, remember the end goal to recognize the changes in the output response **[M. Aruna, 2012].**

Initially, RSM is initiated to demonstrate model responses **[Box and Draper, 1987]**, and afterward relocated into the displaying of numerical experiments. The distinction is in the sort of error created by the response. In physical investigations, incorrectness might be a direct result of estimation error in computer tests, numerical noise results about fragmented merging of iterative procedures, round-off errors or the discrete portrayal of continuous physical phenomena **[Giunta, 1996, van Campen, 1990, Toropov, 1996]**.

The use of RSM for design optimization is diminishing the cost of expensive investigation techniques (e.g. finite element method or CFD examination) and their related numerical clamor. The issue can be approximated with smooth functions that enhance the convergence of the optimization procedure since they diminish the impacts of clamor and they take into account the utilization of subordinate based calculations. **[Venter et al., 1996]** have examined the upsides of utilizing RSM for design optimization applications.

The reaction can be shown to graphically, either in the 3D space or as contour plots that assistance envision the shape of the response surface. Contours are curves of consistent reaction attracted the x1, x2planeshown in Figure 1.11 keeping every single other variable settled. Each shape compares to a specific stature of the reaction surface.

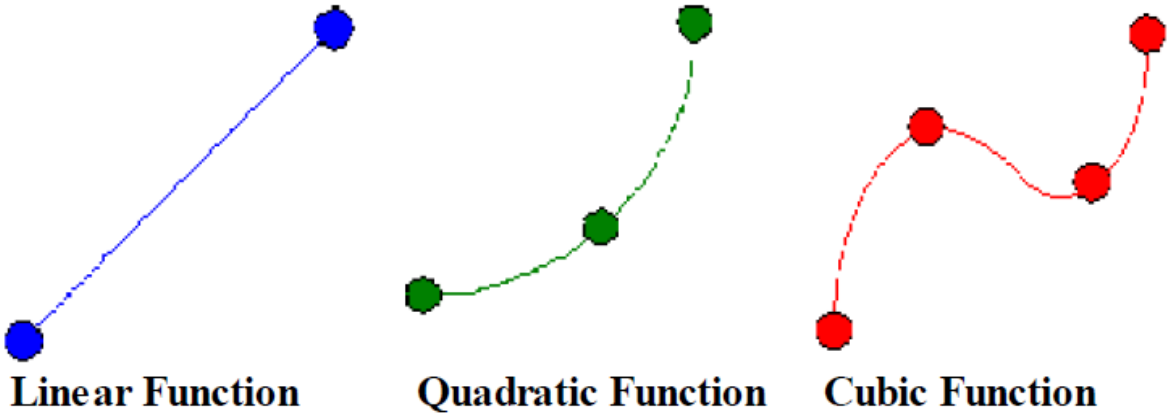

Figure 1.11 Possible practices of response as functions of factor settings

Two-level factorial outline with focus points can recognize yet may not fit quadratic impacts. A 3-level factorial plan can fit quadratic models however they require numerous runs when there are in excess of 4 factors. Fractional factorial design made to maintain a strategic distance from such a large number of runs. But it may have Complex alias name structure and lack of rotatability which is alluring property for 3-level fractional factorial design. **[Shao-Wei Cheng, 2001]**

In a rotatable design, the variance of predicted estimations of y is a function of distance of a point from the focal point of the design as well as it's anything but an function of the direction point lies from the middle. Before examination a little information or no learning may exits about the locale region which contains ideal reasons which ought not predisposition an examination toward any path.

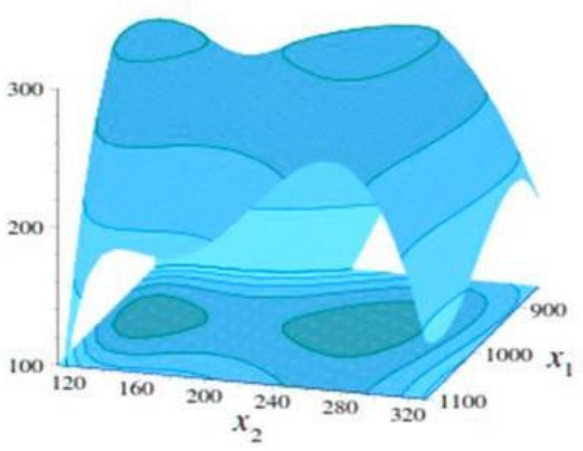

Figure 1.12 Typical Response Surface Contour

1.4.4 Types of RSM Design

- Box-Wilson Central Composite Design
- Box-Behnken outline

1.4.5Box-Wilson Central Composite Design

A Box-Wilson Central Composite Design usually called as a CCD, contains fractional factorial design or an imbedded factorial with central points that is increased with a gathering of `star points' that permits to estimation the shape. On the off chance that the separation from the focal point of the design space to a factorial point is ±1 unit for every factor, the separation from the focal point of the design space to a star point is ±αwith $|\alpha| > 1$. The estimation of α relies upon specific properties wanted for the design and on the quantity of factors included. **[Russell V. Lenth, 2009]**.

To evaluate the curvature, the CCD design plans start with central points or factorial design as well as star points**. [Li Wang, 2006]** as appeared in Figure 1.12.

The classification has been made based on star points and it is divided as three central composite designs. Therefore the CCD contains star points as the same number of factors in the design. The star points speak to new extraordinary qualities (low and high) for each factor in the design.

Table 1.2 summarizes the properties of the three varieties of central composite designs.

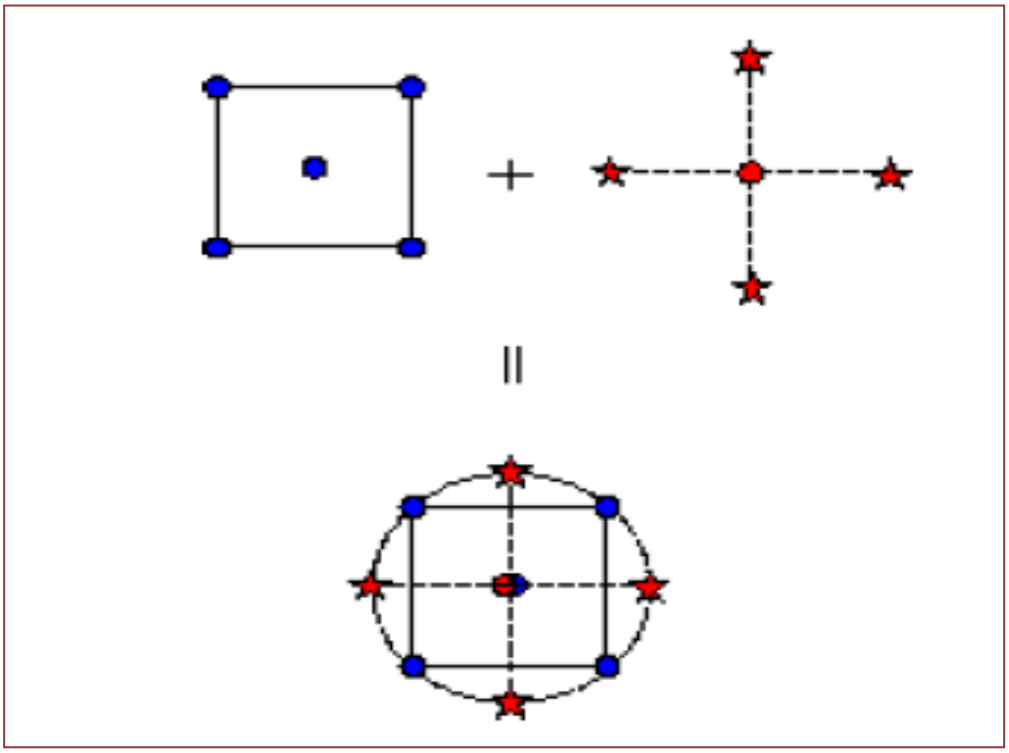

Figure 1.13 Generation of a Central Composite Design for Two Factors

It is to take note of that the CCC (Central Composite Circumscribed) investigates the biggest procedure space and the CCI (Central Composite Inscribed) investigates the smallest procedure space. Both the CCC and CCI are rotatable design; however the CCF (Central Composite Factorial Design) is definitely not a rotatable design. In the CCC design, the design points about the factorial square.

The factorial portion of the central composite design:

$$\alpha = (\text{numberoffactorialruns})^{1/4} \qquad (1.2)$$

If the factorial is a full factorial, then

$$\alpha = (2^k)1/4 \qquad (1.3)$$

Table 1.2 Comparisons of the Three Types of Central Composite Designs

CCD Type	Terminology	Comments	Pictorial Representation
Circumscribed	CCC	CCC plans are the first type of the focal composite design plan. The star focus points are at a distance from the inside in light of the properties wanted for the plan and the quantity of variables in the plan of design. The star focus points set up new extremes for the first to last settings for all components. Figure 5 represents a CCC plan of design. These plans have circular, round, or hyper round symmetry as well as its require 5 levels for every factor. Enlarging a current factorial or determination V fractional factorial design (FFD) with star focus points can deliver this plan of design.	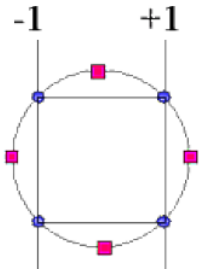
Inscribed	CCI	For those circumstances in which the breaking points indicated for factor settings are genuinely confines, the CCI configuration utilizes the factor settings as the star focus points and makes a factorial or FFD inside those cutoff points This is additionally requires 5 levels of every factor.	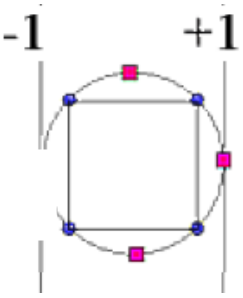

Face Centered	CCF	In this plan the star focuses are at the focal point of each and every face of the factorial space, so α= ± 1. This assortment requires 3 levels of every factor. Enlarging a current factorial or determination V plan of design with suitable star focus points can create this design. (Building Statistics Handbook)	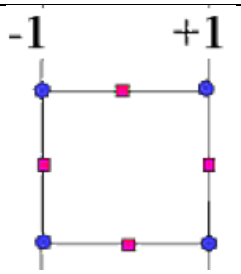

1.4.6 Box-Behnken Method

The Box-Behnken configuration is a free quadratic outline design in that it doesn't contain an implanted factorial or partial factorial plan. In this plan of design, the treatment blends are at the midpoints of edges of the procedure space and at the middle. These outlines are rotatable and require 3 levels of each factor appeared in Figure 1.9. The plans have constrained capacity for symmetrical blocking contrasted with the CCD **[David J. Edwards, 2007].**

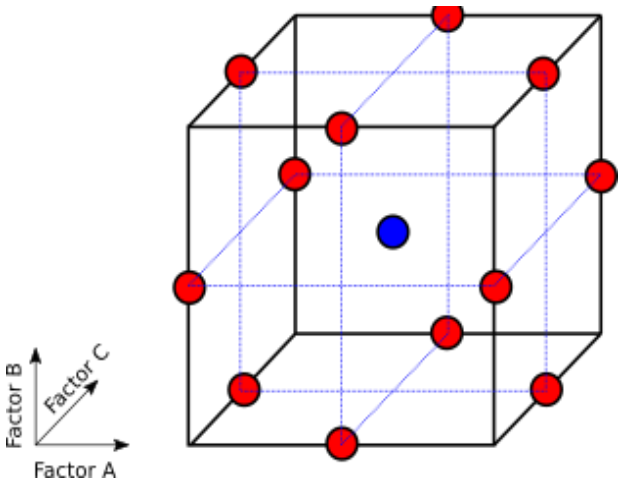

Figure 1.14 Box-Behnken design plan for 3 factors

Properties of RSM design are:

- Fitted esteems are as close as conceivable to watched esteems. Which limit residuals or blunder of forecast
- Internal gauge of mistake.
- Lack of fit detection is good.
- Satisfactory dispersion of data over the test locale rotatability.
- Suitability for blocking.
- Transformations can be evaluated.
- Sequential development of higher request plans from more straightforward outlines
- Combinations of treatment are minimum.
- Good graphical examination through straightforward information designs.

1.4.7 Steps in DOE

Getting great outcomes from a DOE includes these seven stages:

- Set destinations
- Select procedure factors
- Select a trial design plan
- Execute the plan of design
- Check that the information is steady with the test suppositions
- Analyze and decipher the outcome results
- Use/display the results outcome (may prompt further runs or DOE **[N. Aslan, 2006]**

1.5 Minimum Quantity Lubrication (MQL)

Minimum quantity lubrication (MQL) refers to the application of a miniscule quantity of coolant, typically of a flow rate of 10 to 100 ml/hour **[Kamata and Obikawa, 2007].** Minimizing the ecological impacts of cutting process is needed to get the continual and neat manufacture. The alternative process for machining are developing is still an excessive task to avoid the negative environmental impact of machining can be achieved by operating modification of obtainable processes **[Hanafi et al., 2012]**. As the manufacturing world is in a continuous pursuit of investigating the methods in order to increase the process performance and to reduce the production costs, in addition to the growing environmental concerns **[Fratila, 2013]**, minimum quantity lubrication process can offer the near-term solution to the problem. Driven by pressure from international environmental protection agencies, energy consumption and natural resources

conservation laws enforced by public authorities, manufacturing industry and the concerned research centers are forced to focus their efforts on researching alternative production processes, creating technologies to minimize the use and production of environmentally hostile residues. MQL has demonstrated as a successful near-dry machining technique as well as a globally acknowledged option compared to complete dry and wet cutting conditions from the perspective of cost, ecological, human health issues and machining process performance [**Lawal et al., 2013]**. MQL is a sustainable manufacturing approach which is vital in the current scenario of manufacturing industry as it incorporates all the issues related to sustainability. The cost of cutting fluids range from 7 to 17% of the total machining cost while another estimate gives this cost as 15-20 % of total machining cost compared to the 2 tool cost which ranges from 2 to 4% **[Attanasio et al., 2006; Lawal et al., 2013; Li et al., 2014]**. Therefore, the minimization of metal working fluids can serve as a direct gauge of sustainable manufacturing. Machining with MQL has been extensively applied in many machining processes such as drilling **[Filipovic and Stephenson, 2006; Davim et al., 2007]**, milling **[Lacalle et al., 2006; Liao and Lin, 2007]**, turning **[Davim, 2007; Kamata and Obikawa, 2007]** and MQL grinding **[Silva et al., 2005; Shen et al., 2008]**. Since no huge power consuming auxiliary equipment such as compressors, chillers and pumps are required as compared to flooded machining, hence a marked reduction in energy consumption in MQL machining. The use of empirical approach together with the implementation of experimental design techniques as well as application of statistical data analysis techniques are gaining recognition on account of the simplicity involved in the model making procedure and the accuracy of the prediction obtained for the specific cutting conditions domain **[Kannan and Baskar, 2013]**. Aluminium alloys are the most machinable amongst the metals with a wide range of applications due to mechanical and corrosion resistance with lower cutting forces as well as low cutting temperatures **[Kelly and Cotterell, 2002; Ariff et al., 2012]**. However, due to highly adhesive characteristics of aluminium and its alloys more effective lubrication is required for these alloys although these are not hard and difficult-to-cut especially with alloys containing hard inclusions such as aluminium oxide, silicon carbide, or free silicon **[Kelly and Cotterell, 2002; Wakabayashi et al., 2007]**. The machining of aluminium alloys results in the generation of very fine metallic particles in the form of ultrafine dust particles with longer air-borne suspension time hence harmful for the health of the operator **[Songmene et al., 2011]**. Significance of machining processes optimization arises from the prerequisite for an economic and feasible performance of the machining processes. Practical manufacturing

processes are illustrated by conflicting and often incompatible measures of performance such as quality and productivity **[Kumar and Chhabra, 2014]**.

1.5.1 Principle of MQL system

[Steidle Gmbh Est. 1979] Minimum Quantity of lubrication is mainly based on two approaches one is targeted lubrication and another one is quantity optimization. In conventional lubrication, an emulsion consists of 5 percent (approx) of lubricant and 95 percent (approx) of water is normally adopted. Consider the effect of this mixture most of the emulsion aids only to cool down the heat that is produced by its indigent lubricant effect. If we optimized the lubrication it leads to reduce the heat to dissipate. Furthermore, only a small volume of the lubricant is required for the lubrication process. Everything over and above this amount is listed. MQL means using only the definite quantity of lubricant required due to this it is also called as "Near dry lubrication".

[SteidleGmbhEst, 1979] Minimum Quantity of lubrication is defined as the amount of lubricant required between 10 to 100 ml per processing hour. When we compare with the closed circuit cooling the ratio will be approximately, 1: 10,000. In other words, for every liter of emulsion we require only one drop of MQL. The spray painting on gun is used on cutting surface and the minimum quantity of lubrication demands greater speed and higher pressure through gun. Contemplating the circumstances needed for the current work as well as by MQL transfer process, the pressure is maintained at 5 bar for long cutting operations. In this process, an air compressor is utilized to maintain high pressure into the gun and mix with the fluid comes from the liquid reservoir chambers. The fluid reservoir is connected at the top with the spray painting gun. A gun is used at chip tool interface to provide high velocity of MQL, which is prepared by blending of air and vegetable oil. While processing, the high velocity thin stream of minimum quantity of lubrication is envisaged at the tip of the cutting tool and the coolant will reach the interfaces near to the work-tool interfaces as well as the chip–tool. To allow the high dimensional quality, the MQL is mainly applied on flank and rake surface to convert the auxiliary flank.

As per the available literature, researchers were mainly concentrated on rotary turning but on the rotary milling limited research work is done. **Baro *et al.* (2005)** studies rotary face milling operations and proposed a model with self propelled rotary milling cutter. The assumptions were made to study this based on chip cross sectional area of both rotary milling cutter and surface grinding process are comparable. The aerospace with rotary tool milling process have very

limited operational attempts and it is motivated to do research in this area. Radial rake angle in conventional machining is considered as inclination angle in rotary machining which has great importance while dealing with the mechanics of rotary machining. Hence, various inclination angles are developed as well as performed on four inserts in rotary face milling process and represented in this research with the help of a Nickel based superalloy Inconel 625. Also, cutting force, Cutting Temperature and surface roughness models have been developed.

1.5.2 Thermal conductivity of Nano fluids

Traditional conduction of heat methods for liquid solid combinations are developed such as Maxwell method Jeffrey method and Hamilton–Crosser method **[Jeffrey, 1973],** Maxwell model **[Maxwell, 1904].** Though this type of traditional methods of heat conduction is restricted to mixtures, which are contained micrometer-sized particles. When applying to Nano fluids, the thermal conductivity was usually underestimated.

[Choi et al. 2001] has studied and observed that the thermal conductivity of ethylene glycol was improved equal to 40% when 0.3 Vol% Cu nanoparticles of 10 nm mean diameter are used, while **[Xuan and Li, 2000]** stated that the thermal conductivity of water was improved to 78% of 7.5 Vol% Cu nanoparticles of 100 nm mean diameter **[Hong et al, 2005**] observed that the ferrous nano fluids are improved the thermal conductivity equal to 18% as the volume fraction of particles is increased up to 0.55 Vol%. **[Patel et al. 2003]** Ag and Au nanoparticles are combined with water and observe that the water soluble Au nano particles of diameter 10–20 nm, prepared with citrate stabilization gives thermal conductivity development of 5–21% in the range of 30–60ºC temperature at a loading of 0.021 Vol%.

Non-metallic nano fluids such as Al_2O_3, CuO, SiC, TiO2 and carbon nanotubes also have been studied. **[Masuda et al. 1993]** observed the thermal conductivity of water with the mixing of 4.3 vol% Al_2O_3 Nanoparticles (mean dia of 13 nm) 30% improvement. **[Lee et al. 1999],** conversely stated that the thermal conductivity at the same nano particle loading only a 15% enhancement in (mean dia of 33 nm). **[Xie et al, 2002]** observed that an approximately 21% improvement was obtained while using 5 Vol% of nano particle loading (mean dia of 68 nm). These differences in activities were may be endorsed to differences in average particle size in the samples. Nano fluids consisting of CuO nanoparticles dispersed in water and ethylene glycol seem to have larger enhancements in thermal conductivity than those containing Al_2O_3nanoparticles **[Lee et al., 1999]**.

1.6. Genetic Programming

Genetic programming (GP) was introduced by **[Koza. J. R 1992],** belongs to a group of evolutionary algorithms derived from the concept of genetics and natural selection. GP is comparatively new to a group of other evolutionary algorithms, evolutionary programming **[Schwefel, H.-P, 1981]**, evolution strategies **[Fogel, L.J., A.J. Owens, 1966]** and genetic algorithms **[Goldberg, D.E. and J.H. Holland, 1988]**. An evolutionary algorithm (EA) is a part of the evolutionary computation, in turn, a part of artificial intelligence. GP is a technique for generation of genetic mathematical models introduced by [**Koza. J. R 1992** and **1994**].Koza proposed GP as a generalization of GA. The genetic programming method is mainly applied to non-linear regression problems to create mathematical expressions that associate among a set of dependent parameters and independent parameters to provide a good fit **[Poli, R., 2003]**.

1.6.1. Concept of Genetic Programming

Genetic programming (GP) is an addition of the genetic algorithm (GA) in which the genetic population of computer programs exists. GP is used to model while GA is used for optimization. And also, GP differs from GA by utilizing the tree structure and chromosomes of variable length rather than GAs chromosomes of fixed length and structure. The genetic algorithm output is one set, while the genetic programming output is another computer program. The chromosome in a certain way the problem is coded, it can be carried out usually in its current form instead of binary strings. Therefore, in this approach, members of the population may be represented themselves in a particular problem being solved. For an instance, to undertake a regression problem, the members of the population can be symbolized as a mathematical expression with a tree structure **[Koza. J. R 1992]**.

1.6.2. Execution of GP

The procedure of GP comprises the following basic steps **[Koza. J. R 1992]**:

i. Identification of functional set and terminal set, together with fitness measure.

ii. Generation of the initial random population of terminal and functional sets.

iii. On the basis of value of fitness, estimate the each individual fitness.

iv. Application of the selection operators. The grater the fitness values of an individual, the higher the probability that the individual is elected, and leads to the next generation (the strongest survival). This population is called as the mating pool.

v. Based on the crossover possibility, pairs of individuals from the mating pool are selected and the crossover is carried out.

vi. The next step is to apply a mutation operator, depending on the mutation probability, helps the mutation to ensure that no point in the individual search space stays unexplored.

vii. Copy the individuals to a new population.

viii. Repeat steps (iii) to (vii) for a determined number of iterations or until or until a specified fitness value is achieved.

These steps are discussed with an emphasis on the relevance of modeling with the genetic Programming.

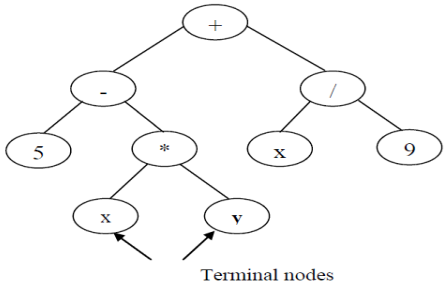

$f = (5\text{-}xy) + x/9$

Figure 1. 15: General tree representation of Genetic Programming

The models are presented as a tree structure, and generate a large population of these models. Each model consists of a functional and a terminal set. The functional set comprises of basic mathematical operators (+, -, ×, /), trigonometric functions (sin, cos, tanh etc.,), exponential functions and boolean algebra operators (eg AND and OR).The problem of the input variables is represented by a terminal set **[Garg, A., K. Tai, and M.M. Savalani, 2014]**.

The representation of a functional tree is shown in Figure 1.6. The connection points are shown as nodes in the tree. The nodes are classified based on their position in the tree. The inner nodes in the tree are called functions. They may be Arithmetic operations, Boolean operations, Mathematical functions etc…The ending nodes (leaf nodes) are called terminal nodes. Here the "+", "*", "/" functions have two sub-trees. The right sub tree is (x / 9). Similarly, Figure 1.6 shows f = (5-xy) + x/9.

For a GP model, there are four essential elements that need to be designed:

i. ***Create random initial population*:** The first step is to create random GP population. The random individuals here are random trees. These trees are created by selecting and combining terminal and functions in the trees.

ii. ***Fitness evaluation**:* Designing a fitness function which can determine the ability of a model to solve the problem is an important step in GP. Based on the error between actual data and the model induced by GP a numerical value is obtained. This numerical value is fitness. Each individual in GP will have a fitness value.

iii. ***Selection:*** The individuals with higher fitness values must be selected over the process of lower fitness values for reproduction. This is ensured by the process of selection. The probabilities of choosing a model for reproduction are directly proportional to its fitness value. There are a number of ways of selecting models. Roulette wheel selection, truncation selection, tournament selection, fitness proportionate selection, ranking selection etc. are some of them.

ii. ***Genetic operators*:** After selecting an individual from the population three genetic operators reproduction, mutation and crossover are used.

a. *Reproduction* is where selected individual copies itself into the new population. Elitism is a special reproduction operator. Elitism ensures that the superior individual is always selected.

b. *Crossover* is the primary genetic operator for modifying the program structures. With the help of information gathered from parents and by combining them crossover is carried out. Thus by combining the important information from two parents, a more superior individual is formed. This is done in GP by swapping the sub trees in them as shown in Figure 1.16.

c. *Mutation* is considered as a secondary genetic operator for modifying program structures. Unlike crossover here, there is no involvement of two parent individuals. In GP mutation of an individual is made by selecting a subtree of that individual and replacing it with a newly created subtree as shown in Figure 1.17

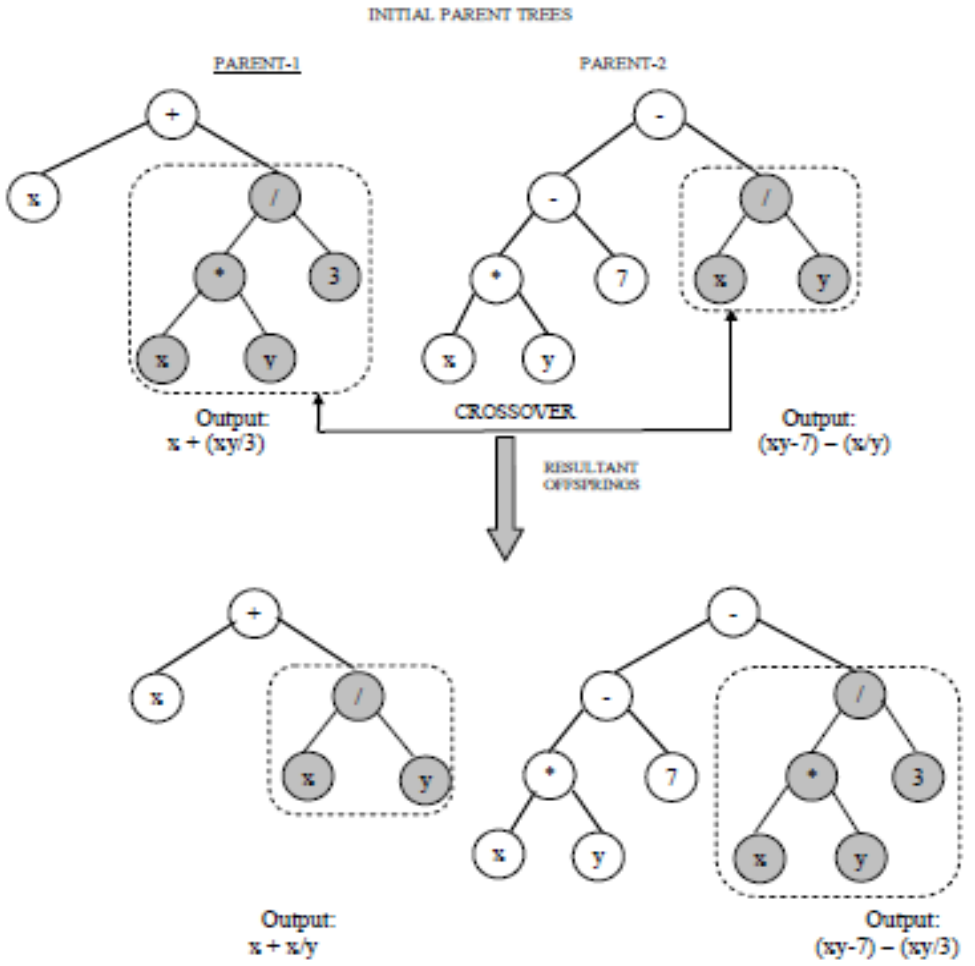

Figure 1. 16: Crossover operator

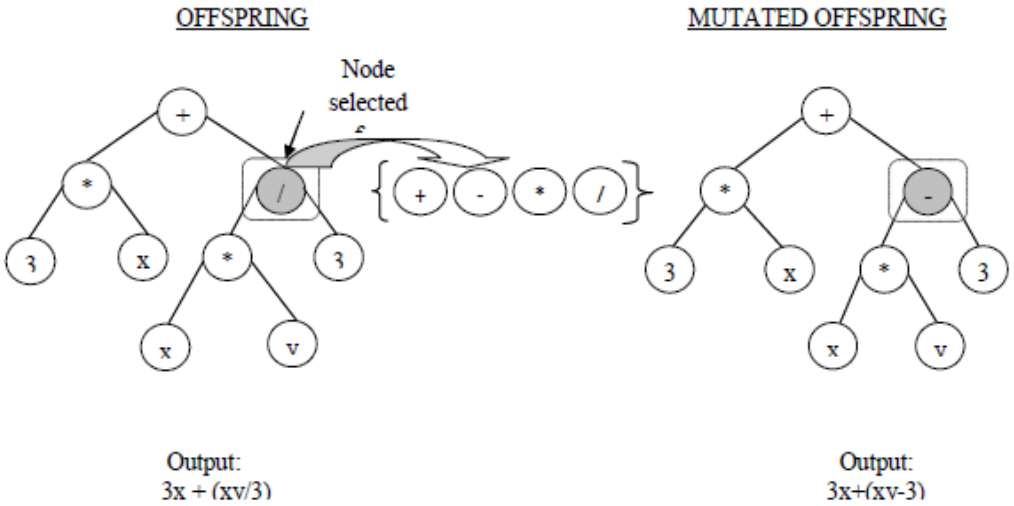

Figure 1. 17: Mutation operator

1.6.3. Multi Gene Genetic Programming

Multi Gene Genetic Programming (MGGP) is a newly developed method of genetic programming **[Koza, J.R, 1999]**. It mainly helps in the improvement of precision of GP. MGGP mainly differ from GP in the number of trees that can be used in MGGP. GP mainly uses single trees whereas MGGP uses a combination of trees. The advantage of multi gene genetic programming process based on previous models is that it is a data-driven method based on data which depends on experimental data to develop models. This avoids errors by reason when building a model of the differential equation is used.

In MGGP the final structure of the target model is made in a linear form by combining two or more non-linear gene. The general form of a MGGP model is:

$y = a0 + a1\mathrm{Gene}1 + a2\mathrm{Gene}\,2 + \cdots + an\,\mathrm{Gene}\,n$

Where, $y$is the output, $aa0$is the bias term, $\mathrm{Gene}_1$are the non-linear genes, $a_1$is the coefficient of related genes, n is the number of genes.

The outline of MGGP algorithm is **[Searson, D.P., D.E, 2010]**:

---

i. Define the problem

ii. MGGP Algorithm

Begin

a. Set terminal set and function set, the genetic operators, the population size, number of generations and the maximum number of genes

b. Generation of genes initial population

c. The models are generated by joining the set of genes by the least squares method

d. Evaluation of models performance based on RMSE

e. Employ the genetic operators and create new population

f. Checking the performance of the models according to the termination criteria and, if not satisfied,

GO TO Step ii (e).
End;
END;

A model formulated using MGGP algorithm. Then the method of least squares is used in the MGGP algorithm to find the coefficients $a_0, a_1 \ldots a_n$.

1.6.4. MGGP Execution

The efficient achievement of MGGP algorithm is mainly determined by the parameter settings. These parameter settings are selected by the trial and error technique. The problem complexity determines the size of the population and the number of generations. Based on literature review **[Garg, A. and K. Tai, 2012, Garg, A. and K. Tai, 2013]** large size of the population and a large number of generations are to be avoided in case of large number of data samples and this helps in avoiding the problem of over-fitting. The size of the search space and number of models are influenced by a maximum no. of genes and the maximum depth of the gene.

The study of the GP of processing applications and Tai Garg shows that the size of population and the no. of generations must be attached to a high number for the smallest quantity of data or data, of higher dimensions. The size and the different forms of the model for the space of the global solutions are evaluated by the values of the maximum number of genes and the depth of the genes **[Garg, A. and K. Tai, 2013]**.

The performance of the individual in the initial population from the fitness function, i.e. the Mean square error (RMSE) given as follows:

$$RMSE = \sqrt{\sum_{i=1}^{n}(|G_i - A_i|^2)/n}$$

Where G is the predicted value data of the i^{th} sample of the MGGP model, A_i is the real value of the data of the i^{th} sample, and N is the number of training samples [50].

GA and Genetic Programming are similar in almost every aspect, except that the playback operator cut a tree view. In the process of structural adjustment GP population of computer programs is hierarchical. The GP procedures are most commonly used to model the complex system, but also a system can be used effectively for modeling

1.7. Concept of Optimization

Optimization is a method of making things superior. Optimization is a modification of input parameters to obtain the minimum or maximum output(s). The input parameters are the variables, the process or function is called an objective function or cost function and the output is fitness value or cost **[Haupt, R.L. and S.E. Haupt, 2004]**. Optimization techniques that have reached a maturity level in recent years come in a variety of industries, including automotive and aerospace manufacturing industries, chemical energy. Optimization refers to the search for one or more possible solutions, extreme values or more goals. The need to find a solution to the problem of this nature is above all the ultimate goal of a solution with a minimum cost of production for maximum reliability. Due to these extreme properties of optimum solutions, optimization methods of great practical importance, especially in engineering design, experiments and business decisions of the company.

1.7.1. Single Objective Optimization

In single objective optimization, it is the only best solution that is generally the global maximum or minimum based on the type of optimization issue **[Goldberg, D.E, 1989]**. If there are multiple conflicting objectives, there doesn't exist one solution that is best compared to all targets. It cannot be an optimal combination of parameters in practice for all objectives. The parameters influence differently. There is, therefore, a require for a multi objective optimization technique to the present problem to arrive at the optimal solutions **[Srinivas, N. and K. Deb, 1994]**.

1.7.2. Multi Objective Optimization

Optimization is the most important to find an optimal solution. An optimization process consists of three basic elements: variables, objective function and constraints. This process is to minimize or maximize the objective function to satisfy constraints. The problem is based on many variables and therefore must have different combinations of values of the variables are reviewed by the optimism of the objective function **[Fonseca, C.M. and P.J. Fleming, 1995]**. Sometimes many contradictory criteria such as cost, performance, capacity and reliability should be considered at the same time. It is very complicated to choose which is best for the selection criteria because the criteria can variance with each other. This is also known as the multi-objective optimization technique.

Many real world design problems involve simultaneous optimization of multiple objectives. In the case of multiple objectives, there cannot be a solution that is best (global maximum or minimum) of all objectives. In a usual multi-objective optimization problem, there are a number of superior solutions for the rest of the solutions in the search space if all valid objectives, but are lower than other solutions in space in one or more goals. These solutions are known as non-dominated solutions or Pareto optimal solutions **[Rangaiah, G.P, 2016]**. The rest of the solutions are identified as dominated solutions. The choice of a solution to another problem requires knowledge and a series of factors related to problems. Therefore a solution that can be selected by a designer may not be adequate for another designer or in a modified situation. Hence, it may be useful for the multi-objective optimization problem to know Pareto optimal solutions.

In the case of multiple conflicting objectives, there is no solution that is best with respect to all objectives. In practice, it may not be a single best possible combination parameter for cutting force, surface roughness and cutting temperature. The parameter influences them differently. Therefore, there is a necessity for a multi-objective optimization technique to arrive at solutions to this problem. In the case of several contradictory objectives, there is no solution that is best for all targets.

The multi-objective problem was designed as follows:

Minimization \ Maximization

$F(x) = [f_1(x), f_2(x),\ldots\ldots..,f_k(x)]$

Subjected to $g_j(x) \leq 0$ where $j = 1,2,3,4,\ldots\ldots..,j$

$h_k(x) = 0$ where $k = 1,2,3,4,\ldots\ldots.,k.$

Where $f_1(x)$, $f_2(x)\ldots\ldots\ldots..f_k(x)$ are the objective functions. The objective function can be of minimization or maximization type. In multi-objective optimization, preferably an attempt has to be made in obtaining a set of trade–off optimal solution by considering all objective to be significant. The objective function can be minimized or maximized. In the multi-objective optimization, preferably an attempt has to be made in obtaining a set of trade–off optimal solution by considering all objective to be significant.

1.7.3. Concept of dominance and Pareto optimality

Multi Objective Optimization uses a dominance model by comparing two solutions. If an optimal solution is not dominated by any other possible solution to the problem of multi objective optimization, it is said that a solution is a non-dominated solution. To find a set of non-dominated solutions the following procedure can be adopted. If x (1) is not worse than x (2) then x (1) dominates x (2) all targets and x (1) is strictly better than x (2) in at least one target. It is said that the solution x (1) dominates x (2) or x (1) is dominated by x (2), if the two above conditions are true.

A single solution is not obtained to a multi-objective optimization problem, but a set of numerical equal solutions of fine optimal solutions known as non-dominated Pareto solutions. These solutions are strongly based on the concept of dominance, where one factor dominates another if it is better than the other in at least one target and not a bad function in relation to all other objectives. Pareto front depicts the tradeoffs among opposing objectives and recognizes non-dominated solutions. It consists of members of the population, for whom there is no solution, which is better in criteria than the Pareto set member. The ability to characterize the Pareto front can focus on inspection and compensation for conflicting variables. The representation of the Pareto front can be quickly used to find promising solutions to large populations of expressions and focus the efforts of subsequent analysis of these solutions.

Although several conventional methods for obtaining solutions are available for multi-projection problems, they have some disadvantages of conventional methods of minmax optimization, weighted sum, and distance function methods. These techniques change the multi-objective problem to a single objective, in which the respective weights are based on relative performance. These methods have the disadvantage that the deep knowledge of the meeting manufacturer must have a best knowledge of the classification of the objective functions. If the objective functions are discontinued the methods will fail. On the other side of the non-dominant genetic algorithm (NSGA-II) has the benefit that it does not need ascent information and natural parallelism and thus provides a robust adaptive optimization technique **[Srinivas, N. and K. Deb, 1994].**

1.8 Non-dominated sorting genetic algorithm-II (NSGA-II)

There is one method of solution to multi-objective problems are to change the vector objectives to scalar objectives into single objective by averaging the objectives with a weight vector. The method which is permitted a simple algorithm of optimization is used. The scalarization process is used the weight vector. In addition to the alternate solutions were known by a decision maker if he interested. Since the genetic algorithms (GAS) obtained a number of Pareto-optimal results may be taken using GAS work with a point population. A novel approach is suggested by [**Schaffer 1984]** i.e. EGA (vector evaluated genetic algorithm), gave good results, but it has a disadvantage of bias toward some Pareto-optimal solutions. A new algorithm was developed according to Goldberg (1994) theory is called nonedominated Sorting Genetic Algorithm (NSGA). The bias problem in VEGA was eliminated and distributes the population over the entire Pareto optimal regions. Although there exist two other implementations **[Fonesca & Fleming, 1993; Horn, Nafpliotis, & Goldberg, 1994]** based on this idea, NSGA is different from their working principles and is closer to Goldberg's suggestion **[Kalyanmoy Deb, 2002]**.

1.8.1 General Description of NSGA-II

NSGA-II establishes the following steps like traditional GAs. First, it initializes a random population of N individuals, then it gives children/offspring by recombination and mutation, evaluates the individuals, and finally selects the fittest ones.

- ✓ Through a tournament selection a parental population is selected. This selection procedure recommends selecting a parent based on both convergence and spreading, while maintaining a reasonable diversity amongst the population.
- ✓ The genetic operators used inside NSGA-II are generally the Simulated Binary Crossover and the Polynomial mutation. These operators use a stochastic approach to determine children genes, based on the genes of their parents. They are extremely efficient when real variables are used.
- ✓ The selection process is computed at each generation on an intermediate population combining both parents and offspring. Therefore, no valuable solution can be lost, which makes NSGA-II elitist **[Laurent Magnier, 2008]**.

1.8.2 Principle of NSGA-II

Initially, a random parent population P_{gt} (the subscript t indicates the generation) of size N is created. Non dominated principle is used to short the population. Every solution is assigned a fitness up to its non domination level (1 is the best level, 2 is the next-best level, and so on). Thus, the maximum value of fitness is implicit. At first, the usual binary tournament selection, recombination, and mutation operators are used to create an offspring population Q_{gt} of size N. Since elitism is introduced by comparing current population with the previously best found nondominated solutions, the procedure is different after the initial generation. The procedural steps are illustrated in Figure 5.4. First, a combined population $R_{gt} = P_{gt} \cup Q_{gt}$ is formed. The population R_{gt} is of size 2N. Then, a fast non-domination sorting algorithm is used to rank the solutions according to their dominance rank and organize fronts of equal rank.

According to the available literature, research was mainly focused on rotary turning while rotary milling received limited attention. [**Baro *et al.* 2005]** developed a cutting force model for rotary face milling with self-propelled rotary milling cutter. The model was based on assumption that the chip cross-sectional area in rotary cutting is analogous to that of chip in surface grinding operation. Only a few attempts have been made on application of rotary tool milling of aerospace materials. Thus there is a need for further research in rotary milling process especially when machining aerospace materials. Radial rake angle in conventional machining is considered as inclination angle in rotary machining which has great importance while dealing with the mechanics of rotary machining. Therefore, in this work, a rotary face milling cutter with four insert inclination angles has been developed and its performance has been evaluated while machining of Inconel 625 in dry, MQL and nano coolants conditions. Also cutting force, surface roughness and cutting temperature models have been developed.

1. 9 Research Problem and Objectives of the present work

Inconel 625 is nickel based superalloys with high temperature mechanical properties and outstanding oxidation resistance whose applications include gas turbine engines and Aerospace engines. Along with these properties they also exhibit very high hardness at high temperature which causes problem in machining. Defense organizations like DRDL have been working with Inconel 625 for their scramjet engines. During the interaction with the scientists of DRDL it is found that the machinability data of Inconel 625is not available with rotary machining.

Knowledge of interaction of machining process variables on surface finish, cutting force, and temperature and models for prediction of output variables are scarcely available. Generation of such rotary machining data, response and models are very much required for the user industries such as aerospace and defense. In machining super alloys, the consumption of cooling fluids remain very important, the coolant acquisition, use, disposal and the cleaning of the machined components lead to increase in cost more than four times than the without coolant. Thus, minimizing machining costs and making the processes environmentally safe must be the objective. The goal for this is to move toward dry cutting by eliminating or minimizing the cutting fluids (MQL) use and to improve material removal rate with rotary machining. To conduct the experiments, there is need of manufacturing self propelled rotary face milling cutter with four distinct inclination angles 20^o, 30^o, 40^o and 50^o.

Thus the present work is initiated with the following objectives to achieve.

1.9.1 The main objectives of the present work

1. Develop a self-propelled rotary face milling cutter with provision for four different inclination angles..
2. To study the machinability of Inconel 625 and to find out the effect of cutting parameters (speed, feed and depth of cut) on surface roughness, cutting forces and temperatures while machining with self propelled rotary face milling cutter.
3. To develop RSM models for the surface roughness, cutting forces and cutting temperature in terms of cutting parameters.
4. To find-out the optimum level of cutting parameters for providing the desired surface roughness, cutting force and cutting temperature.
5. To study the machinability characteristics of Inconel 625 with different coolants (MQL and MQL with Al_2O_3, SIC and combination of both Nano coolant).
6. To develop soft computing models like MGGP and NSGA - II for the analysis and prediction of the relationship between input and output parameters.
7. To compare the cutting forces of Inconel 625 with that of SUS 304 Steel.

1.9.2 Expected Outcome

The expected outcome of the present work is presented below:

1. The generated machinability data would be useful to the industry for estimation of Cutting forces, Surface finish and Cutting temperature and thus industry may take necessary precautions while machining Inconel 625 alloys and then cut down wastages like scrap and rework and in turn lead to cost reduction.

2. The industry can predict Cutting force, Surface Finish and Cutting Temperature and their adverse effects on machined components through various soft computing models being developed. And discussion on optimum cutting conditions may lead to better surface finish and enhanced tool life.

3. The concept of MQL is slowly picking up in the industry. The outcome of this research would establish that the application of MQL as a necessity while machining nickel based super alloys (Inconel 625) by rotary machining.

4. The data on Cutting forces, Cutting Temperatures and Surface finish by conducting several experiments on Inconel 625 using self propelled rotary face milling cutter. The reason may be due to expensive nature of materials. Inconel 625 is very expensive, but the machining data on these materials is highly useful to the user industry.

1.9.3 Proposed work:

The flow chart outlining the proposed work is shown in Fig.1.18.

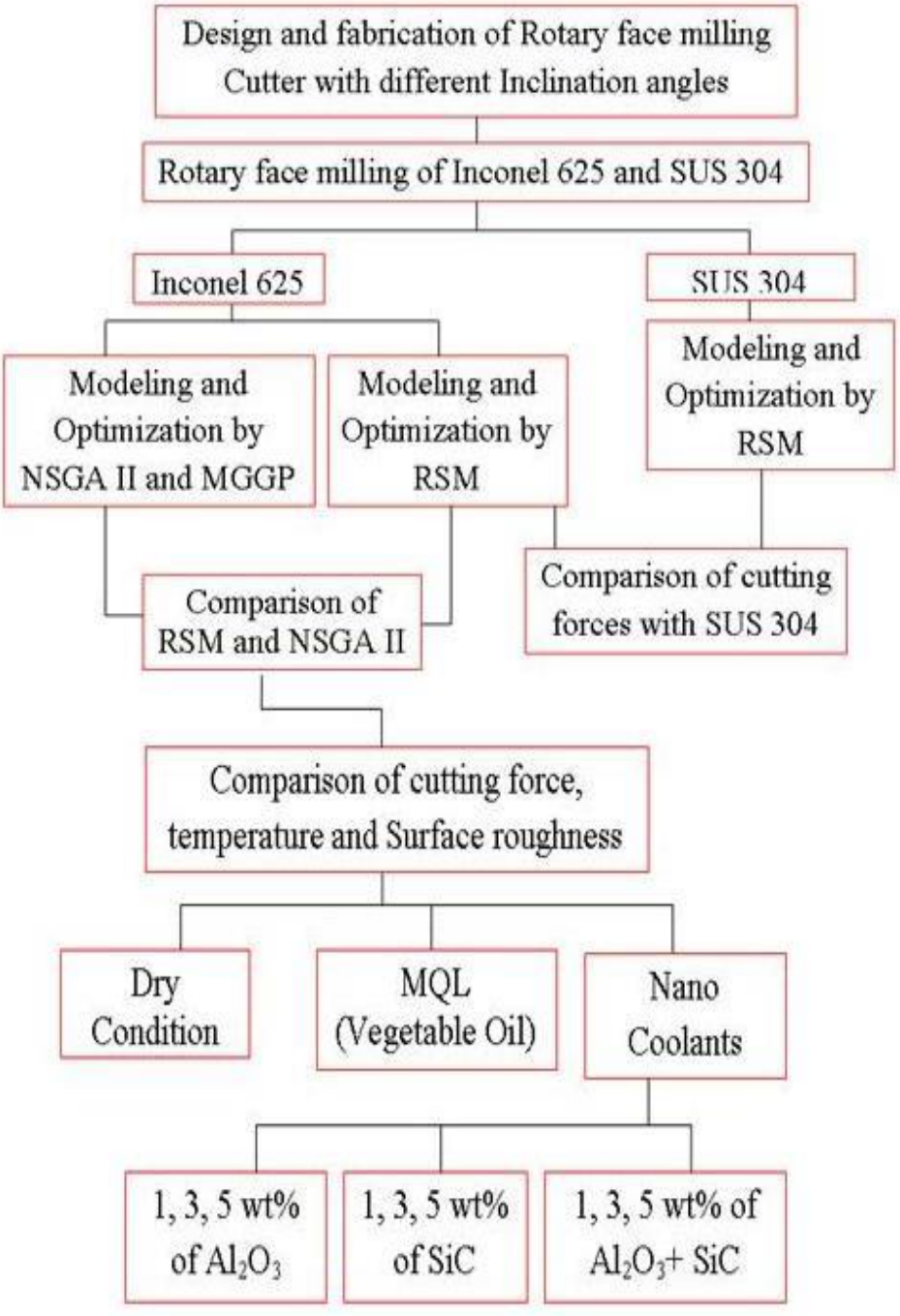

Fig.1.18. Flow Chart of the proposed methodology

1.9.4 Organization of the thesis

The thesis is organized as follows:

- Chapter-1 – This chapter discusses the introduction of rotary cutting, advantages and applications
- Chapter-II - This chapter discusses the review of literature on rotary tool machining
- Chapter-III – This chapter discusses design and analysis of rotary face milling cutter with different inclination angles. It also discusses the manufacturing aspects such as material selection, heat treatment, machining of critical profiles of cutter body, front and rear clamps.
- Chapter-IV – This chapter discusses the experimentation details such as machine tool, work piece materials and experimental setup
- Chapter-V – This chapter discusses the experimental investigations carried out to determine cutting forces developed in face milling operation using the developed self propelled rotary face milling cutter and compared with the cutting forces developed in face milling operation with SUS 304. And also discusses the experimental investigations carried out on surface finish and cutting force generated in face milling operation using self propelled rotary face milling cutter.
- Chapter-VI–This chapter discusses the effect of MQL and Nano coolants on Cutting force, Surface roughness and cutting temperature.
- Chapter-VII – This chapter discusses the development of predictive models for estimation of cutting forces in face milling operation using self propelled rotary face milling cutter
- Chapter-VIII – discusses the conclusions and scope for future work
- Chapter IX – References

1.10 Summary

Introduction and importance of machining is presented in this chapter. Introduction on Nickel based super alloys, their properties and machinability problems were emphasized. Introduction on self propelled rotary tools and their types were explained. DOE and MQL concepts were introduced and planned to conduct tests on Nickel based super alloy particularly Inconel 625 which is difficult to machine materials. Introduction of the soft computing models like MGGP and NSGA – II are presented in this chapter.

The objectives and necessities of the present research and expected outcome and organization of the thesis of this work are also presented.

CHAPTER 2

REVIEW OF LITERATURE

In this chapter, the basic principle of operation of rotary tools and introduction to rotary milling has been presented. Also, the salient features of some of the earlier works related to cutting forces, cutting temperature, surface finish, chip formation, etc. in rotary cutting process and applications and advantages of soft computing techniques have been reported.

2.1 Rotary cutting Principle

The principle of rotary machining differs from traditional machining processes because of its distinct kinematics property. In rotary machining the significant conditions in rotary machining are chip flow angle, cutting edge inclination angle, chip deformation, tool wear, and cutting speed. The inclination angle (*i*) is the major role of a rotary cutting performance during the operation. According to [**Shaw *et al.* 1952]**, this cutting angle may be high accurately

described as the angle between the tool reference plane as well as the tangent of the cutting edge at the tool.

The cutting tool has a major panorama during the performance of operation is the cutting insert, which is rotate separate from cutter. Thus, third movements, i.e. tool rotational speed occurs while the machining operation. The consequences of this peculiar involvement the chip formation process of the mechanics and the kinematics, Consequently, the tool frame mechanism is studied, where the cutting edge is arrogated to be a straight line since radius of the tool is bigger as compared to another geometric parametric quantity (Fig 2.1). Here V_C, V_r and V_w are absolute chip velocity, rotary insert velocity and work piece velocity vectors respectively.

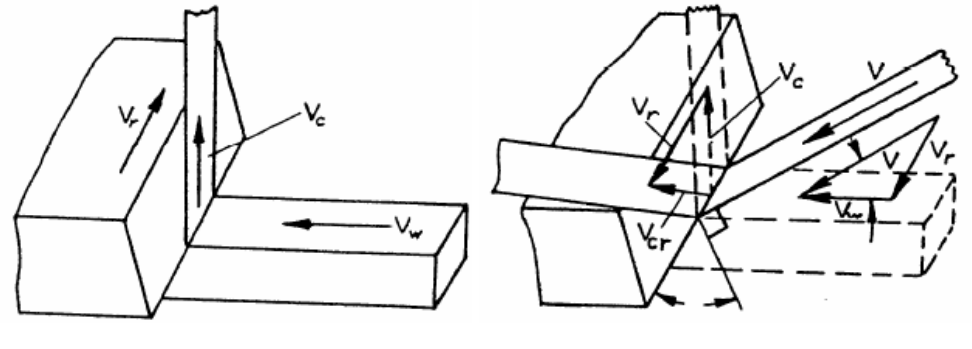

(a) (b)

Fig.2.1. Rotary cutting process as observed from a fixed point

(a) In space and (b) on tool **[Armarego *et al.* 1994a].**

Radial rake angle in conventional face-milling can also be considered as inclination angle in rotary face-milling. The insert rotation in rotary cutting which is the major differentiating factor from conventional cutting process is achieved through inclination angle of the insert. The schematic of the insert rotation is shown in Fig.2.2. Since the actual angle of obliquity (inclination angle) varies along the cutting edge, the nominal inclination angle is taken as the angle of obliquity i_F of the cutting edge which is equivalent to ε as shown in Fig.2.2. In practice, due to the round cutting insert the unwarranted tool wear can be decreased because of its own rotational axis as well as spend a fresh-cut edge happening on the cutting area of tool. Due to this finamina the self-cooling take place at the cutting surface which decreases the heat effect and enhance the tool life.

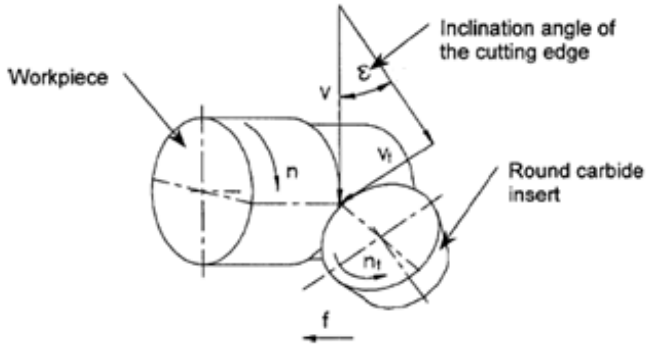

Fig.2.2. Principle of rotary cutting **[Chen *et al.* 1992b]**

2.2 Rotary milling process

There are two types of milling called up milling or Conventional milling and Down milling or Climb milling (Fig. 2.3). Compared to traditional milling process climb milling is highly proposed to avoid rubbing action of insert while entering to the part. This rubbing action will highly promote heat and friction, results in change of tool life of cartridge. But in case of rotary milling operation this will be minimized due to continuous change of cutting edge during the cutting operation.

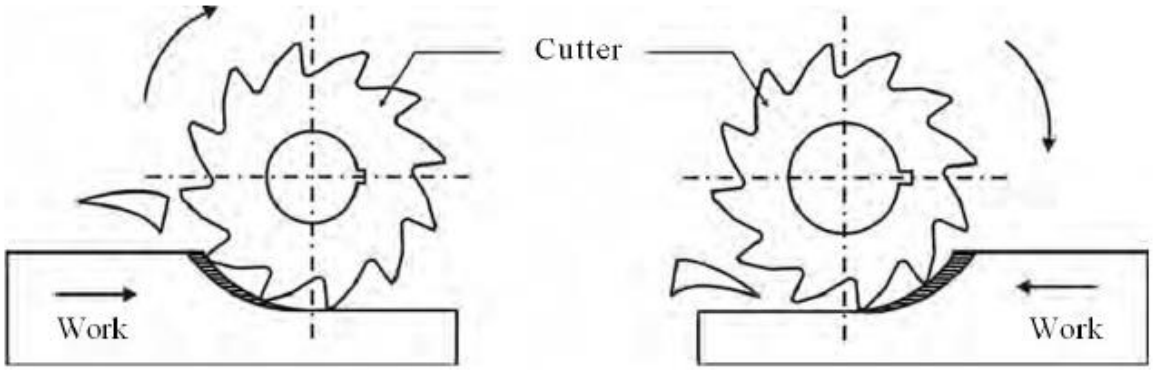

Insert impacts part. Rubbing on entry and exits at thickest chip thickness

Insert impacts at the thickest point and exits at thin point

(a) Conventional milling (b) Climb milling

Fig.2.3. Types of milling process

The concept of rotary tools is not a new one and it has been used in the year 1865 by James Napier for turning operation. The cutting action of rotary tools has been a focus of interest to many researchers. In 1930's, the earliest papers on rotary cutting appeared.

It is envisaged that the cutting action of rotary tools in a plain surface generation can be modeled by incorporating proper changes in the models relating to their stationary insert cutting tools. The cutting action of rotary tool during face milling operation is shown in Fig.2.4.

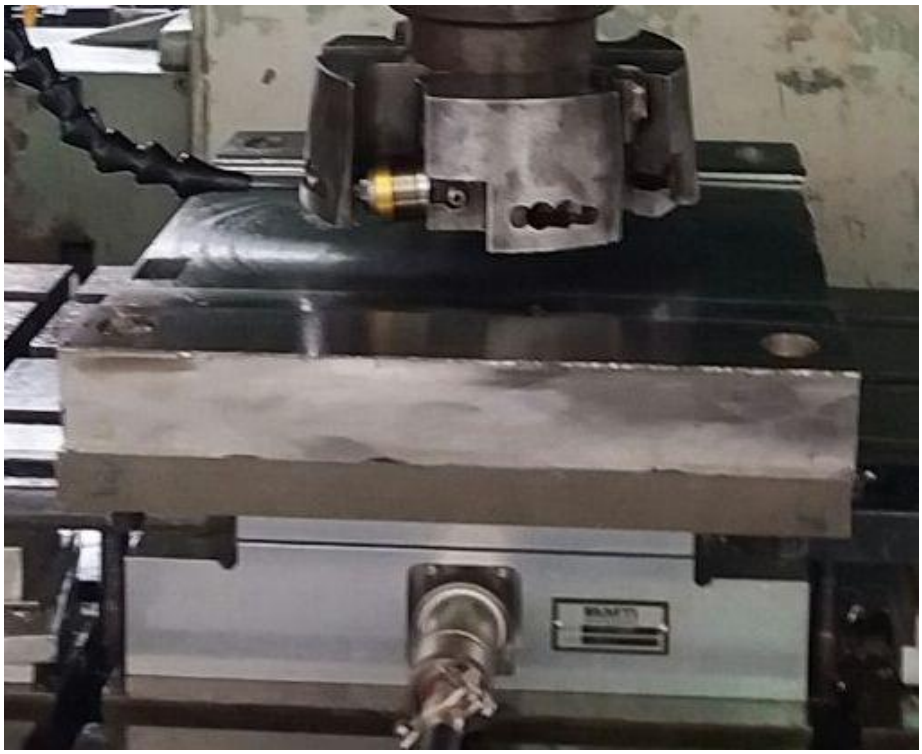

Fig.2.4. Diagram showing rotary milling cuter and work piece interaction

In late 1960s and 1970s the experiments were conducted using rotary tools.In **1956, M.C. Shaw** along with his team developed a driven rotary tool, performed detailed investigations on kinematics of rotary cutting tool. Between 1960's and 1970's, Type-2 rotary tool had been developed in Soviet Union. In **1968, N.R. Iyer and F. Koenigsberger** performed early experiments with self-propelled rotary cutting tools. In **1981, Venuvinod** studied the mechanics of driven rotary tool. In the 1990s extensively investigated the cutting mechanics of rotary tools. In **1990, Gi Heung Choi and David Dornfeld** proposed the analytical predictions of rotary cutting processes. In **1991, E.J.A. Armarego, V. Karri, A.J.R Smith** developed cutting models for simulating orthogonal and oblique rotary cutting processes.

In **1993, E.J.A. Armarego**, **V. Karri, A.J.R Smith** developed computer aided predictive models for rotary tool cutting processes. **In 1994, E.J.A. Armarego**, **V. Karri, A.J.R Smith** conducted theoretical and experimental investigation of driven and self-propelled rotary tool

cutting processes. In **1998, Z. M. Wang, E. O. Ezugwu and A. Gupta** used self-propelled rotary tool for machining aerospace materials. In **2002, Shuting Lei, Wenjie Liu** used driven rotary tool for high-speed machining of titanium alloy. In **2003, Uday A. Dabade** and S. S. Joshi analyzed chip cross-sectional area and surface roughness generated by self-propelled rotary tool. In **2006, H.A. Kishawy** developed a cutting force model for self-propelled rotary tools.

The earlier works related to various aspects in rotary cutting process such as tool life, cutting forces, surface integrity obtained, chip formation, and soft computing techniques pertaining to the rotary cutting process are discussed in next sections.

2.2.1 Cutting Forces

Granin *et al.* (1965) using a set-up with self-propelled rotary cutting tools studied the surface finish obtained in rotary cutting and developed a theoretical surface finish equation. He proved that rotary tools are capable of generating very fine surfaces compared to the finish obtained by a conventional stationary tool at the same feed rate.

Wear and surface finish in face milling with self-propelled rotary tools have been treated by **Venkatesh *et al.* (1972)**. Cutting speeds as high as 200 m/min for HSS and above 600 m/min for carbide rotary inserts were possible when machining steel. The high degree of surface finish obtained with rotary inserts (Ra value of 1.6-1.7 μm compared to 2.5 μm of fixed insert) could eliminate surface grinding to some extent. The author also showed that the built-up edge (BUE) formation in the case of rotary tools was not pronounced and wear rate was low. The author concluded from observing the color of the chips produced that the machining temperatures using rotary cutting tool are much lower than the stationary cutting tools.

Shaw *et al.* (1952) estimated that of 10^0 inclination angle of a rotary tool is capable of reducing the total power consumption to make a given cut by about 30% and at the same time to operate with a temperature of about 200 ^{0}C lower than that for the equivalent stationary tool. He found that the friction ratio was smallest possible when the angle of inclination was about 30^0. The shear energy per unit volume decreased while the frictional energy per unit volume increased with effective rake angle$\propto_e$ so that the total specific cutting energy exhibited a minimum when the inclination angle was about 40^0 for the conditions tested.

Zemlyanskii *et al.* (1966) used HSS self-propelled rotary tools with huge range of cutting conditions to machine Cu, Zn, steel, brass, Ni-Cr alloys, Ti and cast iron. They showed that when turning 0.45% C steel and an alloy steel, the tangential cutting force decreased by 42%, back force increased by 49%, feed force remain unchanged. They also showed that the cutting speed had a significant effect on the forces, the extent of which depended on the work material used. Further, with the rise in angle from 5 to 20 degrees, a slight increase in forces was noted. Moreover, an increase of 67% and 46% in cutting forces was noted when the depth of cut and feed respectively were doubled. The results showed no significant effect in the cutting forces in the presence of cutting fluids but showed an increase in back and main cutting forces by 25%-30% when the diameter of the tool was increased by 2.3 times. In studying the nature of chip deformation it was inferred that the maximum deformation of the chip material was not only along the material near the rake surface, as in conventional cutting, but also along the surface of separation between the chip and the work material.

Aronovich *et al.* (1991) considers the sliding motion of the cutting edge as a friction coefficient. The results indicate that the friction coefficient decreases as the inclination angle increases. Furthermore, the dependence correlates quite well with the oxide films thickness and its effect on shear strength.

Aronovich *et al.* (1991) considers the sliding motion of the cutting edge as a friction coefficient. The results indicate that the friction coefficient decreases as the inclination angle increases. Furthermore, the dependence correlates quite well with the oxide films thickness and its effect on shear strength.

According to **Chen *et al.* (1992)** the main cutting force is found to be 10-15% lower; the axial force about the same and the radial force 30-40% lower than for a fixed circular tool when machining SiC/MMC composite.

Armarego *et al.* (1993, 1994a, and 1994b) reported a wide range of analysis on the mechanics of driven and self-propelled rotary cutting tool processes. Force components, shear stress, friction angles, chip flow angles and chip length ratios are calculated and experimentally verified. The mathematics behind equations is complex and computer aided computation is needed to solve

them. Still the equations include unknown variables with unclear degree of dependency. Equations are same for both driven rotary tool (DRT) and self-propelled rotary tool (SPRT).

Armarego *et al.* (1997) presented a predictive cutting model for forces and power in rotary tool. The model is restricted to self-propelled rotary tools and turning operations. Hundreds of tests were carried out on both coated and TiN uncoated cemented carbide tool. This model is depending on the approach of unified cutting mechanics, and this model shows the operations can be indicated by no. of equivalent 'classical' oblique cutting elements of positive and negative inclination angles about similar 'classical' orthogonal cutting element. This element governs the speed of the rotary tool and is located at the point on the active cutting degree where the torque on the rotary tool is zero for frictionless tool spindle axis.

Ezugwu *et al.* (2002) evaluated wear of round uncoated carbide of self-propelled rotary tool (SPRT) inserts in the finish turning of IMI 318. It was observed that Self-propelled rotary tool (SPRT), round inserts shows higher wear resistance to round and rhomboid shaped carbides as well as to the rhomboid shaped PVD TiN-coated carbide inserts used for traditional (conventional) turning of titanium alloy IMI 318. The performance of Self-propelled rotary tool (SPRT) is very high at grater inclination angles, because of the reduction of the temperature achieved by continuous changing of cutting edge and relative cutting speed is lower while machining. When machining IMI318, the main cutting force and radial force were 15-20% and 25-35% lower than those obtained under traditional machining with round inserts. The main cutting force decreased with the inclination angle due to increased rotary speed and higher effective rake angle, while the feed force increased.

Ramesh kumar *et al.* (2002) compared both conventional turning and rotary turning processes in respect to tool life, surface roughness and material removal rate and concluded that the results obtained in rotary cutting are better than that of conventional machining.

Kishawy *et al.* (2004) developed a finite-volume heat transfer model and used to study the heat transfer property of rotary tools. The investigation has included that increasing the tool cutting velocity ratio reduces the typical tool temperature to a lower value. Further, an increase of the velocity ratio increases the typical temperature of the tool. However, the model shows that a lesser temperature of the tool is occurred at a velocity ratio much higher than that utilized in

practice for self-propelled rotary tools. This suggests that the longer tool life is due to continuous cutting edge but not self-cooling feature of SPRT.

Baro *et al.* (2005) proposed a cutting force model for a self-propelled face-milling with round inserts and experiments were conducted to validate the proposed model. The proposed model studied that the difference in the cutting mechanics of self-propelling inserts and conventional milling tools. Aluminum alloy (Al 1100) used as work piece material to conduct the experiments on a specifically designed and fabricated self-propelled round insert face-milling cutter with tungsten-carbide round inserts of 20 mm dia. It was observed that the proposed model captures the trend in the corresponding experimental values more accurately. The average prediction errors are obtained 10%, 12% and 17% respectively in the magnitudes of F_X, F_Y and F_Z.

Li *et al.* (2006) developed a force model for self-propelled rotary tool operation. They validated the model by performing experiments at various conditions and the estimated cutting forces were within the limit of deviation. This model was used to estimate the coefficient of friction at cutting zone for a typical self-propelled rotary tool. It was observed the coefficient of friction is lower when the speed and feed rate increase. On the rake face the normal force was found to be very sensitive to the changes in feed.

Patel *et al.* (2006), the application of rotary tools investigated in face-milling operation. The work involved analysis of chip characteristics and cutting forces, and the development of mathematical as well as conceptual models to estimate the cutting forces. The author stated that all the cutting forces are reduced for an inclination angle up to 45^o and after the cutting forces are increased. The initial reduction of cutting force up to 45^o, because of the inclination increases, then the effective rake angle increases and unnecessary deformation of material will be takes place when the angle of inclination beyond $45^{o.}$ It results in reverse of flank and rake surfaces. Due to the thermal softening of the work material during the cutting speed increment resulting feed and cutting forces decreases and also increment in angle of shear plane, decrement in co efficient of friction. Similarly all the forces are increases with the depth of cut due to undeformed chip area increment.

2.2.2 Cutting Temperature

The machine tool efficiency is major problem with the cutting temperature dissipation at the cutting zone and mainly on the cutting tool aspects. More number of studies was investigated on the issue of temperature dissipation from the both experimental and mathematical aspects with various degrees of achievement yet there is no particular experimental technique that can be used to confirm the analytical results **(M. Bacci da Silva *et al.*)**.Finding of the maximum temperature and its distribution along the rake face of the cutting tool has a certain importance because of its control influence on tool life, as well as, the quality of the machined part **(N.A. Abukhshim*et al.*)**.

T.I. El-Wardany*et al.* (1996) discussed an experimental and analytical investigation into the different factors which influence the distribution of temperature on AI203-TiC ceramic tool rake face while machining of difficult-to-cut materials, like case hardened AISI 1552 steel (60-65 HRC) and nickel-based super alloys. The distribution of temperature was estimated by using the FEA. The author reported that the experimental methods developed wereused to measure the temperature of the cutting edge without major difficulty, there is a little temperature reduction tool occurs, and the heat induced from the cutting process is concentrated in the vicinity of the tool tip, while turning Inconel 718 with ceramic tools, it is found that an optimum speed of 510 m/min for minimum cutting edge temperature was estimated. Also, an optimum feed of 1.25 mm/rev for minimum cutting temperature was found. The cutting temperature raised with increase of depth of cut and the temperature is reduced when the nose radius is increased.

N.A. Abukhshim*et al.* (2006) has emphasized more on the comparability of test results and the importance of temperature measurement method related to high speed cutting. The author reported that the prediction of cutting temperatures is a major challenge in metal cutting because of the numerous practical difficulties involved in the process. The author stated that the analytical models for metal cutting operations suffer mainly due to the simplified assumptions. Due to the complexity and the severity of the deformation in high-speed machining process, it is clear that purely analytical approaches are severely restrictive. One of the very important results of the author was that accuracy and reliability of HSM machining simulation models is significantly limited by uncertainties in material friction models. Therefore, more research is needed to buildup mathematical models to estimate the contact geometry and separating contours between the sticking and sliding zones.

2.2.3 Surface finish

Granin *et al.* (1965) using a set-up with self-propelled rotary cutting tools studied the surface finish obtained in rotary cutting and developed a theoretical surface finish equation. He proved that rotary tools are capable of generating very fine surfaces compared to the finish obtained by a conventional stationary tool at the same feed rate.

Wear and surface finish in face milling with self-propelled rotary tools have been treated by **Venkatesh *et al.* (1972)**. Cutting speeds as high as 200 m/min for HSS and above 600 m/min for carbide rotary inserts were possible when machining steel. The high degree of surface finish obtained with rotary inserts (Ra value of 1.6-1.7 µm compared to 2.5 µm of fixed insert) could eliminate surface grinding to some extent. The author also showed that the built-up edge (BUE) formation in the case of rotary tools was not pronounced and wear rate was low. The author concluded from observing the color of the chips produced that the machining temperatures using rotary cutting tool are much lower than the stationary cutting tools.

Venuvinod *et al.* (1981) stated that triangular chips appear at higher values of inclination angle and chip flow angles in the range of 70^0-90^0. This chip form is associated with high cutting forces, severe sub-surface deformation, over cut and tearing. They may be avoided by the use of reverse feed, reverse rotation, low inclination angles and high rotary speeds in either direction. The machined surface is normally cleaner and finer with reverse feed and at high rotary speeds.

Aronovich *et al.* (1991) stated that cutting speed and feed rate have significant effects on surface finish. However, these effects are quite different from those observed under conventional turning. Increase of feed only gave a slight deterioration in the surface finish generated. This may be associated with increased smearing action between the tool and the work piece at high feed rate. Higher inclination angle greater than 45° resulted in a lower Ra value due to reduction of the effective nose radius. The elimination of built-up edge at high cutting speed and increase of surface finish was disturbed by a poor stability of the rotary cutting system.

According to **Chen *et al.* (1992b)** micro structure analysis of the machined SiC/MMC‘s composite surface formed by either diamond tool or the rotary tool has much less whisker reorientation and material flow in the surface layer than with fixed carbide tools. The surface roughness increases moderately with the inclination angle until approximately 45° whereas beyond this point roughness increases steeply with the angle observed.

Dabade *et al.* (2003) explained the influence of various parameters on surface roughness in rotary milling with the model shown in Fig.2.5. The author stated that surface roughness in rotary milling operations is significantly influenced by insert inclination angle and feed rate. Statistically designed experiments based on Taguchi methods were conducted using the L27 orthogonal array to analyse surface roughness and area of chip cross sectional as response variables. An increase in inclination angle reduces the surface roughness (Ra) and increase in feed increases Ra.

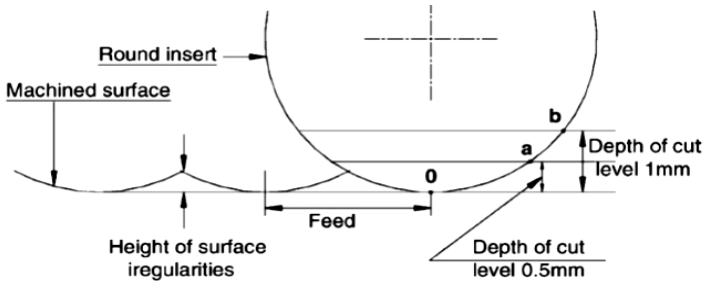

Fig.2.5. Model for surface roughness in rotary machining **[Dabade*et al.* (2003)]**

Franco *et al.*(2004) proposed a analytical model for estimate the surface finish in rotary face milling operations. The author stated that from the proposed model, for surface roughness that related to existed results of axial and radial run outs can be found easily, as well as the range of surface roughness due to the random values that can be adopted by these tool errors. Milling experiments were also made to validate the mathematical model and good agreement was found between the predicted and experiment results. According to the results, for decreased values of feed, the arithmetic average roughness (R_a) related to the tool errors random values is very similar to the surface roughness that would be given by one tooth. But, as feed increases, Ra tends to the ideal situation in which axial and radial run outs are equivalent to zero.

Kishawy *et al.* (2004) more no. of experiments were conducted to estimate the self-propelled rotary tool performance, during machining of Waspaloy and titanium alloys. The author states that a different surface pattern was achieved by rotary inserts with the relative movement of the rotary tool and work piece. Extensive tool life was obtained while machining waspaloy and titanium alloys, and surface roughness is obtained less than 0.5 µm.

2.2.4 Minimum Quantity Lubrication

In metal industries, the usage of cutting fluid plays a major role in terms of both environmental pollution and health of the employee. But the usage of cutting fluid generally obtained economy of tools and it becomes easier to get close tolerances and to retain work piece surface characteristics without spoil. Because of them in machining operations some alternate techniques are adopted to reduce or avoid the usage of cutting fluid. A few of these alternate methods are dry machining and minimum quantity of lubrication (MQL) **[N.R. Dhar*et al.* (2006)]**.

Y. Kamata*et al.* (2007) applied the minimum quantity lubrication technique in high speed finish turning of nickel based alloy, Inconel 718. Three different types of coated carbide tools are used by the author. The author selected three different coatings as three layers coating of CVD with TiCN/Al_2O_3/TiN (Coating A), a PVD super lattice coating of TiN/ AlN (Coating B) and a PVD monolayer coating of TiAlN (Coating C). In MQL system the performances of these tools were evaluated in terms of surface finish and tool life, with comparing of dry and wet cutting. Cutting speeds were set at relatively higher values of 1.5 and 1.0 m/s. The author obtained best performance at the cutting speed of 1.0 m/s, with Coating A in MQL, the second best performance is obtained by Coating B in MQL cutting. The longest tool life was attained by Coating A in wet cutting, but the surface finish was the second worst; It was observed that there is the optimal air pressure in finish-turning of Inconel 718 with MQL unlike MQL grooving of carbon steel. It was also observed in an experiment using argon as a carrier gas of oil mist instead of the air that the carrier gas of MQL plays an important role for cooling the cutting point. the tool life is drastically reduced at the cutting speed of 1.5 m/s. By compare the surface finish with Coating B was enormous in MQL cutting. The increase in the quantity of lubricant improved the tool life of Coating A in MQL cutting to the level in wet cutting, but the surface finish in MQL cutting was not improved.

B. Tasdelen et al. (2008) studied the experimental readings about on minimum quantity lubrication (MQL) and air-cooling at drilling with various oil sums, dry compressed air and emulsion. The author examined the outcomes as far as wear, chip contact, powers/torques and surface roughness. In view of the outcomes got in the experiments of drilling of gear wheel steel with indexable supplements it can be presumed that the most noteworthy wear both for middle and outside inserts was observed utilizing emulsion, followed via air and MQL helped

machining; additionally the most noteworthy cooling capacity of emulsion is presumably the reason behind the unreasonable apparatus wear situated amidst the contact zone; the zone where the chip breaks on the rake confront was comparable for air and MQL-5 ml/h (the least oil amount supply). This zone changes with more oil supply demonstrating the oil impact of oil beads and changing the chip breakage component on the insert; Higher surface unpleasantness for air assisted drilling is caused by the material ill tempers on the slopes of feed denotes; the power and torque estimations did not demonstrate a high distinction but rather yet most noteworthy power was observed for air and the least for emulsion; A quicker "Run-in" time of the new insert/bore was observed all the more clearly for emulsion and air assisted drilling showing higher friction on the tool chip contact zone.

M.M.A. Khan et al. (2009) considered the impacts of minimum quantity lubrication on turning AISI 9310 alloy steel utilizing vegetable oil-based cutting liquid. The minimum quantity lubrication was given a spray of air and vegetable oil. Based on the obtained results from the experimentation, the author announced that MQL gave appreciable amount of enhancements expectedly, however in fluctuating degree, in regard of chip development modes, tool wear and surface roughness all through the scope of cutting speed and feed rate attempted primarily because of diminishment in the normal chip– device interface temperature. The important commitment of MQL jet in machining the low alloy steel by the carbide insert embraced has been the diminishment in flank wear, which would empower either astounding change in tool life or improve in productivity (MRR) permitting higher cutting speed and feed. Surface roughness also enhanced for the most part because of decrease of wear and harm at the tool tip by the use of MQL.

T. Thepsonthi et al. (2009) expressed that applying cutting liquid in a metal-cutting procedure can diminish the rate of tool wear and enhance surface finish. The author detailed that the execution of pulsed jet application was better than that of dry cutting and flood application as far as surface roughness and tool wear and was observed to be exceptionally reasonable for fast end milling process since the performance at high cutting speed was greatly improved than the execution of dry cutting and flood application, particularly as far as tool wear. Likewise, flood application has undesirable affect on tool wear but it enhances surface finish. The astounding performance over flood application and dry cutting and the extreme decrease of cutting fluid utilization prompt the conclusion that Minimal-cutting liquid application in pulsed-jet form is

possible to be utilized as a part of high-speed milling of hardened steel. It is also powerful as an option of flood application and dry cutting.

Bruce L. Tai (2011), The MQL applied in machining process uses optimum amount of lubrication which is an effort to replace conventional flood coolant system. In this study, the author compared nine different commercial MQL fluids and a conventional metal working fluid (MWF) to find the relation of determined properties and MQL machining performance. The author reported that poorer heat removal properties have been observed for the MQL lubricants compared to water based (MWF) fluids, but improved wettability and lubricity results have been observed for MQL. Among the MQL lubricants, machining results showed that low fluid viscosity, high mist concentration, large mist droplet diameter and high wettability were best correlated with good machinability. The author also stated that though it is tough to correlate based on these experimental results, the optimal machining under these mild machining conditions was observed with the low viscosity fluids, which corresponded to high mist concentration, large droplet size and good wettability.

Lukasz M. Barczak (2012) studied the application of the minimum quantity lubrication (MQL) method in abrasive machining compared to conventional and dry grinding. The grinding has been performed on the common steels EN8, M2 and EN31. The performance indicators considered are grinding power, specific forces (tangential and normal), grinding temperature, and workpiece surface roughness. The author reported that the applicable regime for MQL in grinding has been found using this study.

Murat Sarıkaya, Abdulkadir Gullu (2014) studied that the optimization of cutting parameters with multi response outputs using design of experiments in turning. The tests were planned for experimental design depending on taguchi L9 orthogonal array. For experimentation, the difficult to cut material cobalt based super alloy Hynes 25 taken as the wok piece material and the process outcomes such as flank wear, notch wear and surface roughness was measured. The cutting fluid, fluid flow rate, and cutting speed were optimized simultaneously by taguchi based gray relational analysis. the author found that the multi response optimization results, which were obtained from the largest signal to noise ratio of the grey relational grade (GRG), the optimum combination was vegetable base cutting fluid,180 ml/h fluid flow rate and 30 m/min cutting speed to simultaneously minimize the tool wear patterns and surface roughness. In addition, it was found

out that the percentage improvement in GRG with the multiple responses is 39.4%. It was clearly shown that the performance indicators are significantly improved using this approach.

2.2.5 Response Surface Modeling

I.A. Choudhury*et al* (1999) developed response models for tool life, surface roughness and cutting force for turning Inconel 718 using factorial design of experimentation and RSM. Based on the observations the author reported that the influence of feed rate on tool life was higher than the effect of cutting speed in case of coated tools; also the effect of depth of cut on the tool life is greater in the case of uncoated carbide than in the coated carbide; the surface finish obtained by the uncoated and coated tools is mostly affected by the change in feed. The surface finish increases as the depth of cut increases machining with coated carbide tools while surface finish reduces with uncoated tools. The cutting force depends on speed, feed and depth of cut. Cutting velocity has negative impact on cutting force while feed and depth of cut has negative.

A.M.K. Hafiz *et al* (2007) developed an effective method to predict surface roughness for high-speed end milling of AISI H13 tool steel using PCBN inserts. The author used RSM to develop quadratic mathematical model in terms of cutting speed, axial depth of cut and feed. From the model, the author concluded that the feed plays the most leading role on surface finish followed by the cutting speed in high-speed end milling. The influence of axial depth of cut is negligible on surface finish while machining of AISI H13 tool steel. The author also stated that interaction effects between cutting speed and axial depth of cut also have a critical influence on the surface finish.

Ravirajshetty*et al.* (2008) used the Taguchi and RSM methods to minimize the surface roughness in turning of discontinuous reinforced aluminum composites (DRACs) under pressurized steam jet approach. The experiments were planned accordingly with Taguchi and quadratic model was developed using RSM to minimize the surface roughness. The major parameters found to get the minimum surface roughness were steam pressure, feed and cutting speed. Steam pressure is the dominant parameter on the surface roughness.

M. Aruna*et al.* (2010) developed a mathematical surface model using RSM for machining of Inconel 718 with cermet tools. Factorial design and response surface analysis were used to study

and optimize the conditions for machining Inconel 718. The author reported that the most influencing factor on the surface finish is feed rate.

L.B. Abhang*et al.* (2011) developed a response surface model for predicting the surface roughness in machining of EN-31 steel using RSM with factorial design of experiments. A first-order and quadratic mathematical models were developed. The most significant factors influencing the cutting force and surface finish were cutting velocity, feed rate, depth of cut, tool nose radius and concentration of lubricants. The adequacy and residual analysis are performed to test the validity of the model. It is observed that the predicted and measured values are close to each other.

BrahimFnides*et al.* (2012) conducted an experimental study to develop mathematical models for cutting forces and surface roughness in hard turning of X38CrMoV5-1 hot work tool steel hardened to 50 HRC using RSM. ANOVA is also adopted to check adequacy of the model. The most inflecting parameter on surface finish and cutting force is feed rate and cutting speed.

2.2.6 Tool Life

Reznikov *et al.* (1971) showed that any one point on the cutting edge of a self-propelled rotary tool remains in contact with the work piece only for a short period of time (0.2 - 0.3 seconds), consequently the temperatures in rotary cutting tools were shown to be 40% lower than those for conventional stationary cutting tools.

Venuvinod *et al.* (1983) stated that compared to conventional cutting, physical and chemical processes accompanying formation and destruction of surface films on rotary tool are of great importance, for instance, for working surface wear friction. The reason for this is the tangential movement of an insert causing decrease of adhesion between the work piece and tool material.

Chen *et al.* (1990) showed that tool wear is proportional to the distance machined on SiC/MMC composite and cutting speed hardly affected the tool wear. The author suggests that abrasive wear is the main cause of tool failure. For self-propelled rotary tools, the inclination angle controls the relative motion between rotary tool and the work piece (chip). Hence, wear characteristics will change accordingly. On SiC/MMC composite an increase of inclination angle from 15^0 to $30^0$and

further to 45^0 results in a tool life extension of 72% and 145%. This is about 40 times that of the fixed circular insert 100 times that of the square one.

Aronovich *et al.*(1991) studied the characteristics of rolling friction in rotary cutting and its effect on tool life. The author states that the life of rotating tools is approximately 80-100 times greater than the stationary tools.

According to **Chang X. (1995)** a self-propelled rotary cutting tool (SPRT) can be used in metal machining at higher cutting speeds with much longer tool life than conventional cutting tools because of the continuous rotation of its round tool insert.

According to **Wang *et al.* (1998)** SPRT incorporating CVD-coated inserts exhibit superior wear resistance when machining Inconel 718. The tool life increased four and three times as compared to round and rhomboid inserts respectively when machining Inconel 718. When machining IMI318 with self-propelled rotary cutting tool incorporating cemented carbide inserts, there is sixty times improvement in tool life.

Joshi *et al.* (1999) evaluated the wear of rotary carbide tools while machining Al/SiCp composites considering inclination angle, cutting speed, feed rate and SiCp volume process variables. Also a tool life model is proposed considering volume of reinforcement in the composite material apart from tool and process parameters. The author reported that: The chosen input variables were observed to be statistically in influencing the flank wear, the cutting speed being the most predominant influential of all.

Zang *et al.* (2003) studied the performance of rotary tools machining of hardened steel compared with conventional tools. The SPRT shows longer tool life and better resistance to tool wear compared with conventional tools at same cutting conditions.

Lei and Liu (2002) developed a driven rotary lathe tool for high speed machining of titanium-composite (Ti-6Al-4V). Cylindrical turning tests were led utilizing the driven rotary tool (DRT) and a stationary cutting instrument with a similar embed, for correlation in the rapid machining of Ti– 6Al– 4V. The outcomes demonstrated that the DRT can essentially expand apparatus life. Increment in tool life of in excess of 60 times was accomplished under specific conditions. The primary and push drive segments are substantially bigger than the feed constrain utilizing the

round insert in this investigation. Every one of the three power segments are not exceptionally delicate to the difference in cutting velocity for the scope of rates utilized as a part of this study when cutting with the rotary tool.

Kishawy *et al.* (2004b) conducted wide number of experiments to evaluate the performance of SPRT during machining of waspaloy and titanium alloy (Ti-6Al-4V) work pieces. It is observed that the insert diameter had minor influence on the tool wear but insert rotation has major influence tool wear (Fig.2.6). Flank wear was the major tool failure in rotating inserts whereas wear was the dominant mode of tool failure in fixed tools.

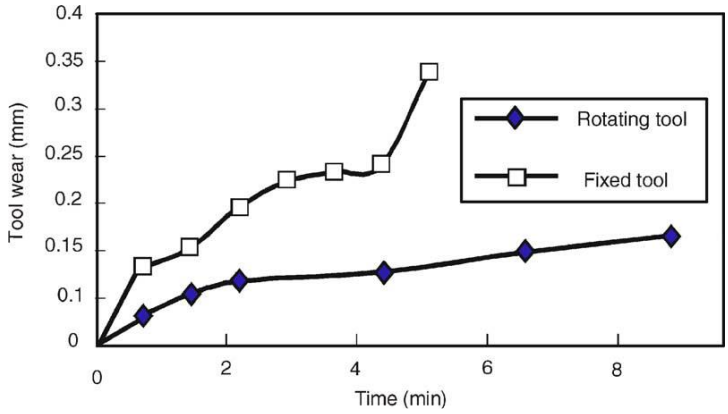

Fig.2.6. Progress of tool wears during machining titanium **[Kishawy*et al.* (2004b)]**.

2.2.7 Chip Formation

Radwan *et al.* (1977), analysed chip formation when machining with SPRT. The author proposed an analytical approach based on single shear plane model of deformation for geometry of the chip formation. According to the author, the chip formation with a self-propelled rotary tool corresponds to plane strain deformation and the single shear plane is adequate for computation of mechanics of cutting with this type of cutting tool.

According to **Boothroyd (1989)**, the chip cross-sectional area in rotary milling is analogous to that of chip cross-sectional area in surface grinding operation.

Dabade *et al.* (2003) stated that the chip cross-sectional area in rotary milling is significantly affected by feed rate, inclination angle, and depth of cut. An increase in inclination angle decreases the height and width of chip cross-section whereas enhancement in feed rate and depth of cut increases the height and width of chip cross-section.

According to **Kishawy *et al.* (2003)**, two sets of experiments were conducted in order to find the influence of tool rotation on the chip morphology. Saw toothed chip was found during machining with fixed tool whereas continuous chip observed with tool set to rotate freely.

Kishawy *et al*. (2006) generated a model to find chip flow angle while machining with SPRT. The validity of the model was examined with residual analysis. It is observed from the analysis that the cutting speed and feed have no significant influence on the absolute chip flow direction. From the observed data, the chip flow angles were limited to 10^o in the SPRT machining process.

Aronovich *et al.* (1991) tested steel 40 (0.4% C) and 12X18H9T (0.12% C, 18% Cr, 9% Ni and 1% Ti) and stated that the optimum inclination angle is 30^0 when machining with P9 HSS inserts. Tool life was increased 200-1000% compared to stationary tool. Tool wear mechanism is dominated by adhesion when the inclination angle is below 30^0 and after the optimum value abrasive wear takes over.

Chen *et al.*(1991) states that while machining Ti-6Al-4V, it was noted that at a lower cutting speed of 60 m/min there is hardly any difference between the rotary tool and the fixed circular tool. However, at a higher speed of 120 m/min, the mean wear rate of the rotary tool is found to be about 14% of the square one resulting in 7 times higher tool life. The rotary tool has hardly any crater wear but chipping and flank wear.

Chen *et al.*(1992) evaluated the performance of SPRT in machining SiC Whisker-Reinforced Aluminium composite, which is one of the difficult-to-cut Metal Matrix Composite (MMC). The author concluded that:

- Carbide rotary tool displays superior wear-resistance as compared to Poly-crystalline diamond tool. Carbide tool life has been tremendously extended by rotary cutting, about 53 times to that of fixed circular tool and 112 times to that of rectangular tool (Fig.2.7).The rotary cutting process capable of high-speed machining i.e., high cutting speeds and high feed rates. Ultimately the SPRT is found to be high performance cutting tool for machining this metal matrix composite (MMC).

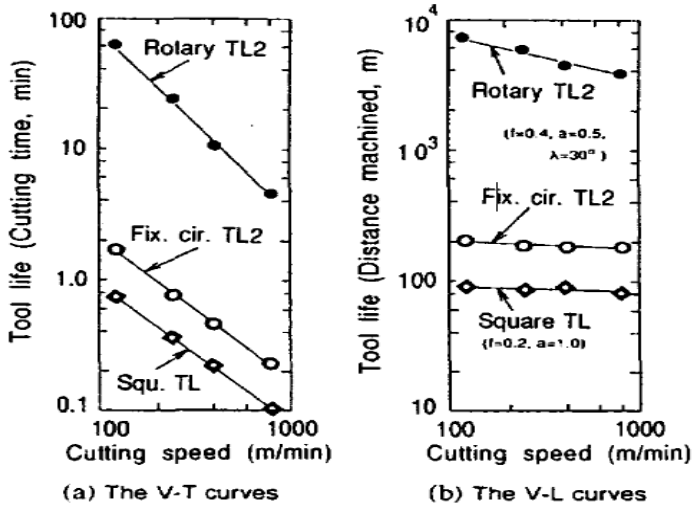

Fig.2.7. Tool life as a function of cutting speed **[Chen *et al.* (1992)]**

Ezugwu *et al.*(1997) explored the drawbacks during machining of titanium, tool wear and reasons for the failure of the tool. The author concluded that Titanium and its alloys are considered as hard to-machine materials because of the high cutting temperature and the high stress at as well as near the forefront while machining. The high cutting temperature is because of the heat produced while machining (catastrophic thermoplastic shear process), the thin chips, a thin secondary zone, a short chip-tool contact length and the poor thermal conductivity of the metal, while the high stresses are because of the little contact region and the quality of titanium even at higher temperature. Straight grade (WC/Co) cemented carbides tools are generally considered as the tool materials for the machining of titanium alloys as an uninterrupted operation. Along with cemented carbides tools, high speed steels and carbide tools are suitable for the interrupted machining. The development of new tool materials is still required. The high cutting stresses and temperatures near the cutting edge develops during machining of titanium alloys which is the main reason for the cutting tools suffer severe thermal and mechanical loads. Flank wear, crater wear, notch wear, chipping and catastrophic failure are the prominent failure modes when machining titanium alloys.

Ezugwu *et al.* (2002) evaluated the wear resistance of SPRT tipped with round uncoated carbide (WC-Co) inserts in the finish turning of titanium alloy IMI 318. The author reported that A SPRT inserts revealed excellent wear resistance compared to round and rhomboid-shaped carbides as well as to the rhomboid-shaped PVD TiN-coated carbide inserts used for traditional turning of titanium alloy IMI 318 on account of the distribution of the cutting energy along the entire tool

edge. Wear mechanism caused due to high temperature was reduced at a higher cutting speed of 129 m/min (beyond the capability of conventional tools) for the SPRT tipped inserts. The main failure mode in SPRT insets was chipping which causing from cyclically fluctuating thermal and mechanical shocks induced by the continuous shifting of the cutting edge during machining. The interaction effect of speed, feed and inclination angle were the major contribution on the average flank wear rate of SPRT inserts revealed from the fitted exponential wear model.

Ezugwu *et al.* (2007) in his work on improvements in machining of aerospace alloys using self-propelled rotary tools concluded that SPRT inserts have excellent wear resistance and amazing tool life compared to conventional turning during machining of difficult-to-cut nickel and titanium base super alloys (Fig.2.8). When properly applied, the rotary tool machining improves heat transfer during machining due to the reduction in relative cutting speed, the use of the entire cutting edge and the lower cutting temperature associated with the rotation of the insert (Fig.2.9).

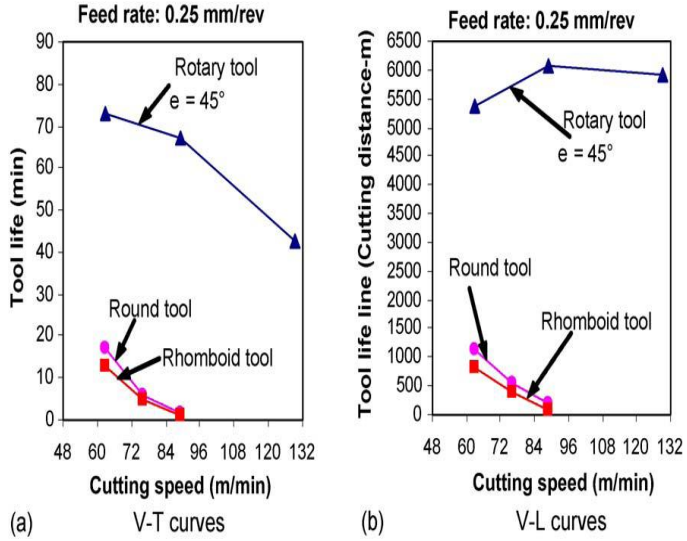

Fig.2.8. Tool life and tool life line as a function of cutting speed when machining IMI 318 with uncoated carbide tools. **[Ezugwu *et al.* (2007)]**

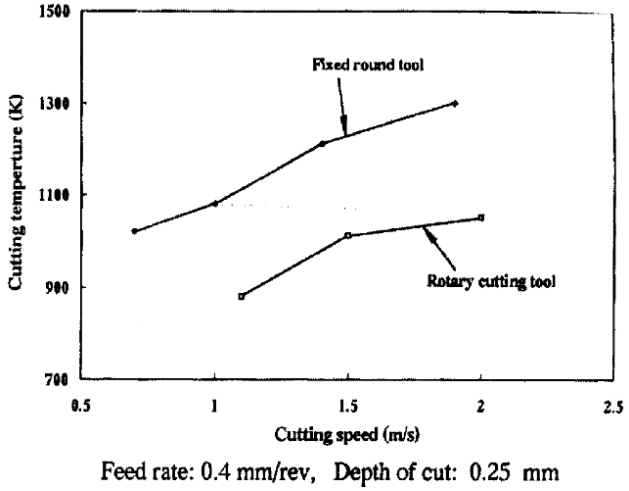

Fig.2.9. Cutting Temperatures with stationary and rotary round tool. **[Ezugwu*et al.* (2007)]**

The Cutting forces obtained with SPRT machining are very lesser compared to traditional (conventional) turning with circular inserts due to the decreased quantity of work done in chip development and lower friction on the rake face of the tool under rotary cutting. The lower cutting temperature generated with the rotary tool causes lower plastic deformation and work hardening of work piece material.

Sasahara *et al.* (2008) proposed a new technique of rotary cutting method related with a multi-tasking lathe. The tool rake face is located on the end face of the tool shank so as to make the resultant cutting force direction and tool axis align almost in parallel so that the machine can have better rigidity against cutting force. It was found that both smaller tool wear and higher efficiencies were achieved by the dry machining of Inconel 718.

A. Hosokawa *et al.* (2010) investigated the cutting prosperities of the actively driven rotary tool in turning from thermal aspects. The tests were conducted on austenitic stainless steel (AISI 304) and heat-resistant Ni-based alloy (Inconel 718) by Dry and MQL techniques. A new innovate fiber coupled two-color pyrometer is used to measure the cutting temperature. It was found that in case of dry turning, the tool temperature decreases with the increase of tool rotational speed up to approximately 250 m/min, but it increases again as the tool turning speed exceeds approximately 250 m/min. In case of MQL external turning with normal biodegradable oil, the tool temperature decreases around 45 ^{0}C within the appropriate tool rotational speed.

2.2.8 Modeling and Multi Objective Optimization

[Myong-Il Kim, 2016] has developed a mathematical model to predict the influence of the drill point angle on the cutting forces in drilling with the twist drills, which was used to optimize the angle to reduce drilling forces. The effectiveness of the proposed model was verified by comparison with published data. It was observed that the proposed model corresponded well with the experimental data and was useful for improving the performance of twist drill.

[Yu, J., H. Wang, and J. Zhang, 2009] Developed empirical models for the performance of Si_3N_4 porous ceramic prepared by gel casting process using an artificial neural network (ANN). The developed ANN model was used to obtain the influence of the composition on the performance of Si_3N_4 porous ceramics.

[Garg and Tai, 2013] compared the performance of MGGP with partial regression of the least squares and ANN in solving multi collinearity studies **[Garg, A. and K. Tai, 2013]**. It has been observed that the ability of MGGP is to remove unnecessary variables automatically. Garg et al also compared and found that the performance of classification driven GP (C-GP) model is similar to the ANN model. The performance of the SVR model is worse than the ANN and C-GP models. June Li et al. developed empirical models of the service life, the residual stress and the surface roughness by regression analysis and optimal grinding parameters to control NSGA-II using technical applications.

Metin Kök et al. proposed to an empirical model for the prediction of surface roughness recessing AWJ 7075 alloy Al-Al2O3 particles with the programming of gene expression (GEP). In the developed models, material properties such as the size and the weight fraction of the reinforcement and the depth of the cut particles were considered as variables in the model **[Li, J., et al, 2015].** Jeyapaul A. et al reported on the use of the genetic algorithm and method ANOVA Taguchi to optimize the gear milling process with several performance characteristics. They have shown that several response optimization problems effectively address genetic algorithms **[Kök, M., E. Kanca, and Ö. Eyercioğlu, 2011]**.SH Yang et al. tried two evolutionary algorithms, i.e., the differential development of the methodology and the permissive-II gene classification algorithm to determine the optimal set of parameters for multi criteria optimization problems, ie to minimize wear on the tool and the metal removal rate in the surface temperature and roughness constraints to maximize **[Jeyapaul, R., P. Shahabudeen, and K. Krishnaiah, 2006]**.

2.3 Summary

In this chapter, earlier works related to rotary machining process from available literature and the salient features of the works are briefly presented. Also, the basic principle of rotary machining and introduction to rotary milling process is discussed. It was found that majority of the literature was focused on rotary turning whereas rotary milling has received limited attention. Application of rotary milling operation on difficult-to-cut materials like titanium based super alloys, nickel based superalloys, etc, has found a little literature. Inclination angle is the key factor that governs the generation of cutting forces in rotary milling and in turn its application practically. Further studies on the effect of inclination angle on rotary milling process for achieving the desired cutting forces is also necessary. A theoretical model for estimating the cutting forces is available in the literature but the estimation of specific cutting pressure which is the key factor in the model is not fully analyzed. According to the literature study, usage of soft computing model for prediction can improve the accuracy of prediction irrespective of applied fields. The brief literature on soft computing models indicates that MGGP and NSGA - II models are better models when compared to other soft computing models.

In this work, rotary milling cutter with different inclination angles was developed and its performance in machining Nickel based superalloy Inconel 625 is evaluated. Full factorial experimentation is carried out for performance evaluation and finding the optimum combinations of process parameters for desired cutting forces. Also, a soft computing model using MGGP and NSGA - II for predicting the cutting forces in rotary machining operation is developed which is trained using a validated theoretical model.

CHAPTER 3

DESIGN AND DEVELOPMENT OF ROTARY FACE MILLING CUTTER WITH DIFFERENT INCLINATION ANGLES

3.1 INTRODUCTION

To study the rotary milling performance, Inclination angle is one of the major parameters. The inclination angle is equal to the radial rake angle in face milling insert geometry. In order to experiment the cutting forces developed during machining with different machining angles, in the design of the cutter, four inclination angles 20°, 30°, 40° and 50° are considered and the CAD model is developed as described below. Cutter body has been provided with slots to hold a round insert which can rotate around its own axis. Initially, milling cutter body model has been proposed to accommodate four inclination angles without considering provision to hold the rotary inserts as shown in Fig.3.1.

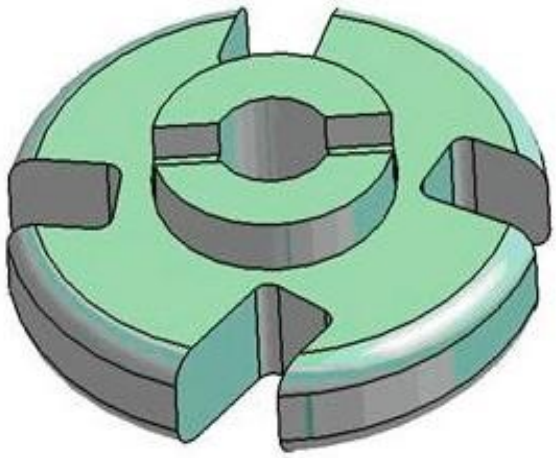

Fig.3.1. Conceptual model with different inclination angles

While designing the rotary tool holder are extra some factors are considered, errors created by the rotational cutting edge and chatter excited by large radial thrust force. A tool holder should acquire adaptable geometry because the geometry of a rotary tool, particularly the inclination angle extensively affects the performance of the tool.

The developed model has to hold the rotating cartridge assembly designed by Rotary Technologies Corporation, USA. The cutter model is designed to suit the cartridge assembly by providing the dove tail slot and v-groove. These dimensions are extracted from the commercial rotary milling cutter by inspecting it under flash microscope and coordinate measuring machine. Cutter body model concept has been designed by considering the importance of different inclination angles and keeping the radial distance of the cutting tip from the centre constant at a distance of 55 mm for all the inclination angles. Pockets are provided on the cutter to get some similarities and uniformness in slot dimensions for the clamps. Axial rake angle of 4.5° was provided on the cartridge. Internal bore diameter was fixed by considering the weight of the cutter and it is designed to suit to Ø40mm Morse taper shank adaptor for milling machine. The CAD model of the cutter developed is shown in Fig.3.2.

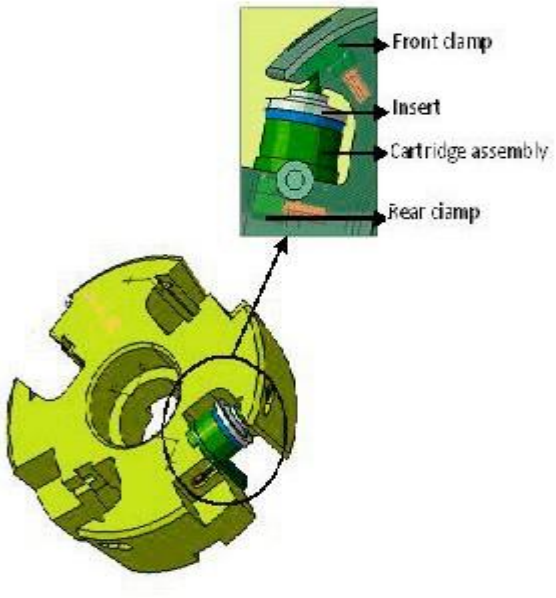

Fig.3.2. CAD model of rotary milling cutter assembly

3.2 Components of the Rotary milling cutter assembly

Rotary milling cutter body has to hold the cartridge assembly which requires front clamps and rear clamps having internal left hand threads. Studs with left hand and right hand M6 threads on respective sides are provided to make sure the clamps are tightly holding the cartridge by locking mechanism. Front clamp has been designed to push the cartridge towards the cutter body to overcome the inevitable play in dovetail slot and rear clamp will hold the cartridge tightly. Rotary Technologies Corporation designed the cartridge assembly with advanced bearing materials which assures negligible wear inside the bearing system.

1. Cutter body
2. Front clamp rear clamps
3. Studs (2 nos.)
4. Cartridge Assembly

The exploded view of the rotary milling Cutter assembly with all the components and the rotary cartridge is shown in Fig.3.3.

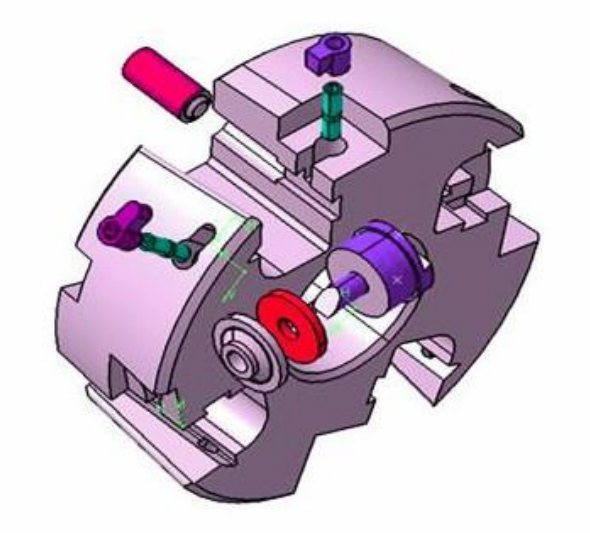

Fig.3.3. Exploded view of the rotary milling cutter assembly

3.3 Work material for the cutter components

The material for the cutter body and the clamps are selected as EN 36 and hardened to 37 HRC. This material is a best quality alloy steel and it combines shock resistance, high tensile strength, good ductility and resistance to wear at defined hardness. It is nickel chromium molybdenum steel with high strength and toughness and having maximum resistance to impact at the hardness around 36 HRC. Due to its extreme resistance to impact loads at 37 HRC, EN 36is selected as work material for the manufacturing of cutter body and the components.

EN 36 is suppliedin annealed condition and is readily machinable. The hardness of raw material is around 20 HRC. In order to achieve high hardness of around 37 HRC, the material is heat treated. Heat treatment cycle for EN 36consists of hardening followed by tempering to 37 HRC and it requires through hardening process to attain uniform hardness throughout the volume. The composition of the EN 36material shown in Table 3.1

Table 3.1. Composition of EN 36

C	Si	Mn	Ni	Cr	S	P
0.12-0.18%	0.10-0.35%	0.30-0.60%	3.00-3.75%	0.60-1.10%	0.05% max.	0.05% max.

The hardening process is used to produce good toughness and high strength when the entire component needs to be toughened. In this hardening, the metal is heated to form austenite,

and then quenched to transform the austenite to martensite, which has a much harder microstructure. Then the part is tempered to the defined temperature to attain the required hardness. Tempering between 250°C-375°C is not suggested as this can sincerely decrease the steels impact value.

3.4. Theoretical calculations of Cutting forces generated

The rotary face milling cutter is designed to have self-propelled rotary inserts. Cutting forces in rotary milling operation are separated into three components i.e. Radial force (F_R), Axial Force (F_A)and Tangential force (F_T),to facilitate rotational movement in the inserts, the inclination angle is kept non-zero. Part of the tangential force on the insert is used to rotate the insert. Inclination angle is the major parameter to study the rotary milling performance. The effect of inclination angle on cutting force is shown in Fig. 3.4.

Due to the influence of inclination angle, the equations to predict cutting forces can be formulated as **[Baro *et al.* (2005)]**:

$$FR* = FT\cos(i) + FR\sin(i) \quad (3.1)$$

$$FT* = FR\cos(i) - FT\sin(i) \quad (3.2)$$

$$FA* = FA \quad (3.3)$$

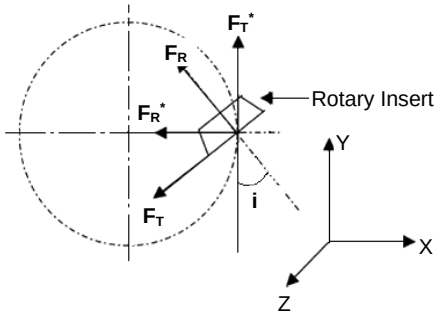

Fig.3.4. Effect of inclination angle on cutting forces in rotary face milling

Ratio of the cutting forces varies with the depth of cut. The ratio of cutting forces can be expressed as follows

$$FT*:FR*:FA* = 1:0.7:0.4 \quad (3.4)$$

i.e., Radial Force (F_R^*) = 0.7 (F_T^*) and

Axial Force (F_A^*) = 0.4 (F_T^*)

The tangential cutting force (F_T^*) can be expressed as the product of specific cutting pressure (K_T)and Chip cross sectional area (A_c)as follows.

$$FT *= KT * Ac \quad (3.5)$$

The chip cross sectional area can be calculated as below

$$A_c = \frac{\frac{1}{6}(f_t)\sin(\psi)\sqrt{h \times D_i}}{Cos\ i} \quad (3.6)$$

Where $\sin(\psi) = \frac{r_i - h}{r_i}$ (3.7)

Where f_t= feed/insert; h= Depth of cut; D_i= Diameter of Insert; r_i= Radius of Insert; i = Inclination Angle. Considering the cutting forces that arise during machining and based on the requirements to mount the inserts and adaptor to cutter, the cutter design is made.

3.5. Stress analysis on the cutter assembly

Rotary milling cutters are designed to machine difficult-to-cut materials and for intermittent cutting operations. Impact loads coming on to the cutter are significant**.** Theoretically basic rotary machining operation is studied for rotary milling cutters and forces are calculated using standard values of the specific cutting energy values of the different materials. Rotary milling cutter assembly model was developed using Solid works CAD package. The stress analysis was carried out using ANSYS package. Stress analysis was carried out in static condition of the cutter body and factor of safety of six to seven is provided. All the dimensions are fixed to minimize the weight of the cutter and it is 4.2 kg.

3.5.1 Specifications of milling cutter

The specifications of the rotary face milling cutter to be developed are shown in Table 3.2.

Table 3. 2. Specifications of rotary face milling cutter

1.	Outer diameter	150 mm
2.	Effective diameter	110 mm
3.	Bore diameter	Ø 40 mm
4.	Thickness	52 mm
5.	Insert diameter	Ø 27 mm
6.	Inclination angles	20°, 30°, 40° and 50°

3.5.2 ANSYS package

ANSYS is one of the most versatile and widely used commercial finite element programs. The Finite element process is generally divided in to three distinct phases:

1. PREPROCESSING i.e., building the model
2. SOLVING i.e., solving the model
3. POSTPROCESSING i.e., evaluating the results

Preprocessing:

In Pre-processor all the material properties of the cutter material are given as provided below.

a. Work material : EN 36
b. Young's modulus : 205 GPa
c. Poisson's ratio : 0.26
d. Tensile strength of the material : 1100 MPa
e. Yield stress : 735 MPa

The physical relationship of the components is defined and the components are glued according to the respective mating components. Tetrahedral element SOLID187 was chosen due to the complexity of the component. Element side length is taken according to the component such that total number of elements does not exceed 200,000. The meshed view of the cutter assembly is shown in Fig.3.5.Distortion energy theory was considered for component failure. The distortion energy per unit volume at a point is a function of single stress component called Von-Mises normal stress. For defining the boundary conditions, all the surfaces coming into direct contact with the milling shank i.e. all the surfaces connected to shank that take load from cutter, are fixed.

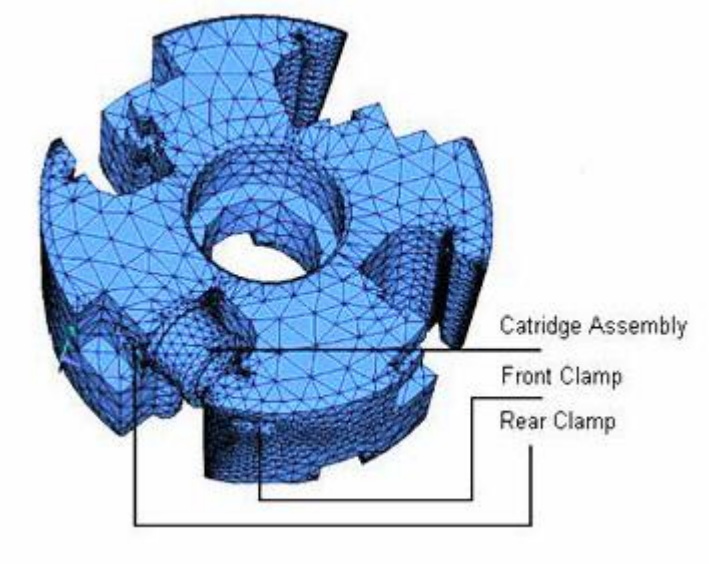

Fig.3.5. Meshed view of the rotary milling cutter assembly

For attaining the maximum load conditions for evaluating the stresses, the strategy followed is described below.

MAXIMUM LOAD CONDITIONS:

Initially a set of experiments have been conducted using the imported rotary face milling cutter developed by Rotary Technologies Corporation. The experiments are conducted based on minimum and maximum levels of cutting speed and feed, keeping depth of cut constant. The experimental table is shown in Table 3.3.

Table 3.3. Experiments conducted with Rotary Technologies Corporation rotary face milling cutter

Experiment No.	Speed (rpm)	Feed (mm/min)	Depth of cut (mm)	Force Fx (N)	Force Fy (N)	Force Fz (N)
1	40	40	0.6	2157	1561	1358
2	40	80	0.6	3946	2758	2355
3	100	40	0.6	1161	871	827
4	100	80	0.6	2039	1504	1363

The experiments are performed using the rotary cutter and vertical machining centre (VMC). The radius of the rotary insert considered is 13.5 mm. From the Table.3.3, it can be observed that the maximum cutting forces obtained for F_X, F_Y and F_Z are 3946 N, 2758 N and

2355 N respectively. The instantaneous cutting force at the start of the cut will be around 1.5 times the continuous cutting force. Also the rotary cutting process is an ambiguous cutting process; the cutter is designed for the maximum load conditions which are taken as 2.5 times the experimentally obtained cutting forces using the imported rotary face milling cutter. Hence, for the analysis, the load conditions at the tip of the insert for the analysis are considered as below:

Considering cutter rotation angle θ to be 90^0 for the maximum cutting condition, the load conditions are

$Fx = F_T^* = 3946$ N

$Fy = F_R^* = 2758$ N

$Fz = F_A^* = 2355$ N

where F_T is Force component perpendicular to insert, F_R is Force component tangential to insert and F_A is Force component perpendicular to F_T& F_R.

Post processing:

The von-Mises stresses developed for the above conditions are plotted using ANSYS package and shown in Figs.3.6-3.9.

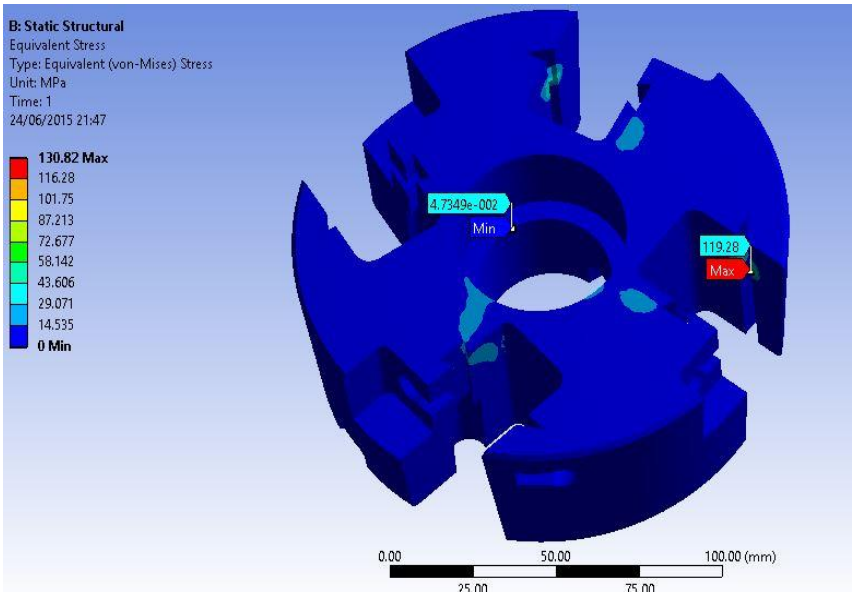

Fig. 3.6. Deformation developed on the cutter insert (Max: 27.6 µm)

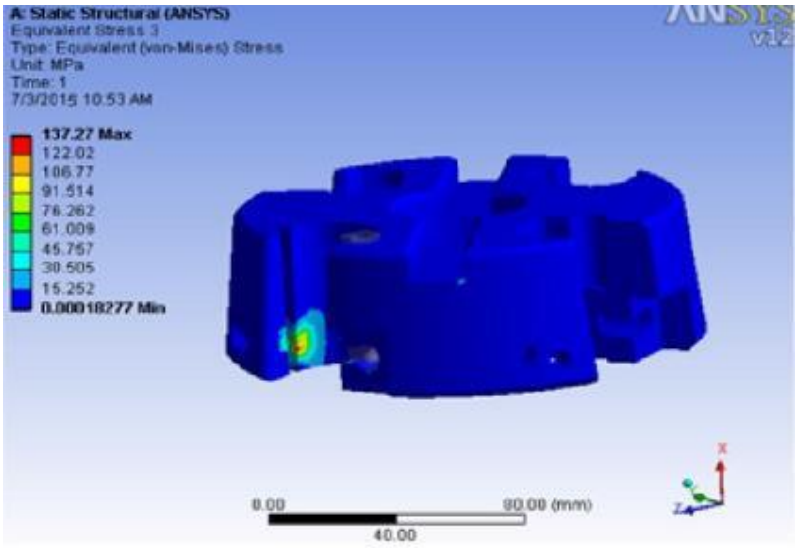

Fig. 3.7. Stress developed on the cutter (Max: 137 MPa)

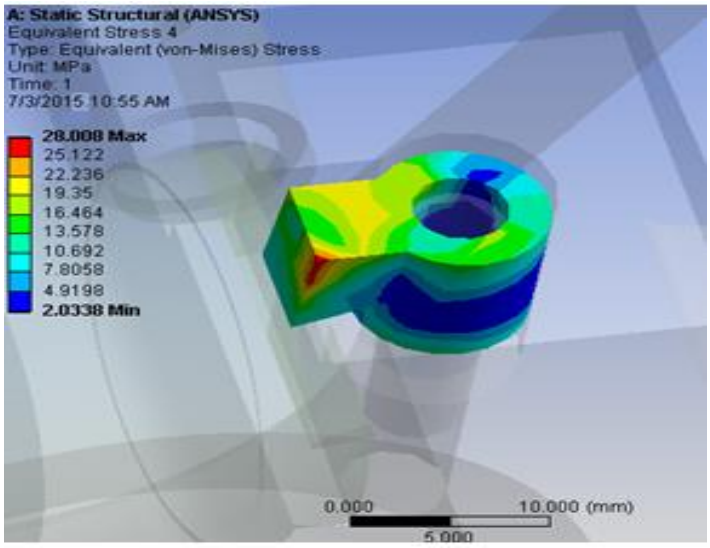

Fig. 3.8. Stress developed on the Rear clamp (Max: 28 MPa)

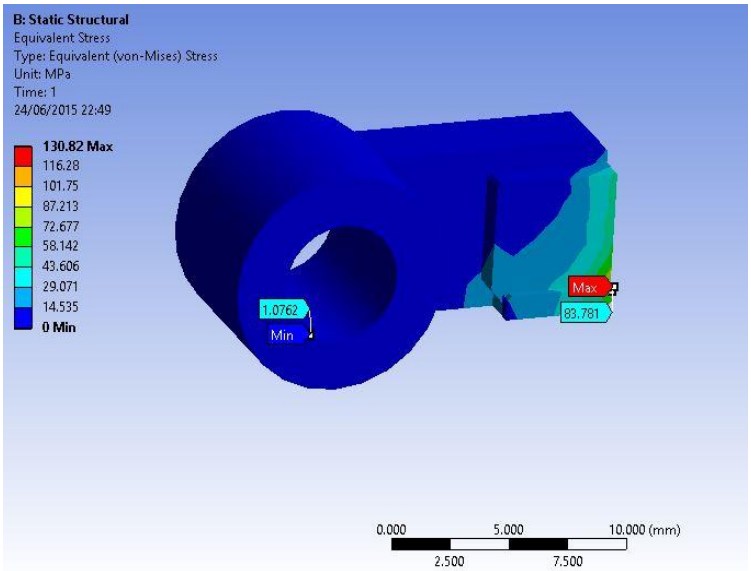

Fig. 3.9. Stress developed on the Front clamp (Max: 102 MPa)

The maximum stress developed on the cutter body with single rotary cartridge was very minimum and found to be around 137 MPa whereas the yield strength of the cutter material is 755 MPa. Hence, the design of the cutter is having a factor of safety of about 5.5 and the design is found to be safe. The stress calculations results were verified with the literature [56].

3.6. Manufacturing of rotary milling cutter

Rotary milling cutter is designed and modeled to hold the cartridge assembly at different inclination angles. Manufacturing drawings are extracted from the model by freezing the model at different stages and close tolerances are provided. Sequence of operations is prepared according to the different stages of manufacturing. Rotary milling cutter assembly comprises cutter body, cartridge assembly, rear clamp, front clamp and studs.

Generally, milling cutter is subjected to impact loads and cutter components should have enough resistance to impact loads. EN 36 is the work material and it is a high quality alloy steel supplied readily in machinable condition. It combines high tensile strength, shock resistance, good ductility and resistance to wear after proper heat treatment.

3.6.1 Machine tools used in developing the cutter

1. Center lathe
2. Surface grinding machine
3. Universal milling machine
4. Vertical machining center (VMC)
5. CNC milling machine
6. Wire electric discharge machine (WEDM)
7. Jig grinding machine
8. Conventional milling machine

3.6.2 Different stages of manufacturing

The manufacturing of the cutter body was carried out in five major stages as per the sequence mentioned below.

Stage-1 of manufacturing: Block Machining

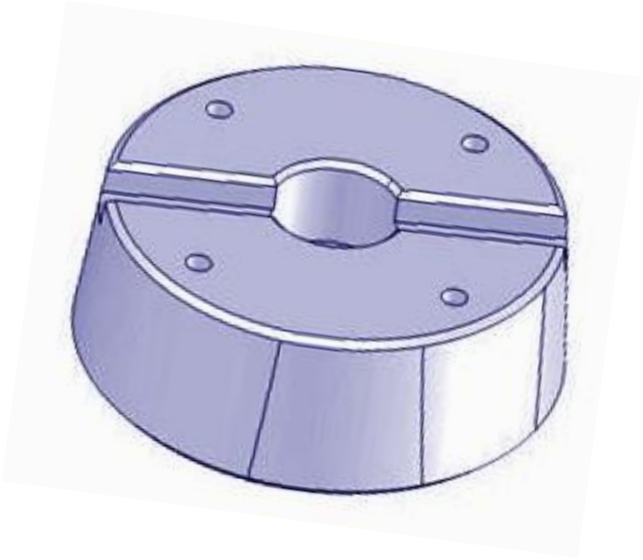

Fig.3.10. Stage-1 of manufacturing

Stage-2 of manufacturing: Milling of pockets, for clamps of cartridge body with different inclination angles.

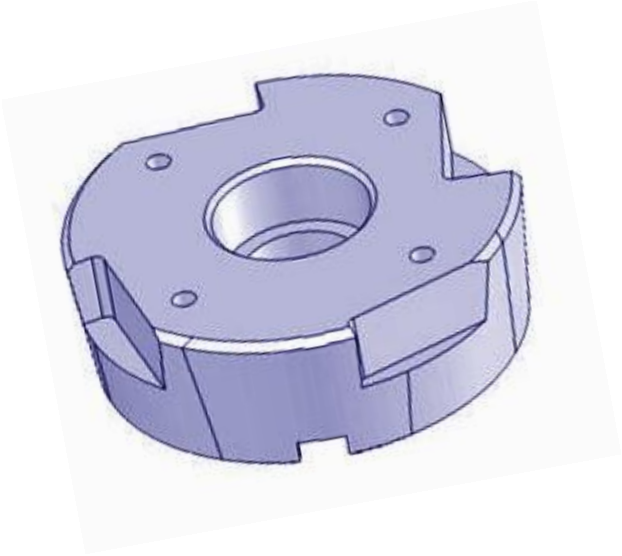

Fig.3.11. Stage-2 of manufacturing

Stage-3 of manufacturing: Drilling, Reaming and Milling of slots for clamps and tapping of holes.

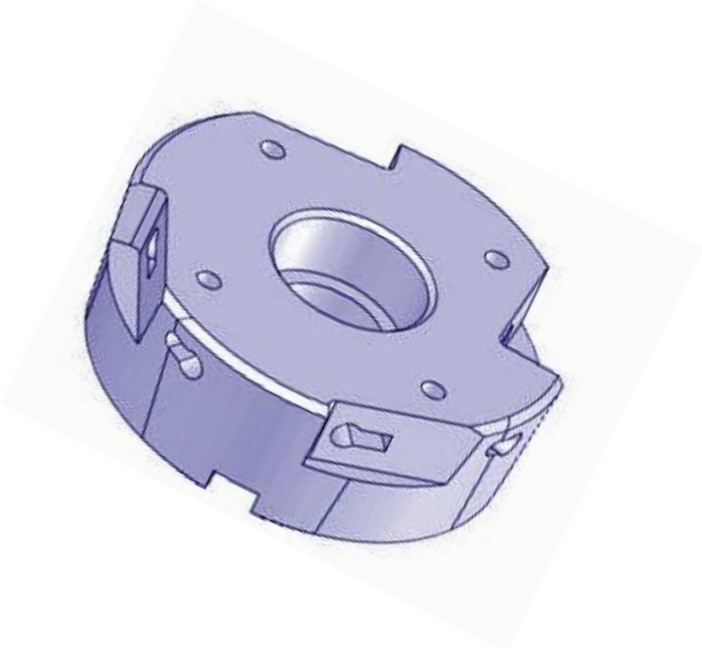

Fig.3.12. Stage-3 of manufacturing

Stage-4 of manufacturing: Slot cutting for mounting of cartridge assembly using Wire EDM.

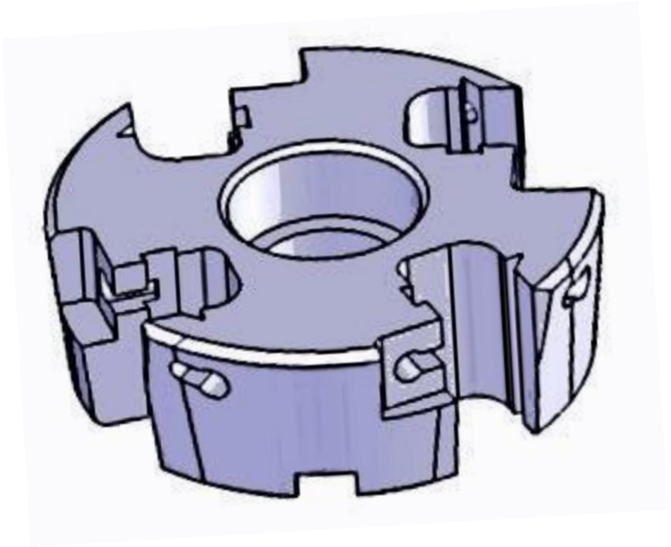

Fig.3.13. Stage-4 of manufacturing

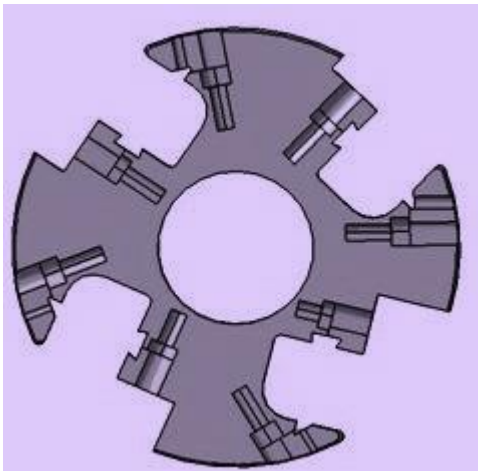

Fig.3.14. Sectional view of the cutter at Stage-4

Stage-5 of manufacturing: Heat treatment to achieve 32 HRc.

Fig.3.15. Photograph of the developed rotary milling cutter with four inclination angles

Scheme of measuring the inclination angle (i) on CMM:

In rotary face milling operation inclination angle (i) is defined as the angle between cutting velocity vector and axis of rotation of the insert. Cutting velocity vector is tangential to the effective diameter of the cutter at the tool workpiece contact point. Geometrically this inclination angle is equal to the angle between the plane containing the cutting edge and radial axis passing through the point of intersection of plane containing cutting edge and axis of insert rotation as shown in Fig.3.16. Inclination angle was measured for the 30° slot in fabricated rotary milling cutter using Coordinate Measuring Machine (CMM). The procedure is detailed below.

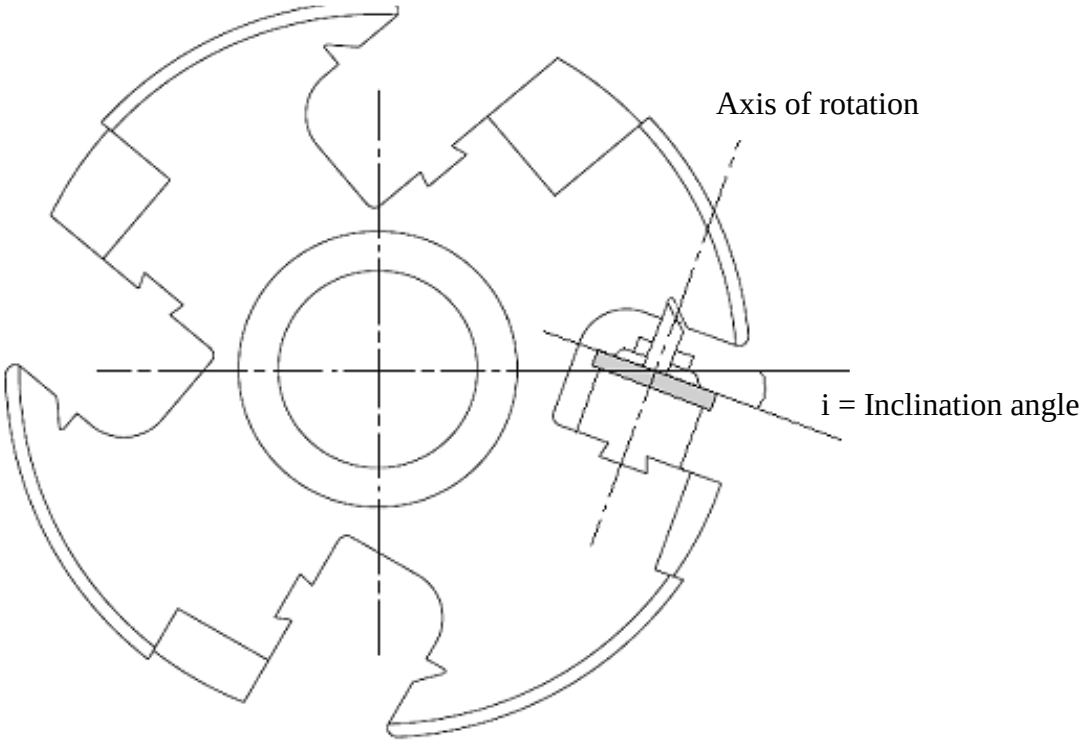

Fig.3.16. Inclination angle in rotary face milling cutter

Step-1Selection of reference plane: By touching the probe on different points of the grounded surface of the cutter body, reference plane was selected.

Step-2Location of vertical axis of cutter body: By touching different points on the inner bore of the cutter, axis was located.

Step-3Location of insert rotating axis: By touching the probe on different points on cylindrical part of the cartridge body, axis was located.

Step-4Location of cutting edge plane: By touching the probe on different points on the circular cutting edge, plane containing cutting edge was located.

Step-5: From the plane of cutting edge and axis of insert rotation intersection point was located. Vertical axis passing through this point is the axis to change the inclination angle of the insert. This is the neutral axis for all slots to guide cartridge assembly and passing through the pitch circle of 110mm diameter.

Step-6: Inclination angle was measured between the plane of cutting edge and radial line passing through the intersection point of cutting edge plane and axis of insert rotation.

3.7 Summary

In this chapter, the design and development of self-propelled rotary face milling cutter has been discussed. The maximum load condition for which the cutter has been developed has also been discussed and the stress analysis of the cutter prior to manufacturing has been presented. The materials used for the manufacturing of the cutter, different stages of manufacturing of the cutter have also been detailed. Different types of machines which are used to manufacture the cutter are presented. The procedure for measuring the accuracy of inclination angles on the cutter for insert using CMM has also been presented.

CHAPTER 4

EXPERIMENTATION

In this chapter, the complete details of the machines and equipment used in the present work and their importance have been described. The methodology that has been used for carrying out the experimentation for cutting forces, cutting temperature and surface roughness measurement has been detailed. Also, the process parameters and their respective levels considered for experimentation have been presented.

4.1 Machine tools and equipment used

The following tools and equipment have been used during experimentation.

Table.4.1. Tools and equipment used in experimentation

Machines used	Vertical Machining Centre (Make: HMT)
	Coordinate Measuring Machine (Make: ZEISS)
Force Measurement	AMTI Dynamometer (Piezoelectric Type)
Roughness Measurement	Ultra Germany (TR 110)
Work Piece Material	Inconel 625 (Nickel alloy)
Base plate	250 mm x 250 mm x 20 mm
Rotary Milling Cutter	
Cutter diameter	150 mm
Effective diameter	110 mm
Inclination angles (radial rake angle)	20° 30° 40° & 50°
Insert diameter	27 mm
Insert Type	K20 Coated Carbide

The rotary milling cutter that is to be used for experimentation has been designed and developed by the author for the present research. The details of the design and development of the rotary milling cutter have been discussed in the chapter-3. The developed rotary milling cutter, parts of the cartridge and assembly of cartridge are shown in the Figs. 4.1-4.3 respectively. The position of the insert in the cutter along with its holding cartridge assembly is shown in Fig.4.4.

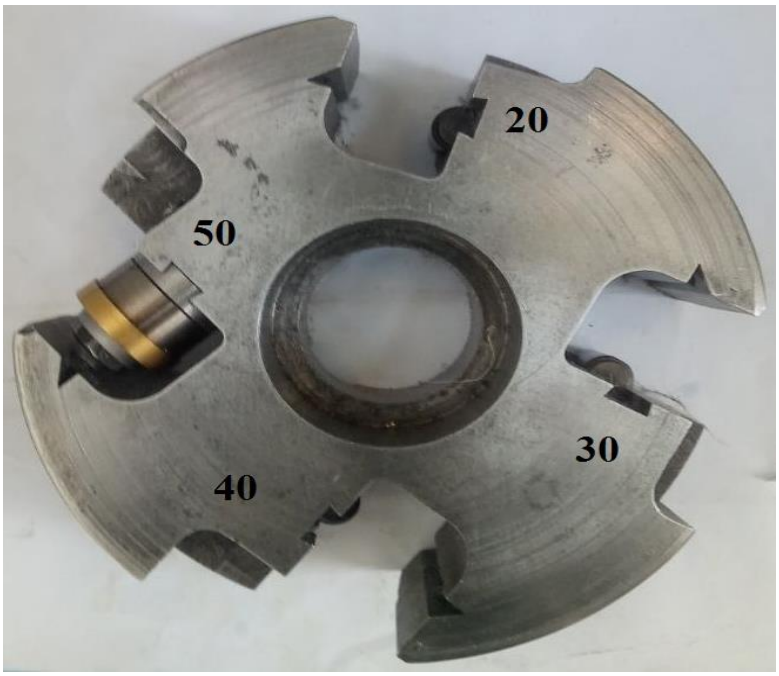

Fig.4.1. Rotary face-milling cutter

Fig.4.2. Parts of cartridge

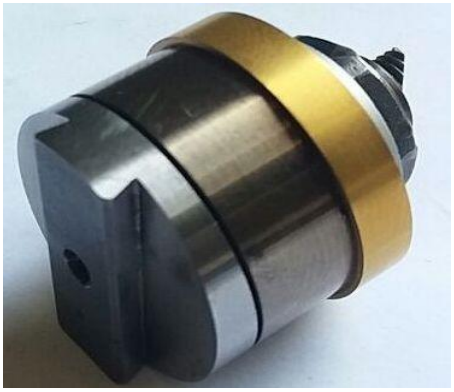

Fig. 4.3 Assembly of cartridge

Fig.4.4. Cartridge assembly fixed in the pocket

4.1.1 Vertical Machining Centre (VMC-HINUMERIK 3100M)

A Vertical Machining Centre (VMC) is a computer controlled milling machine that has the ability to move the spindle vertically along the Z-axis (Fig.4.4). VMC is rigid milling machine generally used for face-milling operations. Most of the VMC machines are 3-axis machines with provisions for attachments for extra two axes. These machining centers are used for machining large wing panels, control surfaces, etc. of aerospace structures. The specifications of the VMC that is used for experimentation are listed in Table.4.2.

Table.4.2. Specifications of Vertical Machining Centre

Make	HMT
Type of control	HINUMERIK 3100M
Number of axes	3
Travel	X-axis 1150 mm, Y-axis 640 mm, Z-axis 425mm
Positional accuracy	25 microns/600 mm
Repeatability	± 12.5 microns
Main motor spindle	5.5/1500 KW/RPM

Fig.4.5. Vertical Machining Centre (Make: HMT)

4.1.2 Cutting force measuring instrument (Dynamometer)

The multi-component AMTI Dynamometer provides dynamic and quasi-static measurement of the three orthogonal components of force (F_X, F_Y&F_Z) acting from any direction onto the top plate. The dynamometer is shown in Fig.4.6. The dynamometer has a great rigidity and accordingly a high natural frequency. Its high resolution enables the smallest dynamic changes in large forces to be measured. The specifications of the dynamometer are given in Table 4.3.

Fig.4.6. Dynamometer (Make: AMTI)

Table.4.3. Specifications of AMTI dynamometer

Measuring range (N) F_X, F_Z, F_Y	2224, 4448, 2224
Sensitivity (μv/v-N) F_X, F_Z, F_Y	0.674 , 0.171, 0.674
Operating temperature range (^{0}C)	-17.78 to 51.67°C
Natural frequency (Hz) F_X, F_Z, F_Y	450, 880, 450
Weight (Kg)	22.73

Functional principle:

The force to be measured is introduced via a top plate and distributed between four 3-component force sensors arranged between the base and top plates. Each of the sensors has three pairs of quartz plates, one sensitive to pressure in the z-direction and the other two to shear in the *X* and *Y* directions respectively (Fig.4.7). Four of these 3-component sensors are installed between a base plate and a top plate under high preload and connected in parallel. They thus constitute a 3-component dynamometer. Piezo-electric sensors produce a charge which varies linearly with the load acting on the sensor. Negative charges give positive voltages at the output of the charge amplifier, and vice versa. The force components are measured practically without displacement. The output charge from the dynamometer is fed to three charge amplifiers. The charge amplifier converts this charge into standardized voltage and current signals, which can then be evaluated by signal processing. The charge amplifier type that has been used is shown in Fig.4.7 and the specifications of the charge amplifier are presented in Table 4.4.

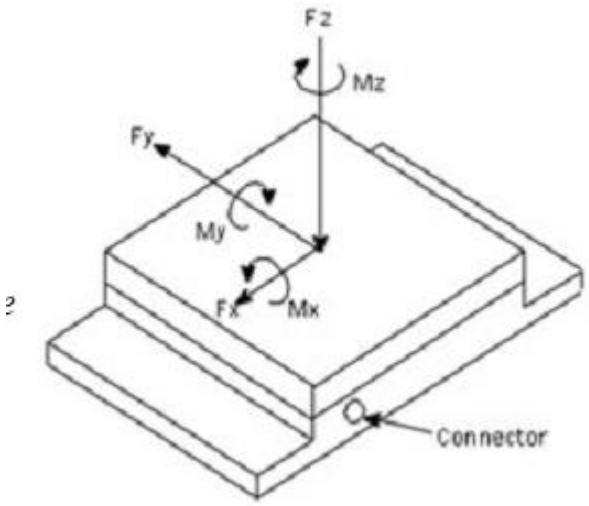

Fig.4.7. Principle of measurement in dynamometer

The charge amplifiers are connected to data acquisition system. Net force is the data acquisition software supplied by AMTI that has been used for cutting force measurement and it is PC based.

Fig.4.8. Charge amplifier (Model: MC12)

Table.4.4. Specifications of charge amplifier

No. of channels	1
Measuring range (pC)	±10 - ±999,000
Output range	±10 V
Frequency range (kHz)	0-200
Special function	Piezotron input

For data acquisition, the cycle time and frequency of acquisition have to be set. For example if the cycle time is 10 seconds and the frequency is 50 Hz, the data will be acquired 50 times in 10seconds. It indicates that once for every 0.2 seconds, the data will be collected. After completion of data collection, the data will be displayed on the PC monitor in the form of three graphs for three individual force components. Numerical data will also be displayed in the form of a table. The setup is shown in the figure 4.9

Fig: 4.9 Dynamometer setup

4.1.3 Cutting Temperature measuring instrument

A thermometer is a device which measures temperature or temperature gradient. The two important fundamental components of this device are the sensor and indicator. Sensor is the component which senses the temperature of a body and indicator shows the value of temperature in a calibrated scale. Infrared thermometers measure the temperature of an object by measuring the infrared energy emitted by that object.

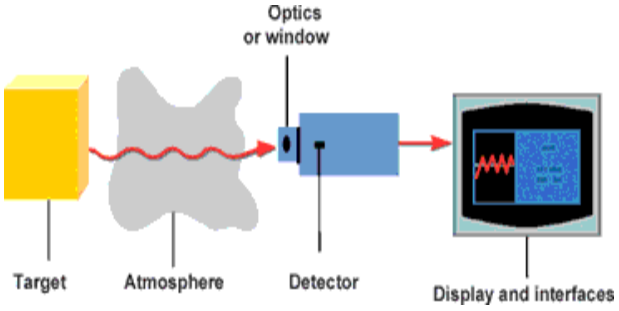

Figure: 4.10 Working Principle of IR Thermometer Figure: 4.11 Infrared thermometers (IR)

4.1.4 Working of Infrared Thermometer

The infrared (IR) energy occupies a certain portion of the electromagnetic spectrum. The frequency of the electromagnetic radiation of infrared rays is below the frequency range of visible light, and that makes the infrared rays invisible to human eyes. The wavelength of infrared radiation is between 0.7 microns to 1000 microns, although these devices can measure the radiation having wavelength in the range between 0.7 microns to 14 microns. However these devices cannot measure the temperature of the air, because, the design is such that, when the sensor of this device senses the radiation from the target, the air between the sensor and the target should not cause any temperature variations in the final measurement.

A property called emissivity is a major factor in the temperature measurements of such devices. Emissivity is defined as the "ratio of the intensity of radiation emitted by the surface at a specified wavelength and direction to that emitted by a black body under the same conditions". So, the emissivity of a black body is 1. The emissivity of all the objects range from 0 to 1. Considering this property, there are two main types of bodies.

- *Gray bodies* have same emissivity at all wavelengths.

- *Non gray bodies* have emissivity which varies according to the wavelength. This change causes accuracy problems in the temperature measurements.

The radiation from an object is sensed by the sensor and it captures the radiation. This sensor is very sensitive as it can even detect a radiation of about 0.0001 watts. The heat energy is converted into electrical energy, which is amplified and modified into output voltage. A central processing unit digitalizes the electrical signal using a 16-bit, Analog-to-Digital Converter, and the Arithmetic Unit inside the processor calculates the temperature value of the object, using *Planck's Radiation Law*, where the value of ambient temperature and emissivity of the object is substituted, which results in a temperature reading on the infrared display.

The camera device captures the image of a target object. The laser emission hole focuses at a single point on the target object, wherein the temperature of the single point position needs to be measured. The infrared measure hole measures the single point temperature of the object, which is instantly displayed on the color liquid crystal display screen. The image and the data are simultaneously stored in the SD card.

This model can be more efficient in working because, the Field of View (FoV) is reduced as the single point temperature is measured, and the temperature variance due to other materials or mediums can be reduced considerably. This advantage is not there in other models.

4. 1. 5 Working Principle of Infrared Thermometer

The basic function of these devices is to capture the infrared rays energy, emitted by anybody having the temperature value above absolute zero (0 kelvin). This is because everybody is made up of atoms and molecules. The higher the temperature of the body, the more will be the vibrations in the molecules of the body and the radiation emission. The above phenomenon is scientifically known as *Stefan-Boltzmann law*, which states that "total radiation energy emitted by a body is proportional to the fourth power of the absolute temperature".

$E \alpha T^4$

where,

- E is the total radiation energy.
- T is the absolute temperature.

Wien's displacement law is also applied in the working of such devices. This law states that, "the wavelength carrying the maximum energy is inversely proportional to the absolute temperature of a black body".

$\lambda_{max} \mathbf{x\ T = b}$

where,

λ_{max} is the maximum wavelength.
T is the temperature of the black body in Kelvins.
b is $2.8977685 \pm 51 \times 10^{-3}$ meters. Kelvins

4. 1. 6 Applications Depending upon Wavelength

Wavelength (μm)	*Applications*
0.7 - 1.1	High precision measurements in industries
1.1 - 1.7	Medium range of temperature and is used in glass and metal industries
2.2 - 2.5	General purpose measurements
3.43	To measure the temperature of thin-film plastics, oil and paints, etc.
3.9	To measure high temperature gas and oil-fired furnaces
4.4 - 4.4	To measure flame temperature
4.8 - 5.2	Glass and Ceramics temperature measurements
7.9	To measure the temperature of glass, polyesters, polyamides, etc.
8 – 14	Long range measurements

A *non contact infrared thermometer* is another type which can measure the temperature of an object, without touching it. This application can be used to measure the temperature of the chips in the computers just by pointing the device above the CPU of the computer. This device employs a laser pointer to aim at the target. These devices are widely used in many working sectors, for temperature measurements.

4.1.7 Surface roughness measuring instrument

Surface roughness, often called roughness, is a measure of the texture of a surface. It is quantified by the vertical deviations of a real surface from its ideal form. These deviations can be measured in different forms like R_a, R_t, etc.

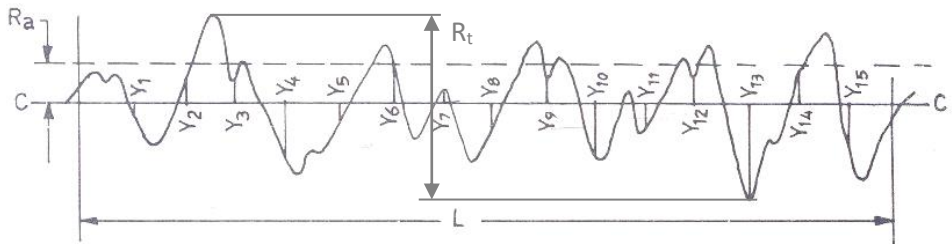

Fig.4.12. Measurement of surface roughness

Ra is Arithmetic Average (AA) or Centre Line Average (CLA) of the roughness profile. This defined as the average height from a mean line of all ordinates of the surface. It is given by

$$R_a = \frac{1}{n}\sum_{i=1}^{n} Y_i$$

Where *n* is the number of ordinates in the sampling length *L* and *Y* is the ordinate height. Similarly, R_t is the maximum peak to valley height within the sampling length *L* (Fig.4.9.).The instrument that has been used for the roughness measurement is shown in Fig.4.13.

Fig.4.13. Surface roughness measuring instrument (Ultra- Germany Make), Model: TR 110

Fig.4.14. Movement of probe on surface during roughness measurement

Table.4.5. Technical Specification for Portable Surface Roughness Tester - TR110

Parameters		Ra, Rz
Measuring range		Ra: 0.05 -10.0 µm Rz: 0.1- 50.0 µm
Straightness accuracy		0.05 + 1.0L/1000 µm L: Measuring length (mm)
Cut-off values		0.25, 0.8 and 2.5 mm
Tracing Speed		1.0 mm/sec
Measuring Lengths		1.25, 4.0 and 5.0 mm
Accuracy		+/- 15%
Repeatability		<12%
Dimensions		110 mm X 70mm X 24 mm
Weight		Approx. 200g
Detectors	*Stylus material* *Stylus radius* *Measuring force*	Diamond 2 µmR 0.75 mN
Sensing method	*Z-axis(vertical)* *X-axis(horizontal)*	Differential inductance Moiŕ striped scale

4.1.8 Coordinate Measuring Machine (CMM)

A 3- dimensional device used to measure physical geometrical properties of an object is called as Coordinate Measuring Machine. The specifications of the CMM used for measurement are given in Table 4.6.The geometrical dimensions are measured by a probe fixed to the third moving axis of this machine. The readings are measured by a CMM is in six degrees of freedom and displays these readings in mathematical form when connected to PC. The CMM that has been used for measuring the inclinations angles of the pockets provided on the cutter for insert position is shown in Fig.4.15.

Fig.4.15. Coordinate Measuring Machine (WMM-850, Make: ZEISS)

Table 4.6.Specifications of CMM (WMM-850)

Travel	850 mm x 700 mm x 600 mm
Resolution	0.5 µm
Maximum load capacity	500 Kgs
Measurement uncertainty (L in mm)	Linear : 2.9+L/250 µm Volumetric : 4.2+L/200 µm
Operating software	UMESS – UNIX

4.2 Work materials used

Inconel 625

- Nickel Chromium alloy
- Available in hot worked and annealed condition
- High strength and outstanding corrosion resistance
- Range of service temperatures from cryogenic to 980◦C
- Excellent weldability
- Low magnetic permeability
- Commonly referred to as Inconel 625

Alloy 625 is a nickel-chromium alloy which gains its stiffening effect through molybdenum and niobium additions, therefore eliminating the need for this alloy to be aged. It has superior resistance to a wide range of corrosive environments as well as the high temperature effects of oxidation and carburization.

Alloy 625 is excellent for sea-water applications, having freedom from pitting and crevice corrosion, high corrosion fatigue strength and resistance to chloride-ion stress corrosion cracking. This alloy also has high tensile, creep and rupture strength, fatigue and thermal fatigue strength and oxidation resistance, making it suitable for aircraft engine exhaust systems, housing engine controls and aircraft ducting systems. It is also used in the nuclear field for reactor cores, control rod components in nuclear water reactors.

Typical Applications of Inconel 625

Typical applications are combustion system transition liners, propeller blades, seals, fasteners, pumps, turbine shroud rings, heat exchanger tubing, reaction vessels, distillation columns, heat exchangers and valves.

4.2.1 Composition of work piece material (Inconel 625)

Table.4.7. Chemical Composition of Inconel 625 work material

Nickel	58 %	Silicon	0.50%
Chromium	23%	Phosphorus	0.015%
Molybdenum	10%	Sulfur	0.015%
Iron	5%	Aluminum	0.40%
Niobium	3.15%	Titanium	0.40%
Carbon	0.10%	Cobalt	1.0%
Manganese	0.50%		

4.2.2 Properties of work piece material

Table.4.8. Properties of Inconel 625work material

Properties	***Metric units***
Density	8.44 g/cm^3
Ultimate Tensile strength	880 MPa
Tensile strength, Yield	460 MPa
Modulus of elasticity	207.5 GPa
Compressive yield strength	970 x10^{3}MPa
Poisson's ratio	0.278
Shear modulus	81.4 GPa
Ultimate shear strength	223.32 MPa
Hardness, Vickers	325 Hv
Thermal conductivity	9.8 W/mk
Specific heat capacity	410 joules/kg K
Melting point	1290-1350 ^{0}c

SUS 304 (AISI 304)

SUS 304 has excellent corrosion resistance in a wide variety of environments and when in contact with different corrosive media. Pitting and crevice corrosion can occur in environments containing chlorides. Stress corrosion cracking can occur at temperatures over 60°C.

SUS 304 has good resistance to oxidation in intermittent service up to 870°C and in continuous service to 925°C. However, continuous use at 425-860°C is not recommended if corrosion resistance in water is required. In this instance 304 is recommended due to its resistance to carbide precipitation.
SUS 304 cannot be hardened by heat treatment. Solution treatment or annealing can be done by rapid cooling after heating to 1010-1120°C.

SUS 304 has good machinability. Machining can be enhanced by using the following rules:

- Cutting edges must be kept sharp. Dull edges cause excess work hardening.
- Cuts should be light but deep enough to prevent work hardening by riding on the surface of the material.
- Low thermal conductivity of austenitic alloys results in heat concentrating at the cutting edges. This means coolants and lubricants are necessary and must be used in large quantities.

SUS 304 taken as base metal to compare output parameters of Inconel 625.

4.2.3 Composition of work piece material (SUS 304 (AISI 304))

Table.4.9. Chemical Composition of SUS 304 (AISI 304) work material

Carbon (C)	0.08%	Sulphur (S)	0.030%
Silicon (Si)	1.00%	Nickel (Ni)	8.00%
Manganese (Mn)	2.00%	Chromium (Cr)	18.00%
Phosphorus (P)	0.045%		

4.2.4 Properties of work piece material

Table.4.10. Properties of SUS 304 (AISI 304) work material

Properties	***Metric units***
Density	0.803 g/cm^3
Ultimate Tensile strength	505 MPa
Tensile strength, Yield	215 MPa
Modulus of elasticity	207.5 GPa
Compressive yield strength	970 x10^{3}MPa
Poisson's ratio	0.29
Shear modulus	86 GPa
Ultimate shear strength	223.32 MPa
Hardness, Vickers	19 Hrc
Thermal conductivity	16.2 W/mk
Specific heat capacity	510 joules/kg K
Melting point	1455 ^{0}c

The reason to compare Inconel 625 and SUS 304 is both the materials are extensively used in aerospace applications in DRDL – Hyderabad, SUS 304 shows work hardening property like Inconel 625 while machining. Both materials are showing closed properties while machining.

When we conducted the trail experiments, we noticed that the optimum values were obtained in the given range of processes parameters. Hence the process parameters were selected depending on the trail experiments and literature. References: 28, 55, 56 and 69 explained this in detail.

4.3 Experimental Procedure

4.3.1 Experimental setup

The work piece along with the dynamometer is clamped on to the machine table. The complete block diagram of the experimental setup and photograph of set up is shown in Figs.4.16 and 4.17 respectively.

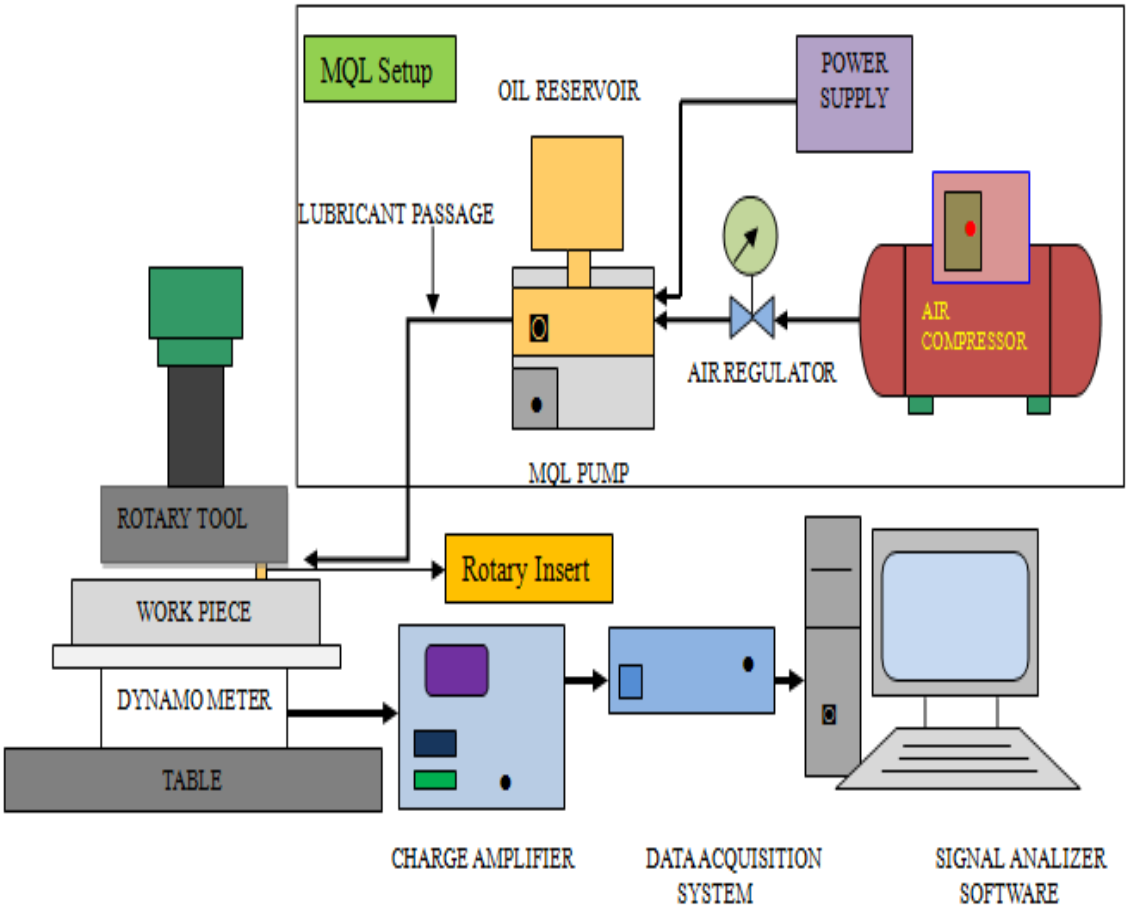

Fig.4.16. Block diagram of the experimental setup

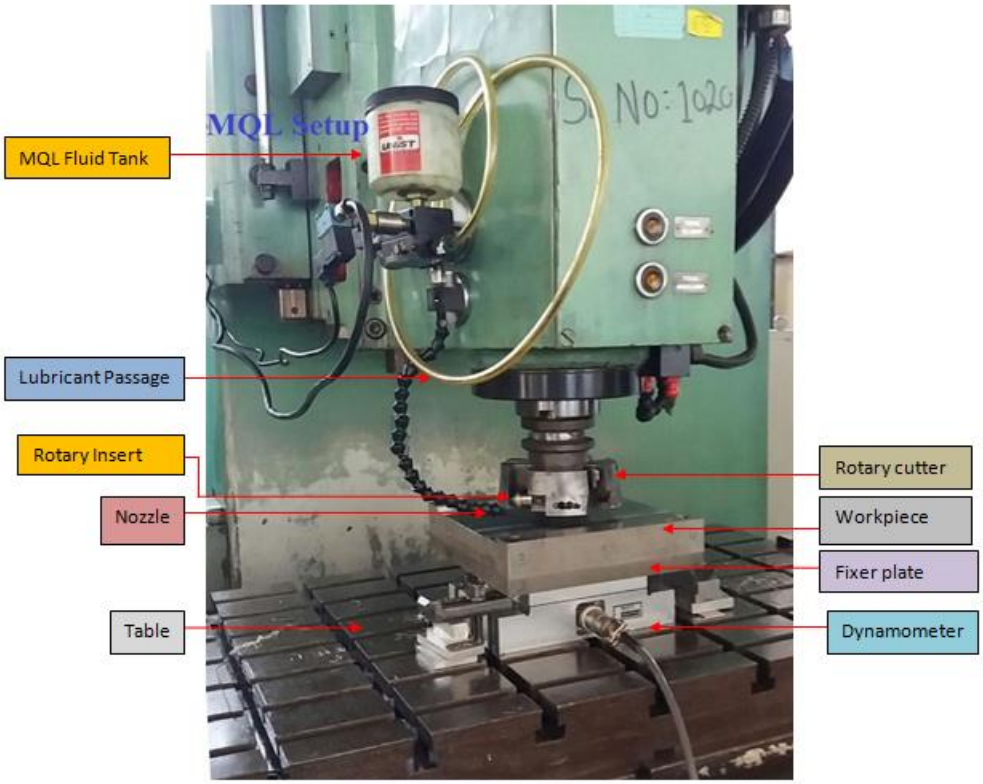

Fig.4.17. Photograph of the experimental setup

4.3.2 Methodology

The preliminary investigation on cutting forces was carried out based on RSM Design of Experiments and full factorial experimentation was followed. The experimentation was carried out as per ISO standards and the average of the cutting forces in X, Y and Z directions are considered. The levels identified for the RSM design of experimentation is shown in Table 4.11. The levels are selected considering dry machining condition and requirement of high specific cutting energy for machining of Inconel 625 Nickel alloys. The methodology followed is shown in Fig.4.18. The ranges of processes parameters are selected depending on the trail experiments and literature [55, 56].

In RSM Design, if we give the inclination angles from 20 to 50, the design used in the study gives 20, 25, 35, 45 and 50, but in the cutting tool, there is provision for only 20, 30, 40 and 50. Hence RSM considered inclination angles, between 20 and 40 while full factorial design angles were between 20^0 and 50^0.

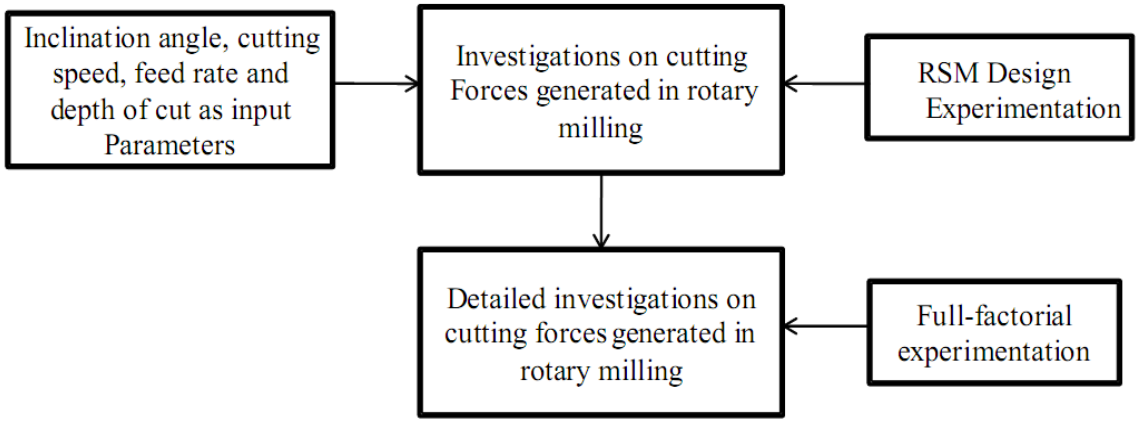

Fig.4.18. Methodology for experimentation (Cutting forces)

Table 4.11.Cutting parameters and their levels for RSM experimentation (Cutting Force, Surface Roughness and Cutting Temperature)

Cutting Parameter	Symbol	Levels		
		1	2	3
Inclination angle (deg)	I	20	30	40
Cutting speed (m/min)	S	14	24	34
Feed rate (mm/min)	F	40	60	80
Depth of cut (mm)	H	0.2	0.4	0.6

In order to study the influence of the process parameters such as cutting speed, feed, depth of cut and inclination angle on cutting forces in X,Y and Z directions, full factorial experimentation is conducted for detailed investigation considering the levels of process parameters shown in Table 4.12. Here the cutting speed is derived from the spindle speed (in rpm) considering the effective diameter of the cutters.

Table 4.12.Cutting parameters and their levels for full factorial experimentation (Cutting Force, Surface Roughness and Cutting Temperature)

Cutting Parameter	Symbol		Level		
		1	2	3	4
Inclination angle (deg)	I	20	30	40	50
Cutting speed (m/min)	S	14	24	34	-
Feed rate (mm/min)	F	40	60	80	-
Depth of cut (mm)	H	0.2	0.4	0.6	-

To compare the cutting forces generated by Rotary Face milling cutter while machining of Inconel 625 with that SUS 304 (AISI 304) for the same process parameters, the RSM Design experimentation and full factorial experimentation were carried out considering the levels as shown in Table 4.12.

The surface roughness investigations are conducted according to the methodology given in Fig.4.19. Full-factorial experimentation as in the case of cutting forces is followed for surface roughness measurement with 4 levels of inclination angle and 3 levels each for cutting speed, feed rate and depth of cut. The levels considered for input parameters are given in Table 4.12. The levels considered for development of Response Surface model is given in Table 4.11.

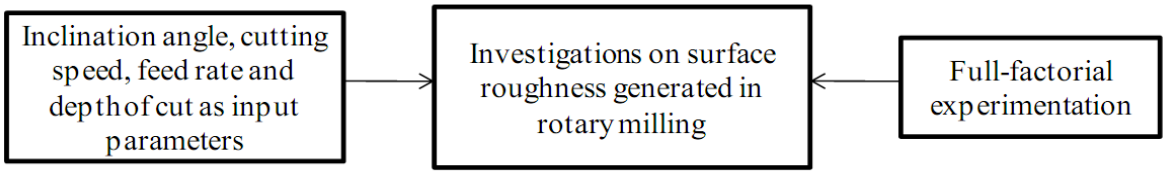

Fig.4.19. Methodology for experimentation (Surface Roughness)

The cutting temperature investigations are conducted according to the methodology given in Fig.4.20. Full-factorial experimentation as in the case of cutting forces is followed for surface roughness measurement with 4 levels of inclination angle and 3 levels each for cutting speed, feed rate and depth of cut. The levels considered for input parameters are given in Table 4.12. The levels considered for development of Response Surface model is given in Table 4.11.

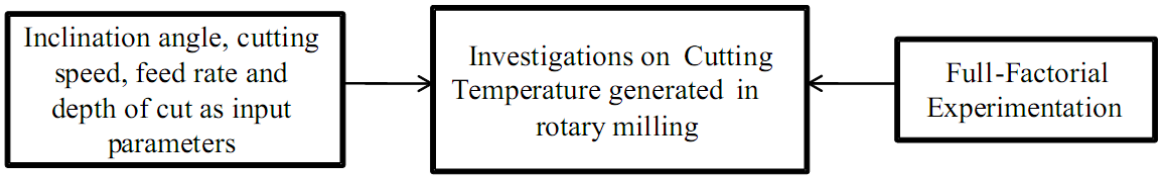

Fig.4.20. Methodology for experimentation (Cutting Temperature)

As the rotary cutting process is a self-heat dissipating operation and in order to study the effect of selected machining parameters on the process and performance of rotary insert while machining Nickel based superalloy Inconel 625, all the experiments have been performed under dry machining conditions. Nine experiments were conducted by Minimum Quantity Lubrication (MQL) process. The nine experiments were taken from RSM Design experimentation list. Three maximum load conditions, three medium load conditions and three minimum load conditions were conducted. Using MQL with Nano coolants, the experiments were also conducted for the above mentioned nine experiments. The levels of nano coolants are 1%, 3% and 5%. If all the experiments will be conducted with MQL and nano coolants the number of experiments will be more (810). Using these nine experiments we conducted three replicates and the no of experiments were 243.

4.4 Summary

In this chapter, the details of the CNC vertical machining centre, rotary and face milling cutters used, work material, force measuring instrument, roughness measuring instrument and Cutting temperature measuring instrument have been discussed. The overall research plan describing the type of experimentation selected in this investigation has been discussed. This chapter also explains the factors and the levels selected for the experimentation. The experimental results are discussed in chapter 5.

CHAPTER 5

INVESTIGATIONS ON CUTTING FORCES, SURFACE FINISH AND CUTTING TEMPERATURE IN ROTARY FACE MILLING OPERATION

This chapter deals with investigating the cutting forces, Cutting Temperatures and surface roughness generated in self-propelled rotary face-milling using the developed rotary face-milling cutter. The experiments are performed with input as a function of four particular controllable factors and statistical analyses are carried out using analysis of variance (ANOVA). The responses considered here are - three cutting forces F_X, F_Y and F_Z, Cutting Temperature and surface roughness. Initially, a preliminary investigation on cutting forces is carried out using RSM Design experimentation. Results of experimentation are given in Table 5.1. Based on the results of cutting forces, cutting temperature and surface finish, a detailed investigation using full factorial experimentation is carried out.

5.1 Results and Discussion

Table 5.1 RSM Design experimentation results for cutting forces (rotary face milling)

S. No	Exp No.	I (Deg)	Speed (m/min)	Feed (mm/min)	Depth of cut (mm)	F_X (N)	F_Y (N)	F_Z (N)	Temp ^0C	SR μ
1	1	20	14	40	0.2	634.58	402.80	500.69	134.9	0.85
2	3	20	14	40	0.6	3471.34	1852.17	1862.44	144.3	1.1
3	7	20	14	80	0.2	921.65	739.78	766.90	152.2	1.05
4	9	20	14	80	0.6	4692.28	2860.26	2959.26	176.4	1.7
5	19	20	34	40	0.2	214.72	162.49	139.98	134.2	1.49
6	21	20	34	40	0.6	813.57	598.91	573.12	168.3	1.51
7	25	20	34	80	0.2	519.81	366.14	348.42	133.2	1.21
8	27	20	34	80	0.6	1753.68	1245.52	1115.77	156.9	1.73
9	28	30	14	40	0.2	521.48	242.96	160.78	135.6	1.54
10	30	30	14	40	0.6	2440.19	1952.57	1647.41	157.3	1.89
11	34	30	14	80	0.2	819.15	773.56	849.06	143.2	1.32
12	36	30	14	80	0.6	3838.99	3399.64	2719.08	194.2	1.84
13	41	30	24	60	0.4	909.22	838.76	720.70	147.4	1.88
14	41	30	24	60	0.4	909.22	838.76	720.70	147.4	1.88
15	41	30	24	60	0.4	909.22	838.76	720.70	147.4	1.88
16	41	30	24	60	0.4	909.22	838.76	720.70	147.4	1.88
17	41	30	24	60	0.4	909.22	838.76	720.70	147.4	1.88
18	41	30	24	60	0.4	909.22	838.76	720.70	147.4	1.88
19	46	30	34	40	0.2	295.044	214.31	240.24	136.8	1.43
20	48	30	34	40	0.6	1299.18	960.05	1273.25	198.3	2.06
21	52	30	34	80	0.2	720.77	399.02	559.46	139.2	1.06
22	54	30	34	80	0.6	2099.28	1525.38	1686.82	202.3	2.26
23	55	40	14	40	0.2	689.09	681.87	740.46	154.7	1.29
24	57	40	14	40	0.6	2664.19	2450.44	1689.86	167.3	1.52
25	61	40	14	80	0.2	948.05	944.04	979.01	148.6	1.32
26	63	40	14	80	0.6	4327.15	4207.97	2933.25	163.8	1.36
27	73	40	34	40	0.2	515.74	324.66	597.68	140.3	1.29
28	75	40	34	40	0.6	1113.84	1038.67	755.17	174.6	1.66
29	79	40	34	80	0.2	868.29	670.75	827.84	151.7	1.26
30	81	40	34	80	0.6	2066.76	1941.40	1265.95	170.4	2.36

5.1.1 Analysis of cutting forces (Fx)

Table 5.2 ANOVA (Fx)

Source	Sum of Squares	df	Mean Square	F Value	p-value Prob > F	
Model	34692104	14	2478007	42.17883	< 0.0001	significant
A-Inclination angle	11771.8	1	11771.8	0.200371	0.6608	
B-Speed	7723237	1	7723237	131.4593	< 0.0001	
C-Feed	2564503	1	2564503	43.65108	< 0.0001	
D-Depth of cut	16845313	1	16845313	286.7286	< 0.0001	
AB	346399.1	1	346399.1	5.896152	0.0282	
AC	14052.6	1	14052.6	0.239193	0.6319	
AD	103900	1	103900	1.76851	0.2034	
BC	48317.96	1	48317.96	0.822433	0.3788	
BD	4339201	1	4339201	73.8587	< 0.0001	
CD	798016.4	1	798016.4	13.58325	0.0022	
A^2	90641.85	1	90641.85	1.542839	0.2333	
B^2	287619.5	1	287619.5	4.895649	0.0429	
C^2	34067.46	1	34067.46	0.579871	0.4582	
D^2	49878.93	1	49878.93	0.849003	0.3714	
Residual	881250.5	15	58750.03			
Lack of Fit	881250.5	10	88125.05	2.060850	0.2517	not significant
Pure Error	0	5	0			
Cor Total	35573354	30				

Table 5.3 Pooled ANOVA (Fx)

Source	Sum of Squares	df	Mean Square	F Value	p-value Prob > F	% Contribution	
Model	34692104	14	2478007	42.17883	< 0.0001		significant
A-Inclination angle	513400.5163	1	513400.52	18.08028178	0.0004	14.43	
B-Speed	7723237	1	7723237	131.4593	< 0.0001	21.71	
C-Feed	2564503	1	2564503	43.65108	< 0.0001	7.20	
D-Depth of cut	16845313	1	16845313	286.7286	< 0.0001	17.35	
BC	4339201	1	4339201	73.8587	< 0.0001	12.19	
BD	798016.4	1	798016.4	13.58325	0.0022	12.43	
A^2	212766.752	1	2127660.8	74.92923108	< 0.0001	5.98	
Residual	881250.5	16	58750.03				
Lack of Fit	881250.5	10	88125.05	2.060850	0.2517		not significant
Pure Error	255292.2488	12	21274.354				
Cor Total	35573354	30					

R-Squared	0.975227
Adj R-Squared	0.952106
Pred R-Squared	0.895976

Fx= 1120.53 +25.57 * A -655.03 * B +377.46 * C +967.39 * D + 29.64 * B * C -80.58 * B * D -54.95 * B * C -520.77 * B * D +187.04 * A^2 +333.18 +138.75 * A^2 (5.1)

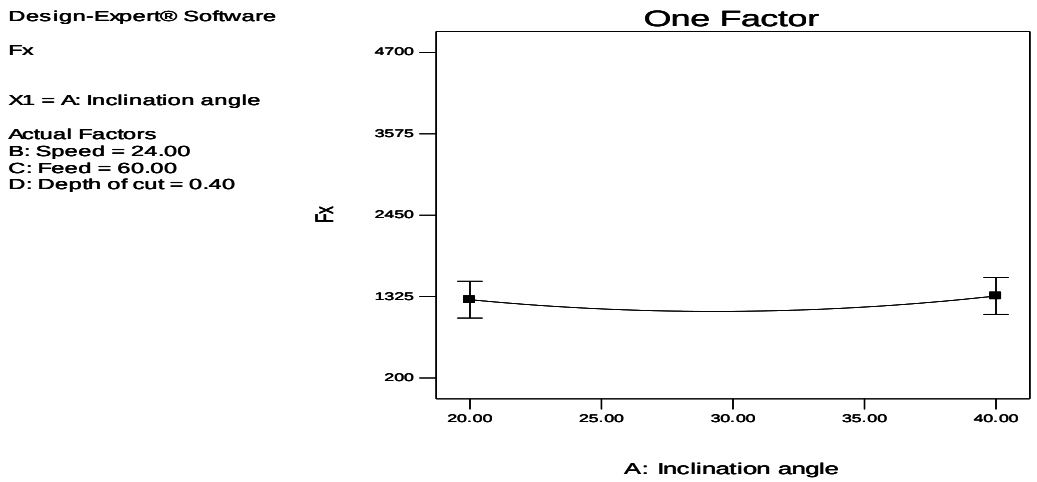

Fig: 5.1.1(a) Effect of Inclination Angle on cutting force (Fx)

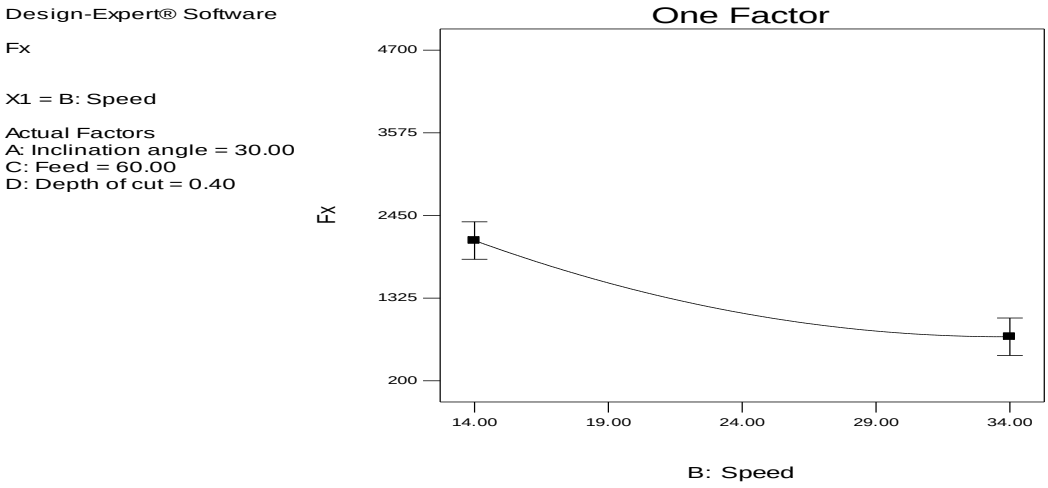

Fig: 5.1.1 (b) Effect of Cutting Speed on cutting force (Fx)

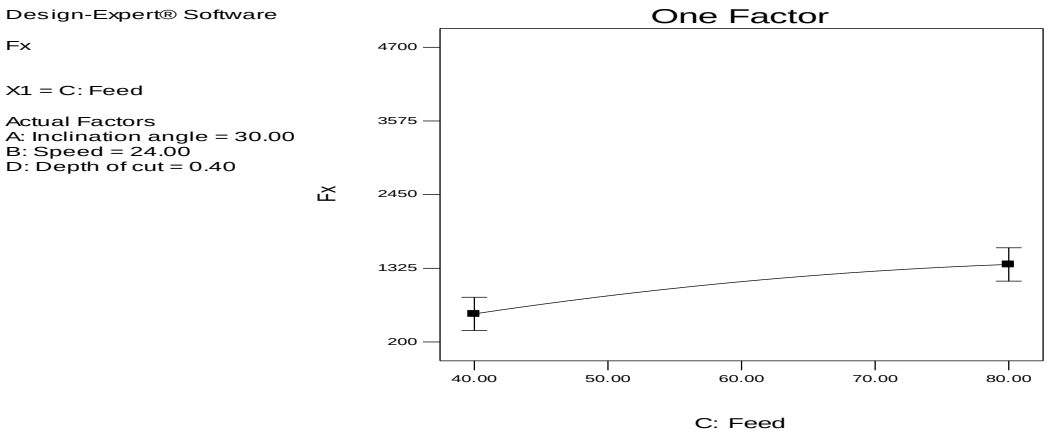

Fig: 5.1.1 (c) Effect of feed on cutting force (Fx)

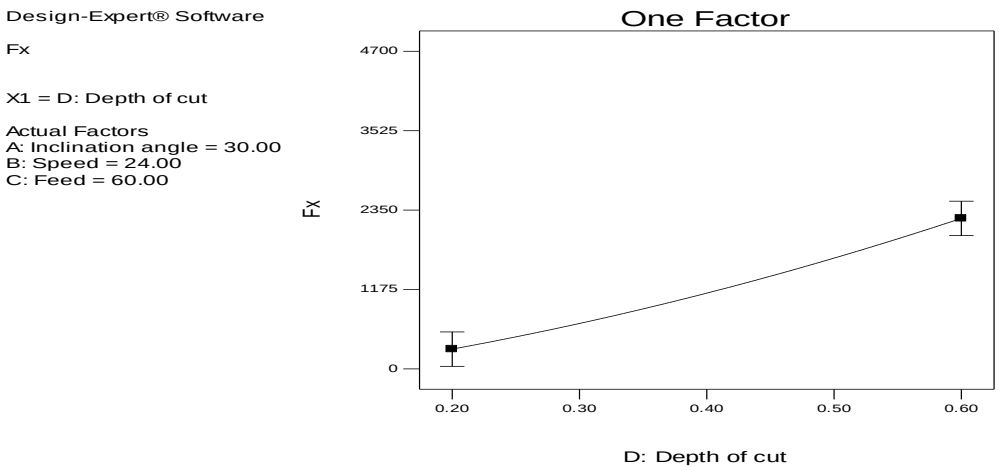

Fig: 5.1.1(d) Effect of Depth of Cut on cutting force (Fx)

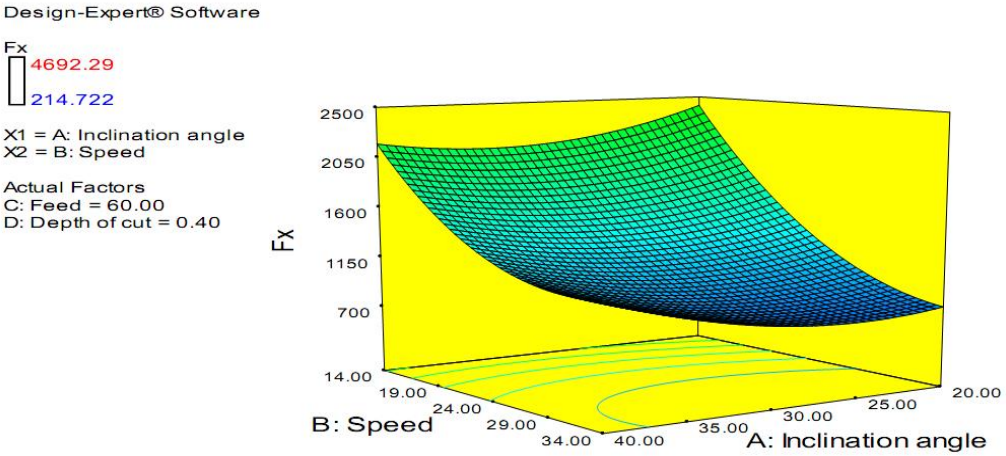

Fig: 5.1.1 (e) Response surface for Cutting force, Speed and Inclination angle

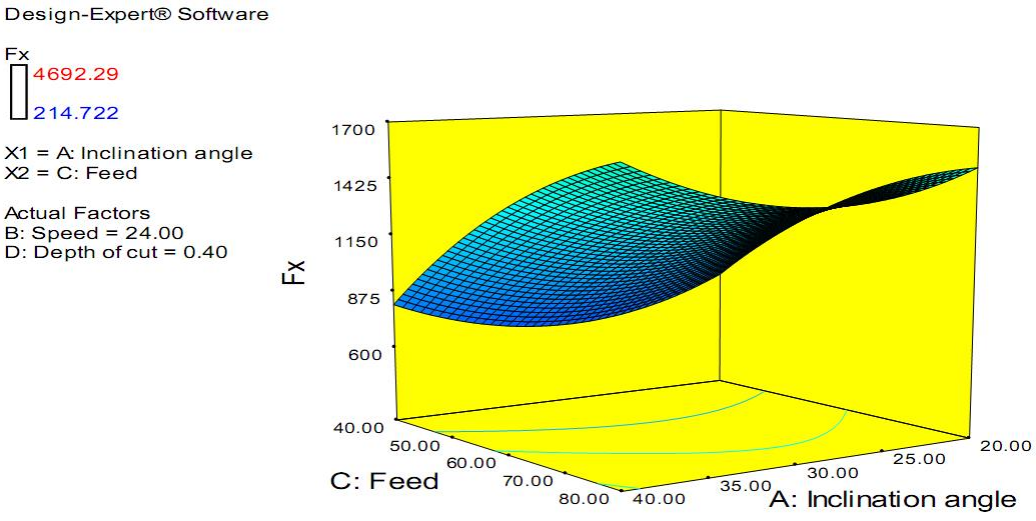

Fig: 5.1.1 (f) Response surface for Cutting force, Feed and Inclination angle

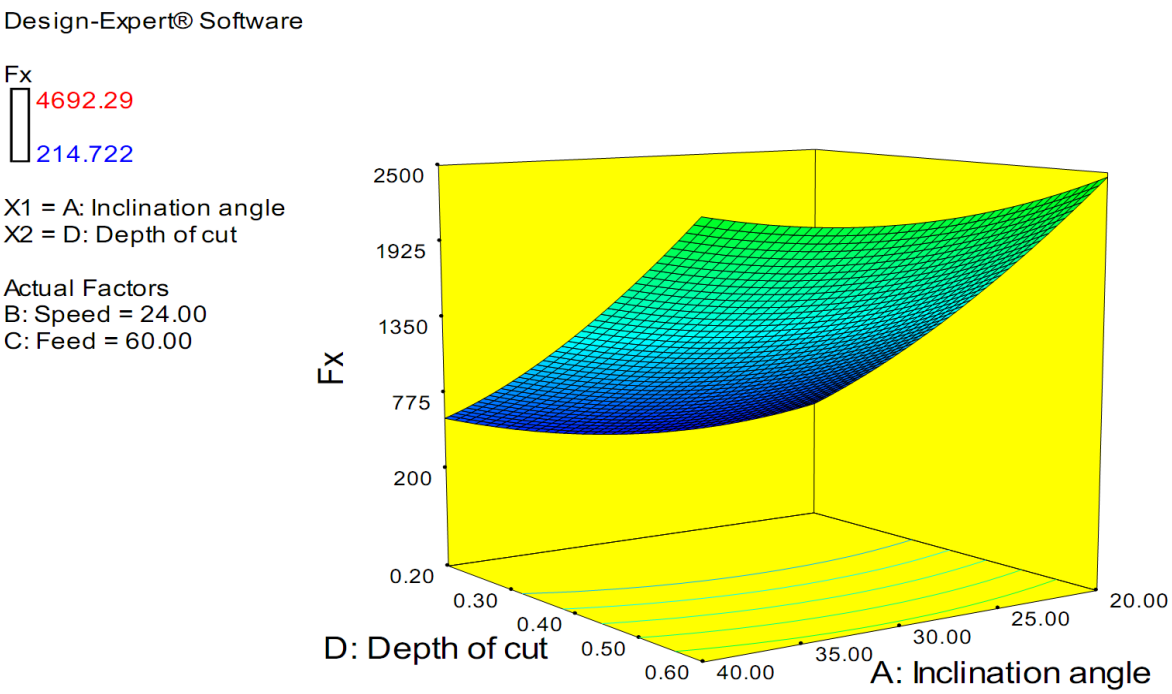

Fig: 5.1.1 (g) Response surface for Cutting force, Depth of Cut and Inclination angle

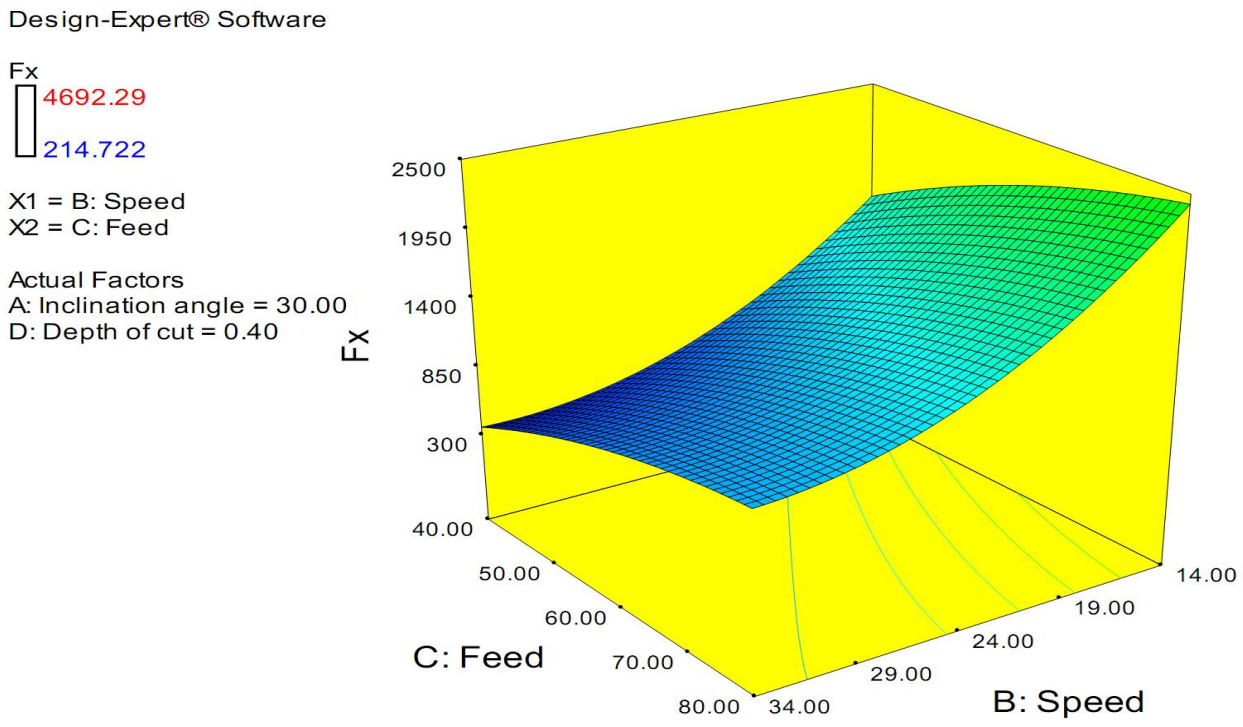

Fig: 5.1.1 (h) Response surface for Cutting force, Feed and Speed

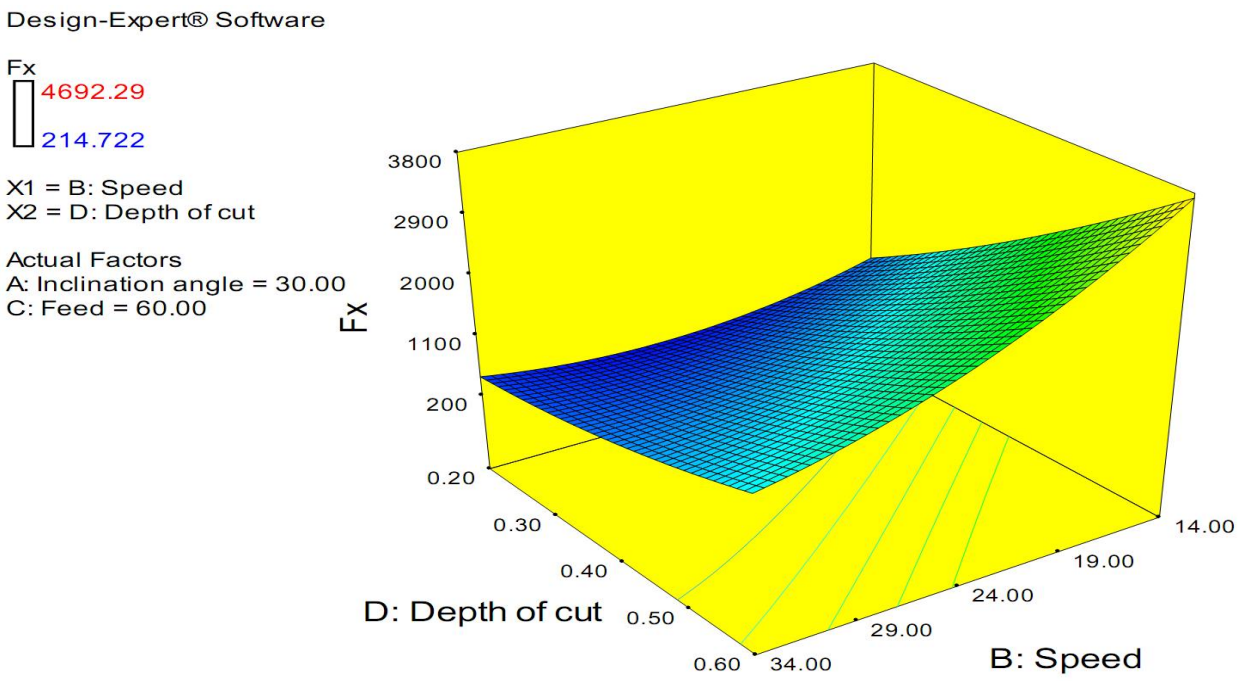

Fig: 5.1.1 (i) Response surface for Cutting force, Depth of cut and Speed

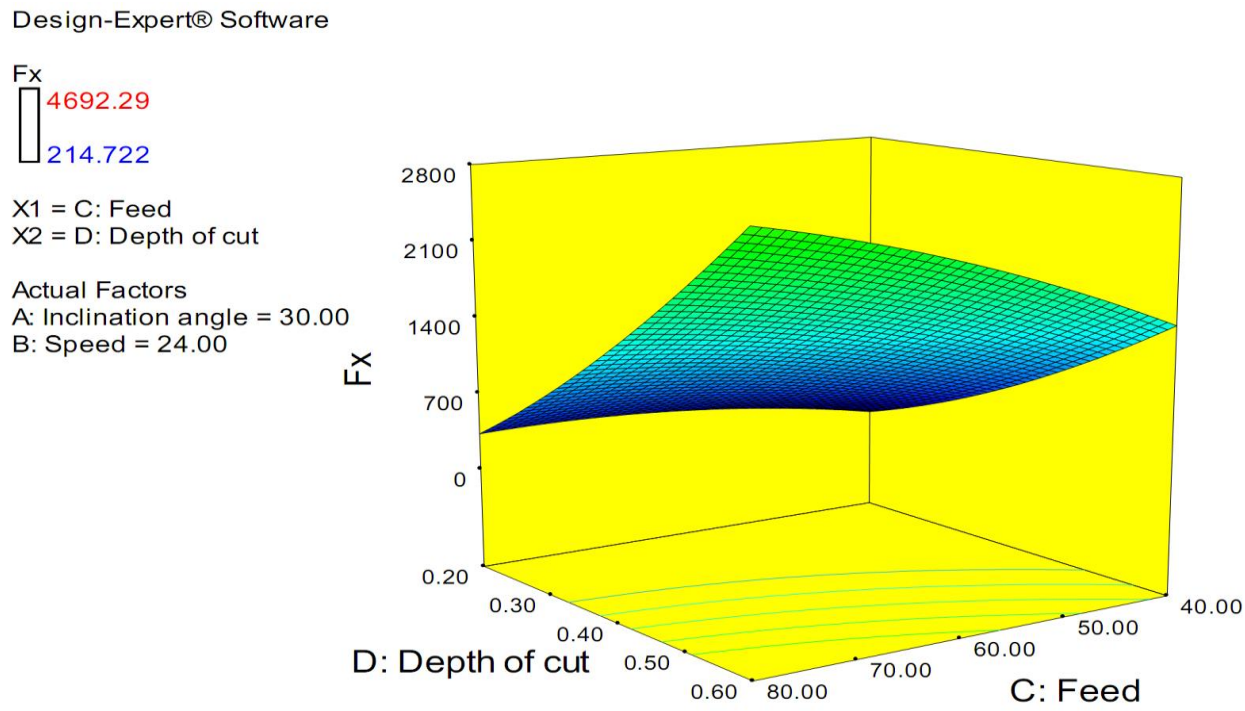

Fig: 5.1.1 (j) Response surface for Cutting force, Depth of cut and Feed

5.1.2 Analysis of cutting forces (Fy)

Table: 5.4 ANOVA (Fy)

Source	Sum of Squares	df	Mean Square	F Value	p-value Prob > F	
Model	20834660	14	1488190	38.8084	< 0.0001	significant
A-Inclination angle	1011523	1	1011523	26.37807	0.0001	
B-Speed	4205996	1	4205996	109.6822	< 0.0001	
C-Feed	2032131	1	2032131	52.99307	< 0.0001	
D-Depth of cut	9711462	1	9711462	253.2514	< 0.0001	
AB	42736.58	1	42736.58	1.114467	0.3078	
AC	71981.6	1	71981.6	1.877106	0.1908	
AD	283955.7	1	283955.7	7.404877	0.0158	
BC	100124	1	100124	2.610992	0.1270	
BD	1756889	1	1756889	45.81542	< 0.0001	
CD	626505.5	1	626505.5	16.33775	0.0011	
A^2	418808	1	418808	10.9215	0.0048	
B^2	58572.02	1	58572.02	1.527416	0.2355	
C^2	146949	1	146949	3.832075	0.0692	
D^2	4.118948	1	4.118948	0.000107	0.9919	
Residual	575206.7	16	38347.12			
Lack of Fit	575206.7	10	57520.67	1.569583	0.3450	not significant
Pure Error	265242.2488	5	23274.354			
Cor Total	21409867	30				

Table: 5.5 Pooled ANOVA(Fy)

Source	Sum of Squares	df	Mean Square	F Value	p-value Prob > F	% Contribution	
Model	20834660	14	1488190	38.8084	< 0.0001		significant
A-Inclination angle	1011523	1	1011523	26.37807	0.0001	4.72	
B-Speed	4205996	1	4205996	109.6822	< 0.0001	19.64	
C-Feed	2032131	1	2032131	52.99307	< 0.0001	9.49	
D-Depth of cut	9711462	1	9711462	253.2514	< 0.0001	25.35	
BD	1756889	1	1756889	45.81542	< 0.0001	8.20	
CD	626505.5	1	626505.5	16.33775	0.0011	2.90	
A^2	418808	1	418808	10.9215	0.0048	1.95	
Residual	575206.7	16	38347.12				
Lack of Fit	575206.7	10	57520.67	1.569583	0.3450		not significant
Pure Error	265242.248	5	23274.354				
Cor Total	21409867	30					

R-Squared	0.973134
Adj R-Squared	0.948058
Pred R-Squared	0.863116

Fy = 985.90 +237.06 * A -483.39 * B +336.00* C+734.52* D -331.37 * B * D +197.88 * C * D +402.05 * A^2 +150 (5.2)

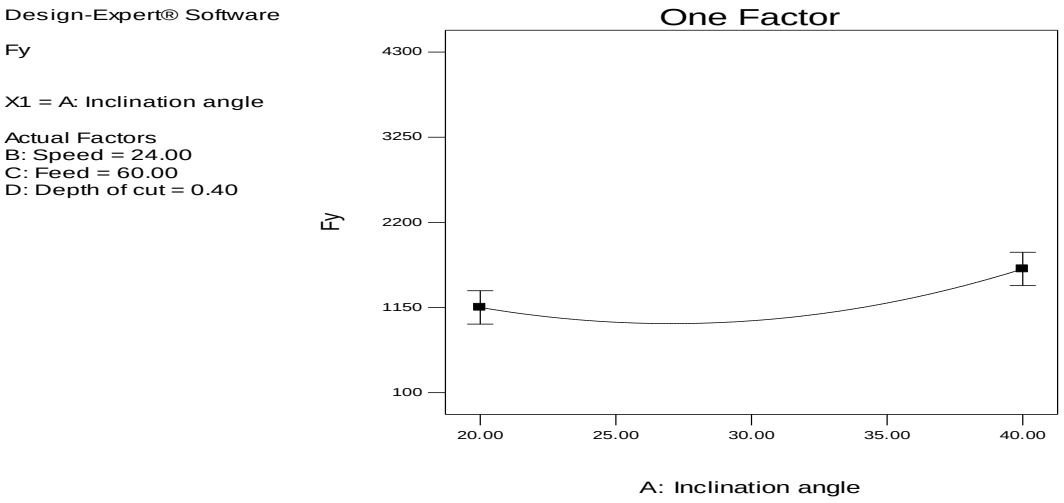

Fig: 5.1.2 (a) Effect of Inclination angle on cutting force (Fy)

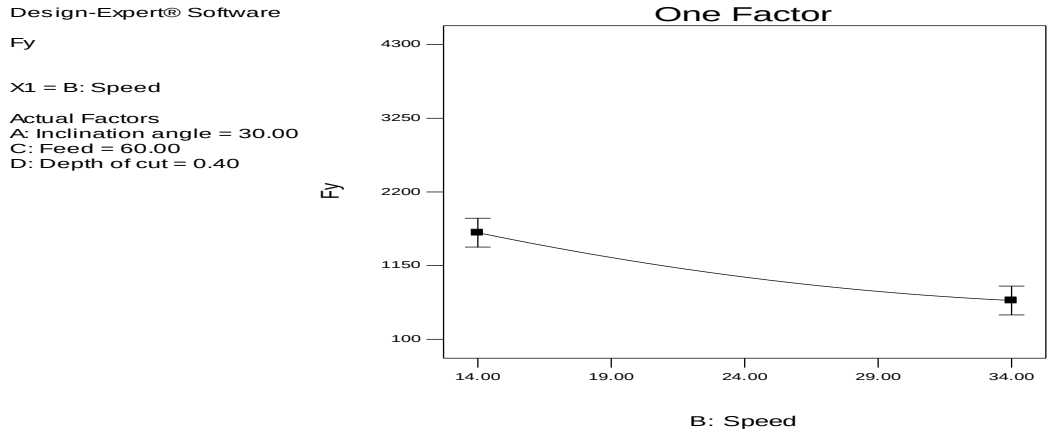

Fig: 5.1.2 (b) Effect of Cutting speed on cutting force (Fy)

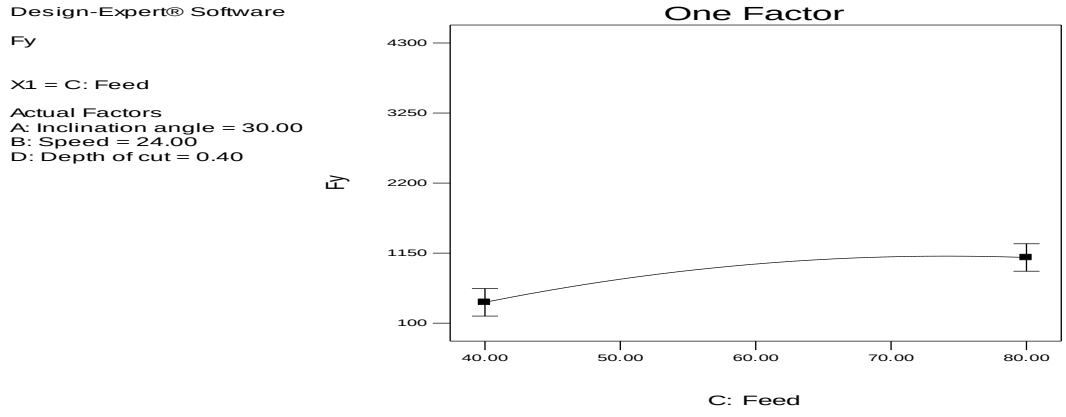

Fig: 5.1.2 (c) Effect of Feed on cutting force (Fy)

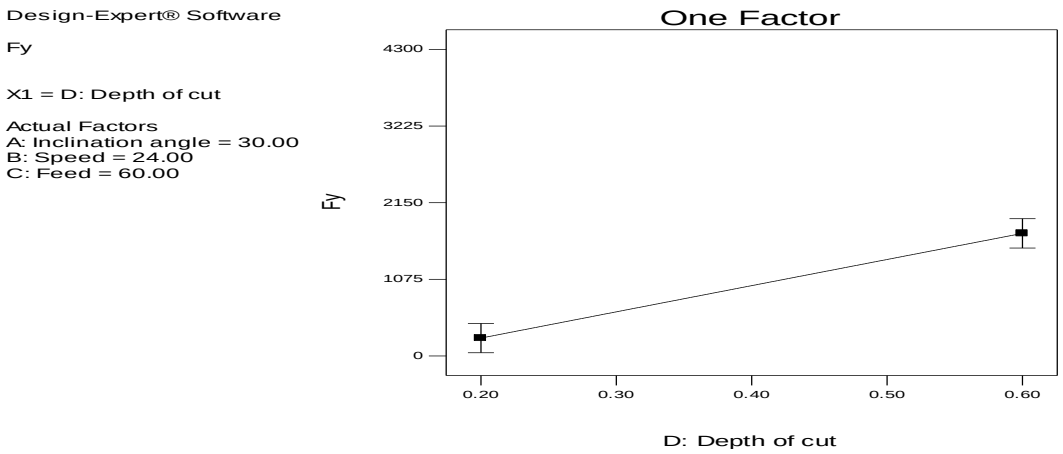

Fig: 5.1.2 (d) Effect of Depth of cut on cutting force (Fy)

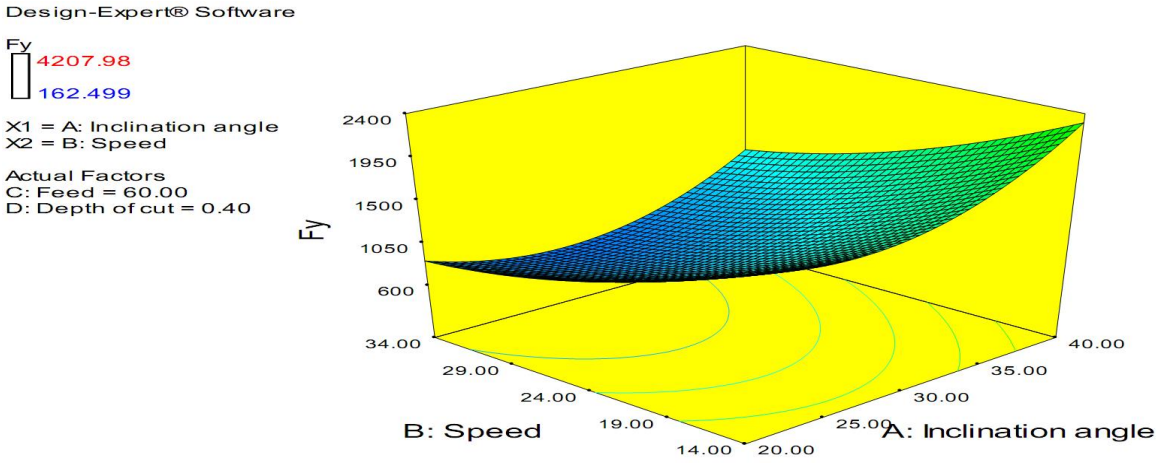

Fig: 5.1.2 (e) Response surface for Cutting force, cutting speed and Inclination Angle

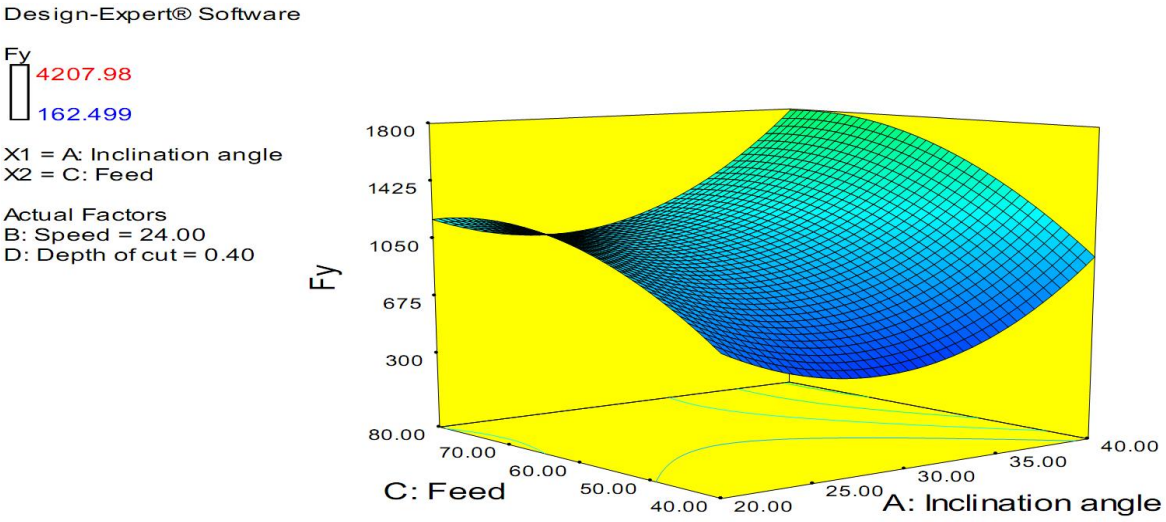

Fig: 5.1.2 (f) Response surface for Cutting force, Feed and Inclination Angle

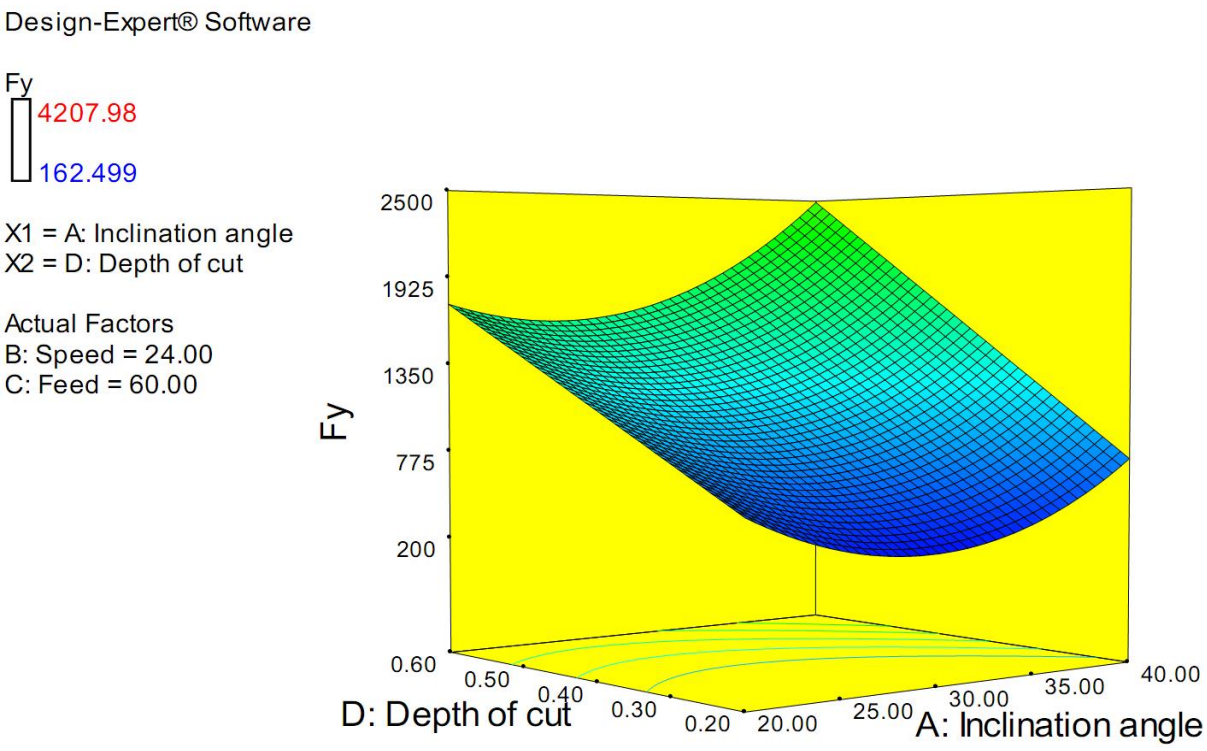

Fig: 5.1.2 (g) Response surface for Cutting force, Depth of cut and Inclination Angle

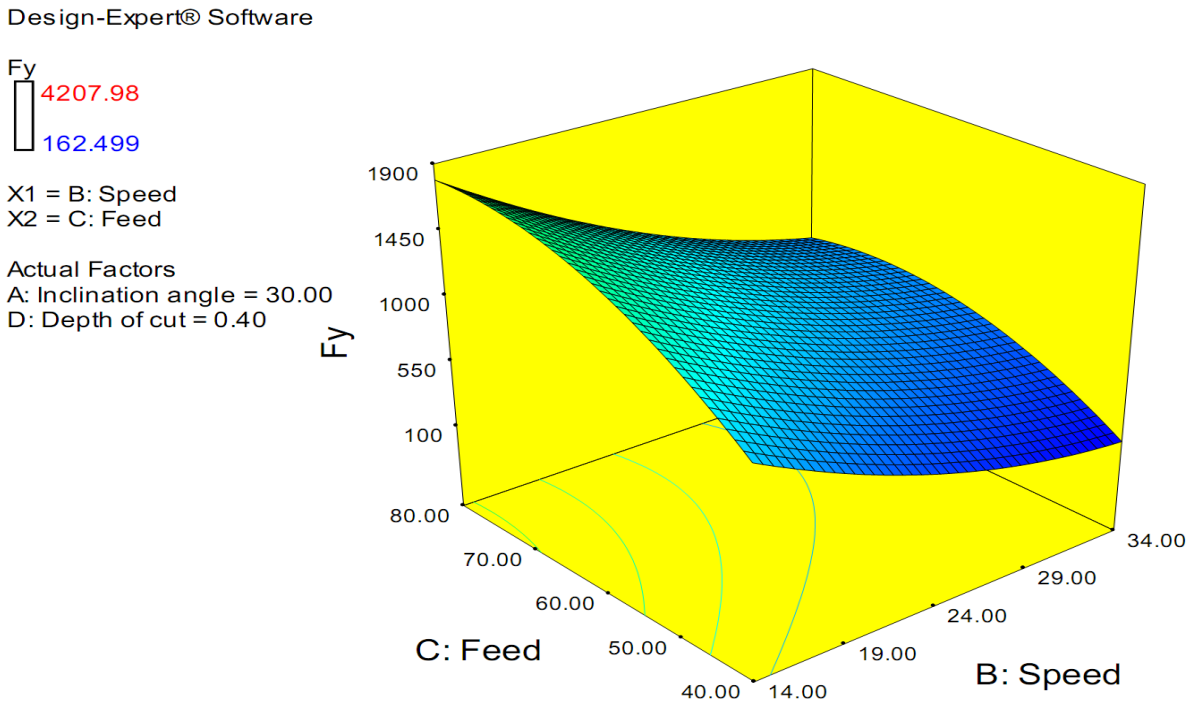

Fig: 5.1.2 (h) Response surface for Cutting force, Feed and Cutting speed

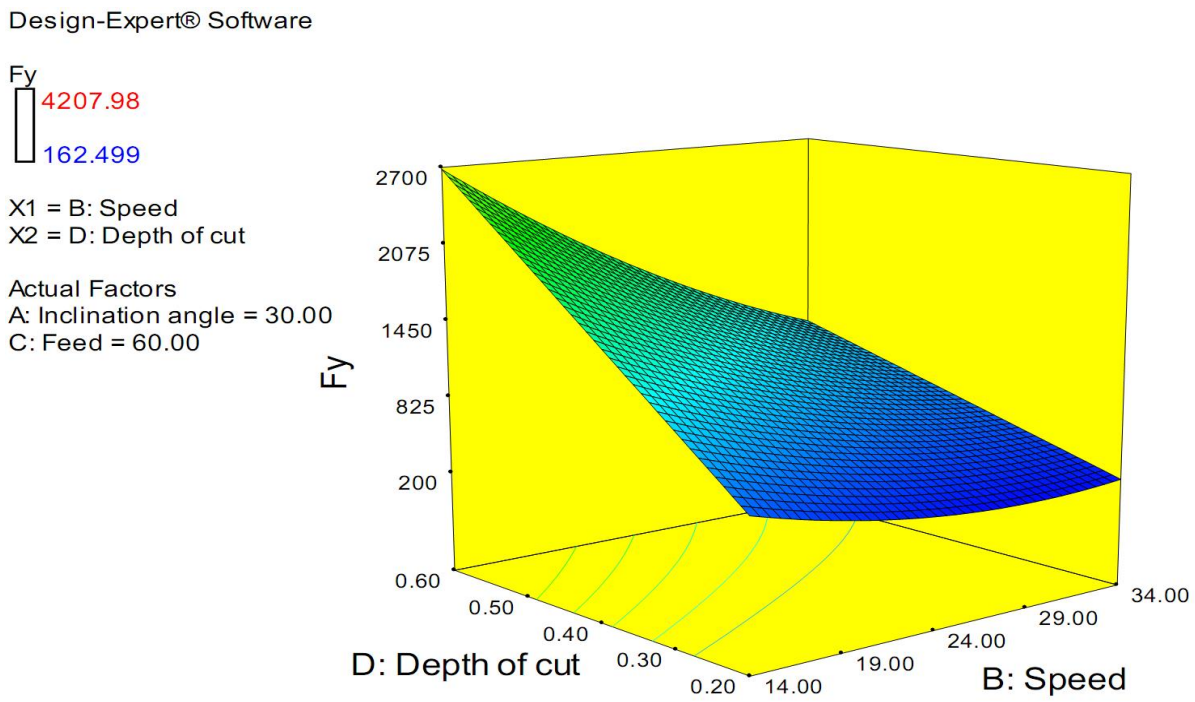

Fig: 5.1.2 (i) Response surface for Cutting force, Depth of cut and Speed

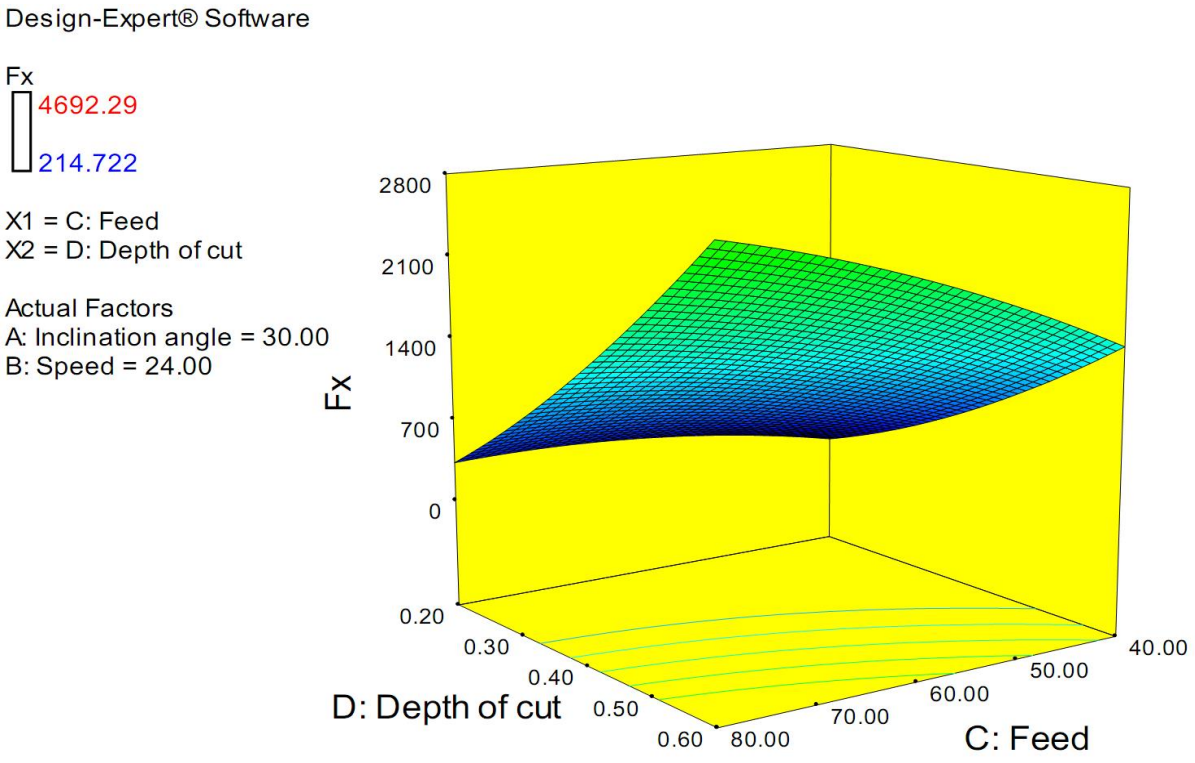

Fig: 5.1.2 (j) Response surface for Cutting force, Depth of cut and feed

5.1.3 Analysis of cutting forces (Fz)

Table: 5.6 ANOVA (Fz)

Source	Sum of Squares	df	Mean Square	F Value	p-value Prob > F	
Model	11990609	14	1332290	44.45267	< 0.0001	significant
A-Inclination angle	195729.4	1	195729.4	6.530631	0.0089	
B-Speed	3048761	1	3048761	101.7238	< 0.0001	
C-Feed	1325824	1	1325824	44.23693	< 0.0001	
D-Depth of cut	4932284	1	4932284	164.5687	< 0.0001	
AD	98497.85	1	98497.85	3.286441	0.0849	
BC	114402.5	1	114402.5	3.817108	0.0649	
BD	1358190	1	1358190	45.31684	< 0.0001	
CD	375238.3	1	375238.3	12.52006	0.0021	
A^2	541683	1	541683	18.07359	0.0004	
Residual	599419.5	20	29970.97			
Lack of Fit	599419.5	16	39961.3	1.27080	0.4352	not significant
Pure Error	215262.2488	5	25214.354			
Cor Total	12590029	30				

Table: 5.7 Pooled ANOVA (Fz)

Source	Sum of Squares	df	Mean Square	F Value	p-value Prob > F	% Contribution	
Model	11990609	14	1332290	44.45267	< 0.0001		significant
A-Inclination angle	195729.4	1	195729.4	6.530631	0.0089	15.35	
B-Speed	3048761	1	3048761	101.7238	< 0.0001	14.21	
C-Feed	1325824	1	1325824	44.23693	< 0.0001	10.53	
D-Depth of cut	4932284	1	4932284	164.5687	< 0.0001	29.17	
BD	1358190	1	1358190	45.31684	< 0.0001	10.78	
CD	375238.3	1	375238.3	12.52006	0.0021	2.98	
A^2	541683	1	541683	18.07359	0.0004	4.30	
Residual	599419.5	20	29970.97				
Lack of Fit	599419.5	16	39961.3	1.27080	0.4352		not significant
Pure Error	215262.2488	5	25214.354				
Cor Total	12590029	30					

R-Squared	0.952389
Adj R-Squared	0.930965
Pred R-Squared	0.893981

Fz = +876.86 *A -411.55 * B +271.40 * C +523.47 * D -291.35 * B * D +153.14 * C * D +274.29 * A2 (5.3)

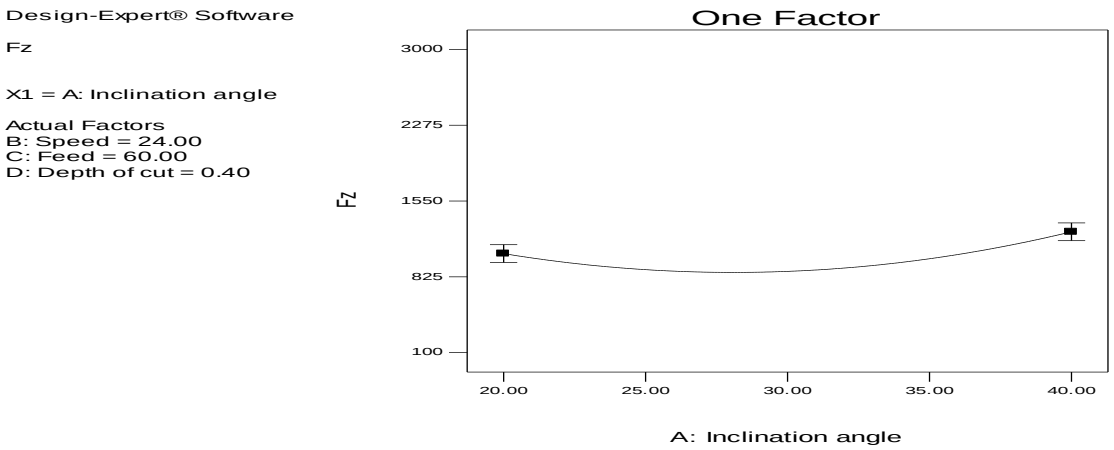

Fig: 5.1.3 (a) Effect of Inclination angle on cutting force (Fz)

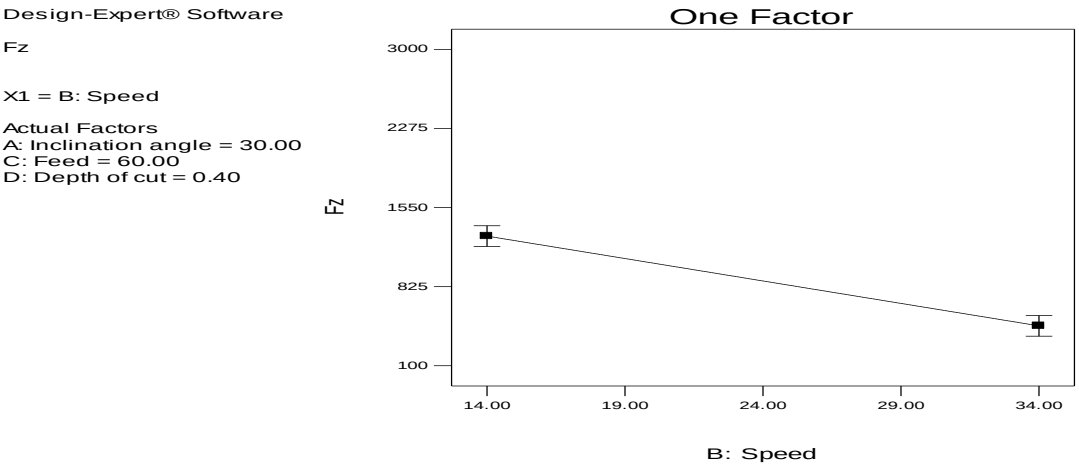

Fig: 5.1.3 (b) Effect of Cutting Speed on cutting force (Fz)

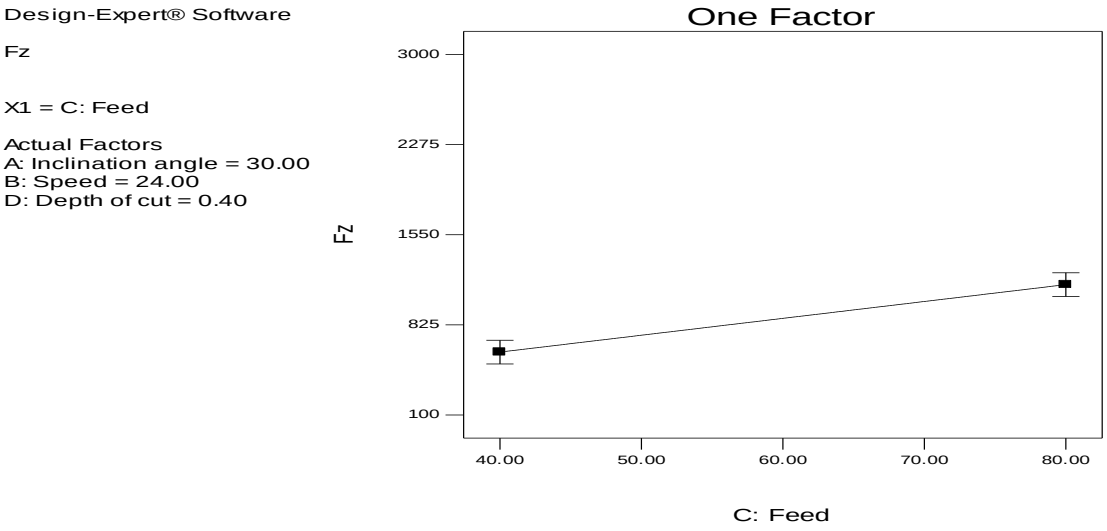

Fig: 5.1.3 (c) Effect of feed on cutting force (Fz)

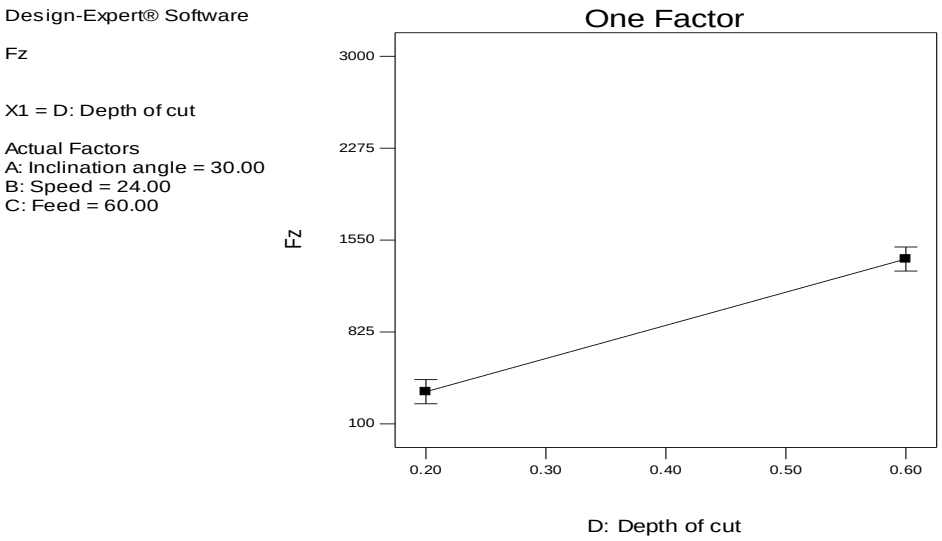

Fig: 5.1.3 (d) Effect of Depth of cut on cutting force (Fz)

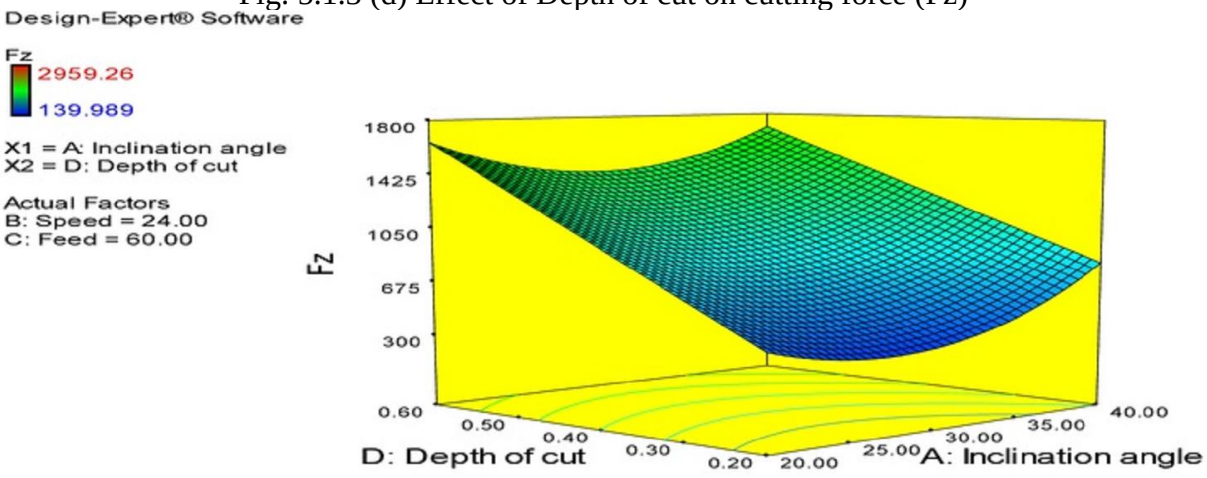

Fig: 5.1.3 (e) Response surface for Cutting force, Depth of cut and Inclination angle

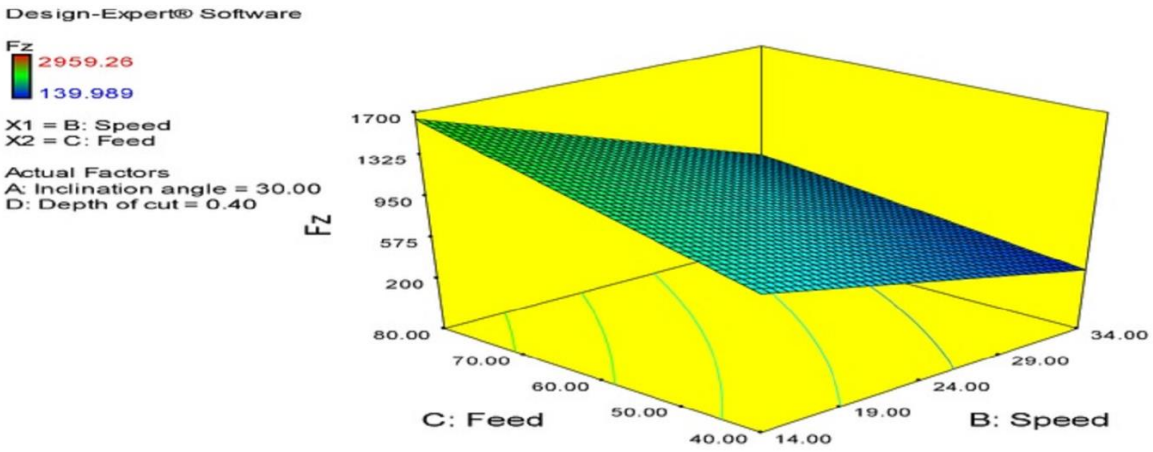

Fig: 5.1.3 (f) Response surface for Cutting force, feed and Speed

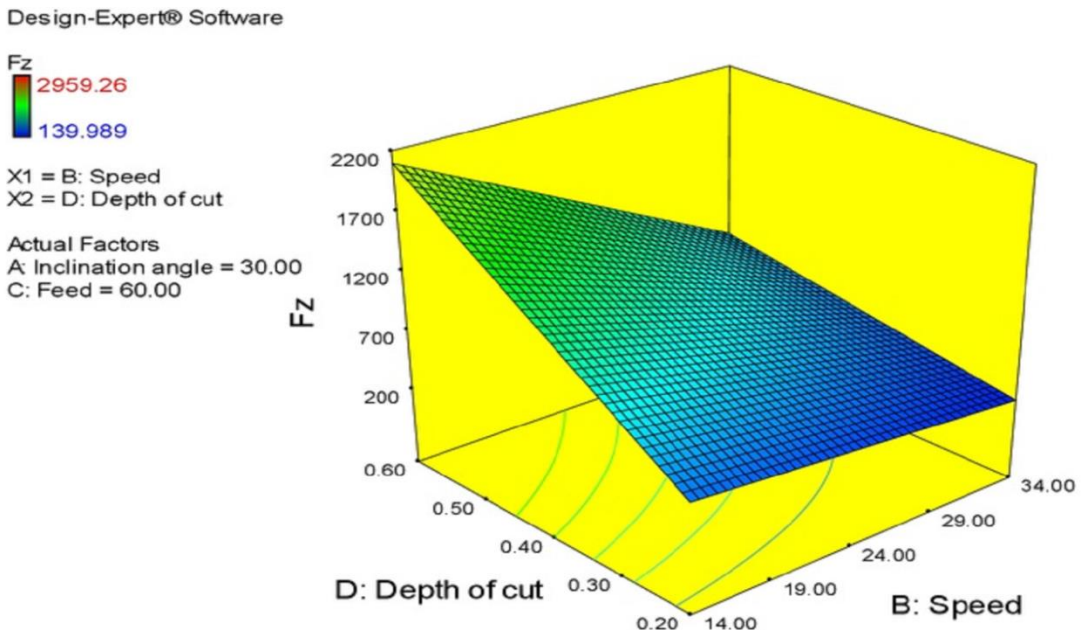

Fig: 5.1.3 (g) Response surface for Cutting force, Depth of cut and Cutting Speed

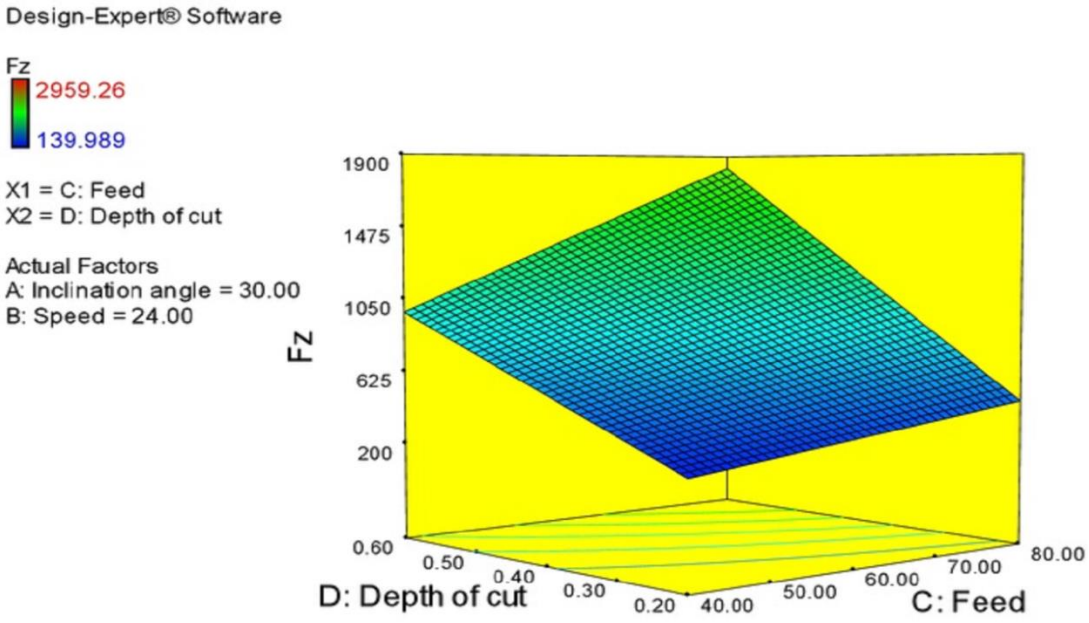

Fig: 5.1.3 (h) Response surface for Cutting force, Depth of cut and feed

The cutting forces values acquired are presented in the table 5.1 two factor interaction (2FI) model has been anticipated to develop which will take into account the linear and interaction influence beside the individual factors shown in tables5.2 , 5.4 and 5.6 (for Fx, Fy and Fz respectively). Tables 5.2, 5.4 and 5.6 present each of the estimated effects, along with their interactions and standard error. In this case B, C, D, BD, CD and $A^2$are significant model terms at

95% confidence interval for having P-values less than 0.05. By pooling some of the insignificant values (P-values greater than 0.005), a new ANOVA Table is formed which is shown in table 5.3, 5.5 and 5.7 (Pooled ANOVA). These tables comprise the P-values for the 2FI order model and lack of fit. It is observed in table 5.3, the models F -values are42.17, 38.08 and 44.45 which justifies that the models are significant for the prediction of cutting forces (Fx, Fy and Fz) for Inconel 625 alloy. There is 0.01% of chance that the model F-value of this occurred due to noise. The proposed cutting forces prediction model is shown by the following equations.

$$Fx = 1120.53 + 25.57 \times A - 655.03 * B + 377.46 * C + 967.39 * D + 29.64 * B * C - 80.58 * B * D - 54.95 * B * C - 520.77 * B * D + 187.04 * A^2 + 333.18 + 138.75 * A^2 \quad (5.1)$$

$$Fy = 985.90 + 237.06 * A - 483.39 * B + 336.00 * C + 734.52 * D - 331.37 * B * D + 197.88 * C * D + 402.05 * A^2 + 150 \quad (5.2)$$

$$Fz = +876.86 * A - 411.55 * B + 271.40 * C + 523.47 * D - 291.35 * B * D + 153.14 * C * D + 274.29 * A2 \quad (5.3)$$

where, A = Speed, V m/min;
B = feed, f mm/rev and,
C = depth of cut, mm.

The effect of inclination angle and process variables on cutting forces is shown in figures 5.1.1(a) –5.1.1 (d) for Fx, figures 5.1.2 (a) – 5.1.2 (d) for Fy and 5.1.3 (a) – 5.1.3 (d) for Fz. It is known from the fundamental theory of machining that the feed rate and depth of cut play an important role in cutting forces (Fx, Fy, and Fz) of the machining process. From figure 5.1.1(a) –5.1.1 (d), 5.1.2 (a) – 5.1.2 (d) and 5.1.3 (a) – 5.1.3 (d) we observe that cutting forces decrease with increase in inclination angle from 20^o to 30^o. This could be due to improper rotation of insert at lower inclination angles. The cutting force has slight variation with increase in inclination angle from 30^0 to 40^o. The cutting force increases with increase in feed rate. This may be due to an increase in cross-sectional area of uncut chip. As the depth of cut increases, the cutting forces also increase. This may be due to an increase in the area of undeformed chip cross-section with increase in depth of cut. It is observed that the cutting force decrease with increase in cutting speed to a certain extent. It may be due to thermal softening effect at high temperature as the cutting temperature increases with increase in velocity. Figures 5.1.1(e) – 5.1.1(j), 5.1.2 (e) – 5.1.2 (j) and 5.1.3 (a) – 5.1.3 (h) are showing three dimensional trends and the effects are explained above.

5.1.4 Analysis of Surface Roughness

Table: 5.8 ANOVA (Surface Roughness)

Source	Sum of Squares	df	Mean Square	F Value	p-value Prob > F	
Model	2.458757	14	0.175626	4.144854	<0.0049	significant
A-Inclination angle	0.13005	1	0.13005	3.069248	0.0052	
B-Speed	0.3362	1	0.3362	7.934495	0.0030	
C-Feed	0.121689	1	0.121689	2.871921	< 0.0001	
D-Depth of cut	0.853689	1	0.853689	20.1475	< 0.0001	
AB	0.0016	1	0.0016	0.037761	0.8485	
AC	0.0025	1	0.0025	0.059001	0.0014	
AD	0.005625	1	0.005625	0.132753	0.7207	
BC	0.000225	1	0.000225	0.00531	0.9429	
BD	0.0441	1	0.0441	1.040783	0.0038	
CD	0.1296	1	0.1296	3.058627	0.1007	
A^2	0.060706	1	0.060706	1.432699	0.2499	
B^2	0.002041	1	0.002041	0.04818	0.8292	
C^2	0.049391	1	0.049391	1.165664	0.2973	
D^2	0.008737	1	0.008737	0.206196	0.6563	
Residual	0.635579	16	0.042372			
Lack of Fit	0.635579	10	0.063558	2.0608505	0.2517	not significant
Pure Error	0.538552	5	0.043655			
Cor Total	3.094337	30				

Table: 5.9 Pooled ANOVA (Surface Roughness)

Source	Sum of Squares	df	Mean Square	F Value	p-value Prob > F	% Contribution	
Model	2.458757	14	0.175626	4.144854	<0.0049		significant
A-Inclination angle	0.13005	1	0.13005	3.069248	0.0052	3.17	
B-Speed	0.3362	1	0.3362	7.934495	<0.0030	8.22	
C-Feed	0.121689	1	0.121689	2.871921	< 0.0001	2.97	
D-Depth of cut	0.853689	1	0.853689	20.1475	< 0.0001	20.85	
AC	0.0525	1	0.0525	0.059001	0.0014	12.83	
BD	0.0441	1	0.0441	1.040783	0.0038	10.75	
Residual	0.635579	16	0.042372				
Lack of Fit	0.635579	10	0.063558	2.0608505	0.2517		not significant
Pure Error	0.538552	5	0.043655				
Cor Total	4.094337	30					

R-Squared	0.945992
Adj R-Squared	0.910289
Pred R-Squared	0.907241

Surface roughness = 1.78 +0.085 * A +0.14 * B +0.082 * C +0.22 * D -0.013 * A * C +0.052 * B * D (5.4)

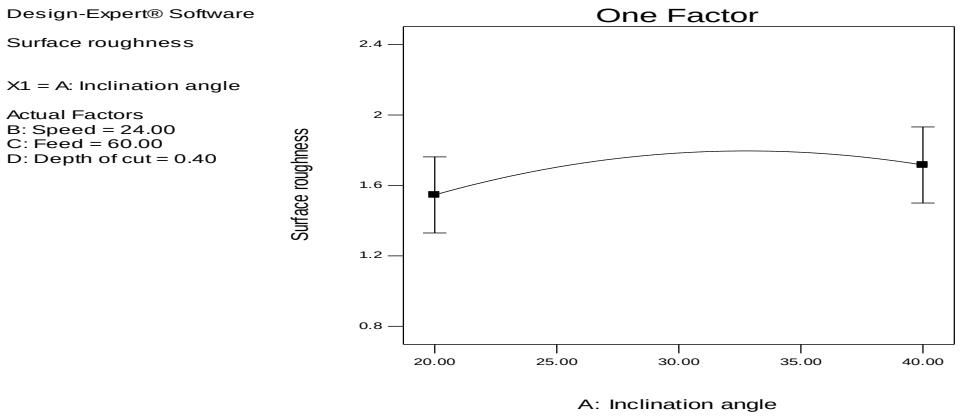

Fig: 5.1.4 (a) Effect of Inclination angle on Surface roughness

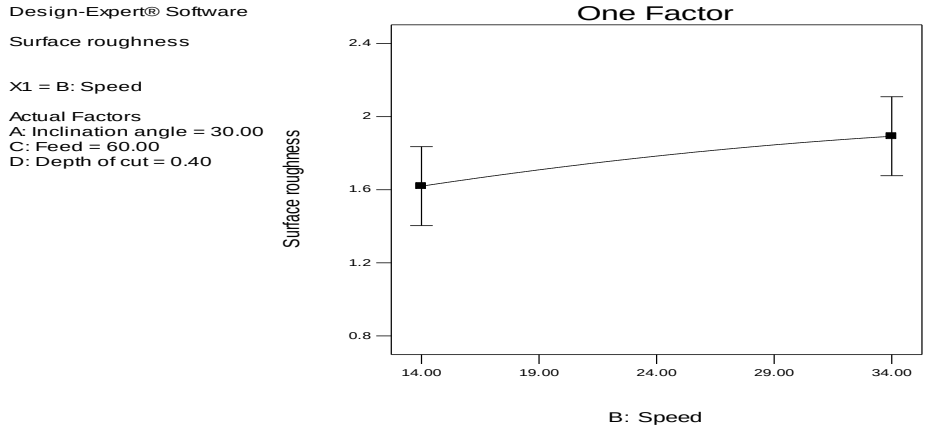

Fig: 5.1.4 (b) Effect of Cutting Speed on Surface roughness

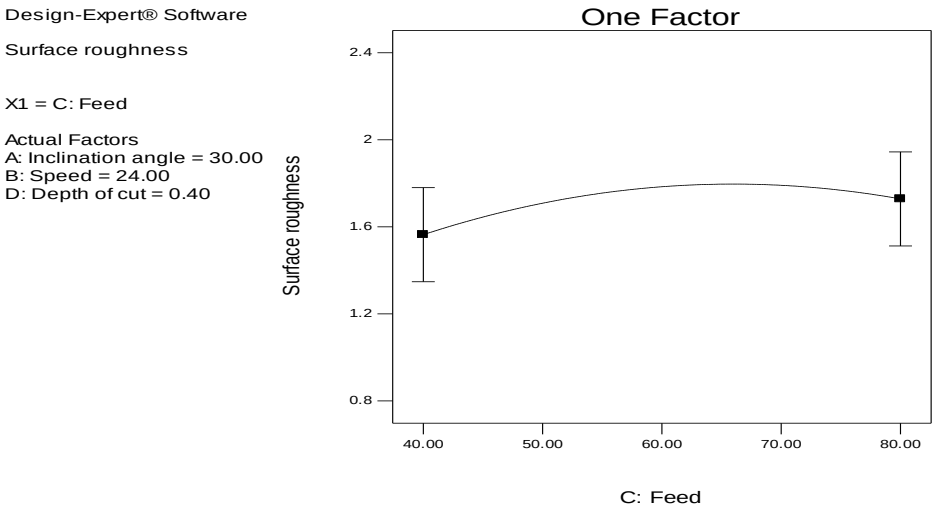

Fig: 5.1.4 (c) Effect of Feed on Surface roughness

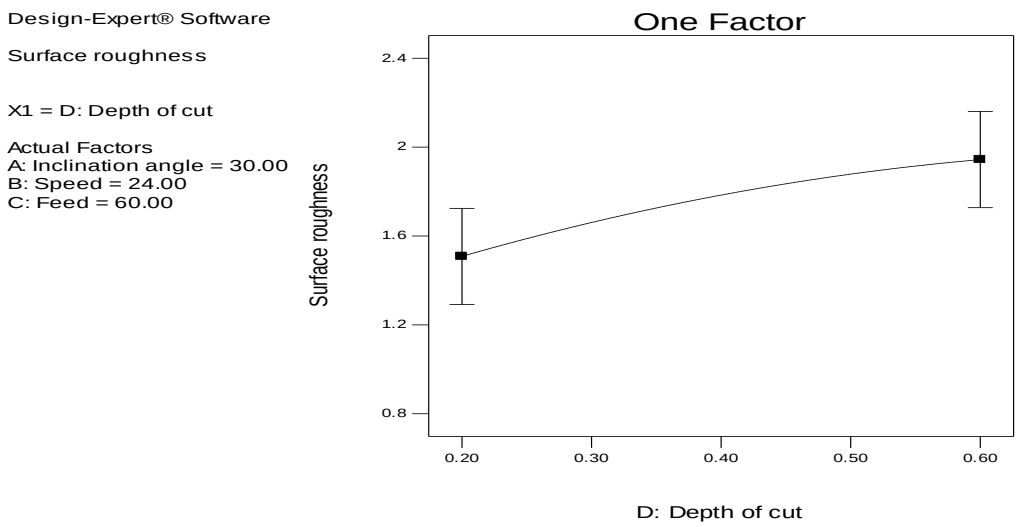

Fig: 5.1.4 (d) Effect of Depth of cut on Surface roughness

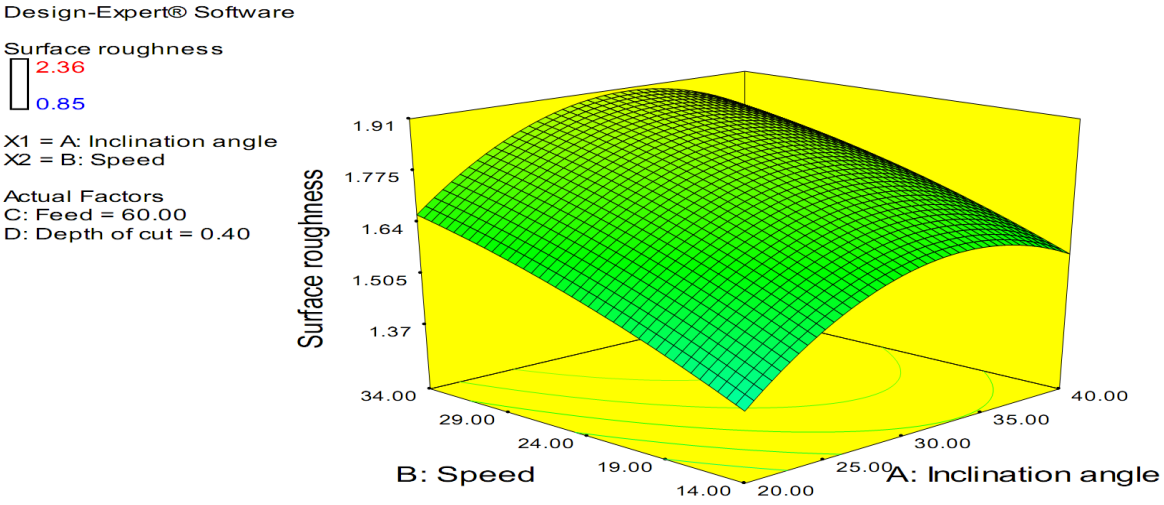

Fig: 5.1.4 (e) Response surface for Surface Roughness, Cutting speed and Inclination angle

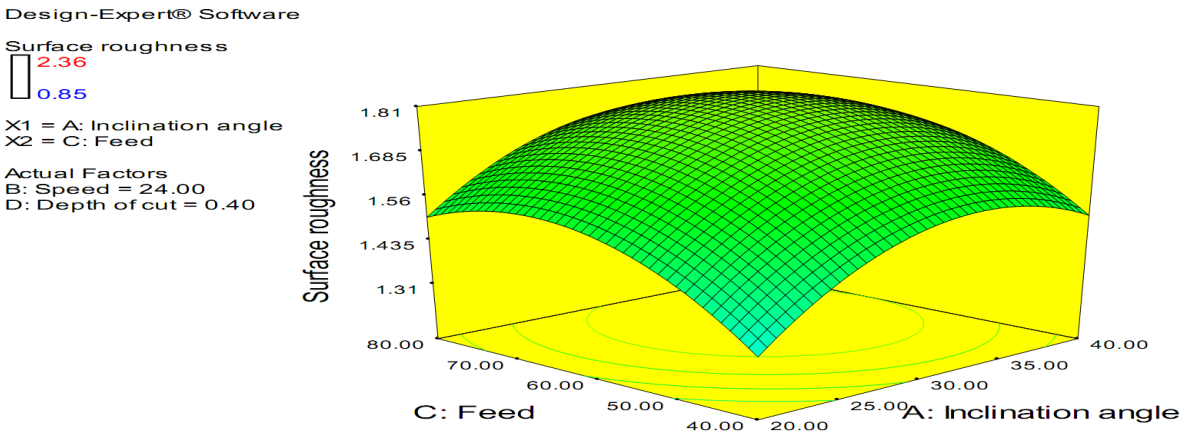

Fig: 5.1.4 (f) Response surface for Surface Roughness, Feed and Inclination angle

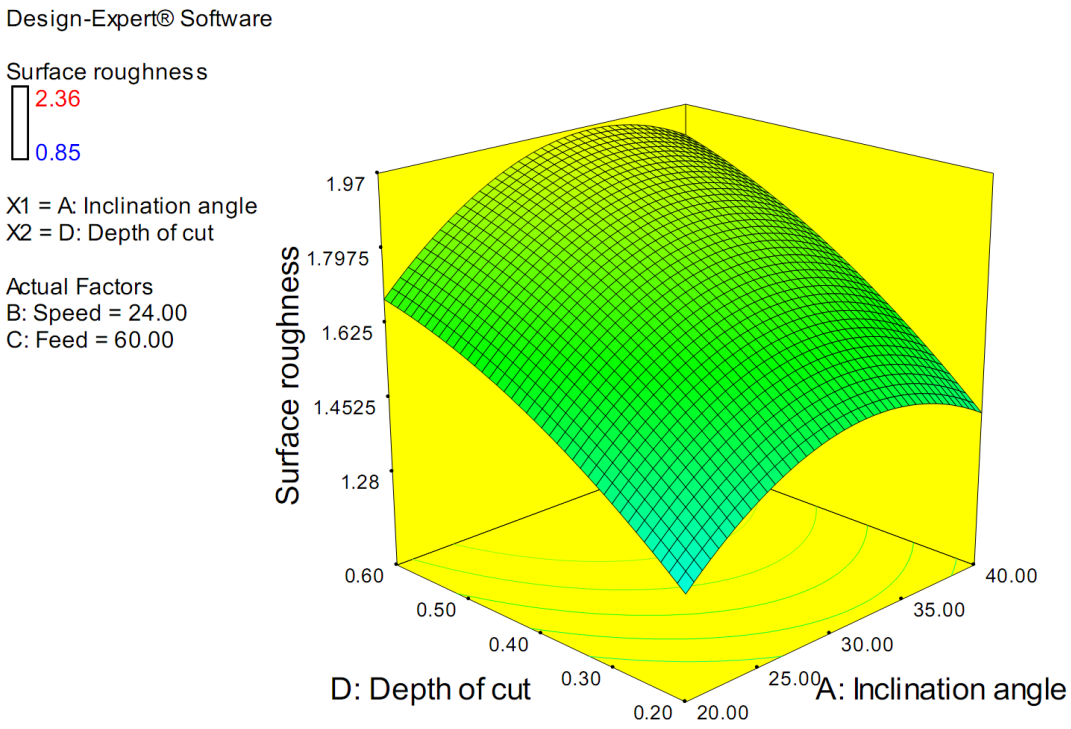

Fig: 5.1.4 (g) Response surface for Surface Roughness, Depth of cut and Inclination angle

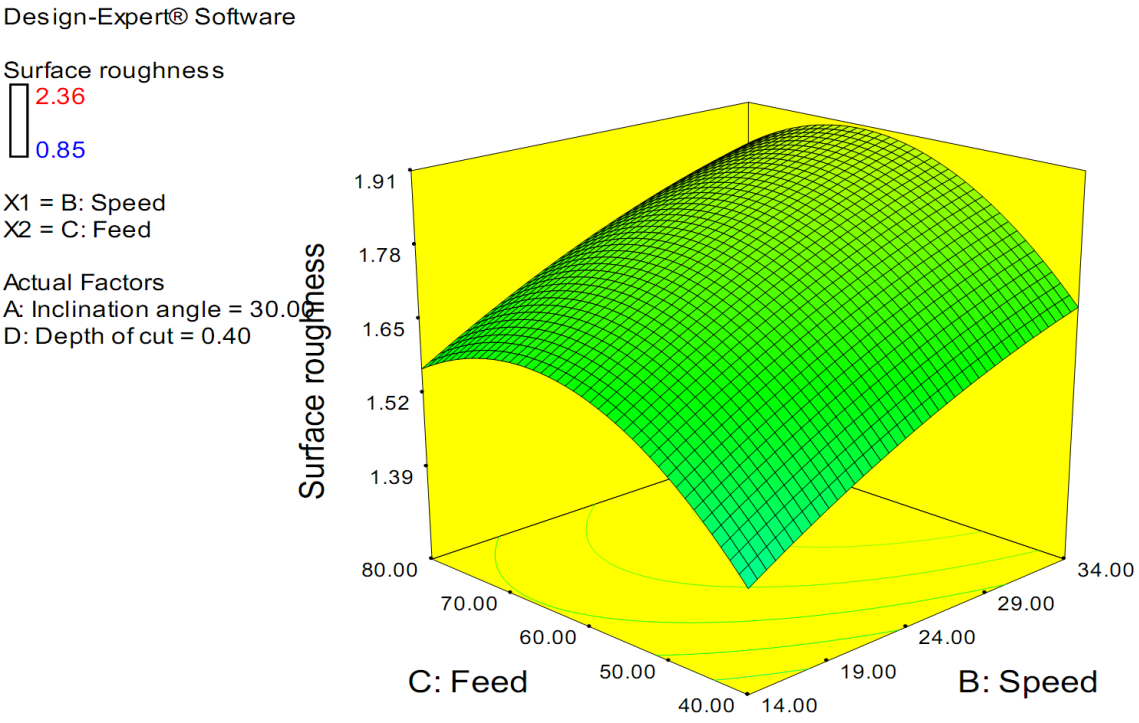

Fig: 5.1.4 (h) Response surface for Surface Roughness, Feed and Cutting speed

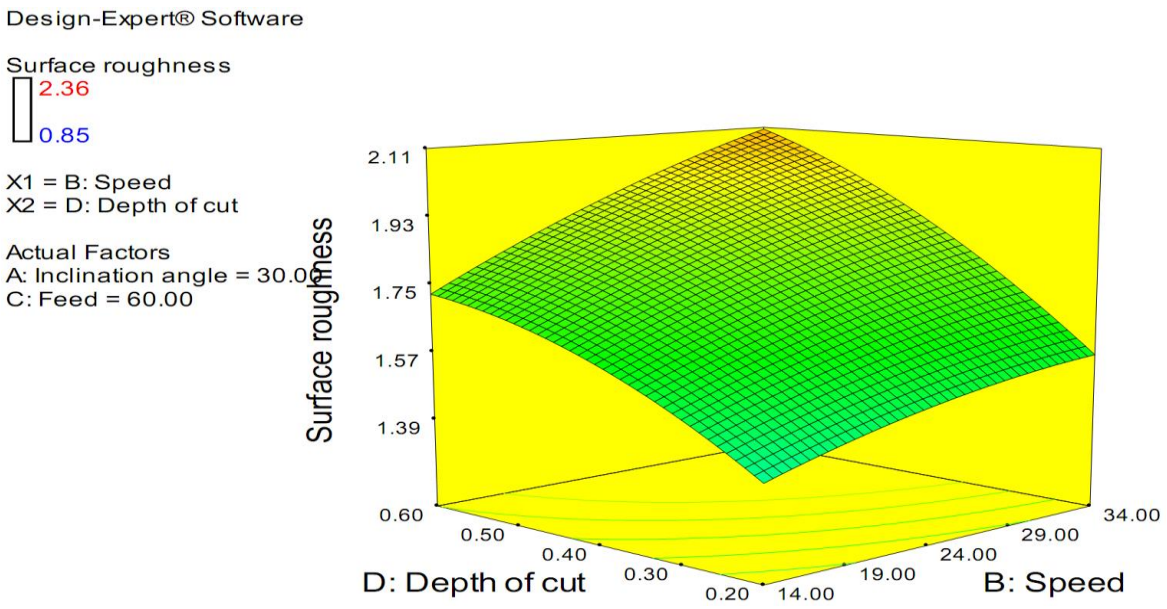

Fig: 5.1.4 (i) Response surface for Surface Roughness, Depth of cut and cutting Speed

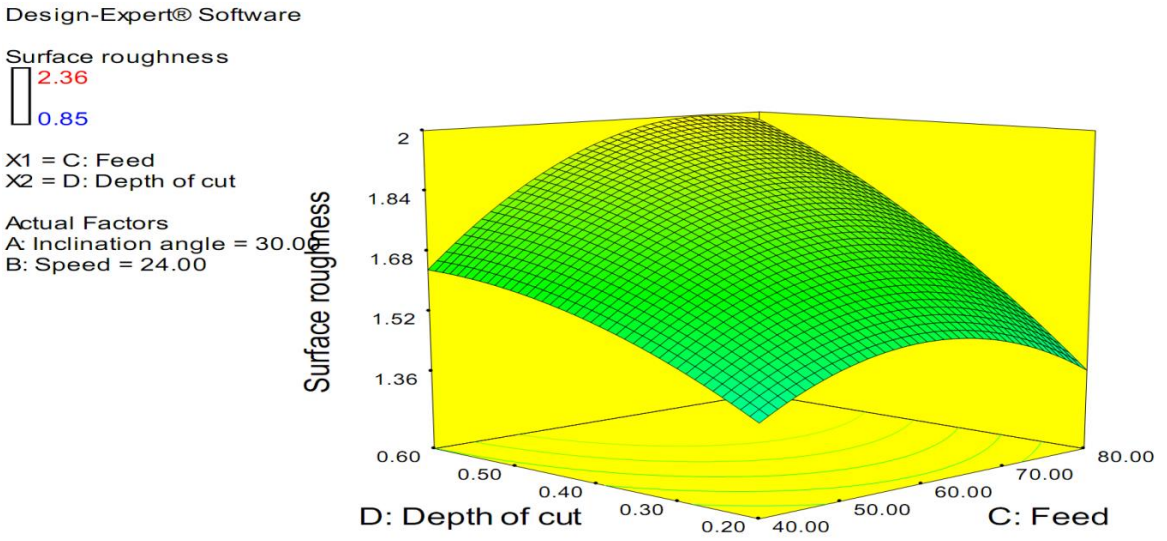

Fig: 5.1.4 (j) Response surface for Surface Roughness, Depth of cut and cutting Feed

The surface roughness values obtained are presented in table 5.1. A model of quadratic has been anticipated to develop which will be taken into account the quadratic and interaction influence with the individual factors shown in table 5.8. Table 5.8 presents each of the expected influence, through their interactions and standard error. The ANOVA table checks the numerical significance of each effect by comparing the mean square against an estimate of the experimental error [**J.Vivancos, 2005**]. In this case A, B, C, D, AC and BD are significant model terms at 95% confidence interval for having P-values less than 0.005. By pooling some of the insignificant

values (P-values greater than 0.005), a new ANOVA table is formed which is shown in table 5.9. This table comprises the P-values for the quadratic order model and lack of fit. This model F value is 4.14, which justifies that the model is significant for the prediction of surface roughness for Inconel 625 alloy. There is 0.01% chance that the model F-value may not be significant as this may be due to noise. The lack of fit test represents is the selected model is sufficient to explain the experimental data or a more complex model is required to be used. This test is conducted by evaluating the unpredictability of the present model residuals to the variability among the observations at replicate settings of the factors. Since the P-value for lack of fit in ANOVA table is greater than 0.005, the model is to be adequate for the experimental data. The proposed surface roughness prediction model is shown by

Surface Roughness (Ra) = 1.78 +0.085 * A +0.14 * B +0.082 * C +0.22 * D -0.013 * A * C +0.052 * B * D (5.4)

Where, A = Speed, V m/min;

B = feed, f mm/rev and,

C = depth of cut, mm.

The response surfaces are also plotted to study the effect of process variables on the surface roughness and as shown in figures 5.1.4 (a) – 5.1.4(d). It is known from the fundamental theory of machining that the feed rate and nose radius play an important role in roughness of the machined surface when the cutting edge is sharp, as given by:

$$Ra = \frac{f^2}{32r} \quad (5.5)$$

Where, f is feed rate and r is nose radius.

From the figures5.1.4 (a) – 5.1.4(d) that the surface roughness has an increasing trend with increase in inclination angle, feed cutting speed and depth of cut. Sometimes the reduction is occurred in surface roughness due to the increase in speed, because if the temperature of the cutting zone increases, it will leads to make the work piece little ductile and continuous chips are produced, and the speed may cause premature tool wear, breakages and tool chatter, all of such factors may lead to poor surface finish. Figures 5.1.4(e) – 5.1.1(j) are showing three dimensional trends and the effects are explained above.

5.1.5 Analysis of Cutting Temperature

Table: 5.10 ANOVA (Temperature)

Source	Sum of Squares	df	Mean Square	F Value	p-value Prob > F	
Model	3181.983	14	244.7679	3.394335	0.0115	significant
A-Inclination angle	61.605	1	61.605	0.854311	0.0031	
B-Speed	1.227222	1	1.227222	0.017019	< 0.0001	
C-Feed	34.445	1	34.445	0.477668	< 0.0001	
D-Depth of cut	2119.005	1	2119.005	29.38544	< 0.0001	
AB	19.8025	1	19.8025	0.274612	0.6074	
AC	97.0225	1	97.0225	1.345466	0.2631	
AD	7.0225	1	7.0225	0.097385	0.0040	
BD	152.5225	1	152.5225	2.115116	0.0032	
A^2	3.761617	1	3.761617	0.052164	0.8222	
C^2	275.4823	1	275.4823	3.820268	0.0683	
D^2	207.4616	1	207.4616	2.876988	0.1092	
ABD	0.0625	1	0.0625	0.000867	0.9769	
AC^2	2.200278	1	2.200278	0.030512	0.8635	
Residual	1153.771	16	72.11071			
Lack of Fit	1153.771	11	104.8883	1.5932306	0.3437	not significant
Pure Error	152.5225	5	152.5225			
Cor Total	4335.755	30				

Table: 5.11 Pooled ANOVA (Temperature)

Source	Sum of Squares	df	Mean Square	F Value	p-value Prob > F	% Contribution	
Model	3181.983	14	244.7679	3.394335	0.0115		significant
A-Inclination angle	61.605	1	61.605	0.854311	0.0031	1.42	
B-Speed	122.7222	1	122.7222	0.017019	< 0.0001	2.81	
C-Feed	134.445	1	134.445	0.477668	< 0.0001	3.09	
D-Depth of cut	2119.005	1	2119.005	29.38544	< 0.0001	48.88	
AD	157.0225	1	157.0225	0.097385	0.0040	3.65	
BD	152.5225	1	152.5225	2.115116	0.0032	3.53	
ABD	625.325	1	625.325	0.000867	0.9769	14.41	
Residual	1153.771	16	72.11071				
Lack of Fit	1153.771	11	104.8883	1.5932306	0.3437		not significant
Pure Error	152.5225	5	152.5225				
Cor Total	4335.755	30					

R-Squared	0.933894
Adj R-Squared	0.907682
Pred R-Squared	0.915926

Temperature = 152.37 +5.55 * A -0.26 * B -4.85 * C +11.55 * D -0.66 * A * D +3.09 * B * D +0.062 * A * B * D (5.6)

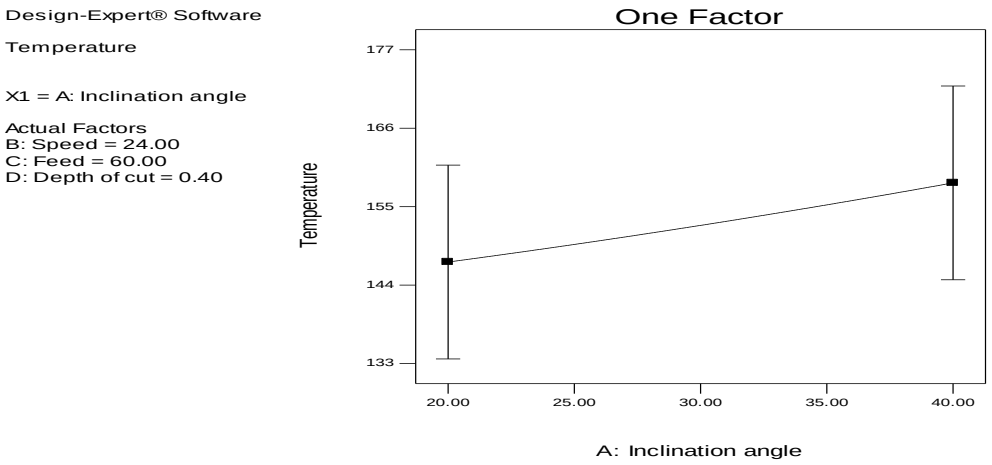

Fig: 5.1.5 (a) Effect of Inclination angle on Cutting Temperature

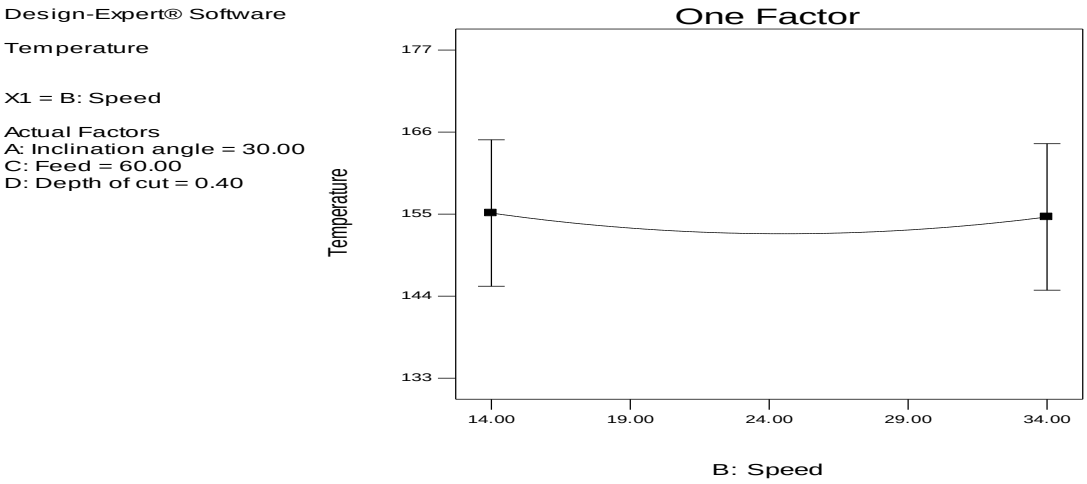

Fig: 5.1.5 (b) Effect of Cutting Speed on Cutting Temperature

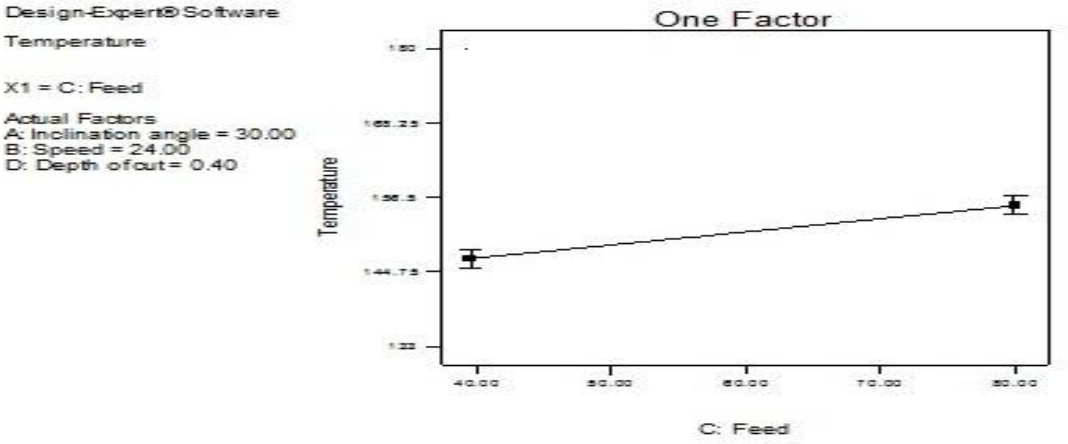

Fig: 5.1.5 (c) Effect of Feed on Cutting Temperature

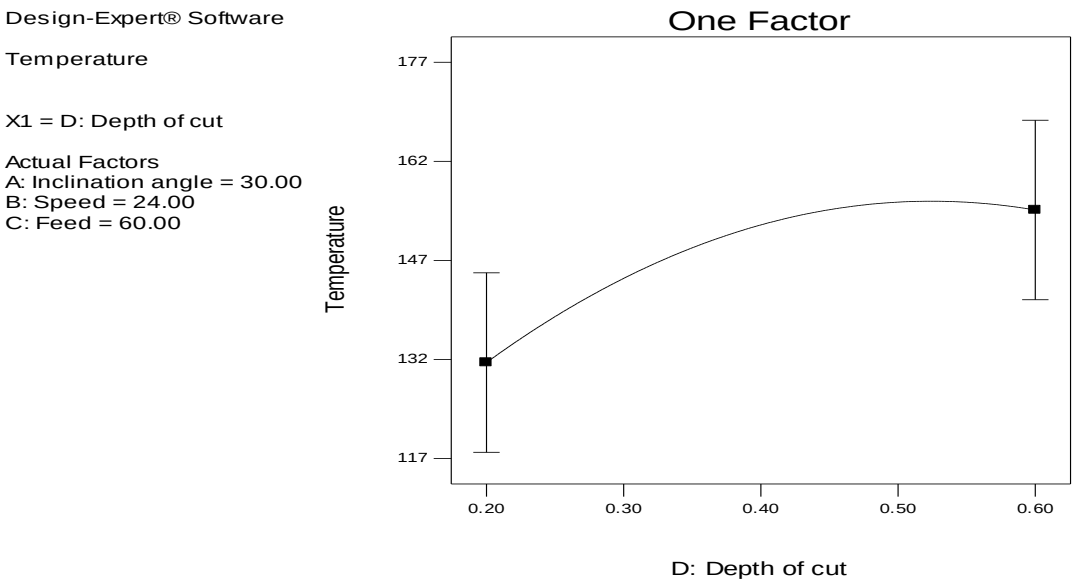

Fig: 5.1.5 (d) Effect of Depth of cut on Cutting Temperature

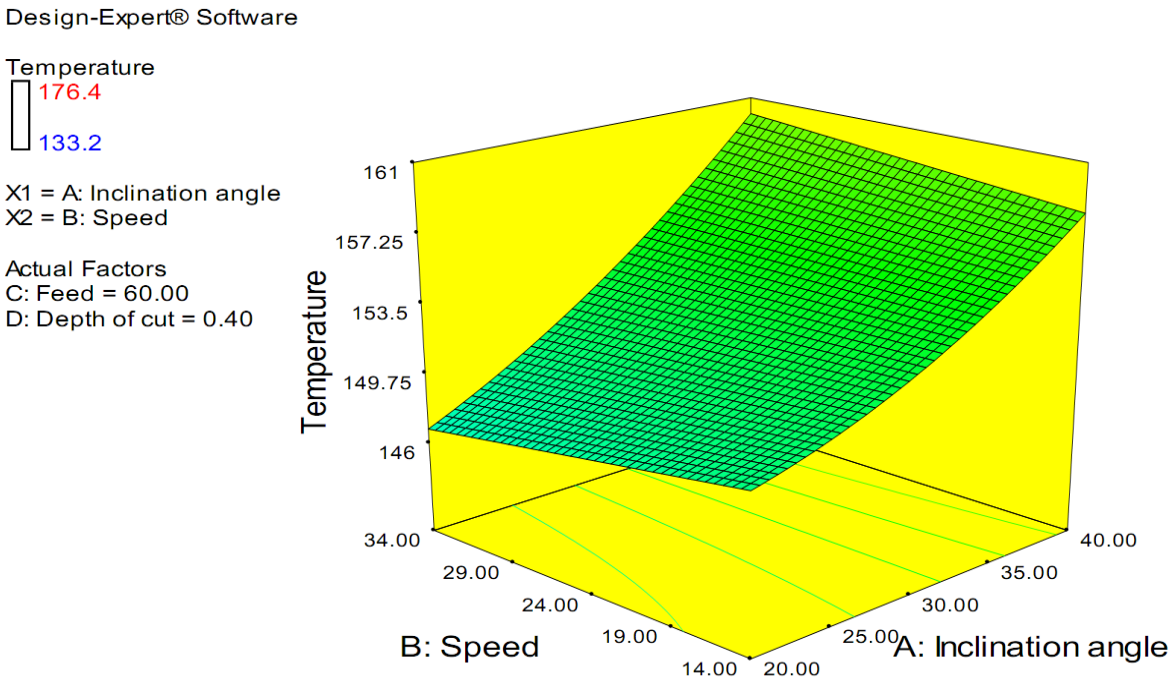

Fig: 5.1.5 (e) Response surface for Cutting Temperature, Cutting Speed and Inclination angle

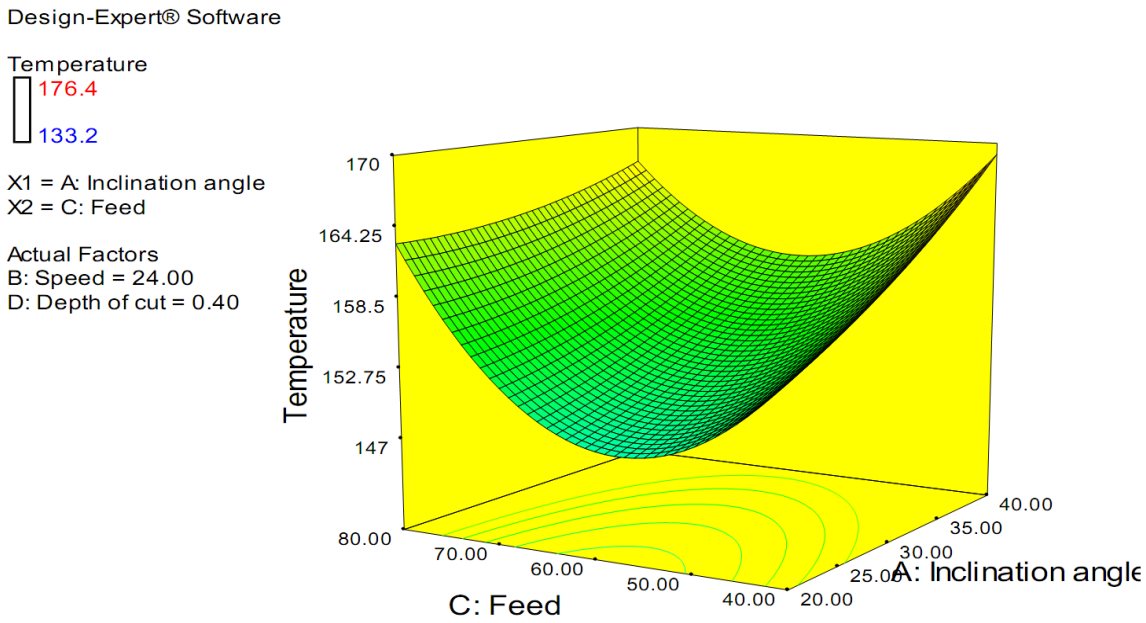

Fig: 5.1.5 (f) Response surface for Cutting Temperature, Feed and Inclination angle

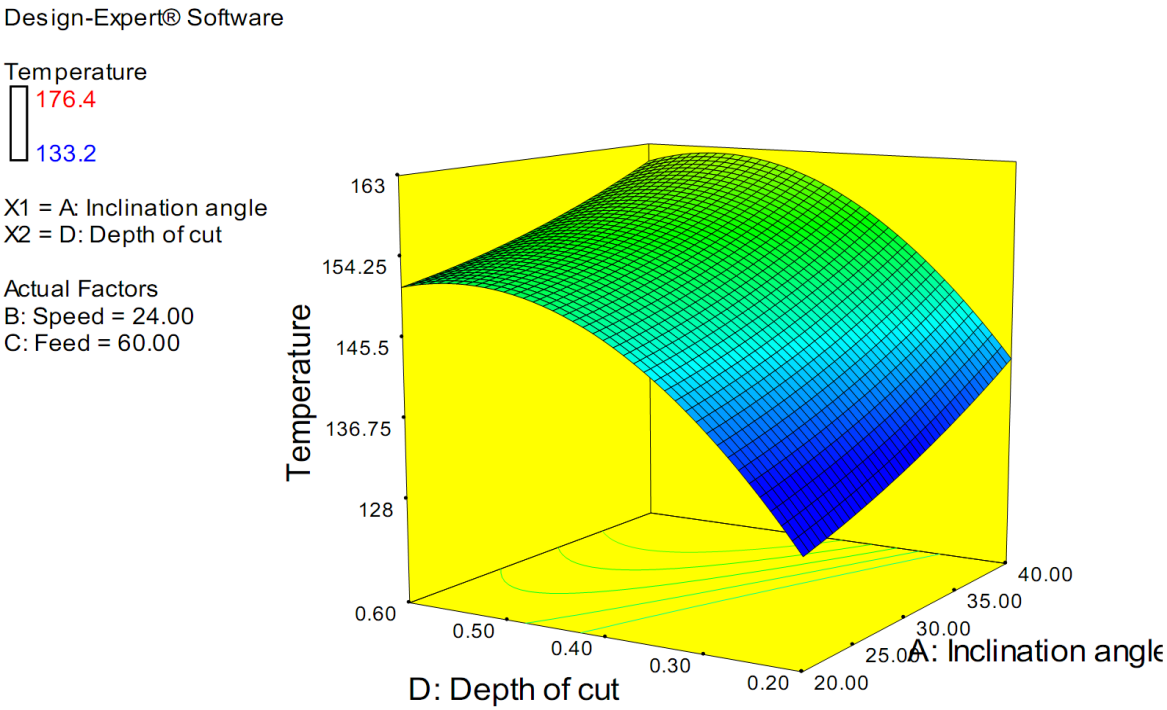

Fig: 5.1.5 (g) Response surface for Cutting Temperature, Depth of cut and Inclination angle

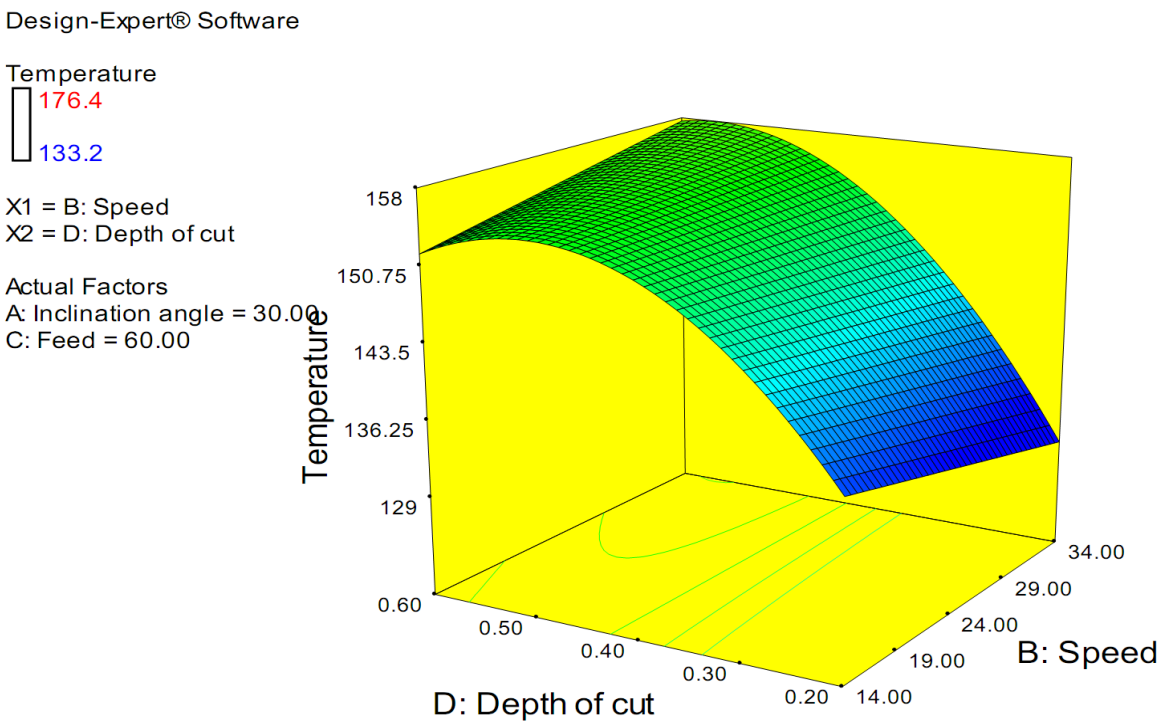

Fig: 5.1.5 (h) Response surface for Cutting Temperature, Depth of cut and Cutting Speed

The cutting temperature values obtained are presented in the table 5.1. Two factor interaction (2FI) models have been planned to develop which will take into account the linear and interaction influence beside the individual factors shown in table 5.10. Here A, B, C, D, AD and BD are significant model terms shown in table 5.10 at 95% confidence interval for having P-values less than 0.05. By pooling some of the insignificant values (P-values greater than 0.005), a new ANOVA Table is formed which is shown in Table 3.11. This Table comprises the P-values for the 2FI order model and lack of fit. It is seen from the Table, the models F value is 3.39, which justifies that the model is significant for the prediction of cutting forces for Inconel 625 alloy. There is 0.01% of chance that the model F-value is not significant this may be due to noise. Since the P-value for lack of fit in ANOVA Table is greater than 0.005, the model appears to be adequate for the observed data. The proposed cutting temperature prediction model is shown by

Temperature = 152.37 +5.55 * A -0.26 * B -4.85 * C +11.55 * D -0.66 * A * D +3.09 * B * D +0.062 * A * B * D (5.6)

Where, A = Speed, V m/min;
B = feed, f mm/rev and,
C = depth of cut, mm.

It is known from the fundamental theory of machining that the Cutting Speed plays an important role in cutting temperature of the machining process. The higher the cutting speed, the faster the surface feed that the tool travels and thus more heat is generated by friction. As cutting speed increases, there is less time for the heat generated to be dissipated and hence the temperature may also increase. The figures 5.1.5(a) – 5.1.5 (d) shows the increase in cutting temperature while increasing of inclination angle, cutting speed, feed and depth of cut. The same trend shows in figures 5.1.5 (e) – 5.1.5 (h) with three dimensional ways.

5.2. Multi Objective Optimization

Objective Functions:
Minimization of Fx, Fy, Fz, Ra and Temperature
Constraints: 20 < Inclination Angle < 50
14 < Cutting speed < 34
40 < Feed < 80
0.2 < Depth of cut < 0.6

Table: 5.12 Optimized values

No.	Incl. angle	Speed	Feed	DOC	Fx	Fy	Fz	Temp	Surface roughness	Desirability	
1	*20.84*	*20.77*	*40*	*0.2*	*214.1067*	*201.6004*	*309.4653*	*133.3198*	*1.142958*	*0.94361759*	*Selected*
2	20.61	21.95	40	0.2	184.7713	212.516	320.4326	133.1998	1.151163	0.941569511	
3	20.34	18.29	40	0.2	358.745	275.9309	335.0813	133.1995	1.093978	0.940056983	
4	20.1	18.03	40	0.2	384.5396	298.8346	345.1113	132.9671	1.081706	0.938930477	
5	20.69	25.93	40	0.2	84.66709	188.9449	295.9008	133.0661	1.1896	0.93834034	
6	20.74	26.28	40.1	0.2	81.72683	187.987	293.3202	133.1994	1.195128	0.937678623	
7	20.35	28.22	40	0.2	89.45285	230.0715	299.2995	132.9632	1.19541	0.935241661	
8	20	29.96	40	0.2	116.9858	279.7677	305.3959	132.8923	1.194531	0.932605771	
9	20.02	30.54	40	0.2	127.7266	288.1041	302.681	133.2	1.198845	0.931708881	
10	20	31.16	40.3	0.2	146.9458	308.3254	302.0592	133.1998	1.205969	0.92964436	

Table 5.13 Full factorial experimentation results for cutting forces, surface roughness and cutting temperature (rotary face milling operation)

Exp No.	Inclination angle (Deg)	Speed (m/min)	Feed (mm/min)	Depth of cut (mm)	F_X (N)	F_Y (N)	F_Z (N)	Ra µm	Temp ºC
1	20	14	40	0.2	689.83	2054.65	2771.34	1.92	132.9
2	20	14	40	0.4	681.87	1802.44	1952.17	1.48	142.5
3	20	14	40	0.6	740.45	1844.71	1862.44	1.82	167.3
4	20	14	60	0.2	796.31	2850.70	3785.98	2.12	146.4
5	20	14	60	0.4	797.40	2528.48	2462.23	1.69	151.3
6	20	14	60	0.6	812.87	2428.24	2275.98	2.02	187.2
7	20	14	80	0.2	948.00	3298.14	4692.28	2.58	152.2
8	20	14	80	0.4	944.04	2977.25	3260.26	1.86	166.9
9	20	14	80	0.6	979.01	2864.72	2959.26	2.30	199.8
10	20	24	40	0.2	776.62	1428.4	1748.96	1.71	154.2
11	20	24	40	0.4	668.17	1213.65	1528.61	1.45	153.5
12	20	24	40	0.6	669.21	1184.57	1466.65	1.92	174.3
13	20	24	60	0.2	1101.13	1663.30	2359.29	1.85	160.2
14	20	24	60	0.4	856.81	1652.72	1890.43	1.58	162.2
15	20	24	60	0.6	778.12	1509.60	1749.29	2.13	183.5
16	20	24	80	0.2	1237.21	2474.91	3151.16	2.15	173.2
17	20	24	80	0.4	1038.96	2304.90	2486.72	1.65	179.2
18	20	24	80	0.6	952.21	2220.12	2114.69	2.23	198.2
19	20	34	40	0.2	515.74	947.23	1313.57	1.39	138.3
20	20	34	40	0.4	324.66	933.23	1198.91	1.73	145.8
21	20	34	40	0.6	597.68	841.53	923.126	1.82	168.3
22	20	34	60	0.2	729.48	1145.71	1551.37	1.55	144.2
23	20	34	60	0.4	497.85	1118.13	1503.88	1.96	155.6
24	20	34	60	0.6	719.66	973.81	1124.20	2.01	181.2
25	20	34	80	0.2	868.29	1546.31	2353.68	1.61	151.7
26	20	34	80	0.4	670.75	1359.16	1945.52	2.09	166.4
27	20	34	80	0.6	827.84	1302.48	1615.77	2.25	202.3
28	30	14	40	0.2	634.52	1657.51	2490.19	1.38	125.6
29	30	14	40	0.4	402.80	1640.01	1852.57	1.17	134.5
30	30	14	40	0.6	513.96	1504.23	1689.41	1.52	157.3
31	30	14	60	0.2	741.36	2619.35	3657.59	1.51	137.3
32	30	14	60	0.4	471.46	2336.29	2146.65	1.29	143.9
33	30	14	60	0.6	660.78	2069.41	2067.55	1.67	178.4
34	30	14	80	0.2	931.65	3206.45	4038.99	1.92	143.2
35	30	14	80	0.4	773.56	2736.88	2999.64	1.58	156.6
36	30	14	80	0.6	849.06	2766.35	2785.08	1.84	194.2

37	30	24	40	0.2	411.13	940.56	1685.23	1.65	133.3
38	30	24	40	0.4	224.37	703.34	1126.18	1.38	153.3
39	30	24	40	0.6	352.03	742.02	1142.38	1.81	152.3
40	30	24	60	0.2	859.46	1374.45	2281.69	1.76	143.2
41	30	24	60	0.4	472.45	1417.43	1652.08	1.48	157.4
42	30	24	60	0.6	489.73	1155.22	1658.28	2.00	159.6
43	30	24	80	0.2	1007.23	1985.95	2984.11	1.99	156.2
44	30	24	80	0.4	662.15	1821.60	2375.45	1.62	171.6
45	30	24	80	0.6	749.46	1614.65	1930.49	2.10	175.3
46	30	34	40	0.2	295.04	863.95	1199.18	1.33	131.8
47	30	34	40	0.4	214.32	730.20	1060.06	1.43	138.9
48	30	34	40	0.6	279.24	615.85	773.25	1.41	146.3
49	30	34	60	0.2	521.26	1010.69	1429.09	1.45	135.6
50	30	34	60	0.4	256.15	928.26	1351.26	1.74	147.8
51	30	34	60	0.6	401.62	875.42	1116.42	1.67	160.6
52	30	34	80	0.2	720.77	1353.55	1999.28	1.54	145.2
53	30	34	80	0.4	399.09	1108.11	1625.38	1.82	152.7
54	30	34	80	0.6	559.46	1200.48	1386.82	1.85	186.9
55	40	14	40	0.2	601.45	1528.78	2464.19	1.22	121.7
56	40	14	40	0.4	381.80	1524.92	1750.44	1.13	131.3
57	40	14	40	0.6	500.69	1456.07	1642.86	1.41	144.3
58	40	14	60	0.2	701.33	2311.29	3428.63	1.34	132.8
59	40	14	60	0.4	452.46	2138.49	2124.12	1.26	140.3
60	40	14	60	0.6	637.56	1975.43	2031.70	1.54	164.3
61	40	14	80	0.2	899.12	2854.00	3827.15	1.72	139.6
62	40	14	80	0.4	739.78	2670.14	2707.97	1.54	151.6
63	40	14	80	0.6	826.90	2567.73	2719.25	1.75	176.4
64	40	24	40	0.2	369.68	810.37	1625.09	1.48	129.7
65	40	24	40	0.4	194.22	602.79	1117.45	1.28	142.9
66	40	24	40	0.6	334.68	695.54	1060.57	1.69	148.3
67	40	24	60	0.2	778.42	1109.22	2163.10	1.56	137.8
68	40	24	60	0.4	452.66	1338.76	1552.72	1.42	148.3
69	40	24	60	0.6	458.32	1020.70	1509.60	1.82	153.3
70	40	24	80	0.2	937.45	1623.96	2918.71	1.75	155.6
71	40	24	80	0.4	588.33	1786.94	2243.88	1.61	163.1
72	40	24	80	0.6	699.39	1523.70	1927.34	1.95	172.3
73	40	34	40	0.2	270.72	731.09	1113.84	1.18	125.2
74	40	34	40	0.4	162.49	739.59	938.67	1.24	131.5
75	40	34	40	0.6	289.98	533.69	695.17	1.38	148.2
76	40	34	60	0.2	463.57	937.35	1355.34	1.31	131.9

77	40	34	60	0.4	231.14	891.46	1217.68	1.37	141.7
78	40	34	60	0.6	377.15	798.62	952.68	1.53	159.3
79	40	34	80	0.2	689.81	1246.44	1866.76	1.46	141.2
80	40	34	80	0.4	366.14	1093.58	1531.48	1.44	149.8
81	40	34	80	0.6	548.42	1070.17	1265.95	1.66	178.2
82	50	14	40	0.2	702.32	2108.96	3068.16	1.61	131.2
83	50	14	40	0.4	589.32	1753.16	2820.13	1.54	162.3
84	50	14	40	0.6	669.30	1939.98	2248.68	1.95	170.8
85	50	14	60	0.2	753.95	2729.10	4012.70	1.74	145.2
86	50	14	60	0.4	762.62	2327.83	4067.65	1.67	170.3
87	50	14	60	0.6	750.07	2287.27	3119.12	2.20	186.4
88	50	14	80	0.2	1056.56	3126.92	4848.47	2.31	151.2
89	50	14	80	0.4	840.55	2782.61	4663.19	1.81	176.5
90	50	14	80	0.6	956.58	2853.94	3853.81	2.42	198.3
91	50	24	40	0.2	733.82	1336.76	2163.06	1.68	143.2
92	50	24	40	0.4	543.14	1343.03	2113.06	1.62	149.2
93	50	24	40	0.6	534.30	944.29	1314.89	1.96	156.3
94	50	24	60	0.2	1025.41	2049.09	2934.64	1.79	152.2
95	50	24	60	0.4	772.68	1936.97	2961.78	1.78	155.3
96	50	24	60	0.6	728.08	1433.83	2645.62	2.32	165.6
97	50	24	80	0.2	1297.54	2549.72	3899.86	2.1	163.2
98	50	24	80	0.4	981.34	2434.52	3845.42	1.88	166.8
99	50	24	80	0.6	912.45	1750.48	3430.81	2.59	181.3
100	50	34	40	0.2	372.21	909.66	1285.32	1.33	140.8
101	50	34	40	0.4	311.35	910.32	1313.52	1.58	154.3
102	50	34	40	0.6	370.45	735.87	823.33	1.88	174.6
103	50	34	60	0.2	585.90	1295.43	1838.52	1.46	145.2
104	50	34	60	0.4	445.57	1192.69	1715.46	1.68	159.7
105	50	34	60	0.6	485.95	1014.55	1156.24	2.37	188.2
106	50	34	80	0.2	758.47	1565.26	2716.38	1.71	149.5
107	50	34	80	0.4	608.91	1434.28	1926.49	1.76	176.7
108	50	34	80	0.6	632.72	1135.68	1574.53	2.49	198.4

5.3 Investigations on Cutting Forces

5.3.1 Influence of process parameters on cutting forces in rotary face milling operation

To estimate the effect of process parameters on cutting forces, full-factorial experiments have been conducted. The variation of Cutting Forces with respect to different process

parameters – cutting speed, feed and depth of cut in Rotary Tool Milling is shown in below graphs.

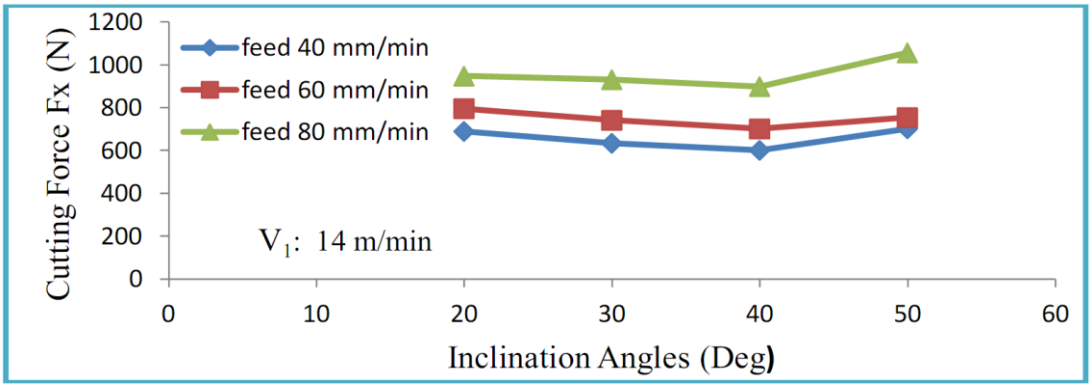

Fig.5.2.2.1 (a). Variation of cutting force F_X at speed 14 m/min and depth of cut 0.2 mm

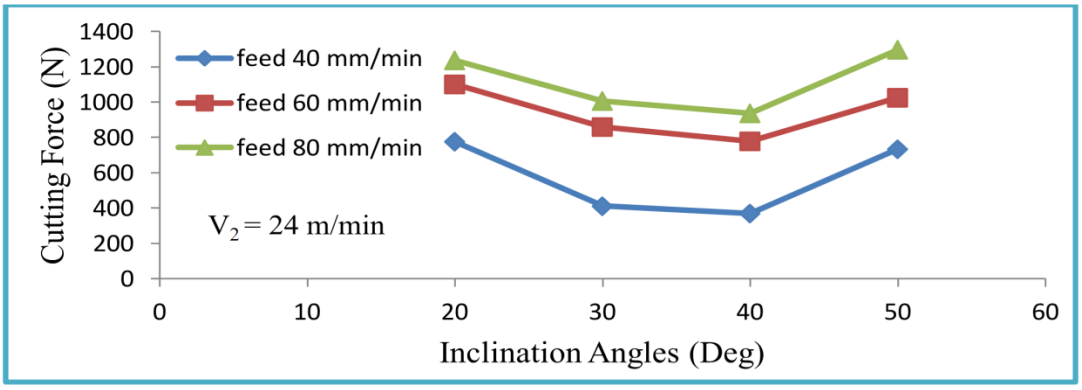

Fig. 5.2.2.1 (b). Variation of cutting force F_X at speed 24 m/min and depth of cut 0.2 mm

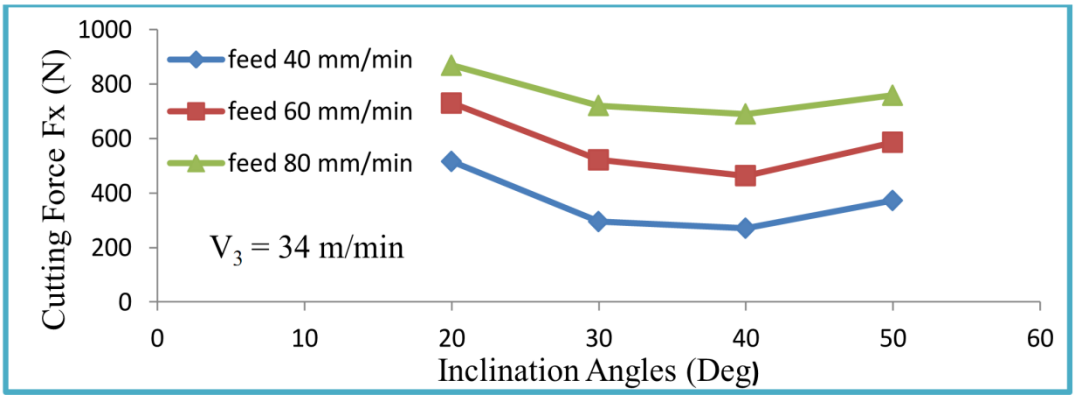

Fig. 5.2.2.1 (c). Variation of cutting force F_X at speed 34 m/min and depth of cut 0.2 mm

Figures 5.2.2.1 (a)-(c) shows the variation of cutting force F_X at constant depth of cut for different cutting speeds, feed rates and inclination angles.

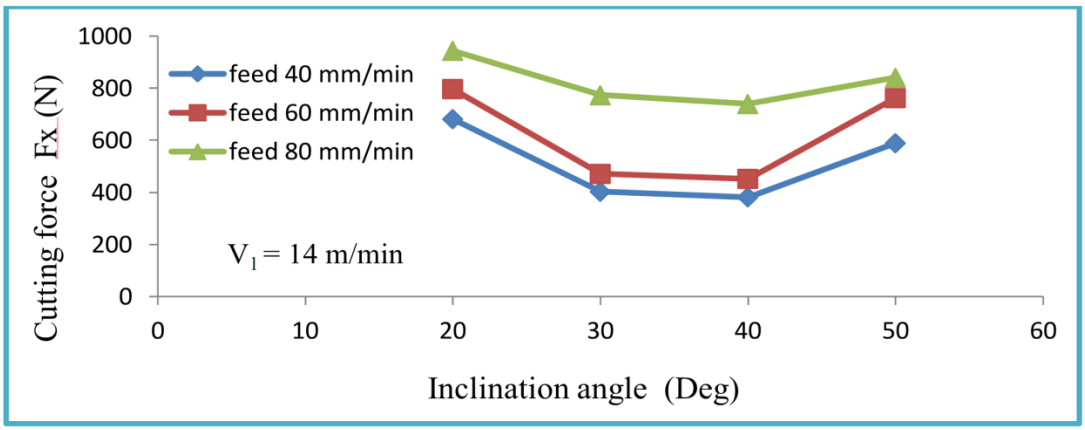

Fig.5.2.2.2 (a). Variation of cutting force F_x at speed 14 m/min and depth of cut 0.4 mm

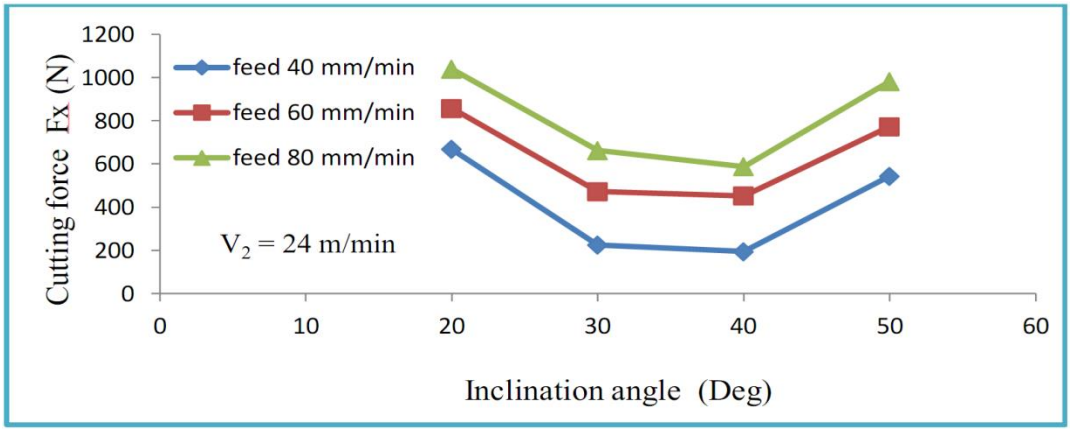

Fig.5.2.2.2 (b). Variation of cutting force F_x at speed 24 m/min and depth of cut 0.4 mm

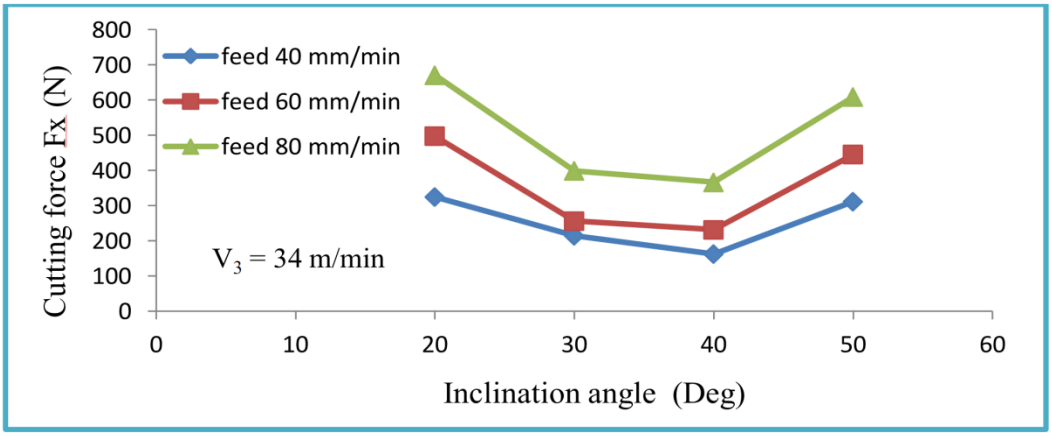

Fig.5.2.2.2 (c). Variation of cutting force F_x at speed 34 m/min and depth of cut 0.4 mm

Figures 5.2.2.2 (a)-(c) shows the variation of cutting force F_X at constant depth of cut for different cutting speeds, feed rates and inclination angles.

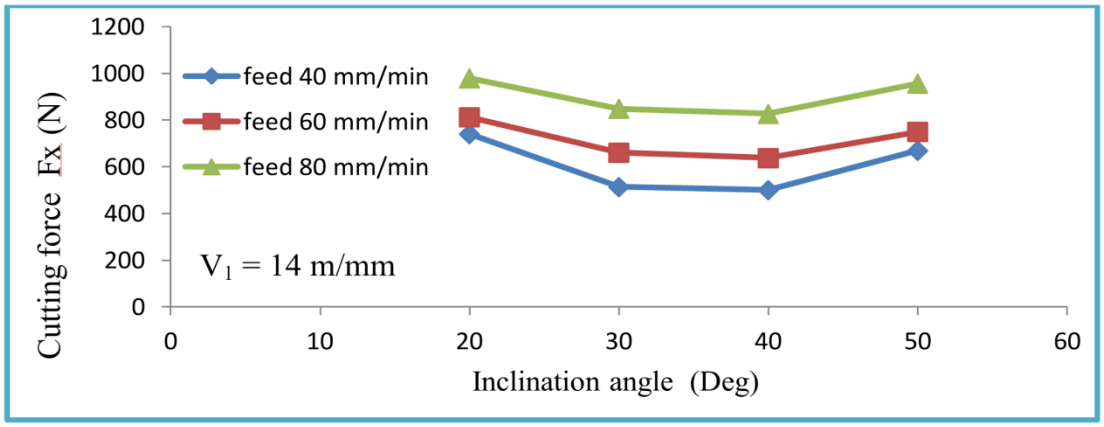

Fig.5.2.2.3 (a). Variation of cutting force F_x at speed 14 m/min and depth of cut 0.6 mm

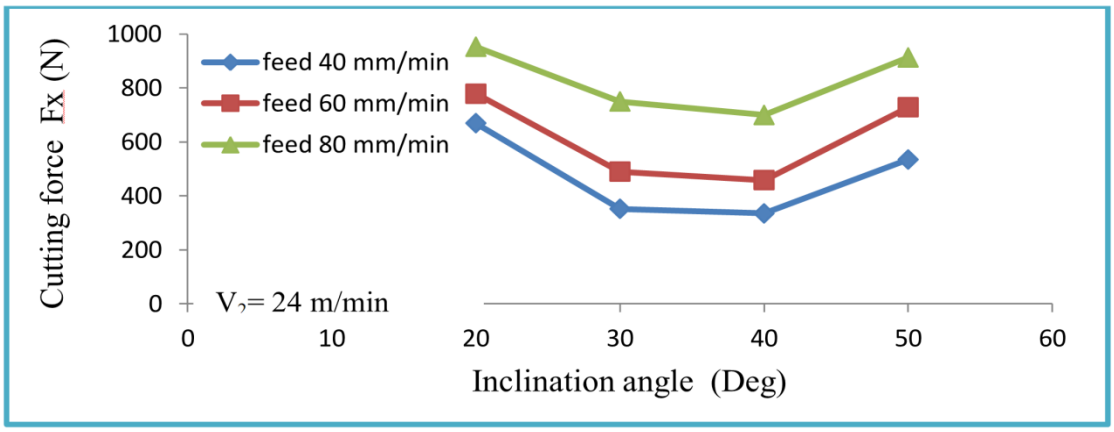

Fig.5.2.2.3 (b). Variation of cutting force F_x at speed 24 m/min and depth of cut 0.6 mm

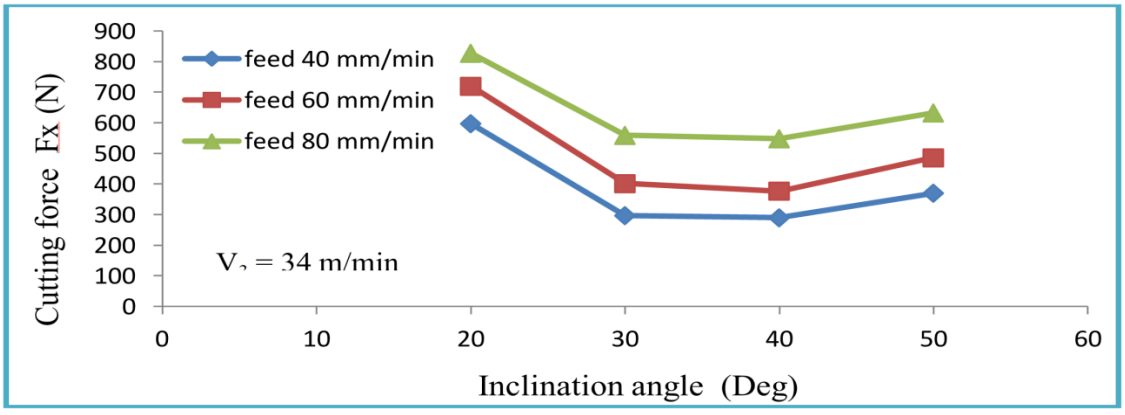

Fig.5.2.2.3 (c). Variation of cutting force F_x at speed 34 m/min and depth of cut 0.6 mm

Figures 5.2.2.3 (a)-(c) shows the variation of cutting force F_X at constant depth of cut for different cutting speeds, feed rates and inclination angles.

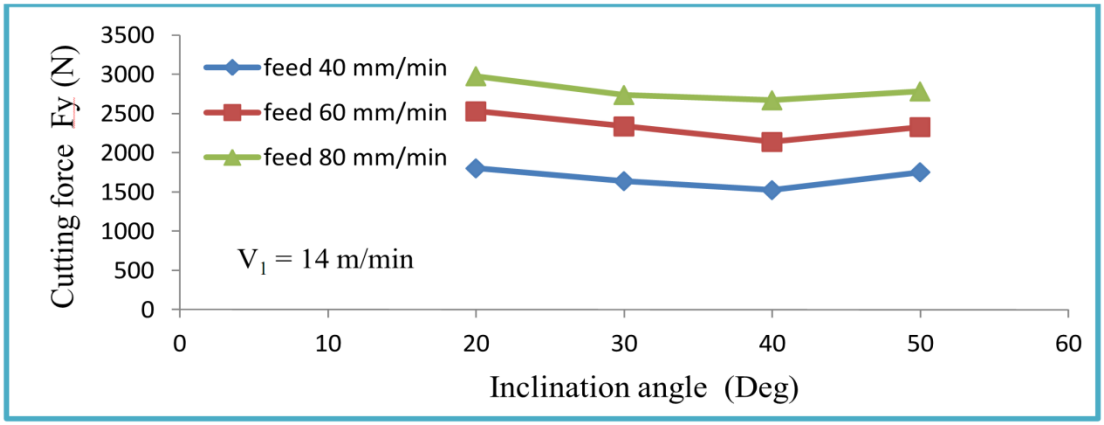

Fig.5.2.2.4 (a). Variation ofcutting force F_Y at speed 14 m/min and depth of cut 0.2 mm

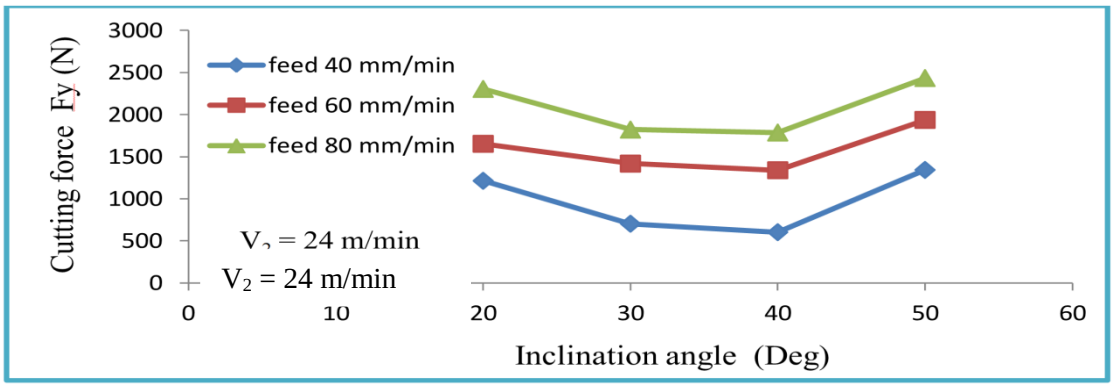

Fig.5.2.2.4 (b). Variation of cutting force F_Y at speed 24 m/min and depth of cut 0.2 mm

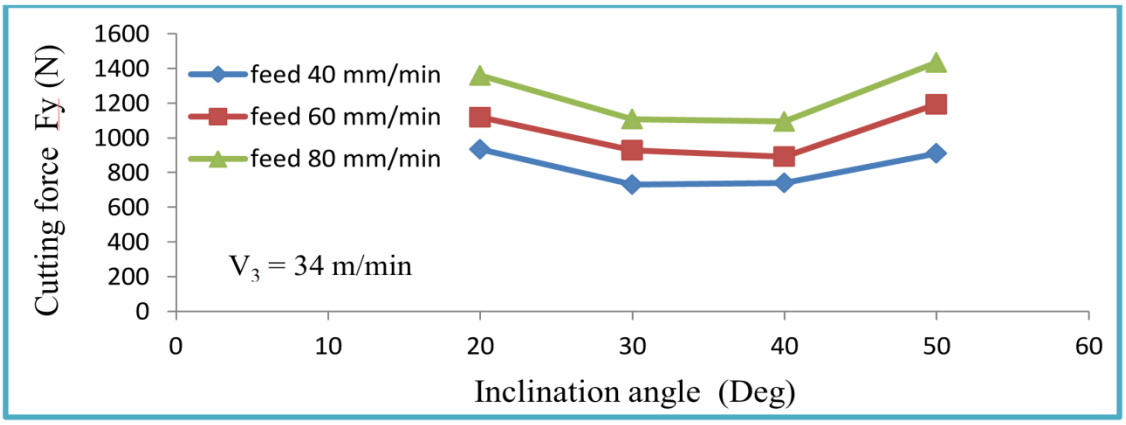

Fig.5.2.2.4 (c). Variation of cutting force F_Y at speed 34 m/min and depth of cut 0.2 mm

Figures 5.2.2.4(a)-(c) shows the variation of cutting force F_Y at constant depth of cut for different cutting speeds, feed rates and inclination angles.

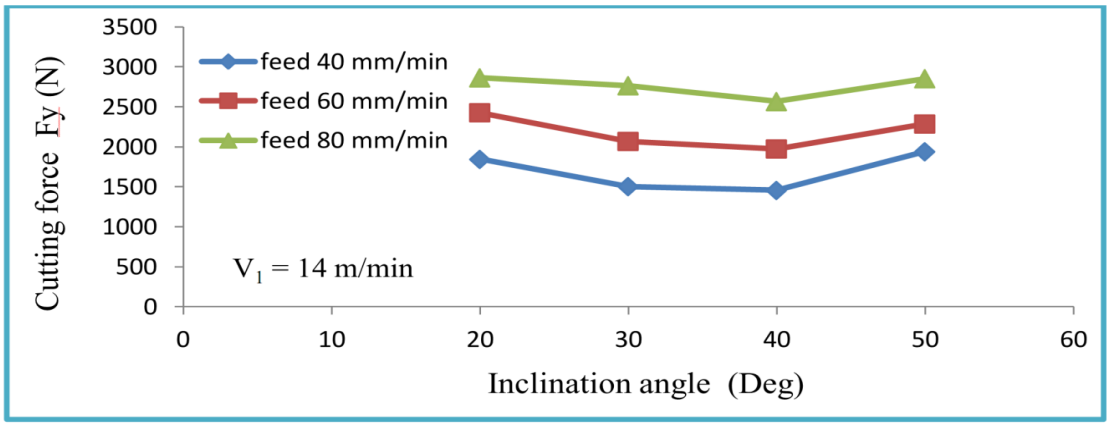

Fig.5.2.2.5 (a). Variation of cutting force F_Y at speed 14 m/min and depth of cut 0.4 mm

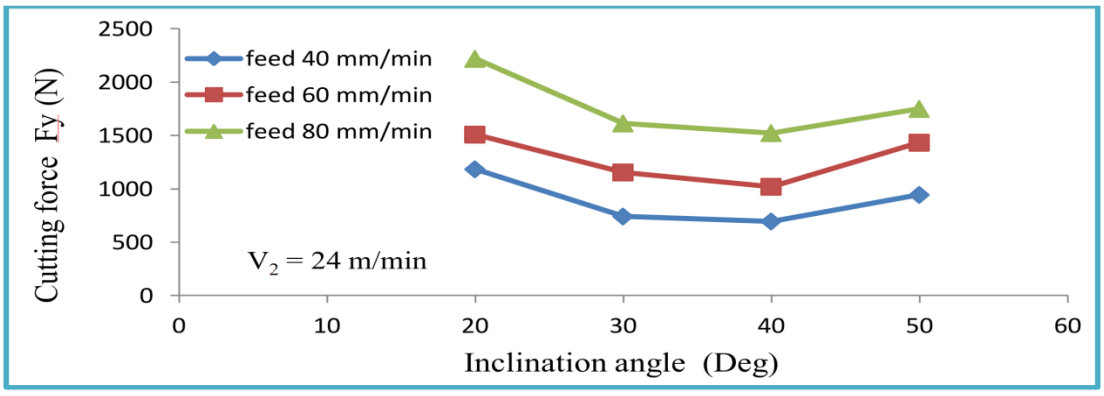

Fig.5.2.2.5 (b). Variation of cutting force F_Y at speed 24 m/min and depth of cut 0.4 mm

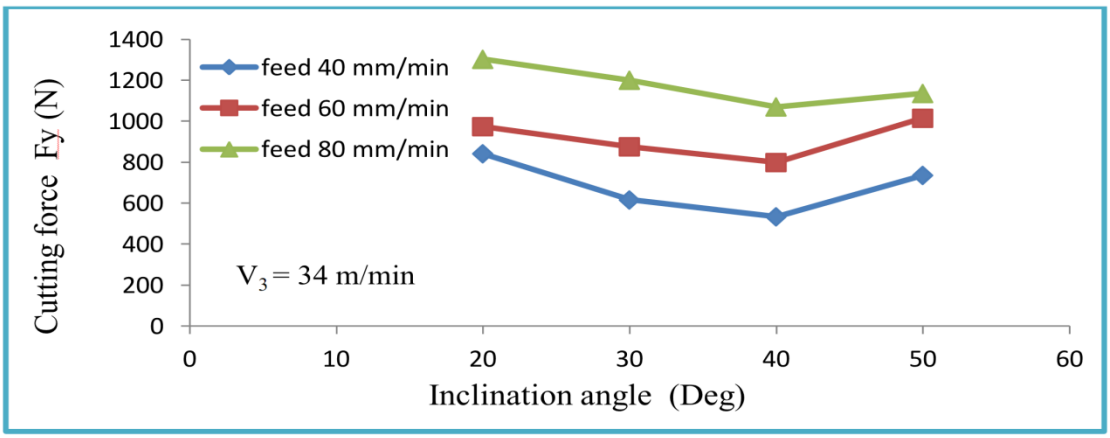

Fig.5.2.2.5 (c). Variation of cutting force F_Y at speed 34 m/min and depth of cut 0.4 mm

Figures 5.2.2.5 (a)-(c) shows the variation of cutting force F_Y at constant depth of cut for different cutting speeds, feed rates and inclination angles.

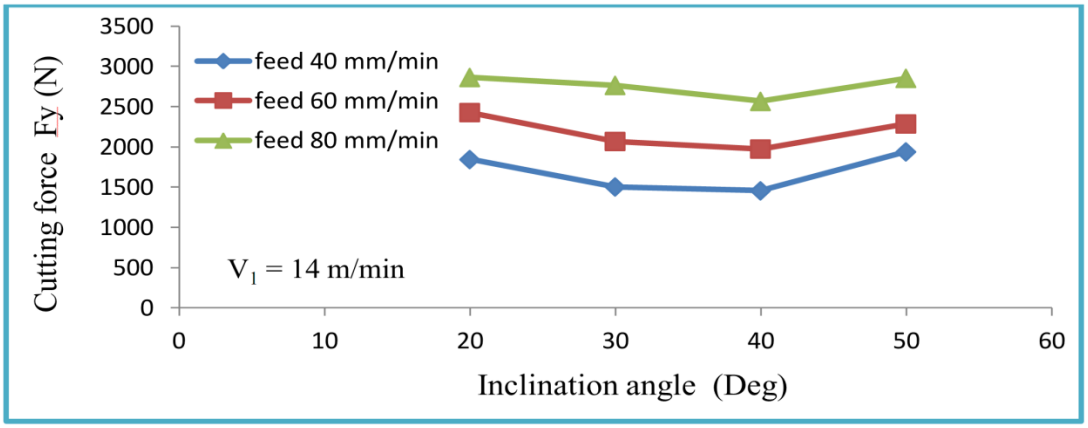

Fig.5.2.2.6 (a). Variation of cutting force F_Y at speed 14 m/min and depth of cut 0.6 mm

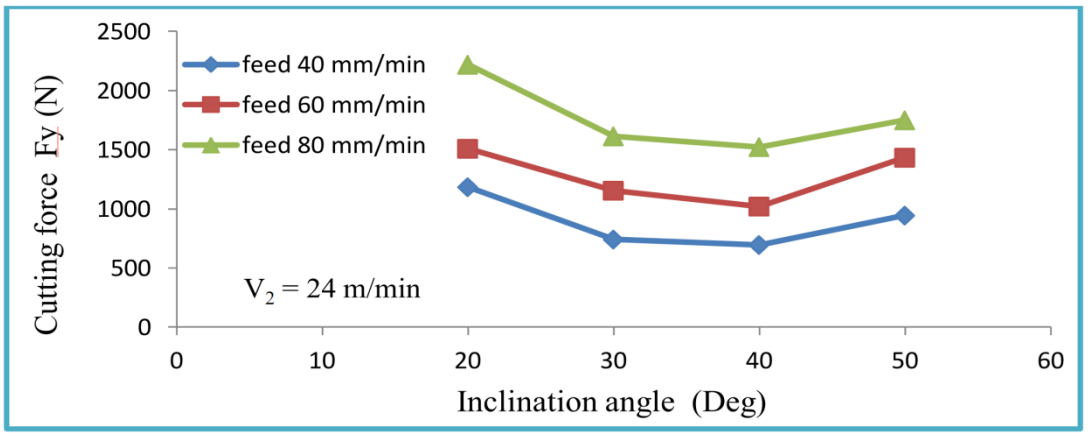

Fig.5.2.2.6 (b). Variation of cutting force F_Y at speed 24 m/min and depth of cut 0.6 mm

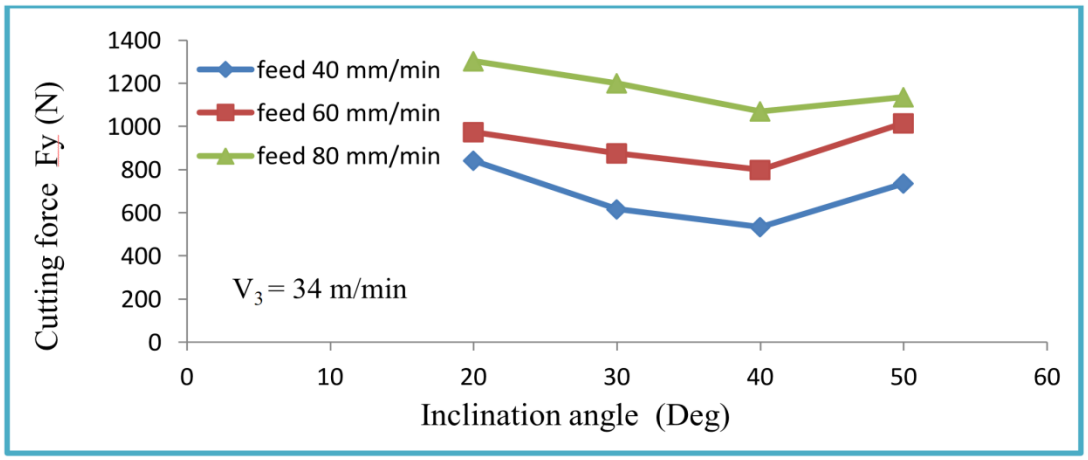

Fig.5.2.2.6 (c). Variation of cutting force F_Y at speed 34 m/min and depth of cut 0.6 mm

Figures 5.2.2.6 (a)-(c) shows the variation of cutting force F_Y at constant depth of cut for different cutting speeds, feed rates and inclination angles.

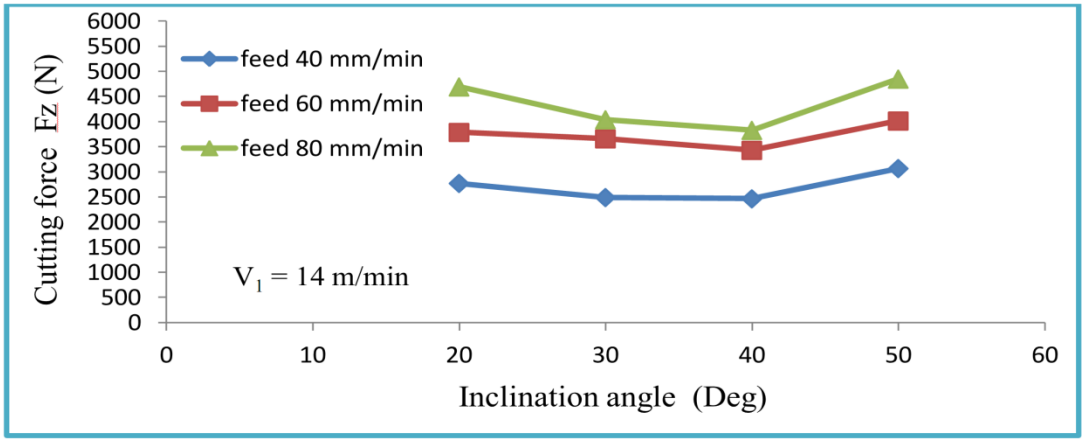

Fig.5.2.2.7 (a). Variation of cutting force F_Z at speed 14 m/min and depth of cut 0.2 mm

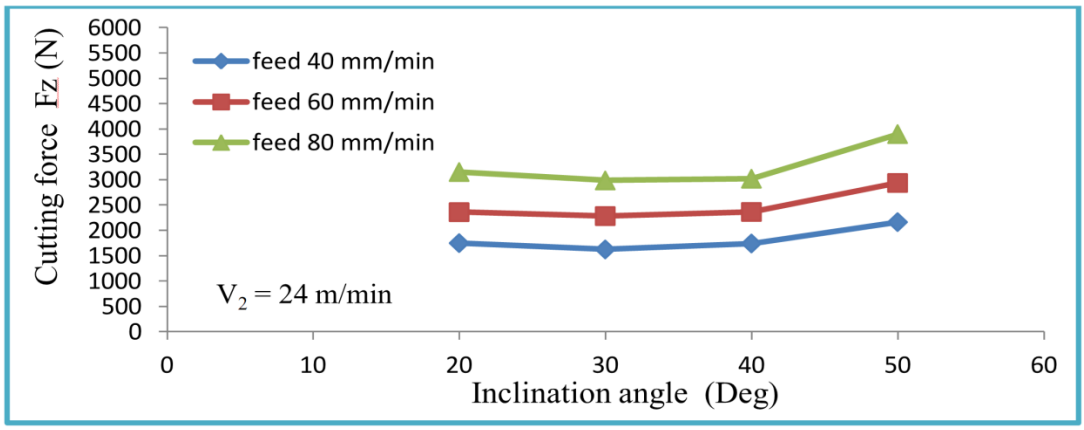

Fig.5.2.2.7 (b). Variation of cutting force F_Z at speed 24 m/min and depth of cut 0.2 mm

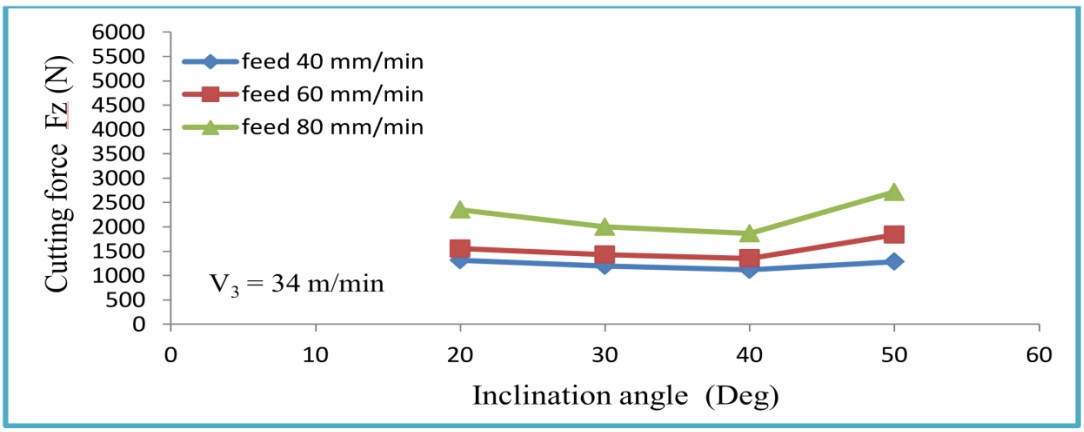

Fig.5.2.2.7 (c). Variation of cutting force F_Z at speed 34 m/min and depth of cut 0.2 mm

Figures 5.2.2.7(a)-(c) shows the variation of cutting force F_Y at constant depth of cut for different cutting speeds, feed rates and inclination angles.

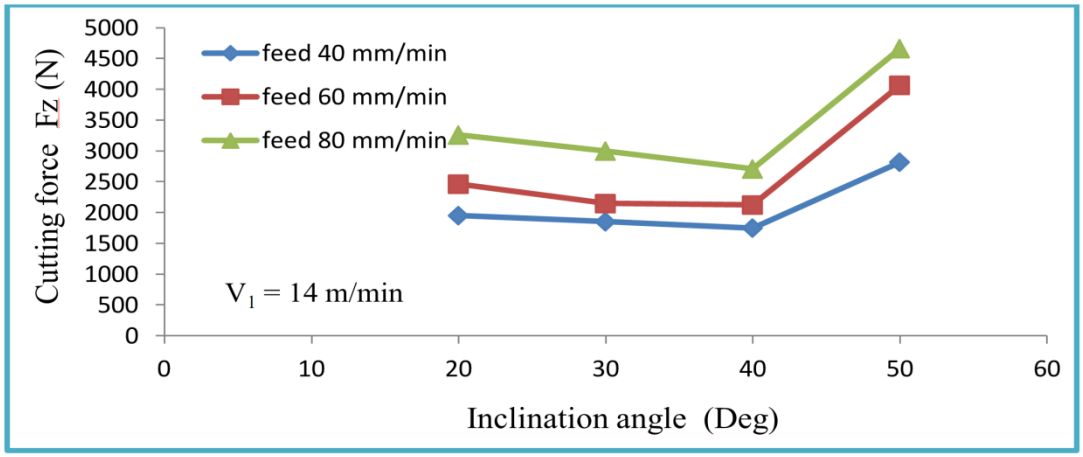

Fig.5.2.2.8 (a). Variation of cutting force F_Z at speed 14 m/min and depth of cut 0.4 mm

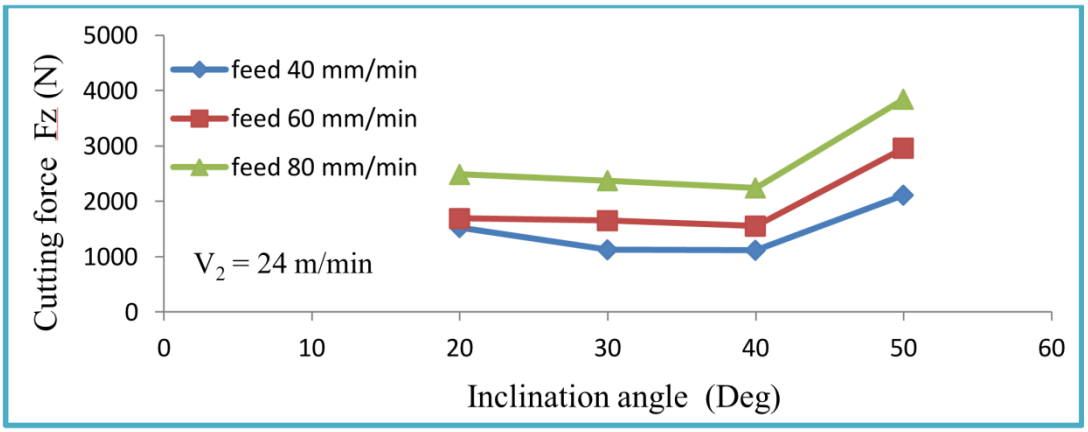

Fig.5.2.2.8 (b). Variation of cutting force F_Z at speed 24 m/min and depth of cut 0.4 mm

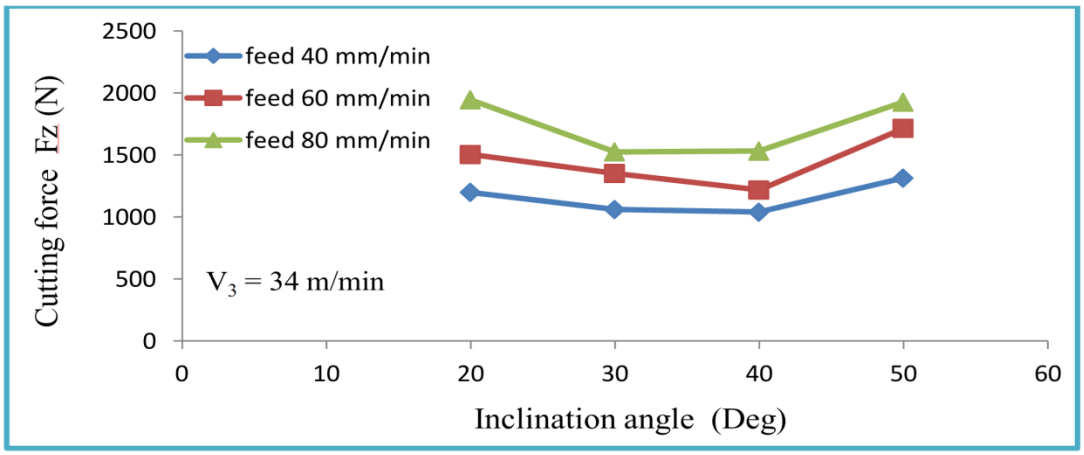

Fig.5.2.2.8 (c). Variation of cutting force F_Z at speed 34 m/min and depth of cut 0.4 mm

Figures 5.2.2.4 (a)-(c) shows the variation of cutting force F_Z at constant depth of cut for different cutting speeds, feed rates and inclination angles.

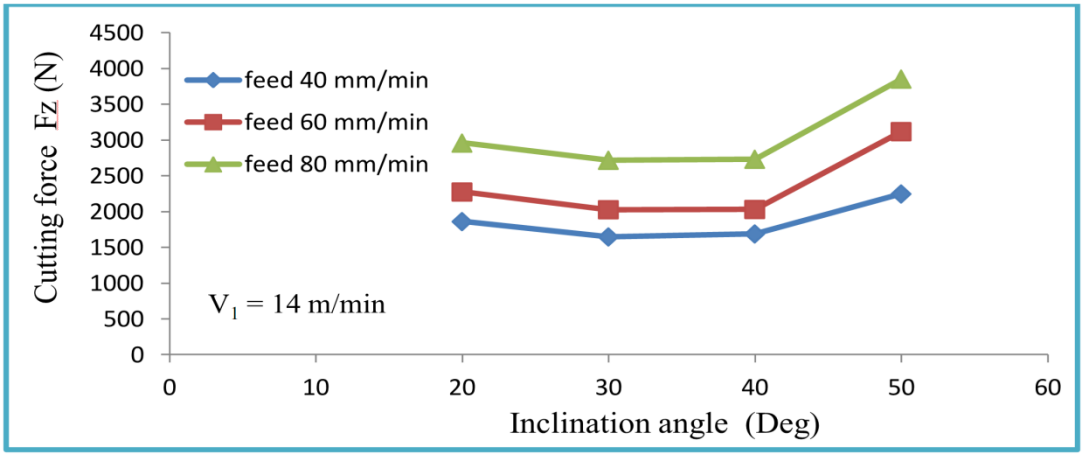

Fig.5.2.2.9 (a). Variation of cutting force F_Z at speed 14 m/min and depth of cut 0.6 mm

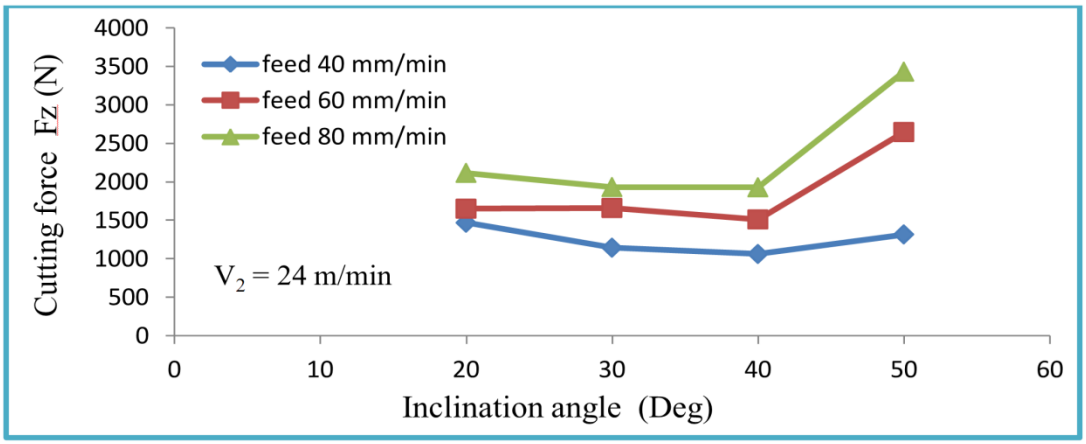

Fig.5.2.2.9 (b). Variation of cutting force F_Z at speed 24 m/min and depth of cut 0.6 mm

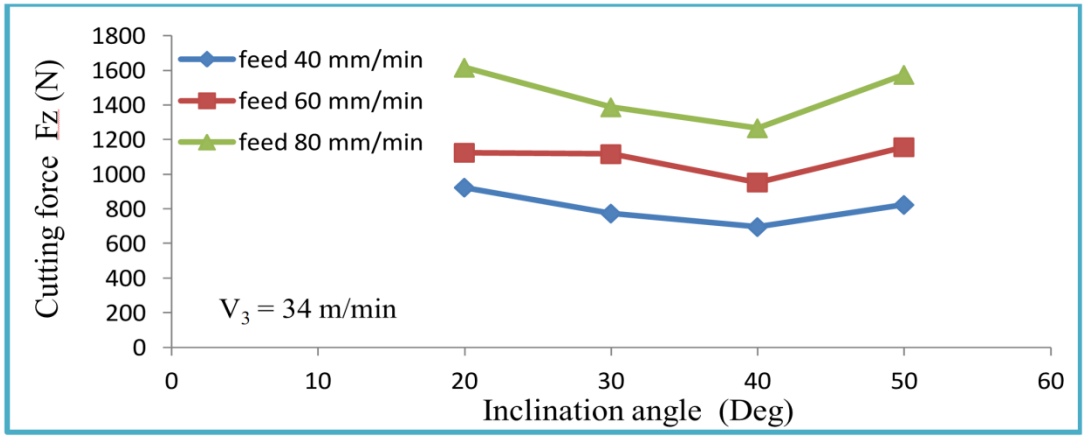

Fig.5.2.2.9 (c). Variation of cutting force F_Z at speed 34 m/min and depth of cut 0.6 mm

Figures 5.2.2.9(a)-(c) shows the variation of cutting force F_Z at constant depth of cut for different cutting speeds, feed rates and inclination angles.

From the results shown in Figs.5.2.2.1-5.5.2.2.9, it is clearly seen that the general trend of increase in cutting forces with increase in feed rate. This could be due to an increase in the cross-sectional area of the uncut chip. Similarly, as the depth of cut increases, the cutting forces also increase. This could be due to an increase in the area of undeformed chip cross-section with increase in depth of cut. It is observed that all of the cutting forces decrease as the cutting speed increases, which may be attributed to the following: (i) with increase in cutting speed, the shear plane angle decreases, thereby reducing the shear forces required to produce deformation, (ii) at high cutting speeds the friction coefficient decreases, hence cutting forces decrease, (iii) at high cutting speeds, thermal softening of the material is significant. All these factors cause the cutting forces to decrease with increase in cutting speed. In the case of Rotary milling cutter, the inclination angle of the insert plays an important role. It is observed that the cutting forces decrease with increase in inclination angle from 20° to 30°. This could be due to improper rotation of the insert at low inclination angles. From 30° to 40°, the cutting forces are showing slight variation.An increase in the magnitude of cutting forces as the inclination angle changes from 40° to 50° could be due to an excessive curling and straightening of chips. Also, cross-section of the chips show an excessive deformation and hence the magnitude of cutting force could increase as the inclination angle changes form 40° to 50°.

At higher depth of cut, and lower cutting speed, lesser cutting forces are observed with the inclination angle of $30^0$and at higher depth of cut, and higher cutting speed, lesser cutting forces are observed with the inclination angle of 40°. At low depth of cut values, lesser cutting forces are observed with inclination angle 50°. Hence, the inclination angle with 30^0 and any other angle in between 30° and 40° are more desirable in cutting of Inconel 625 alloys at higher depth of cut and lower cutting speed in the range of 14 m/min to 24 m/min.

5.4 Investigations on Surface roughness

Surface finish obtained during a machining operation affects the quality of the part being machined and usage of the operation. The higher the surface finish the higher is its qualitative value i.e. the surface roughness should be minimum. For conducting the experiments, four parameters are considered namely inclination angle, cutting speed, feed rate and depth of cut. The levels assigned for each parameter are mentioned in the earlier chapter.

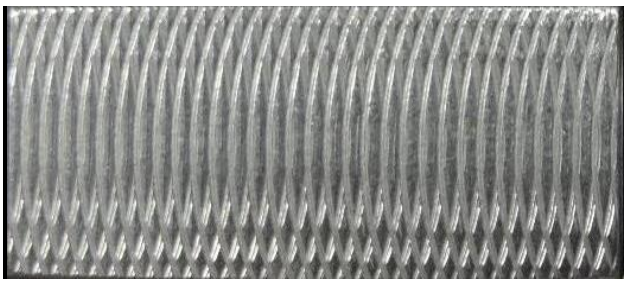

Standard specimen (6.3 µm)

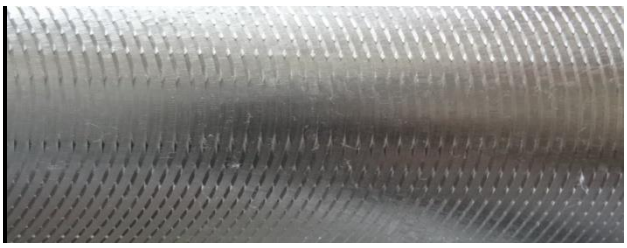

Conventional milling specimen (6.04 µm)

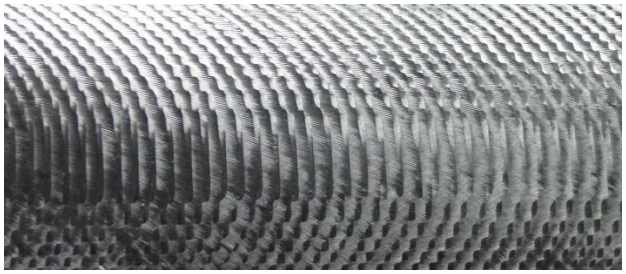

Rotary milling specimen (6.79 µm)

Fig.5.3.1.1. Comparison of roughness layout for conventional and rotary milling with standard specimen.

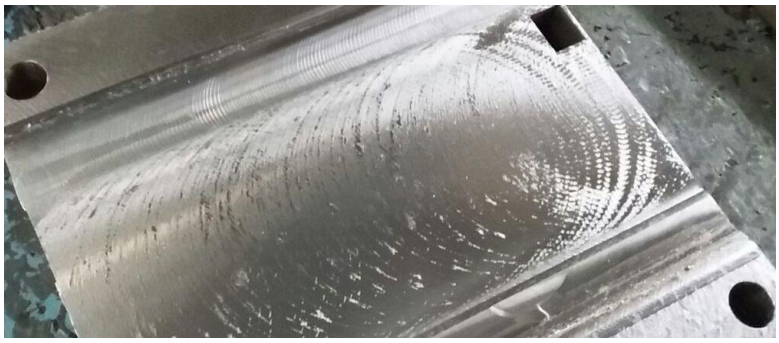

Fig.5.3.1.2Surface roughness pattern generated in rotary face milling

5.4.1 Influence of process parameters on surface roughness in rotary face milling operation

In order to study the influence of process parameters on surface roughness, full-factorial experiments have been conducted. The variation of surface roughness in rotary face milling with

respect to different process parameters – inclination angle, cutting speed, feed rate and depth of cut in Rotary tool milling is shown in below graphs.

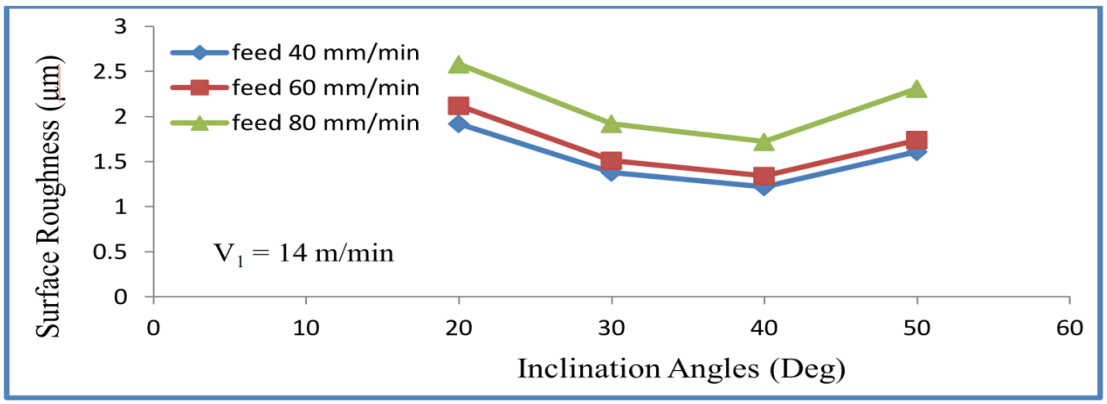

Fig.5.4.1.1(a). Variation of surface roughness at speed 14 m/min and depth of cut 0.2 mm

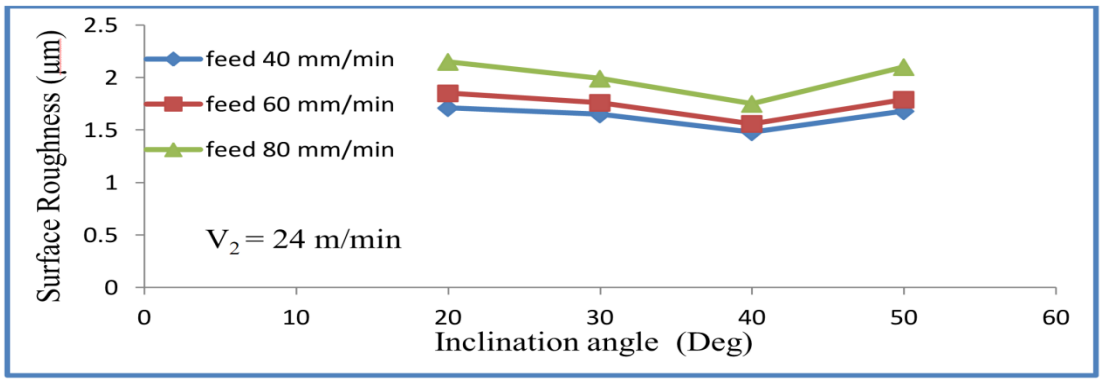

Fig.5.4.1.1 (b). Variation of surface roughness at speed 24 m/min and depth of cut 0.2 mm

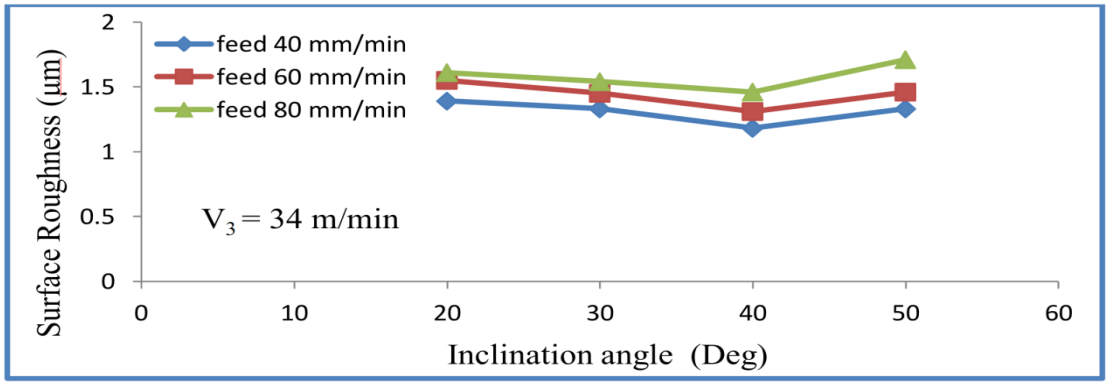

Fig.5.4.1.1 (c). Variation of surface roughness at speed 34 m/min and depth of cut 0.2 mm

Figures 5.4.1.1 (a)-(c) shows the variation of surface roughness R_a at constant depth of cut for different cutting speeds, feed rates and inclination angles.

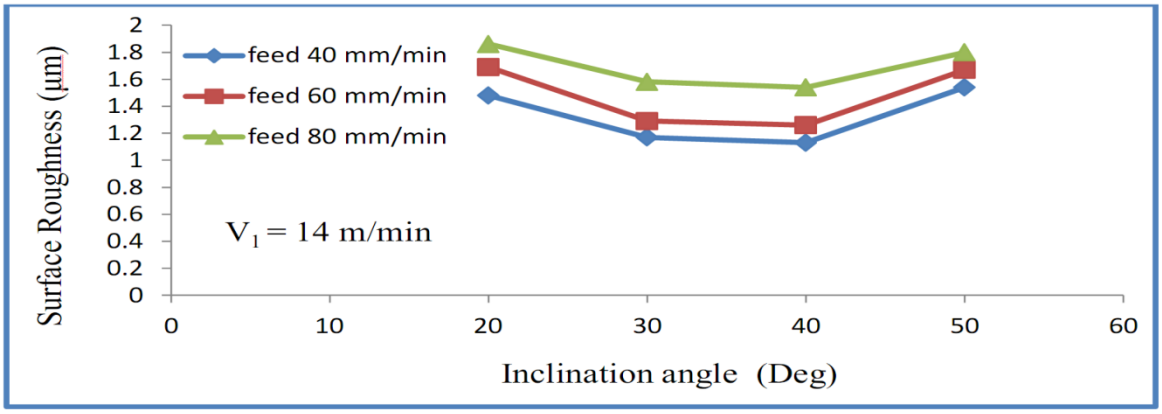

Fig.5.4.1.2 (a). Variation of surface roughness at speed 14 m/min and depth of cut 0.4 mm

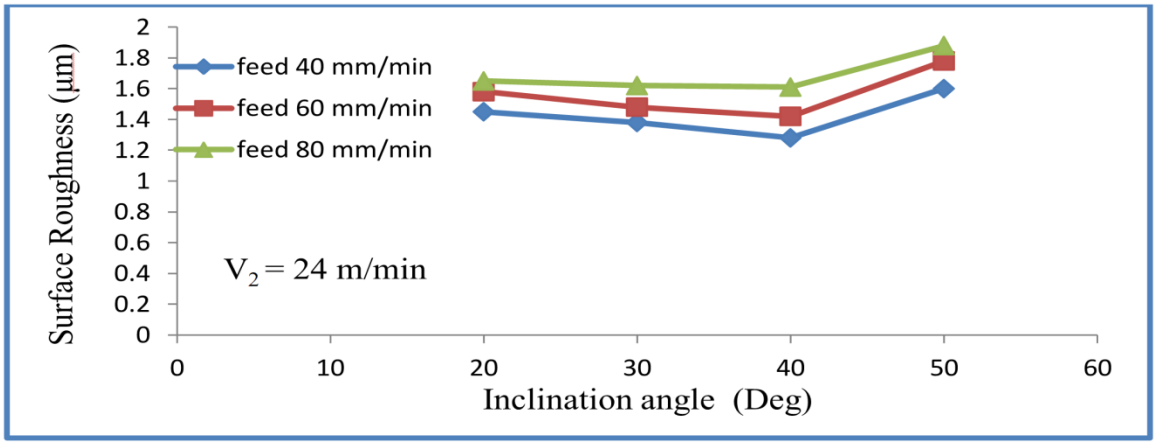

Fig.5.4.1.2 (b). Variation of surface roughness at speed 24 m/min and depth of cut 0.4 mm

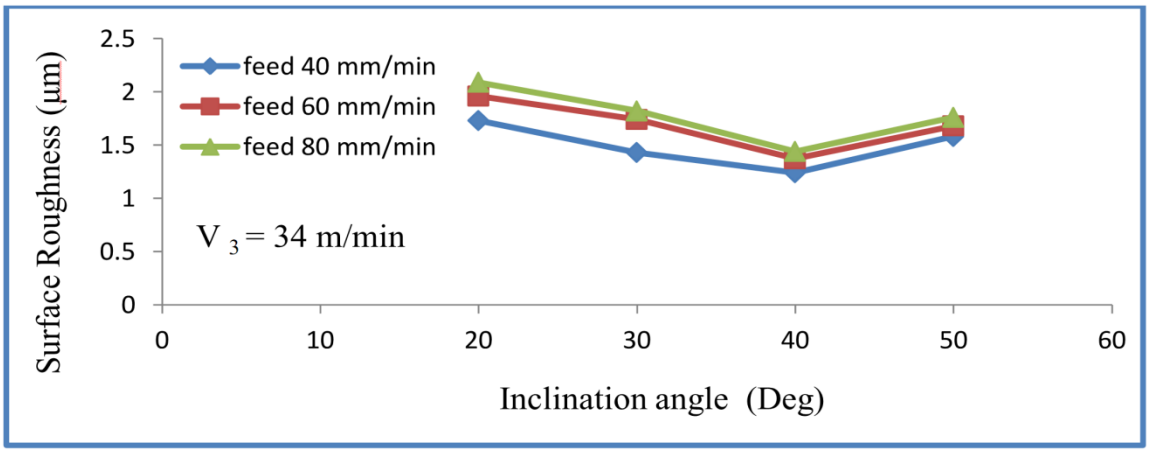

Fig.5.4.1.2 (c). Variation of surface roughness at speed 34 m/min and depth of cut 0.4 mm

Figures 5.4.1.2 (a)-(c) shows the variation of surface roughness R_a at constant depth of cut for different cutting speeds, feed rates and inclination angles.

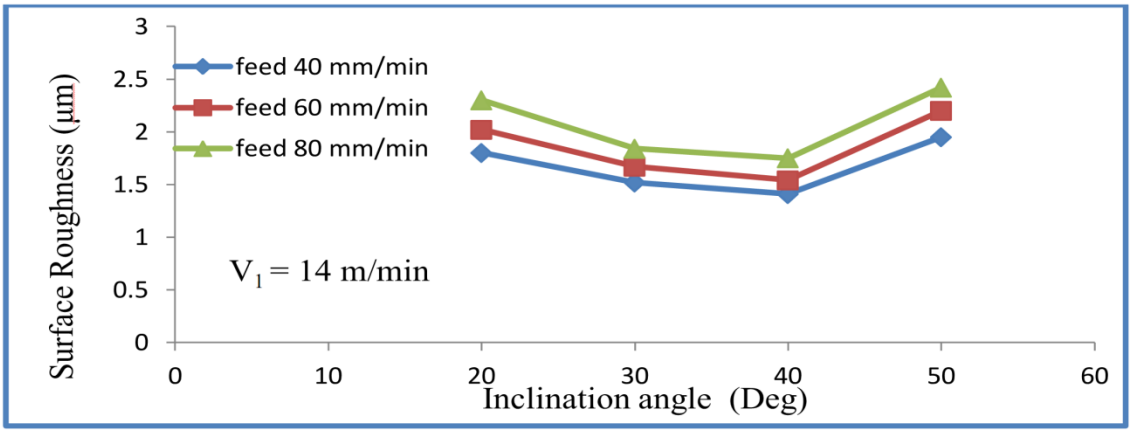

Fig.5.4.1.3 (a). Variation of surface roughness at speed 14 m/min and depth of cut 0.6 mm

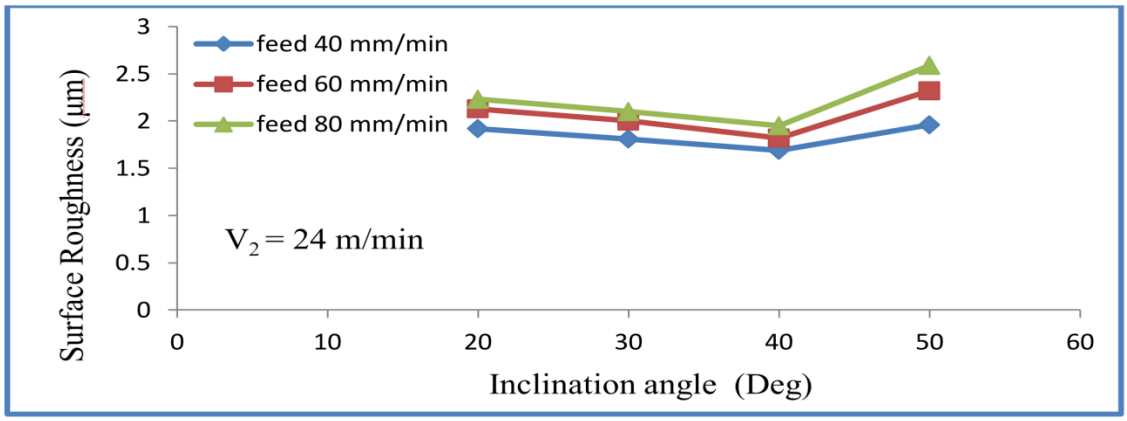

Fig.5.4.1.3 (b). Variation of surface roughness at speed 24 m/min and depth of cut 0.6 mm

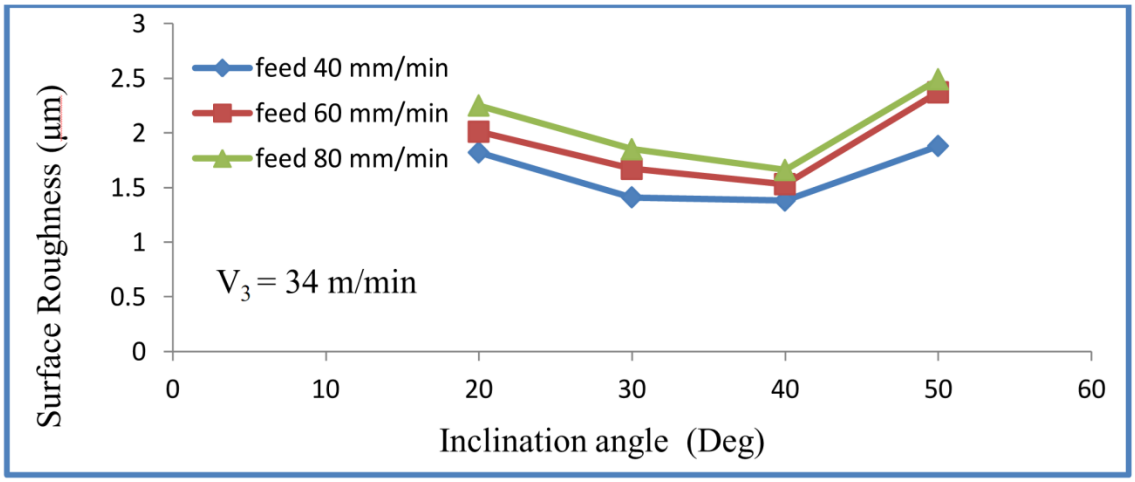

Fig.5.4.1.3 (c). Variation of surface roughness at speed 34 m/min and depth of cut 0.6 mm

Figures 5.4.1.3 (a)-(c) shows the variation of surface roughness R_a at constant depth of cut for different cutting speeds, feed rates and inclination angles.

Figures 5.4.1.1 – 5.4.1.3 shows the variation of surface roughness R_a at constant depth of cut for different cutting speeds, feed rates and inclination angles. From the above graphs, it can be observed that as the feed rate is increasing from 40 mm/min to 80 mm/min, there is significant increase in surface roughness values for rotary milling operation indicating that feed rate is the major influencing factor on surface roughness.

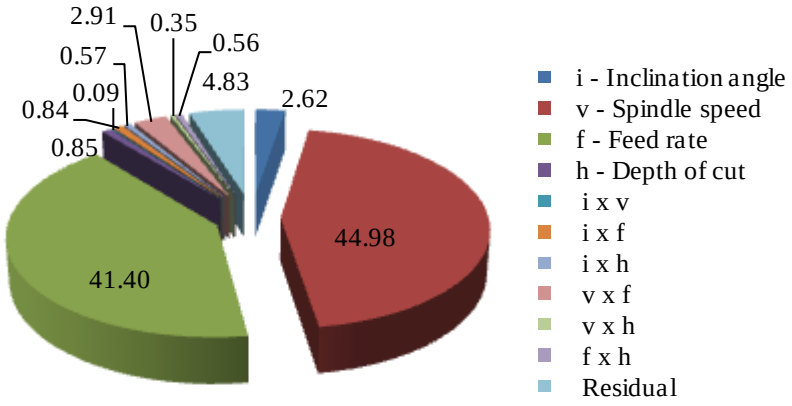

Fig. 5.4.1.3 (d). Percentage Contribution of Parameters on Surface Roughness (Rotary milling)

From the pie chart shown in Fig.5.4.1.3, it can be concluded that cutting speed and feed rate are the major contributing factors for surface roughness generated in rotary milling and inclination angle being next most significant.

5.5 Cutting Temperature Investigations

5.5.1 Influence of process parameters on cutting temperature in rotary face milling operation

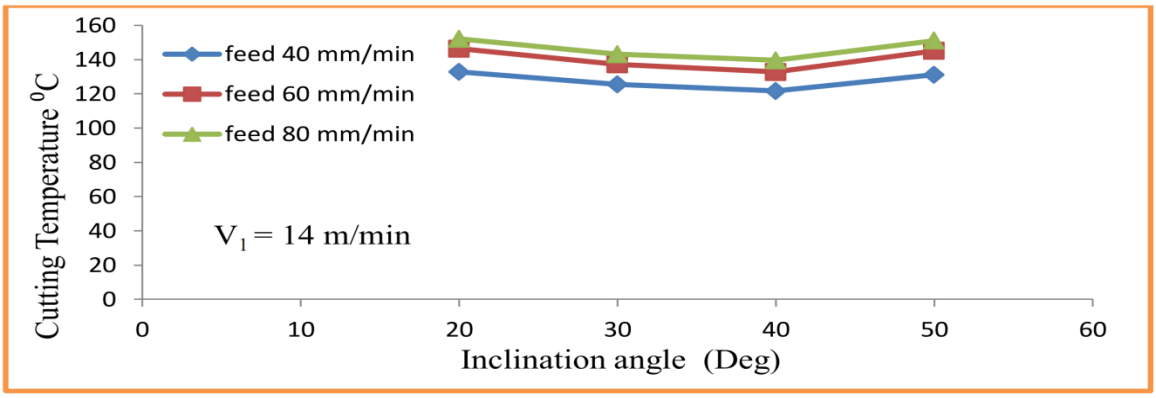

Fig.5.5.1.1(a). Variation of Cutting Temperature at speed 14 m/min and depth of cut 0.2 mm

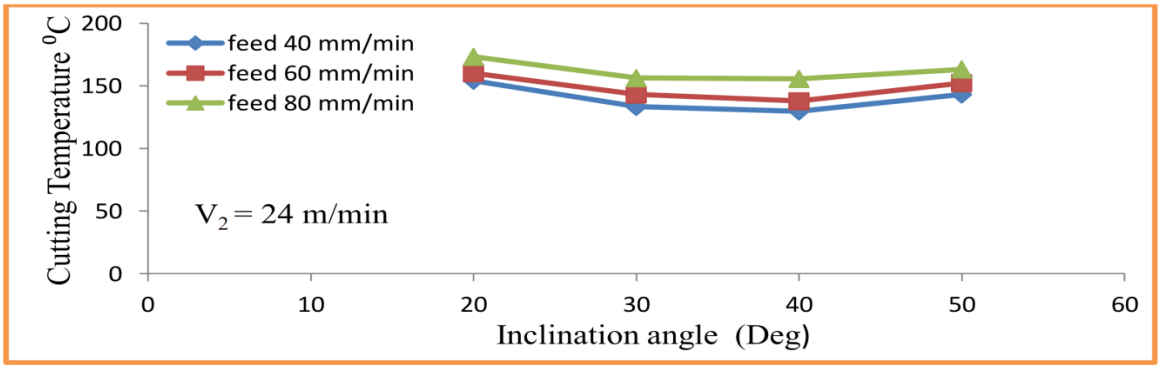

Fig.5.5.1.1 (b). Variation of Cutting Temperature at speed 24 m/min and depth of cut 0.2 mm

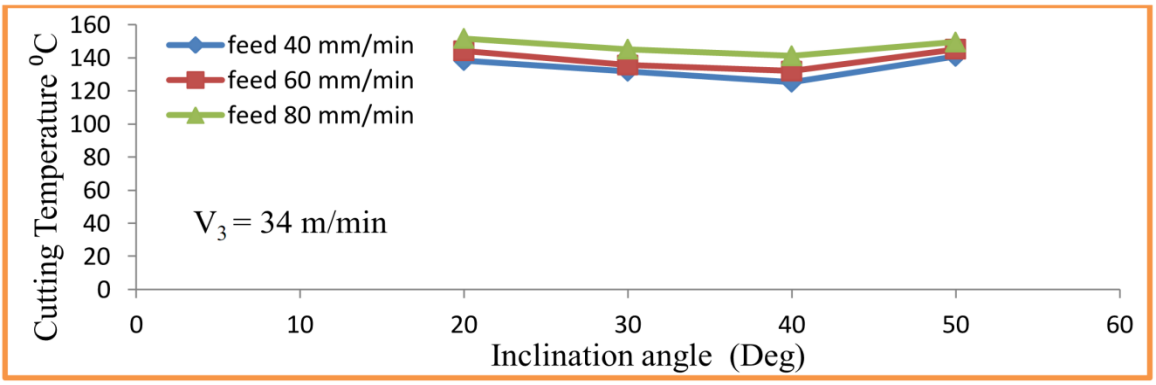

Fig.5.5.1.1 (c). Variation of Cutting Temperature at speed 34 m/min and depth of cut 0.2 mm

Figures 5.5.1.1 (a)-(c) shows the variation of Cutting Temperature at constant depth of cut for different cutting speeds, feed rates and inclination angles.

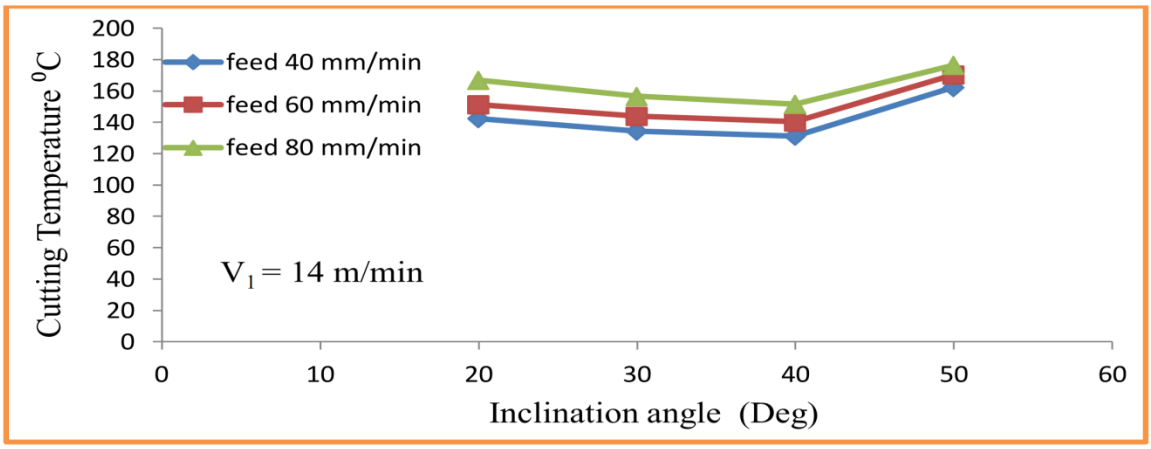

Fig.5.5.1.2 (a). Variation of Cutting Temperature at speed 14 m/min and depth of cut 0.4 mm

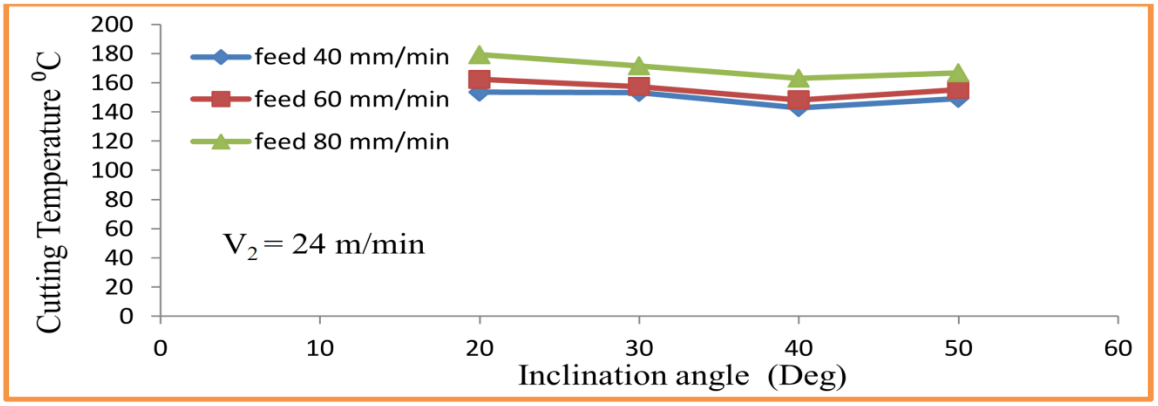

Fig.5.5.1.2 (b). Variation of Cutting Temperature at speed 24 m/min and depth of cut 0.4 mm

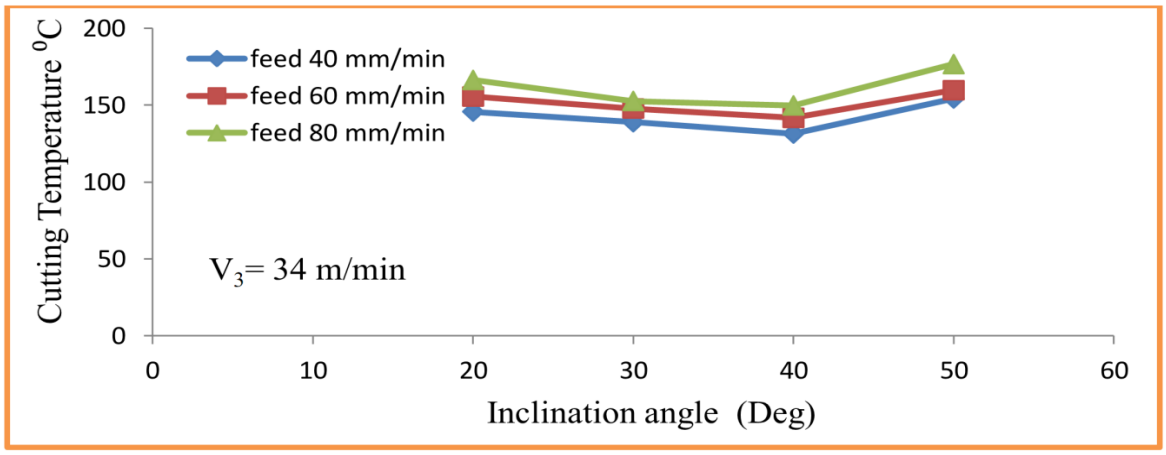

Fig.5.5.1.2 (c). Variation of Cutting Temperature at speed 34 m/min and depth of cut 0.4 mm

Figures 5.5.1.2 (a)-(c) shows the variation of Cutting Temperature at constant depth of cut for different cutting speeds, feed rates and inclination angles.

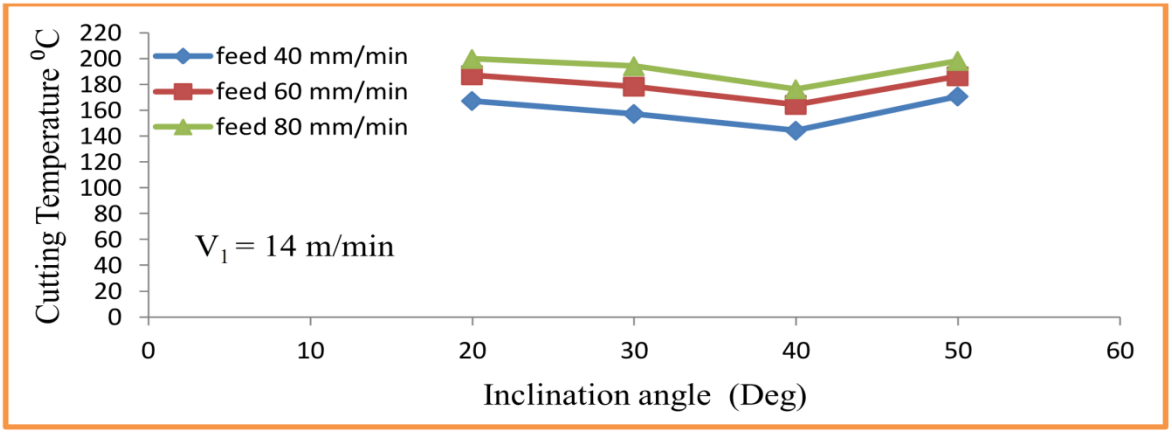

Fig.5.5.1.3(a). Variation of Cutting Temperature at speed 14 m/min and depth of cut 0.6 mm

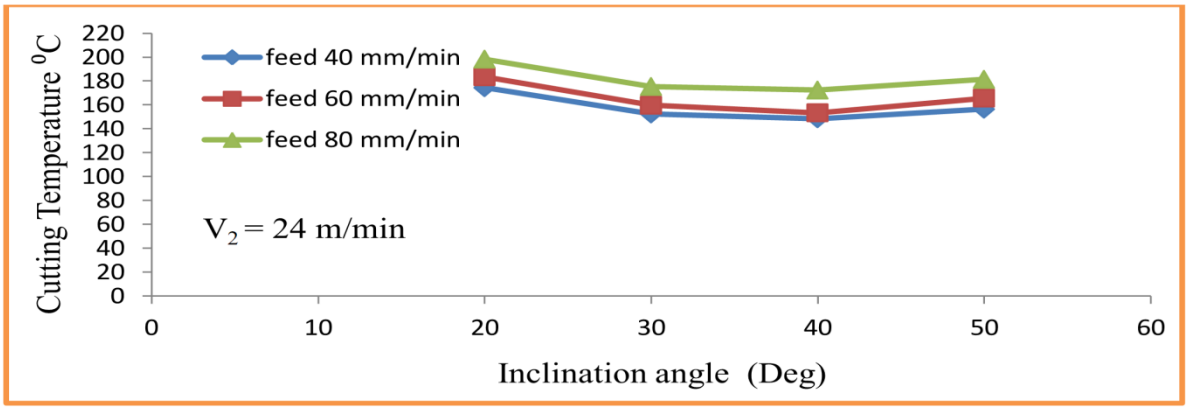

Fig.5.5.1.3 (b). Variation of Cutting Temperature at speed 24 m/min and depth of cut 0.6 mm

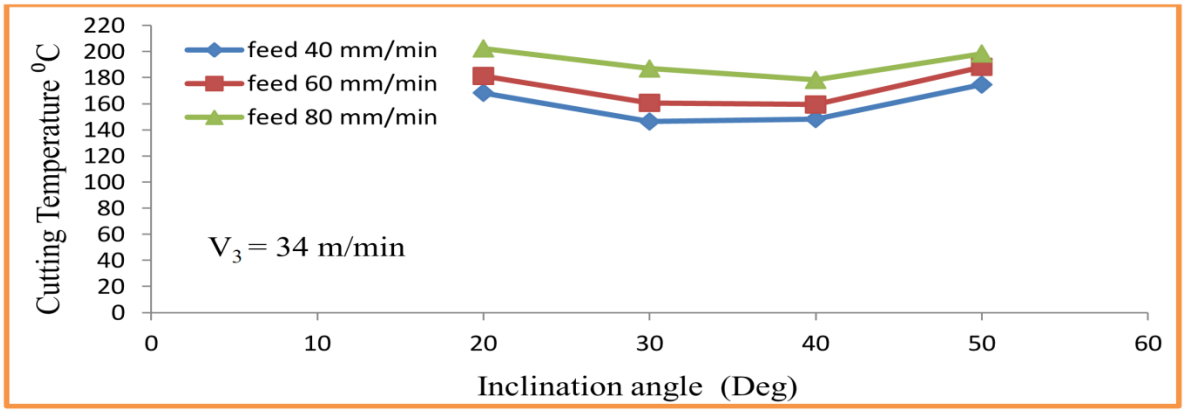

Fig.5.5.1.3 (c). Variation of Cutting Temperature at speed 34 m/min and depth of cut 0.6 mm

Figures 5.5.1.3 (a)-(c) shows the variation of Cutting Temperature at constant depth of cut for different cutting speeds, feed rates and inclination angles.

Figure 5.5.1.1(a) – 5.5.1.3(c) shows the value of cutting temperature at which the experiments were conducted. It is known from the fundamental theory of machining that the cutting Speed plays a key role in cutting temperature of the machining process. The higher the cutting speed, the faster the surface feed that the tool travels, the more heat will be generated by friction. When cutting speed increases, there is less time for the generated heat to be dissipated, hence temperature increases. As feed increases or as the depth of cut increases the chip thickness increases. If the thickness of the chip is very large, the temperature dissipation is very difficult due to the surface larger surface are of chip. There is a little chance to dissipate the temperature, and hence temperature increases.

5.6 Comparison of Cutting Forces of Inconel 625 and SUS 304 (AISI 304)

Table: 5.14 Comparison of Cutting Force (Fz) of Inconel 625 and SUS 304

						Inconel 625 (Dry)		SUS304 (AISI 304) (Dry)
S. NO	Exp No.	I (Deg)	Speed (m/min)	Feed (mm/min)	DOC (mm)	Fz (N)		Fz (N)
1	1	20	14	40	0.2	500.70		356.24
2	3	20	14	40	0.6	1862.45		1717.99
3	7	20	14	80	0.2	766.91		622.45
4	9	20	14	80	0.6	2959.26		2814.81
5	19	20	34	40	0.2	139.99		134.47
6	21	20	34	40	0.6	573.13		428.67
7	25	20	34	80	0.2	348.42		203.97
8	27	20	34	80	0.6	1115.78		971.32
9	28	30	14	40	0.2	160.79		146.33
10	30	30	14	40	0.6	1647.42		1502.96
11	34	30	14	80	0.2	849.06		704.61
12	36	30	14	80	0.6	2719.08		2574.63
13	46	30	34	40	0.2	240.25		195.79
14	48	30	34	40	0.6	1273.25		1128.80
15	52	30	34	80	0.2	559.46		415.00
16	54	30	34	80	0.6	1686.82		1542.37
17	55	40	14	40	0.2	740.46		596.01
18	57	40	14	40	0.6	1689.87		1545.41

19	61	40	14	80	0.2	979.02		834.56
20	63	40	14	80	0.6	2933.25		2788.80
21	73	40	34	40	0.2	597.68		453.23
22	75	40	34	40	0.6	755.17		610.71
23	79	40	34	80	0.2	827.85		683.39
24	81	40	34	80	0.6	1265.95		1121.50
25	82	50	14	40	0.2	469.31		324.85
26	84	50	14	40	0.6	2248.69		2104.23
27	88	50	14	80	0.2	956.58		812.13
28	90	50	14	80	0.6	3853.81		3709.36
29	100	50	34	40	0.2	270.45		125.99
30	102	50	34	40	0.6	823.33		678.88
31	106	50	34	80	0.2	632.73		488.27

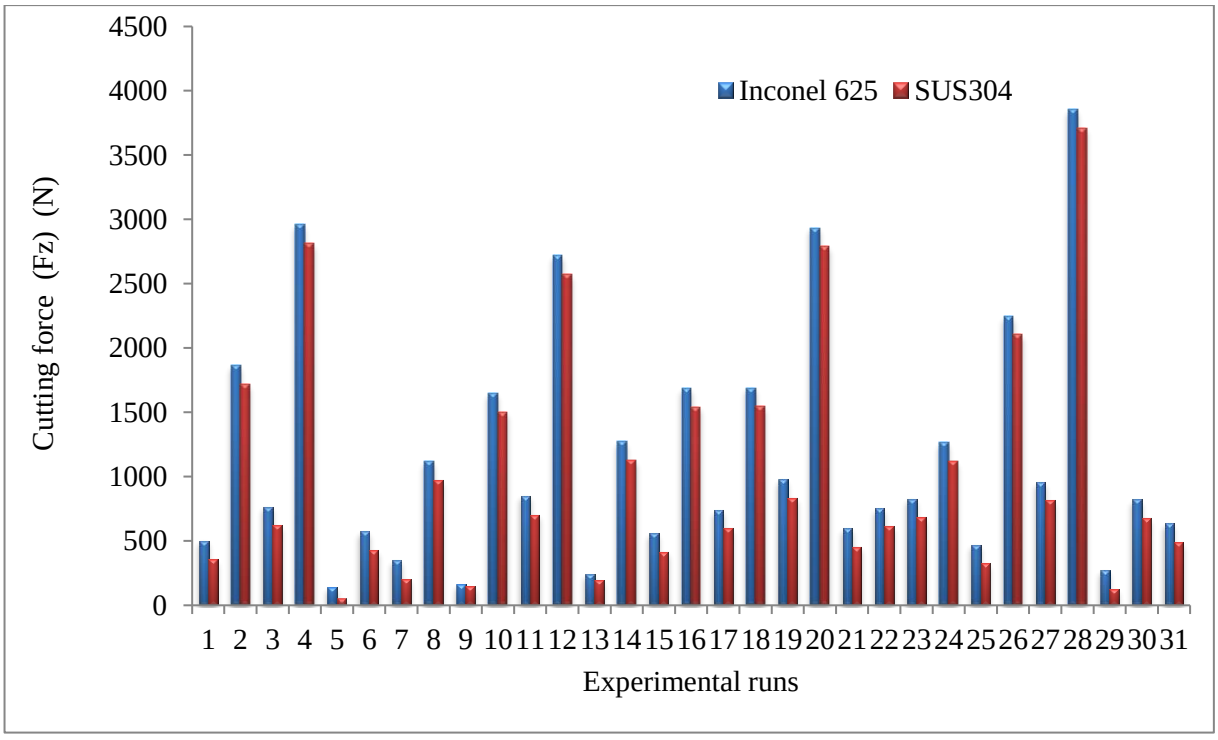

Fig: 5.6 Comparison of Cutting Force (Fz) of Inconel 625 and SUS 304

Cutting forces of Inconel 625 and SUS304 (AISI 304)are compared and depicted in Table 5.6. The Figure 5.6 shows that the cutting forces in SUS304 (AISI 304) is more when compared to Inconel 625. This is because hardness of Inconel 625 alloys is in the range of 30-42 HRC whereas hardness of SUS304 (AISI 304) is 19 HRC i.e. Inconel 625 alloy have more hardness and Dynamic Shear strength compared to SUS304 (AISI 304). Also Inconel 625 super alloys

have FCC crystal structure and they have work hardening properties and hence it is more difficult to penetrate, so more cutting force is required to cut the material as well as Dynamic Shear strength of Inconel 625 super alloys is also high.

5.7 Summary

It can be noticed that the machining with lower inclination angles exhibits lower thrust forces and it is almost 30% of the total thrust force generated in the case of conventional face milling cutters. Hence, rotary milling cutters are recommended for mass production in machining of difficult to machine materials such as Nickel based super alloys and Titanium Alloys for aerospace applications. According to the surface roughness variation graphs, cutting speed and feed rate show a greater influence on surface finish having less surface roughness at low feed rates and high surface roughness at high feed rates. In the case of insert inclination angle, there exists an optimum angle between 30^0 and 40^0 at which the surface roughness is found low. According to the cutting temperature variation graphs, cutting speed and feed rate show a greater influence on cutting temperature. The optimum inclination angles are in between 30^0 and 40^0 to get minimum cutting temperature.

CHAPTER 6

INVESTIGATIONS USING MQL AND NANO COOLANTS ON CUTTING FORCES, IN FACE MILLING OPERATION USING ROTARY FACE MILLING CUTTER

Machining experimentation were also conducted on Inconel 625 alloy using coated tungsten carbide round inserts on Vertical Machining Centre shown in Figure 6.1 at different speed-feed-depth of cut combinations under dry condition, minimum quantity lubrication (MQL) condition and MQL with Nanofluid condition to study the effect of MQL and Nano fluids on the machinability characteristics of the work material Inconel 625 mainly with respect to, Cutting Forces (Fz), Surface Roughness (Ra) and Cutting Temperature. The ranges of the cutting velocity, feed rate and depth of cut were taken as shown in Table 6.1.

Table 6.1: Experimental conditions

Machine tool:	VMC-HINUMERIK 3100M
Work pieces	Inconel 625 Plate 250 mm x250 mm x40 mm
Cutting tool	K20 Coated Carbide
Cutting velocity, Vc	14,24 and 34 mm/min
Feed rate, f:	40, 70 and 100 mm/min
Depth of cut,d:	0.2,0.4. and 0.6 mm
MQL supply:	Air:4 bar, Lubricant: 40 ml/h
Environment:	Dry, MQL and MQL with Nano fluids.
Measurement of surface roughness	(Ultra- Germany Make), Model: TR 110
Measurement of cutting forces	AMTI Dynamometer
Measurement of cutting temperature	INFRARED THERMOMETER

6.1 Cutting Fluid

[O. Cakir, 2007] To minimize the negative effect of friction and cutting temperature generated in cutting zone, the cutting fluids are used. The cutting fluids produce three positive effects in the machining process including heat removal and dissipation, lubrication on the cutting zone and drain out of the chip form machining zone. In order to make machining process more ecological, the Minimal Quantity Lubrication (MQL) has been accepted as successful near-dry applications because of its green environment characteristics.

Minimum quantity lubrication(MQL) refers to the use of only a little quantity of cutting fluids normally at a flow rate of 50–500 ml/h. MQL provides environment friendliness and improves the machinability characteristics**.[M.M.A. Khana, 2009**]. Sometimes this concept of MQL is referred to as micro lubrication or near dry machining. [**MaClure, 2001]** has suggested the concept of MQL since a decade ago as a means of addressing the issues of environmental intrusiveness and industrial problems associated with the airborne cutting fluid particles on factory shop floors. The minimization of cutting fluid also leads to economic advantage by way of saving lubricant costs and cycle time for cleaning work piece, tool, and machine. However, there has been little investigation of the cutting fluids to be used in MQL machining. Here Vegetable Oil is used as coolant in MQL condition and hereafter it is called as MQL.

6.2 Vegetable oil

Vegetable Oil is an environmentally acceptable oil based lubricant. Vegetable Oil will provide the lowest total manufacturing costs of any fluid. Cost savings will be obtained by longer tool life, lower shop maintenance costs, increased productivity, clean chips, clean parts and clean floors. Vegetable Oil is very special to provide greater performance on all ferrous metals. Vegetable Oil exhibits superior lubricant characteristics which allow near dry machining in heavy cutting operations on all CNC, automatic screw, drilling, tapping, milling, turning and hard turning machines. **[Lee, P.-H., 2010].** Its physical and chemical properties are listed in Table 6.2

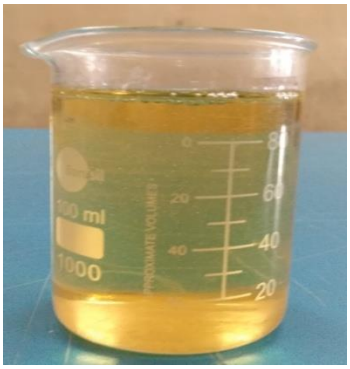

Fig: 6.1 Vegetable oil

6.2.1. Physical and chemical properties

Table 6.2: Properties of vegetable oil

Physical State	Viscosity	Appearance	Weight per Liter	Odor	Water Solubility	Flashpoint
Low Viscous oil	41.87 (mPa)	Clear to Yellow liquid	920 Grams +/- 5.2 Grams	Neutral	Insoluble	Greater than 334 ^{0}C

6.3 Nano Fluid

Nano fluid is a new class of cutting fluid engineered by dispersing nanometre-size solid particles into base fluids such as water, ethylene glycol, lubrication oils, and etc. Nano fluid containing Al2O3 Nano-particles and multi-wall carbon nanotubes were synthesized by two-step physical process. **[Bin Shen, 2008].** Nano fluids have novel properties that make them potentially useful in many applications in heat transfer including microelectronics, fuel cells, and hybrid-powered engines. They exhibit enhanced thermal conductivity and the convective heat transfer coefficient compared to the base fluid.

6.4 Preparation of Nano fluid

In this work the alumina (Al_2O3) Nano particles are mixed with vegetable oil, as a base fluid to make Al_2O3 Nano fluid. The method used to make above Nano fluid is given below. Take one gram of Al2O3 Nano particles and directly mix with 100 ml vegetable oil as a base fluid and prepare the sample. 1Vol% of Al_2O3 Nano fluid = 100 ml of vegetable oil+ 1gm of Al_2O3 Nanoparticles. The above composition has to be mixed continuously about 8 to 9 hours using Magnetic stirrer. The size of Al_2O3 particles is about 5Nm. Here after Nano fluid means a mix of MQL and Al_2O3 particles. Same procedure is used to prepare the SiC nano fluid, and also for hybrid nano fluid (Al_2O_3 + SiC).

6.4.1 Magnetic stirrer

Stirring operation has been carried out for Nano particles into vegetable oil using magnetic stirrer after completion of magnetic stirrer operation we get the Nano fluids. Once the Nano fluid making is over within 2 to 3 hours we have to use the Nano fluid. Otherwise the nanoparticles will precipitate in base oil. The below figure shows depicts Magnetic stirrer, vegetable oil with Nano particles and probe sinicator.

Fig. 6.2Magnetic stirrer and Probe sonication processor

Sonication is a process in which sound waves are used to agitate particles in solution. Such disruptions can be used to mix solutions, speed the dissolution of a solid into a liquid (like sugar into water), and remove dissolved gas from liquids. The sonication process is used to avoid the sedimentation of the nano particles present in the nano fluid which is already prepared using magnetic stirrer. The sonication process is done before using the nano coolant at the machining.

6.4.2 Specifications of the Nano Fluid

Table 6.3: Specification of the Nano Fluid

Base fluid	Vegetable oil
Nano Particles	Al_2O_3 &SiC
Nano Particle size	20-25 nm
Vol. fraction	1%, 3%, 5%
Thermal conductivity of Al_2O_3	31 W/m K
Thermal conductivity of SiC	160 W/m K
Thermal conductivity of vegetable oil	0.162 W/m K
Viscosity of oil	41.87 (mPa-s)

6.5 Experimentation

Experiments have been carried out by Rotary milling on Inconel 625 a nickel based superalloy on VMC-HINUMERIK 3100M using coated carbide inserts. Three optimum conditions obtained by RSM methodology tabulated in Table 5.1 has been selected to explore the role of MQL (Vegetable Oil) and MQL + Nanofluid (Al_2O_3 and SiC) on the machinability characteristics of work material mainly in terms of cutting force (Fz), Surface Roughness (Ra) and Cutting Temperature. The MQL and Nano fluid (i.e. MQL + Nano fluid) has been supplied at high pressure and impinged at high speed through the nozzle at the cutting zone under uninterrupted supply of MQL and Nano fluid conditions at constant pressure around 4 bar. The results are tabulated in the next sections. Nine experiments were conducted by Minimum Quantity Lubrication (MQL) process. The nine experiments were taken from RSM Design experimentation list. Three maximum load conditions, three medium load conditions and three minimum load conditions were conducted. Using MQL with Nano coolants, the experiments were conducted for the above mentioned nine experiments. The levels of Nano particles are 1%, 3% and 5% of weight ratio.

If all the experiments are conducted with MQL and nano coolants the number of experiments goes up and this makes the study rather cumbersome. Data analysis also becomes complex. Using these nine experiments we conducted three replicates and the no of experiments was 243, a very sizable number.

6.5.1 Experimental values of Cutting Force (Fz) on Inconel 625 Under Dry, MQL and Nano fluid

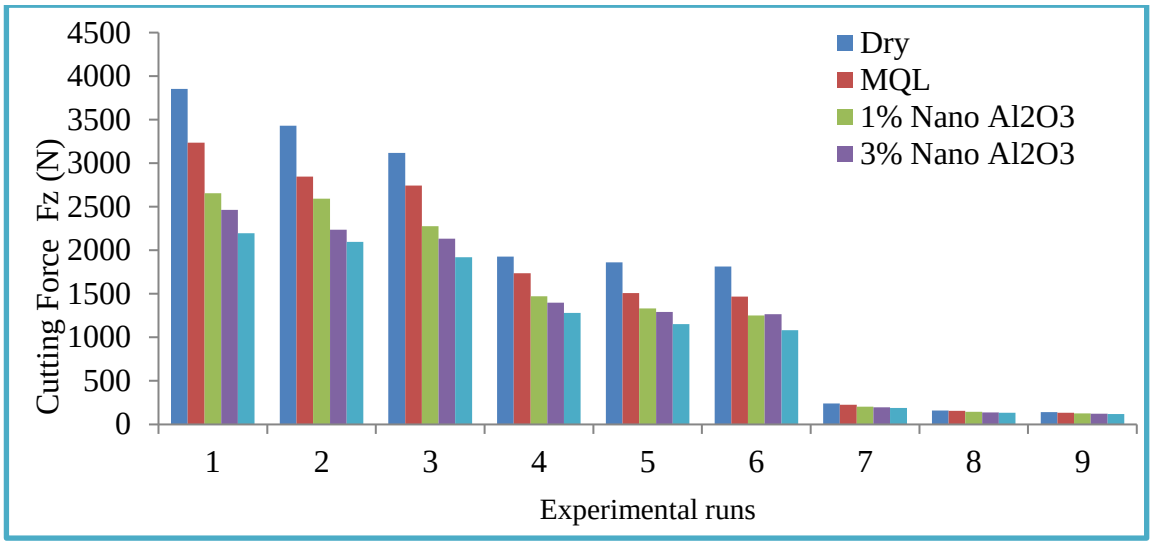

Fig.6.3 Comparison of cutting Force (Fz): Dry, MQL, MQL with Al_2O_3 Nano coolants

6.5.1.1 Comparison of Cutting Force (Fz)for Al_2O_3

Table 6.4 Comparison of Cutting Force (Fz) for Al_2O_3Nano coolant

		% Reduction
a) Dry Condition		-
b) MQL	(a to b)	3-17%
c) 1 % Al_2O_3 Nano Fluid	(b to c)	11-15%
d) 3 % Al_2O_3 Nano Fluid	(c to d)	5-8%
e) 5 % Al_2O_3 Nano Fluid	(d to e)	4-7%

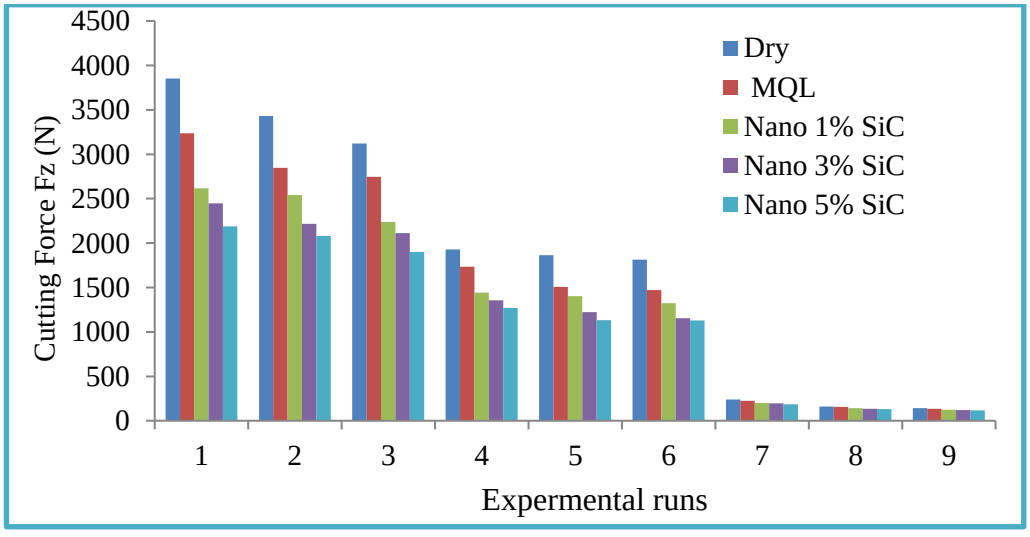

Fig.6.4 Comparison of cutting Force (Fz): Dry, MQL, MQL with SiCNano coolants

6.5.1.2 Comparison of Cutting Force (Fz) for SiC

Table 6.5 Comparison of Cutting Force (Fz) for SiC Nano coolant

		% Reduction
a) Dry Condition		-
b) MQL	(a to b)	3-17%
c) 1 % SiC Nano Fluid	(b to c)	12-16%
d) 3 % SiC Nano Fluid	(c to d)	6-9%
e) 5 % SiC Nano Fluid	(d to e)	5-8%

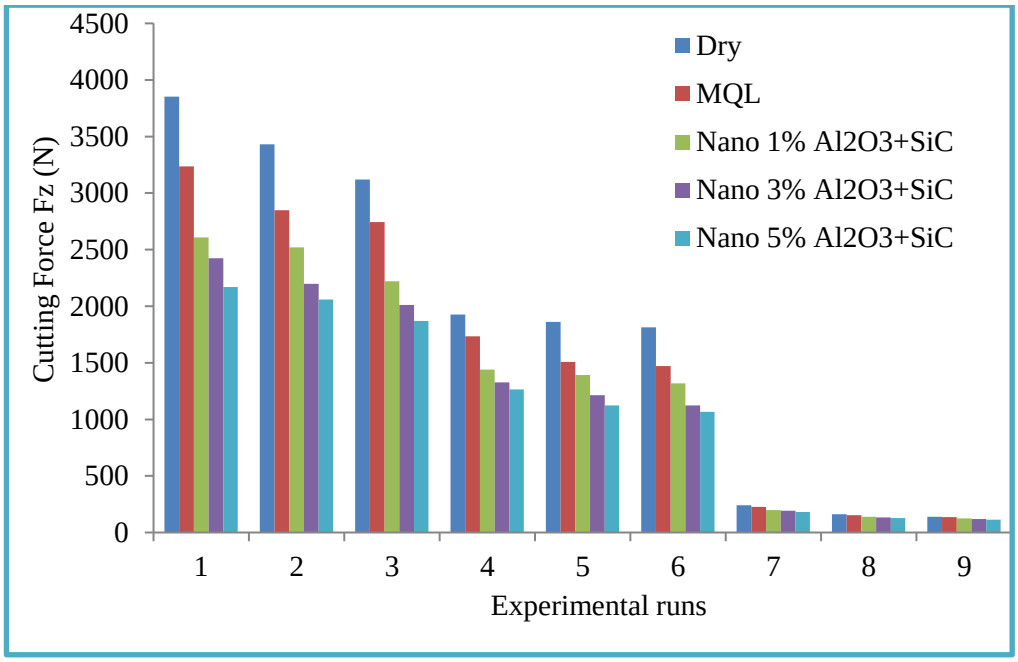

Fig. 6.5 Comparison of cutting Force (Fz): Dry, MQL, MQL with Al_2O_3+ SiC Nano coolants

6.5.1.3 Comparison of Cutting Force (Fz) for Al_2O_3+SiC

Table 6.6 Comparison of Cutting Force (Fz) for Al_2O_3+SiCNano coolants

		% Reduction
a) Dry Condition		-
b) MQL(a to b)		3-17%
c) 1 % Al_2O_3+SiCNano Fluid	(b to c)	15-17%
d) 3 % Al_2O_3+SiCNano Fluid	(c to d)	9-11%
e) 5 % Al_2O_3+SiCNano Fluid	(d to e)	8-10%

Table: 6.7 Overall Comparison of cutting Force (Fz): Dry, MQL, MQL with Nano coolants

Expt.	Dry	MQL	1% Al_2O_3	3% Al_2O_3	5% Al_2O_3	1% SiC	3% SiC	5% SiC	1% Al_2O_3+SiC	3% Al_2O_3+SiC	5% Al_2O_3+SiC
1	3853.8	3237.2	2654.5	2465.6	2194.3	2614.8	2445.5	2188.3	2608.7	2423.9	2168.6
2	3430.8	2847.6	2591.3	2236.9	2095.7	2541.3	2216.7	2079.7	2521	2199	2059.7
3	3119.1	2744.8	2278.2	2132.9	1919.7	2238.4	2112.2	1898.7	2221.7	2012.6	1869.7
4	1927.3	1734.6	1473.6	1396.7	1280.4	1443.3	1356.9	1270.6	1439.2	1327	1263.6
5	1862.4	1508.6	1333.2	1291.5	1152.6	1401.1	1223.9	1133	1392.6	1212.7	1122.8
6	1814.7	1469.9	1252.3	1264.7	1082	1322.4	1153.4	1130.2	1319	1122.6	1065.9
7	240.2	225.8	205.3	198.4	188.5	199.4	196.4	185.7	197.6	191.6	182
8	160.8	154.4	145.4	136.6	132.3	141.5	136	130.3	139.4	131.9	128.8
9	140	135.8	128.4	121.5	118.3	125.4	121.1	115.4	124.1	118.4	113.9

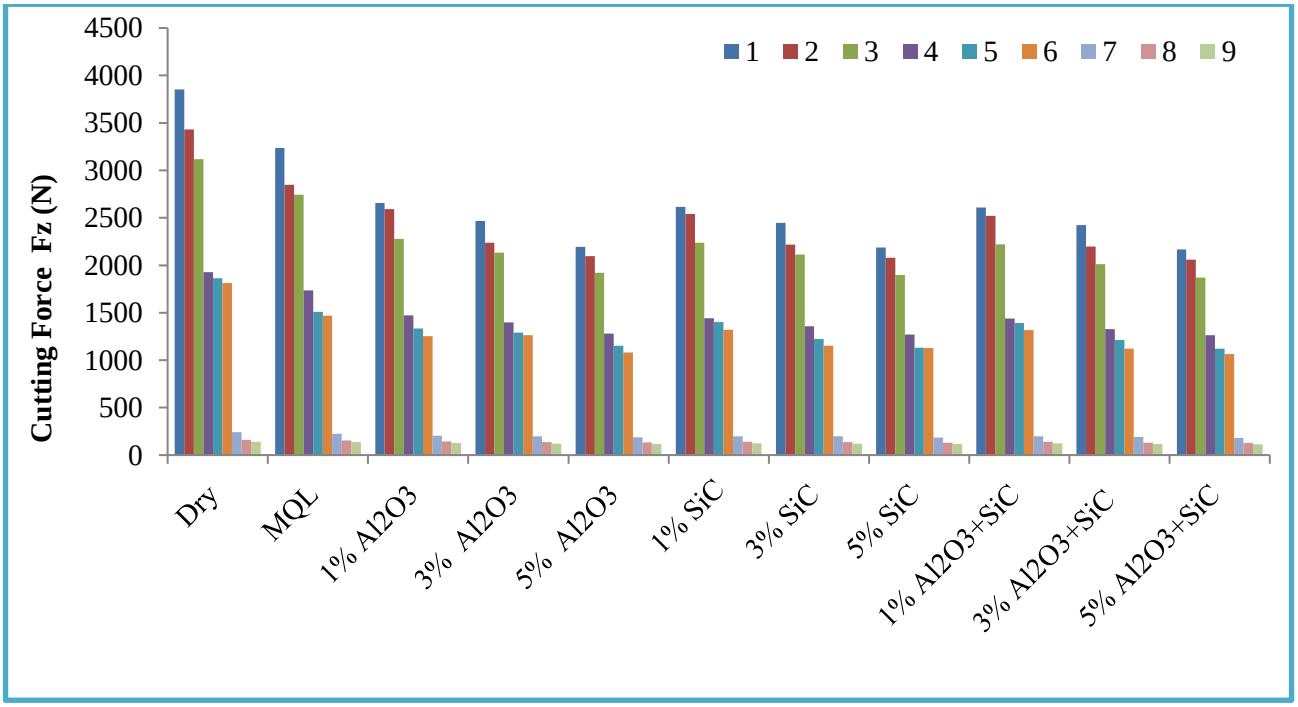

Fig. 6.6 Comparison of cutting Force (Fz): Dry, MQL, MQL with Nano coolants

Figure 6.3 - 6.5shows the Cutting Force at all the three environment conditions i.e. Dry, MQL, Nano fluid, it is clear that the range of the Cutting Force is gradually decreasing from dry to MQL and from MQL to Nano fluid is shown in following tables 6.4, 6.6 and 6.8. The tables 6.5,

6.7 and 6.9 showing the reduction in cutting force (Fz). This reduction of cutting forces from dry condition to MQL may be due to change in the chip tool interaction and retention of cutting edge sharpness due to reduction of cutting temperature. It is observed that there is a reduction of cutting forces in Nano fluid condition as compared to dry, MQL, this may be due to reduction of cutting zone temperatures, which results in less friction and a decrease in the formation of built up edges. Table 6.10 shows the overall Comparison of cutting Force (Fz) in all environments i.e. Dry, MQL, MQL with Nano coolants with all three wt% and figure 6.6 shows the overall comparison of cutting Force (Fz) in all Dry, MQL, and MQL with Nano coolants with all three wt%.

6.5.2 Experimental values of Surface Roughness (Ra) on Inconel 625 Under Dry, MQL and Nano fluid

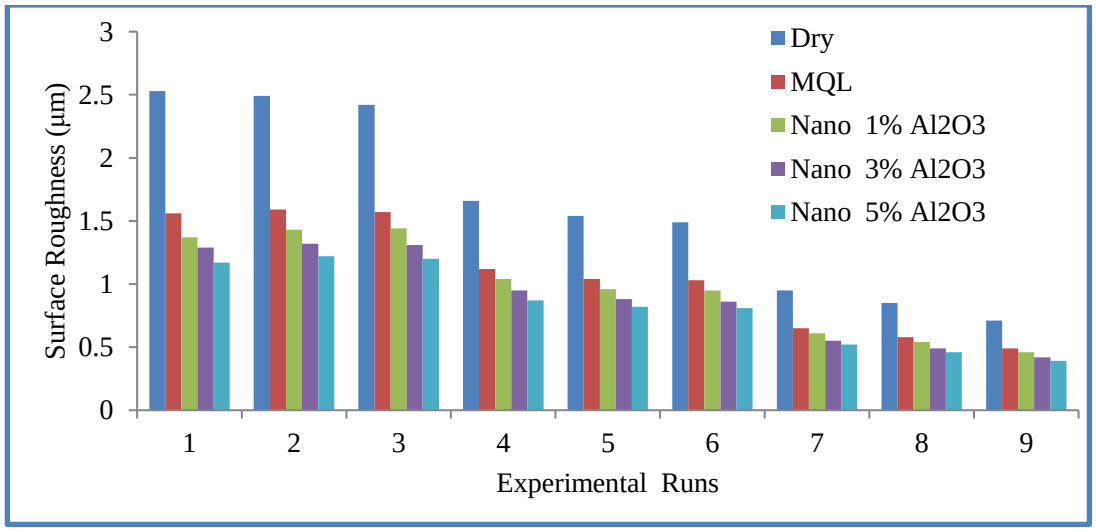

Fig.6.7 Comparison of Surface Roughness: Dry, MQL, MQL with Al_2O_3 Nano coolants

6.5.2.1 Comparison of Surface Roughness for Al_2O_3

Table 6.8 Comparison of Surface Roughness for Al_2O_3Nano coolants

		% Reduction
a) Dry Condition		-
b) MQL	(a to b)	31-38%
c) 1 % Al_2O_3 Nano Fluid	(b to c)	6-12%
d) 3 % Al_2O_3 Nano Fluid	(c to d)	4-8%
e) 5 % Al_2O_3 Nano Fluid	(d to e)	23-25%

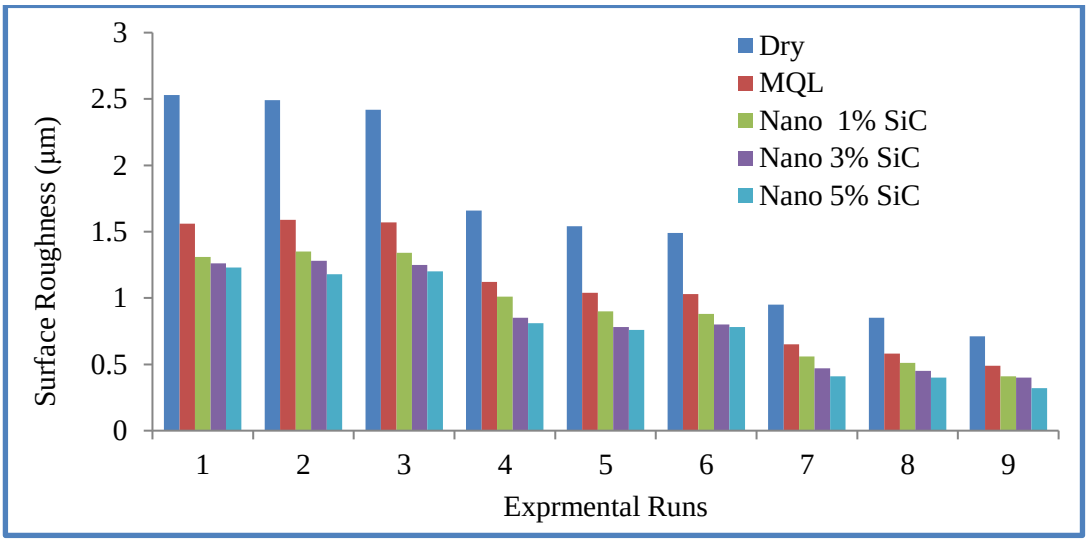

Fig.6.8 Comparison of Surface Roughness: Dry, MQL, MQL with SiC Nano coolants

6.5.2.2 Comparison of Surface Roughness for SiC

Table 6.9 Comparison of Surface Roughness for SiC Nano coolant

		% Reduction
a) Dry Condition		-
b) MQL	(a to b)	31-38%
c) 1 % SiC Nano Fluid	(b to c)	8-14%
d) 3 % SiC Nano Fluid	(c to d)	5-10%
e) 5 % SiC Nano Fluid	(d to e)	24-26%

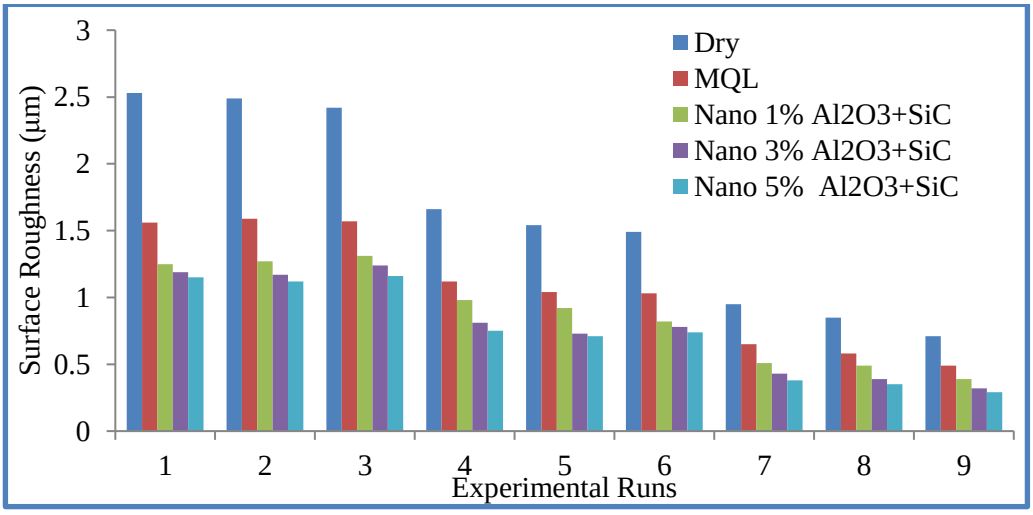

Fig. 6.9 Comparison of Surface Roughness: Dry, MQL, MQL with Al_2O_3+SiCNano coolants

6.5.2.3 Comparison of Surface Roughness for Al_2O_3+SiC

Table 6.10 Comparison of Surface Roughness for Al_2O_3+SiC) Nano coolants

		% Reduction
a) Dry Condition		-
b) MQL	(a to b)	31-38%
c) 1 % Al_2O_3+SiCNano Fluid	(b to c)	10-17%
d) 3 % Al_2O_3+SiCNano Fluid	(c to d)	6-12%
e) 5 % Al_2O_3+SiCNano Fluid	(d to e)	25-28%

Table: 6.11 Overall Comparison of Surface Roughness (Ra): Dry, MQL, MQL with Nano coolants

Expt.	Dry	MQL	1% Al_2O_3	3% Al_2O_3	5% Al_2O_3	1% SiC	3% SiC	5% SiC	1% Al_2O_3+SiC	3% Al_2O_3+SiC	5% Al_2O_3+SiC
1	2.53	1.56	1.37	1.29	1.17	1.31	1.26	1.23	1.25	1.19	1.15
2	2.49	1.59	1.43	1.32	1.22	1.35	1.28	1.18	1.27	1.17	1.12
3	2.42	1.57	1.44	1.31	1.2	1.34	1.25	1.2	1.31	1.24	1.16
4	1.66	1.12	1.04	0.95	0.87	1.01	0.85	0.81	0.98	0.81	0.75
5	1.54	1.04	0.96	0.88	0.82	0.9	0.78	0.76	0.92	0.73	0.71
6	1.49	1.03	0.95	0.86	0.81	0.88	0.8	0.78	0.82	0.78	0.74
7	0.95	0.65	0.61	0.55	0.52	0.56	0.47	0.41	0.51	0.43	0.38
8	0.85	0.58	0.54	0.49	0.46	0.51	0.45	0.4	0.49	0.39	0.35
9	0.71	0.49	0.46	0.42	0.39	0.41	0.4	0.32	0.39	0.32	0.29

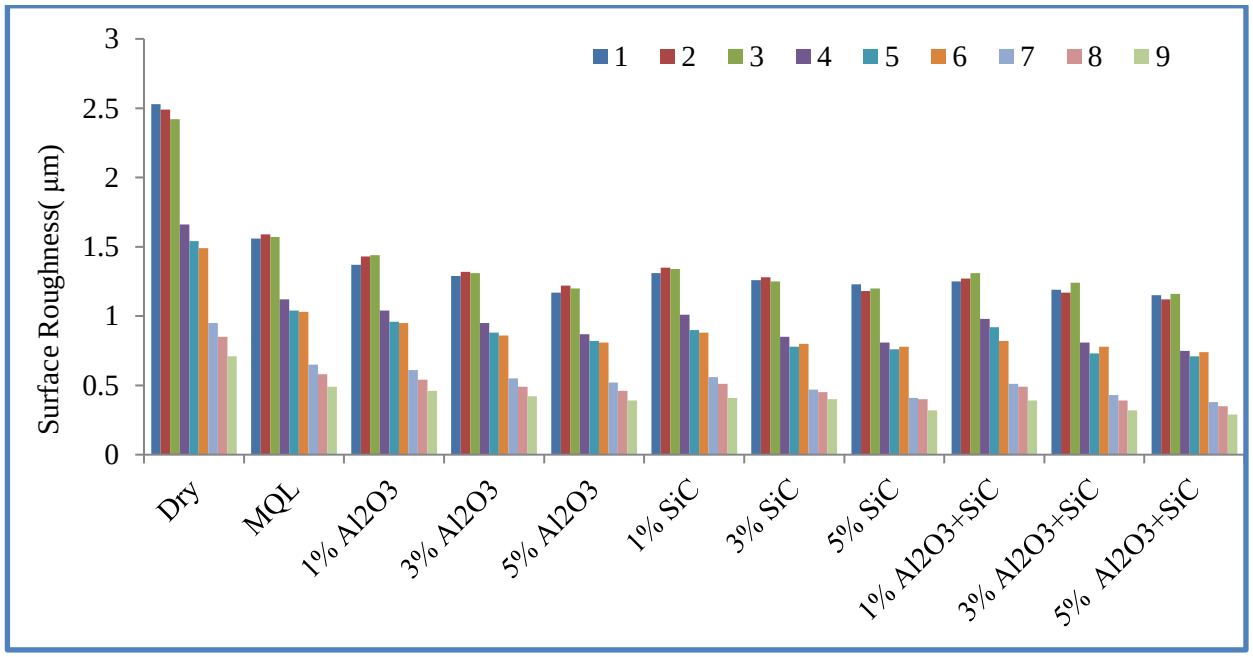

Fig. 6.10 Comparison of Surface Roughness: Dry, MQL, MQL with Nano coolants

Figures 6.7 – 6.9 are showing the surface roughness in all the three environment conditions i.e. Dry, MQL, Nano fluid, it is clear from the Figure 6.7 – 6.9 that the range of the surface roughness is gradually decreasing from dry to MQL and MQL to Nano fluid is shown in following tables 6.11, 6.13 and 6.15.The surface roughness is more in dry condition, this may be due to more intensive temperature and stress at tool chip interface. It is observed that plain MQL condition gives better surface finish than the dry cutting process, this may be due to controlling the deterioration of the auxiliary cutting edge of abrasion, chipping and built up edge formation. It is also observed that Nano fluid further decreases the surface roughness, this is because Nano fluids exhibit enhanced thermal properties such as higher thermal conductivity and heat transfer coefficients compared with the plain MQL. Tables 6.12, 6.14 and 6.16 showing the reduction in surface roughness and figure 6.10 shows the overall comparison of all three environments with all three wt%.

6.5.3 Experimental values of Cutting Temperature on Inconel 625 Under Dry, MQL and Nano fluid

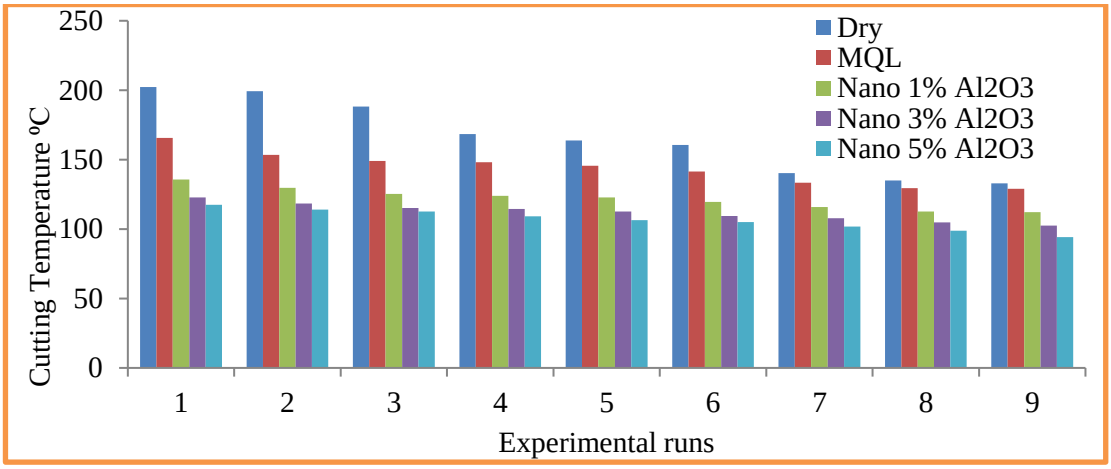

Fig. 6.11 Comparison of Cutting Temperature: Dry, MQL, MQL with Al_2O_3 Nano coolants

6.5.3.1Comparison of Cutting Temperature for Al_2O_3

Table: 6.12 Comparison of Cutting Temperature for Al_2O_3 Nano coolant

	% Reduction
a) Dry Condition	-
b) MQL (a to b)	3-18%
c) 1 % Al_2O_3 Nano Fluid (b to c)	13-15%
d) 3 % Al_2O_3 Nano Fluid (c to d)	3-4%
e) 5 % Al_2O_3 Nano Fluid (d to e)	2-3%

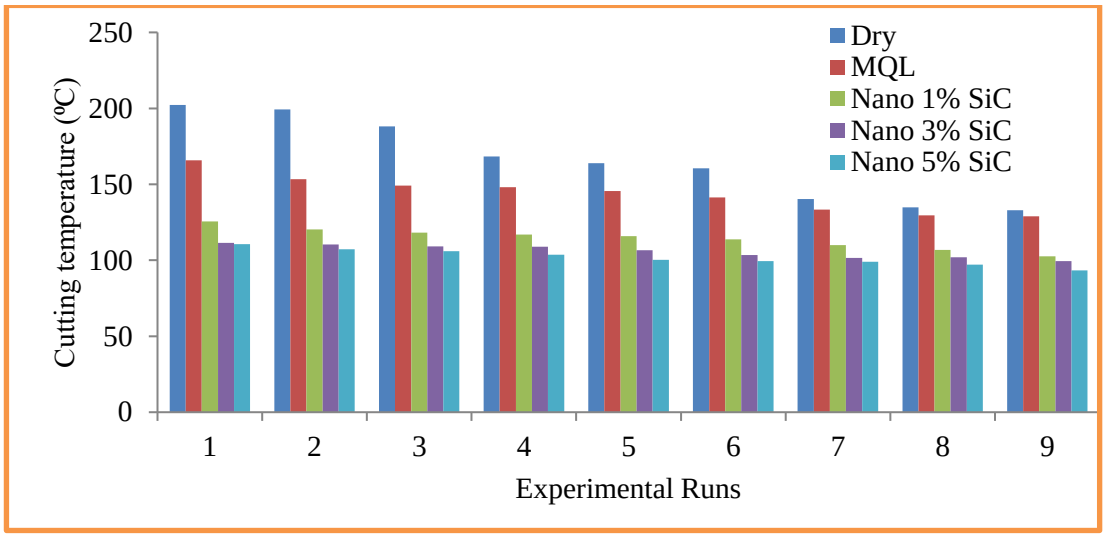

Fig: 6.12 Comparison of cutting Temperature: Dry, MQL, MQL with SiCNano coolants

6.5.3.2 Comparison of Cutting Temperature for SiC

Table: 6.13 Comparison of Cutting Temperature for SiC Nano coolants

		% Reduction
a) Dry Condition		-
b) MQL	(a to b)	3-18%
c) 1 % SiC Nano Fluid	(b to c)	11-18%
d) 3 % SiC Nano Fluid	(c to d)	4-5%
e) 5 % SiC Nano Fluid	(d to e)	2-4%

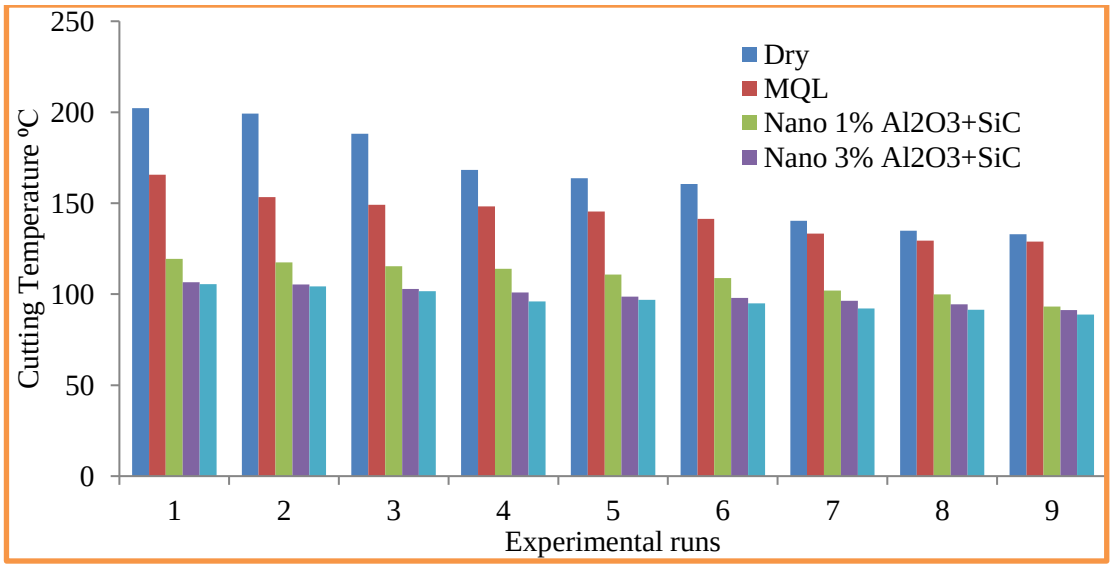

Fig: 6.13 Comparison of cutting Temperature: Dry, MQL, MQL with SiC Nano coolants

6.5.3.3 Comparison of Cutting Temperature for Al_2O_3+SiC

Table: 6.14 Comparison of Cutting Temperature for Al_2O_3+SiCNano coolants

		% Reduction
a) Dry Condition		-
b) MQL	(a to b)	3-18%
c) 1 % Al_2O_3+SiCNano Fluid	(b to c)	12-19%
d) 3 % Al_2O_3+SiCNano Fluid	(c to d)	4-7%
e) 5 % Al_2O_3+SiCNano Fluid	(d to e)	2-4%

Table: 6.15 Overall Comparison of cutting temperature: Dry, MQL, MQL with Nano coolants

Expt.	Dry	MQL	1% Al_2O_3	3% Al_2O_3	5% Al_2O_3	1% SiC	3% SiC	5% SiC	1% Al_2O_3 +SiC	3% Al_2O_3 +SiC	5% Al_2O_3 +SiC
1	202.3	165.7	135.75	122.67	117.47	125.6	111.5	110.71	119.32	106.56	105.56
2	199.2	153.4	129.78	118.45	114.01	120.4	110.4	107.21	117.38	105.32	104.32
3	188.2	149.1	125.29	115.16	112.61	118.3	109.2	105.91	115.29	102.85	101.65
4	168.3	148.2	123.92	114.58	109.29	116.9	109	103.59	113.92	100.86	95.95
5	163.8	145.5	122.86	112.71	106.37	115.9	106.6	100.35	110.86	98.63	96.89
6	160.6	141.4	119.44	109.44	105.05	113.8	103.5	99.55	108.84	97.89	94.98
7	140.3	133.3	115.97	107.85	101.69	110	101.6	98.96	101.97	96.32	92.12
8	134.9	129.5	112.67	104.9	98.78	106.8	101.9	97.18	99.85	94.45	91.45
9	132.9	128.9	112.15	102.42	94.31	102.6	99.42	93.36	91.25	93.25	88.86

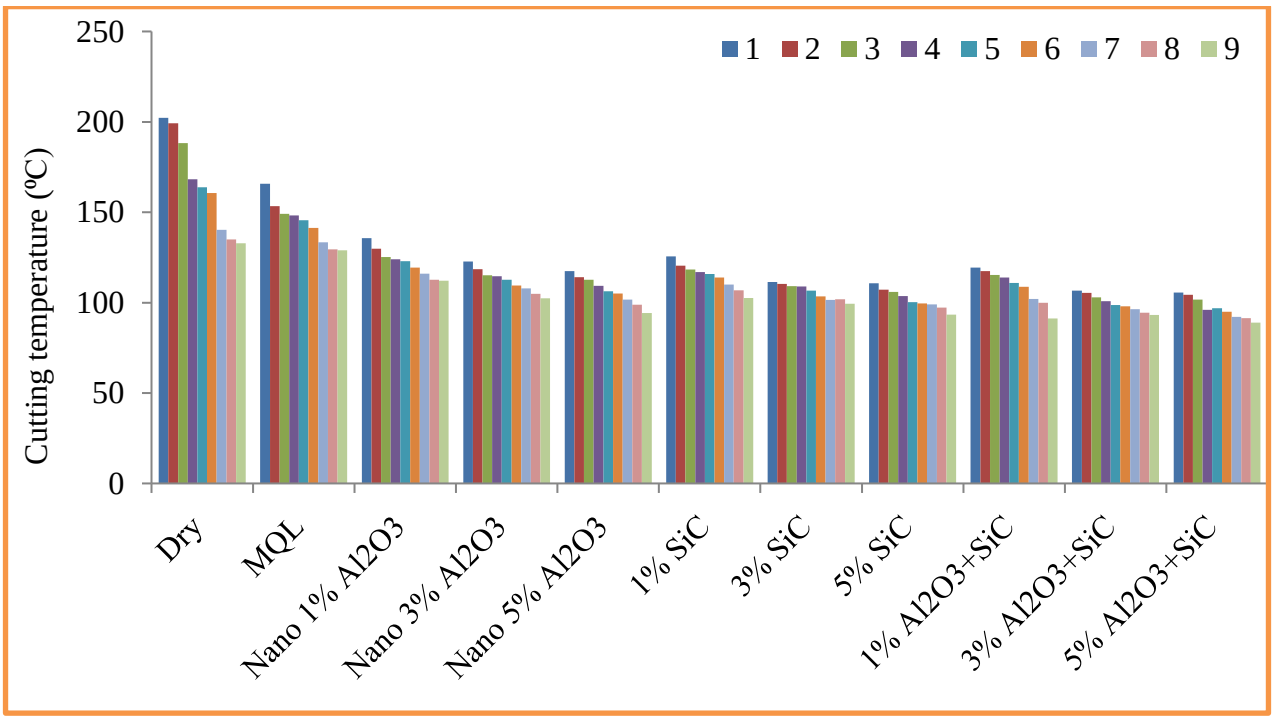

Fig: 6.14 Comparison of cutting Temperature: Dry, MQL, MQL with Nano coolants

Figures 6.11 - 6.13shows cutting temperature in all the three environments i.e. Dry, MQL and Nano fluid, it is clear that the range of the Temperature is gradually decreasing from dry to MQL using Nano fluid as shown in following Table 6.17, 6.20 and 6.22.

It is observed in case of MQL condition chips did not change appreciably but their back surface appeared much brighter and smoother which indicates that the amount of reduction of temperature at chip–tool interaction and eliminates trace of built up edge formation. It is also observed that in the case of Nano fluid condition reduction of cutting temperature is due to Nano fluid exhibits higher convective heat transfer coefficient which enables reduction of average tool work interface temperature. Tables 6.19, 6.21 and 6.23 showing the reduction in cutting temperature and figure 6.14 shows the overall comparison of all three environments with all three wt%.

6.6 Summary

The effect of MQL and Nano fluids (100ml of vegetable oil + 1gm of Al_2O_3or SiC and combination of both) on the machinability characteristics of Inconel 625 mainly with respect to Cutting Forces, surface roughness and temperature dissipation have been thoroughly studied in this chapter. The Cutting Forces for Inconel 625 have been reduced by using Nano fluid of $Al_2O_3$and SiC as compared to dry and MQL. This may be due to reduction of cutting zone temperatures, which results in less friction and decrease in the formation of built up edges. The surface roughness for Inconel 625 is very low when using Nano fluid of $Al_2O_3$and SiC as compared to MQL and Dry conditions. This is may be due to enhanced thermal properties of Nano fluids such as higher thermal conductivity and heat transfer coefficients compared to MQL and dry conditions. The cutting temperature for Inconel 625is found reduced gradually from dry to Nano fluid of $Al_2O_3$and SiC. This may be due to higher convective heat transfer coefficient for Nano fluids and cooling occurs by convective and evaporative heat transfer of coolant. So the best machining conditions to improve quality is machining with Nano fluid of $Al_2O_3$and SiC, and we can get the benefit of saving machining time and machining cost. The combination of $Al_2O_3$and SiC Nano fluid is generate the optimum values for machining of Inconel 625.

CHAPTER 7

DEVELOPMENT OF PREDICTIVE MODEL FOR ESTIMATION OF CUTTING FORCES, SURFACE ROUGHNESS AND CUTTING TEMPERATURE

This chapter deals with the generation of regression models for cutting force, surface roughness and cutting temperature for rotary machining of Inconel 625 using Multi Gene Genetic Programming (MGGP) by considering the experimental data from chapter V. This chapter also deals with prediction of cutting force, surface roughness and cutting temperature using a multi-objective optimization NSGA - II.

7.1. Modeling of Cutting force using Multi gene genetic Programming (MGGP)

7.1.1. MGGP Implementation

In this work, the software tool GPTIPS is used to develop appropriate MGGP models to predict the cutting force, surface roughness and cutting temperature for rotary machining of Inconel 625 **[Searson, D.P., D.E, 2010].**This software is a new code written by "Genetics and Regression Symbolic Programming" on the basis of multi gene genetic programming by means of MATLAB **[Poli, R., A, 2003].** MGGP method is applied to the dataset of Table 5.1 in chapter V. This study aims to determine the cutting force, surface roughness and cutting temperature for rotary machining of Inconel 625and develop a model for prediction of cutting force, surface roughness and cutting temperature for rotary machining of Inconel 625 based on the MGGP. Figure 5.1 shows the architecture of the modeling concept for predicting the cutting force, surface roughness and cutting temperature.

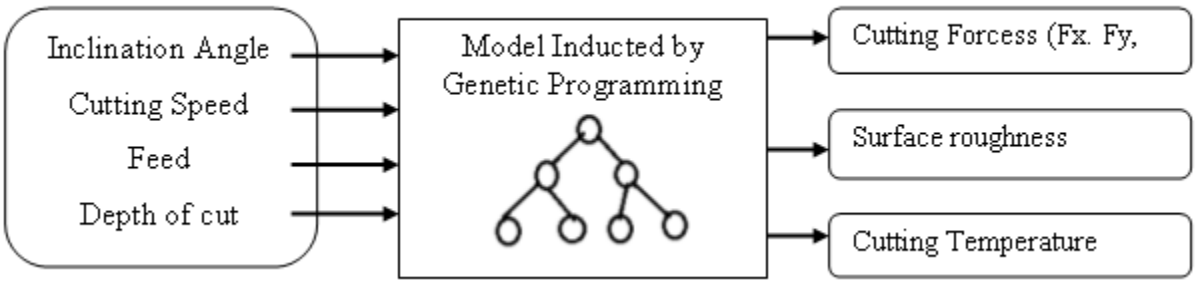

Figure 7. 1 Architecture of the modeling paradigm to predict the cutting variables

GPTIPS has the ability to prevent limitations to the arising of bloating. Bloating is explained as the redundant growth of the tree model without any considerable development in the fitness value **[Kim, M.-I. and P. Zou, 2016, Baziar, M.H., et al 2011]**. This can be prevented when initial parameters were set to certain boundaries, such as a maximum number of nodes per trees, maximum depth of genes, trees, and a maximum number of genes. The tournament selection used was lexicographic, which is an effective method for controlling the bloating of the model **[Luke, S. and L. Panait, 2002]**. The authors examined the value of Root mean square error (RMSE) for evaluating the fitness function. Other initial parameters were established for the implementation of GPTIPS is given in the Table 5.1 **[Searson, D, 2009].**

7.1.2. Setting of parameter for implementation of MGGP

Table 5.1 in chapter V shows the 108 experimental data set values. The experimental data were divided into two groups: the testing dataset as well as the training dataset. The training dataset was employed to compute the equation with input parameters for each response (output parameters) and the testing data was used to verify the developed model and to ensure the widespread implementation of the model for the invisible cases. Selection of testing and training data set has an effect on training models. In this work, about 80 % of the experimental data was chosen randomly for training model while the other 20% of data is used as testing data. The selection is such that the minimum, maximum, mean and standard deviation of the training and testing data sets were reliable. MGGP's best model is based on a minimum RMSE value.

Table: 7.1Initial factor settings for MGGP

Parameters	Values assigned
Population size	100
No. of Generations	200
Runs	10
Size of the tournament	2
Maximum depth of the tree	4
Maximum genes	5
Functional Set	Plus, Minus, Multiply,
Terminal Size	2
Cross over Probability (%)	0.80
Mutation Probability (%)	0.20
Reproduction Probability (%)	0.10

Objective Functions:

Minimization of Fx, Fy, Fz, Ra and Temperature

Constraints: $20 < \text{Inclination Angle} < 50$

$14 < \text{Cutting Speed} < 34$

$40 < \text{Feed} < 80$

$0.2 < \text{Depth of cut} < 0.6$

Basic arithmetic operators, trigonometric and exponential functions are used to obtain optimal MGGP models. The size of the population controls the number of equations in the population. The numbers of levels used by algorithms at end of the run were set by the number of

enervations. The appropriate number of generation and population always depends on a number of the problem complicity and feasible solutions.

A good number of generations and population were thoroughly tested to obtain accurate models for minimum error. The program is executed until the run inevitably completed. The maximum depth of the tree and the maximum number of genes in an individual affects the number of solutions dealt with the search space and the size of the search space. In this case, both complexities of the function and the speed of the developed algorithm decrease simultaneously. The permissible number of genes and the depth of the tree are each set to the optimal values of 4 and 4 as shown in the Table 7.1.

There were several tests performed with different initial parameters of MGGP and the performance of developing equations was calculated for every run. Finally, the best mathematical models were selected for the prediction of Cutting force, Surface Roughness and Cutting Temperature according to performance evaluation criteria.

7.1.3. MGGP model for Cutting Force (Fx)

The best model for Cutting force formulated by MGGP using experimental data given in Table 5.1 is

$$Fx = 1.732*x3-6.854*x2-136.0*x1+11200.0*x4+3.082*x2^2*x4^2+1.732*x1*x2- 450.2* x2*x4 + 90.22*x3*x4 + 4.816*x2^2*x4+ 1.733*x1^2 -4809.0*x4^2- 1.733*x2*x3*x4+ 720.8 \quad (7.1)$$

The accuracy of the equation 7.1 is shown by plotting the Cutting force (Fx) against training and testing data with predicted values as shown in Figure 7.2. The determination of the coefficient (R) and root mean square error (RMSE) are equal to 0.91454 and 289.8977 for testing sets and 0.9681 and 174.1133, for training sets as shown in Figure 7.3(i) and (ii), respectively. There is a good correlation among the predictions from MGGP and the measured values.

A comparison of the errors for the training and testing with experimental data is performed using MGGP and experimental results are shown in Figure 7.2. As can be seen, the training set that includes results of 80 samples and testing set comprising samples of 20 results. It has been observed that the MGGP model can predict the Cutting force (Fx) with a high degree of precision and high variance (96.81% for training and 91.45% testing data) and the root mean square error (RMSE).

Smaller absolute error is better in the GP model, the error found to be is decreased with the increase of number of nodes and thus a MGGP model is more complex. Figure 7.3 shows the actual versus predicted values of Cutting Force (Fx) of training data and testing data Due to this computational difficulty, model was run for the tree depth limited to 4 as shown in Table 7.1. MGGP model was run for 100 times in the same conditions (Table 7.1).This MGGP model is capable of predicting objective (Cutting force) of rotary milling process with high accuracy

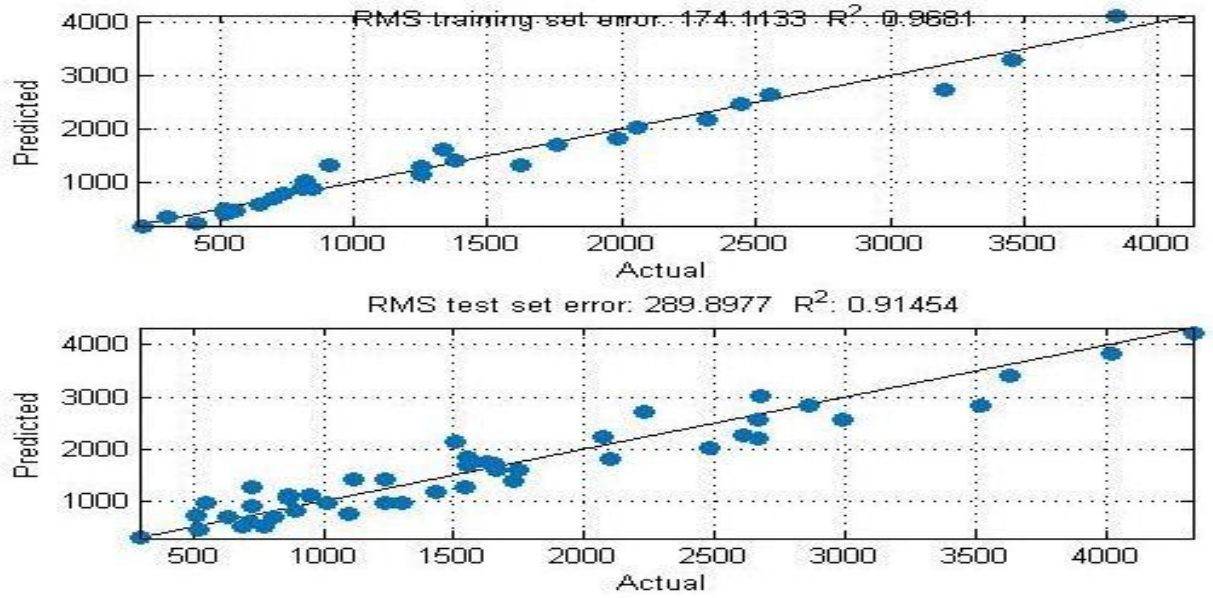

Figure 7. 2: Comparison of experimental results and the MGGP model prediction of Cutting Force (Fx)for (i) training data and (ii) testing data

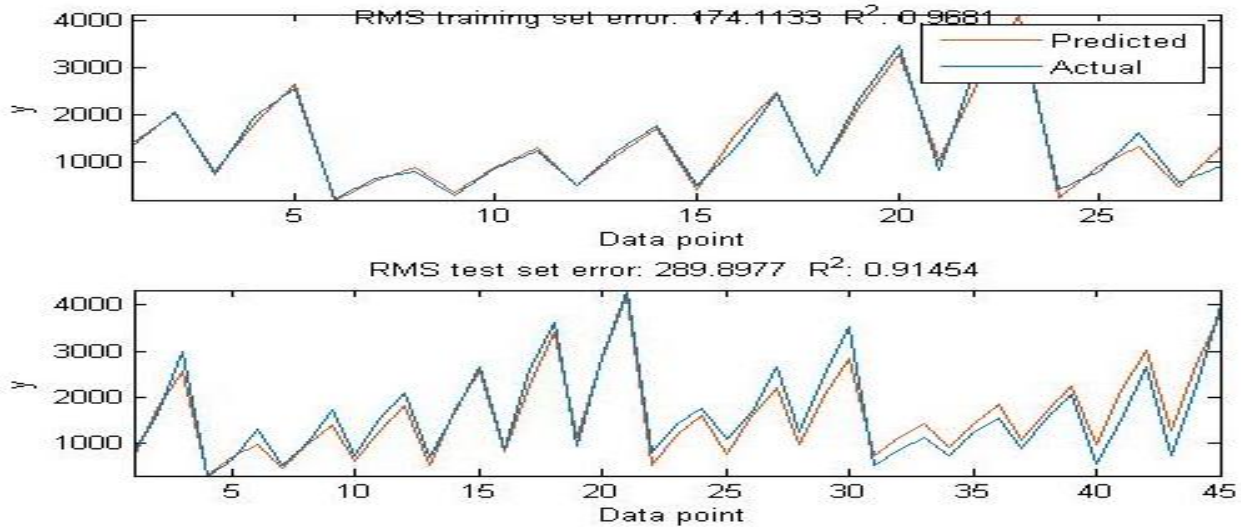

Figure 7. 3: Actual versus predicted values of Cutting Force (Fx) (i) training data and (ii) testing data

The error between the calculated values of MGGP model and experimental results of the training and test data are shown in Figure 7.6. The variation explained is 96.81% and 91.54% for the training and testing data

Table: 7.2 Validation of Cutting Force (Fx)

I (Deg)	Speed (m/min)	Feed (mm/min)	Depth of cut (mm)	F_X (N)	MGGP F_X (N)	% Error
50	24	60	0.4	2049.0979	2235.3256	9.08
50	24	60	0.6	2934.6447	3129.5632	6.64
50	24	80	0.2	1297.5923	1183.2356	8.89
50	24	80	0.4	2549.7235	2735.8923	7.37
50	24	80	0.6	3899.8622	3656.2563	6.24
50	34	40	0.2	372.2178	409.1234	9.91
50	34	40	0.4	909.6607	998.2548	9.72
50	34	40	0.6	1285.3247	1398.2356	8.78
50	34	60	0.2	458.9067	421.3256	8.18
50	34	60	0.4	1295.4316	1358.2356	4.84

7.1.4. MGGP model for Cutting Force (Fy)

The best model for Cutting force formulated by MGGP using experimental data given in Table 5.1 is

$$Fy= 0.9516\ (x1+x2)*(x1+x4-7.362)-33.51*x2*x4-1702.0*x1-431.4*x4^2*(x3+x4-1.0*\ x2*\ x4) – 228.1*(x4-7.362)*(x1+x4-7.447)\ +282.0*x42*(x1-1.0*x2)+173.2*x4*(2.0x3+x4)-4.788 *x1\ *x4^{2\ *}(x2*x4-1.0*x3*x4)-0.02113*x2*x4*(x3+x4)*(x1+x3-1.0*x3*x4)\ +12511.0 \qquad (7.2)$$

The accuracy of the equation 7.2 is shown by plotting the Cutting force (Fy) against training and testing data with predicted values as shown in Figure 7.4. The determination of the coefficient (R) and root mean square error (RMSE) are equal to 0.94118 and 220.9899 for testing sets and 0.9567 and 197.1377, for training sets as shown in Figure 7.4(i) and (ii), respectively. There is a good correlation among the predictions from MGGP and the measured values.

A comparison of the errors for the training and testing with experimental data is performed using MGGP and experimental results are shown in Figure 7.4. As can be seen, the training set that includes results of 80 samples and testing set comprising samples of 20 results. It has been observed that the MGGP model can predict the Cutting force (Fy) with a high degree of precision

and high variance (95.67% for training and 94.11% testing data) and the root mean square error (RMSE).

Smaller absolute error is better in the GP model, the error found to be is decreased with the increase of number of nodes and thus a MGGP model is more complex. Figure 7.5 shows the actual versus predicted values of Cutting Force (Fy) of training data and testing data Due to this computational difficulty, model was run for the tree depth limited to 4 as shown in Table 7.1. MGGP model was run for 100 times in the same conditions (Table 7.1).This MGGP model is capable of predicting objective (Cutting force) of rotary milling process with high accuracy.

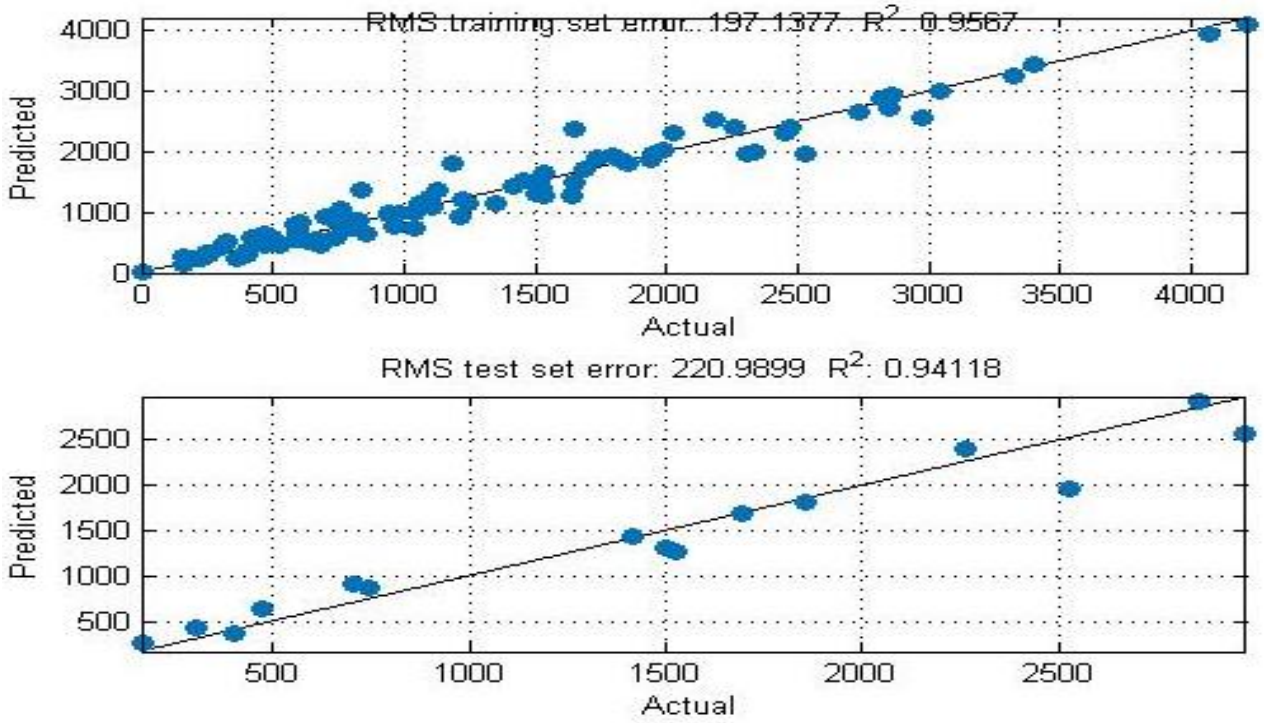

Figure 7. 4: Comparison of experimental results and the MGGP model prediction of Cutting Force (Fy) for (i) training data and (ii) testing data

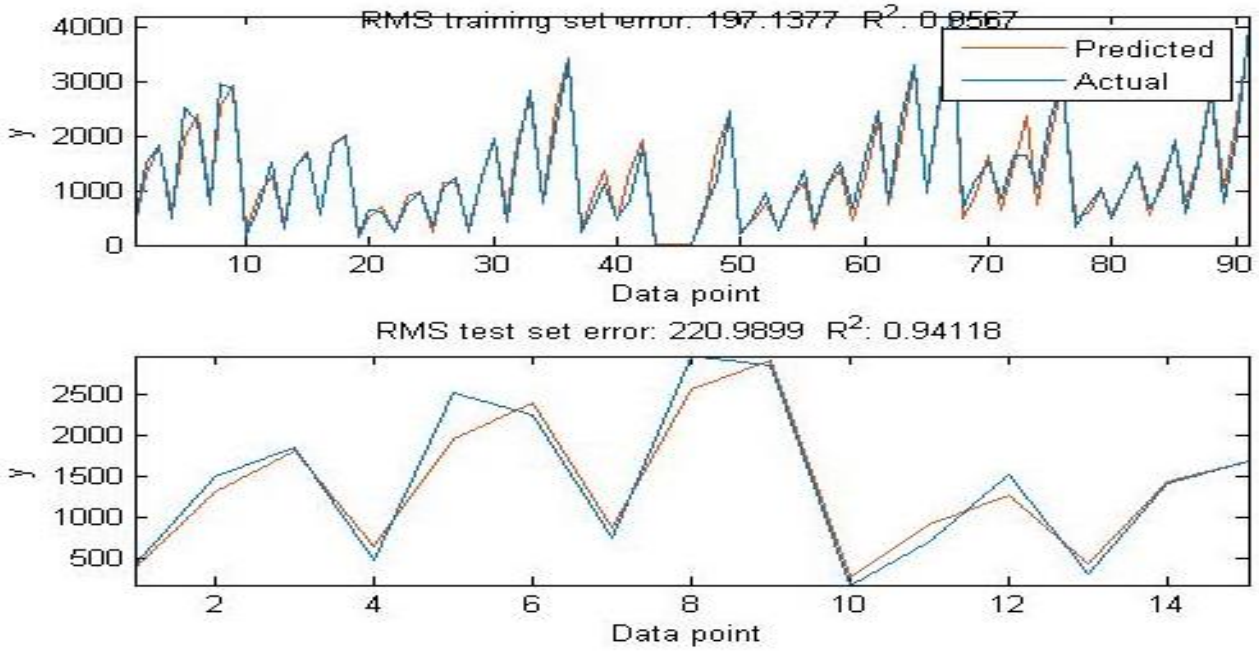

Figure 7.5: Actual versus predicted values of Cutting Force (Fy) (i) training data and (ii) testing data

The error between the calculated values of MGGP model and experimental results of the training and test data are shown in Figure 7.5. The variation explained is 95.67% and 94.11% for the training and testing data

Table 7.3 Validation of Cutting Force (Fy)

I (Deg)	Speed (m/min)	Feed (mm/min)	Depth of cut (mm)	F_y (N)	MGGP F_y (N)	% Error
50	14	80	0.4	2642.6163	2889.2756	9.33
50	14	80	0.6	4663.1916	5059.3658	8.49
50	24	40	0.2	643.1466	699.9856	8.83
50	24	40	0.4	1343.0378	1273.0378	5.26
50	24	40	0.6	2113.0613	2321.9658	9.88
50	24	60	0.2	1072.6801	1060.5689	1.12
50	24	60	0.4	1936.9735	2056.2354	6.15
50	24	60	0.6	2961.7836	3223.8745	8.84
50	24	80	0.2	1251.3442	1370.2596	9.50
50	24	80	0.4	2434.5288	2256.897	7.29

7.1.5. MGGP model for Cutting Force (Fz)

The best model for Cutting force formulated by MGGP using experimental data given in Table 5.1 is

$$Fz= 24.32*x2-48.64*x1-19.19*x3+0.7707*x1*x2-233.8*x2*x4+220.8*x3*x4-1.525*x1*x4^2+ 204*x2 *x4^2+ 0.7546x2^2x4-204*x3*x4^2+1.525x3*x4^3+0.7546x1^2+1561*x4^2-0.7546x1*x2 *x4-1.525x2*x3*x4-15.61 \quad (7.3)$$

The accuracy of the equation 7.3 is shown by plotting the Cutting force (Fz) against training and testing data with predicted values as shown in Figure 7.6. The determination of the coefficient (R) and root mean square error (RMSE) are equal to 0.93683 and 207.3126 for testing sets and 0.9157 and 218.2993, for training sets as shown in Figure 7.6(i) and (ii), respectively. There is a good correlation among the predictions from MGGP and the measured values.

A comparison of the errors for the training and testing with experimental data is performed using MGGP and experimental results are shown in Figure 7.6. As can be seen, the training set that includes results of 80 samples and testing set comprising samples of 20 results. It has been observed that the MGGP model can predict the Cutting force (Fz) with a high degree of precision and high variance (95.67% for training and 94.11% testing data) and the root mean square error (RMSE).

Smaller absolute error is better in the GP model, the error found to be is decreased with the increase of number of nodes and thus a MGGP model is more complex. Figure 7.7 shows the actual versus predicted values of Cutting Force (Fz) of training data and testing data Due to this computational difficulty, model was run for the tree depth limited to 4 as shown in Table 7.1. MGGP model was run for 100 times in the same conditions (Table 7.1).This MGGP model is capable of predicting objective (Cutting force) of rotary milling process with high accuracy.

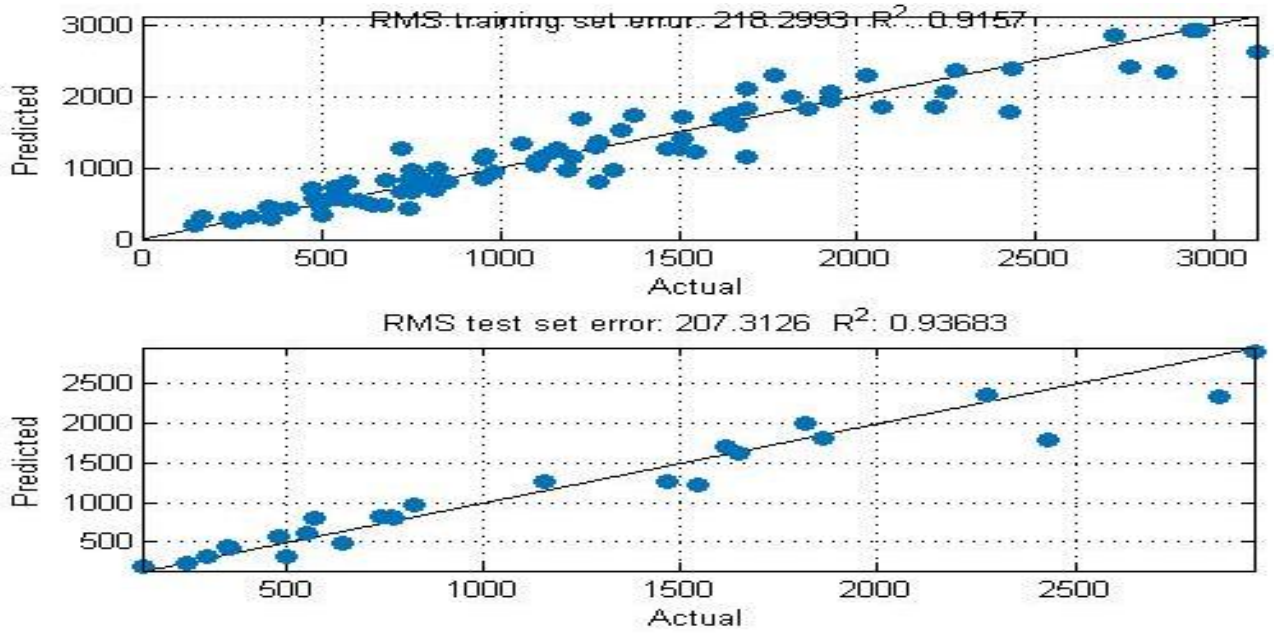

Figure 7.6: Comparison of experimental results and the MGGP model prediction of Cutting Force (Fz)for (i) training data and (ii) testing data

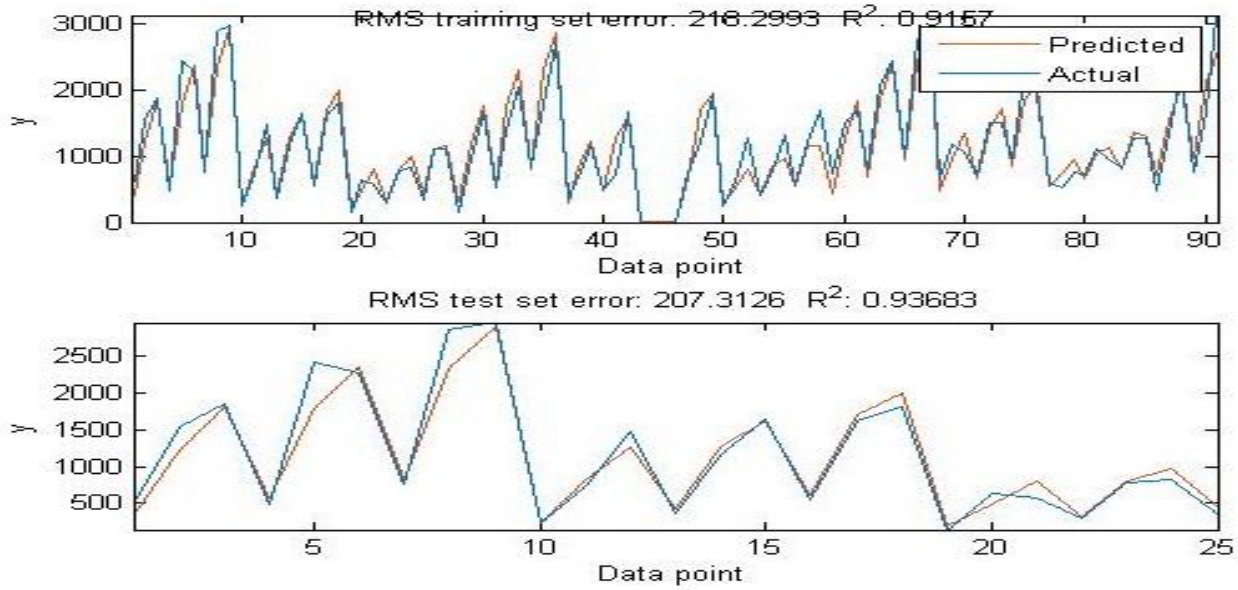

Figure 7.7: Actual versus predicted values of Cutting Force (Fz) (i) training data and (ii) testing data

The error between the calculated values of MGGP model and experimental results of the training and test data are shown in Figure 7.7. The variation explained is 91.57% and 93.68% for the training and testing data

Table: 7.4 Validation of Cutting Force (Fz)

I (Deg)	Speed (m/min)	Feed (mm/min)	Depth of cut (mm)	F_z (N)	MGGP F_z (N)	% Error
50	14	80	0.2	956.5839	1051.5689	7.92
50	14	80	0.4	2253.9434	2459.4596	6.11
50	14	80	0.6	3853.8123	3585.2358	6.96
50	24	40	0.2	534.3096	582.0586	8.93
50	24	40	0.4	944.2989	1029.7895	9.05
50	24	40	0.6	1314.892	1429.3256	8.70
50	24	60	0.2	728.0825	798.586	6.68
50	24	60	0.4	1433.8373	1298.8945	9.41
50	24	60	0.6	2645.623	2897.2385	6.51
50	24	80	0.2	912.4565	998.2596	9.40

7.1.6. MGGP model for Surface Roughness (Ra)

The best model for Cutting force formulated by MGGP using experimental data given in Table 5.1 is

$$Ra= 0.04155*x1-0.004623*x2-0.004623*x3+9.945*x4-0.07639*x1^2*x4^2+ 0.00072729x1^3* x4^2-0.2836* x1*x4+0.0002253* x2* x4+2.905*x1*x4^2-37.94*x4^2-0.7896*x4^3+0.0002253 *x1*x3 *x4+0.0002253*x2 *x3* x4-0.000004968 \quad (7.4)$$

The accuracy of the equation 7.4 is shown by plotting the Surface Roughness (Ra) against training and testing data with predicted values as shown in Figure 7.8. The determination of the coefficient (R) and root mean square error (RMSE) are equal to 0.94843 and 0.1676 for testing sets and 0.9086and 0.17562, for training sets as shown in Figure 7.8(i) and (ii), respectively. There is a good correlation among the predictions from MGGP and the measured values.

A comparison of the errors for the training and testing with experimental data is performed using MGGP and experimental results are shown in Figure 7.8. As can be seen, the training set that includes results of 80 samples and testing set comprising samples of 20 results. It has been observed that the MGGP model can predict the Surface Roughness (Ra) with a high degree of precision and high variance (90.86% for training and 94.84% testing data) and the root mean square error (RMSE).

Smaller absolute error is better in the GP model, the error found to be is decreased with the increase of number of nodes and thus a MGGP model is more complex. Figure 7.9 shows the actual versus predicted values of Surface Roughness (Ra) of training data and testing data Due to this computational difficulty, model was run for the tree depth limited to 4 as shown in Table 7.1. MGGP model was run for 100 times in the same conditions (Table 7.1).This MGGP model is capable of predicting objective (Surface Roughness (Ra) of rotary milling process with high accuracy.

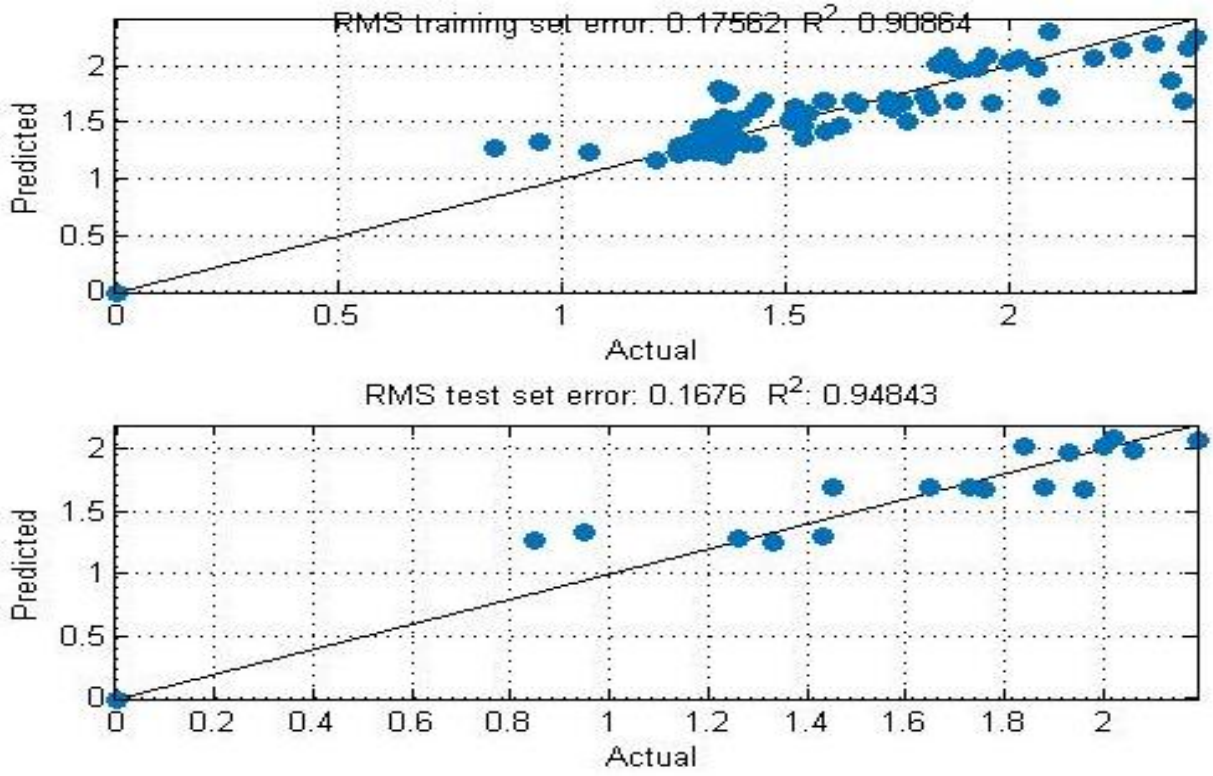

Figure 7.8: Comparison of experimental results and the MGGP model prediction of Surface Roughness (Ra) for (i) training data and (ii) testing data

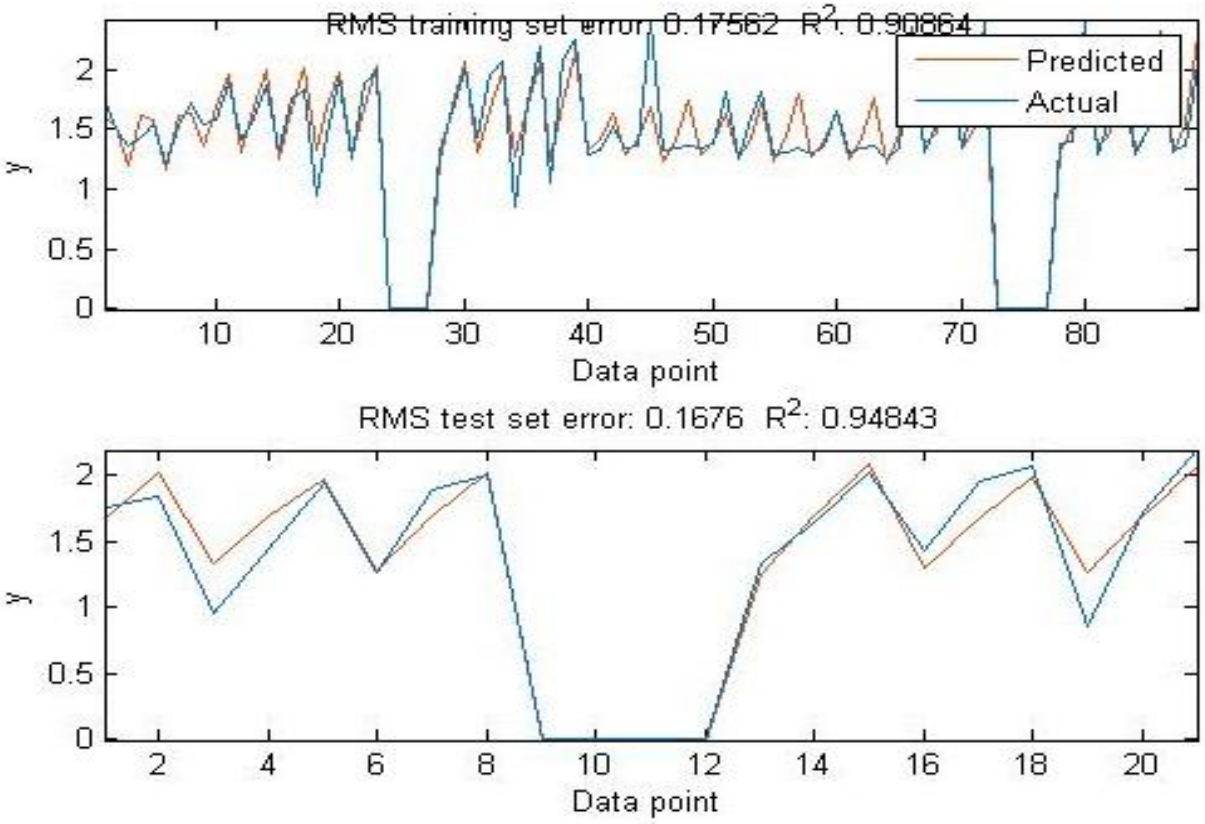

Figure 7.9: Actual versus predicted values of Surface Roughness (Ra) (i) training data and (ii) testing data

The error between the calculated values of MGGP model and experimental results of the training and test data are shown in Figure 7.12. The variation explained is 90.86% and 94.84% for the training and testing data

Table: 7.5 Validation of Surface Roughness (Ra)

I (Deg)	Speed (m/min)	Feed (mm/min)	Depth of cut (mm)	Ra µm	MGGP (Ra) µm	% Error
50	14	80	0.4	1.4	1.52	8.57
50	14	80	0.6	2.42	2.26	6.61
50	24	40	0.2	1.3	1.42	9.23
50	24	40	0.4	1.62	1.46	9.87
50	24	40	0.6	1.86	1.75	5.98
50	24	60	0.2	1.29	1.41	9.30
50	24	60	0.4	1.51	1.65	9.27
50	24	60	0.6	2.32	2.22	4.31
50	24	80	0.2	1.33	1.26	5.26

7.1.7. MGGP model for Cutting Temperature

The best model for Cutting force formulated by MGGP using experimental data given in Table 5.1 is

$$Temp=2.429*x1+3.755*x2+0.7017*x3+259.8*x4-0.007261*x1*x3+10.31*x1*x4-0.01452*x2*x3-4.455*x2*x4-0.02738*(x1+x2)*(x2-1.0*x1*x4)-16.04*x4*(x1+2.0*x4)+0.1952*x1*x2*x4^2-0.0007929*x1^2*x2*x4+0.1222 \quad (7.5)$$

The accuracy of the equation 7.4 is shown by plotting the Cutting temperature against training and testing data with predicted values as shown in Figure 7.10. The determination of the coefficient (R) and root mean square error (RMSE) are equal to 0.97337 and 10.9273 for testing sets and 0.96736 and 9.208, for training sets as shown in Figure 7.10 (i) and (ii), respectively. There is a good correlation among the predictions from MGGP and the measured values.

A comparison of the errors for the training and testing with experimental data is performed using MGGP and experimental results are shown in Figure 7.10. As can be seen, the training set that includes results of 80 samples and testing set comprising samples of 20 results. It has been observed that the MGGP model can predict the Cutting temperature with a high degree of precision and high variance (96.73% for training and 97.33% testing data) and the root mean square error (RMSE).

Smaller absolute error is better in the GP model, the error found to be is decreased with the increase of number of nodes and thus a MGGP model is more complex. Figure 7.14 shows the actual versus predicted values of Cutting temperature of training data and testing data Due to this computational difficulty, model was run for the tree depth limited to 4 as shown in Table 7.1. MGGP model was run for 100 times in the same conditions (Table 7.1).This MGGP model is capable of predicting objective Cutting temperature of rotary milling process with high accuracy.

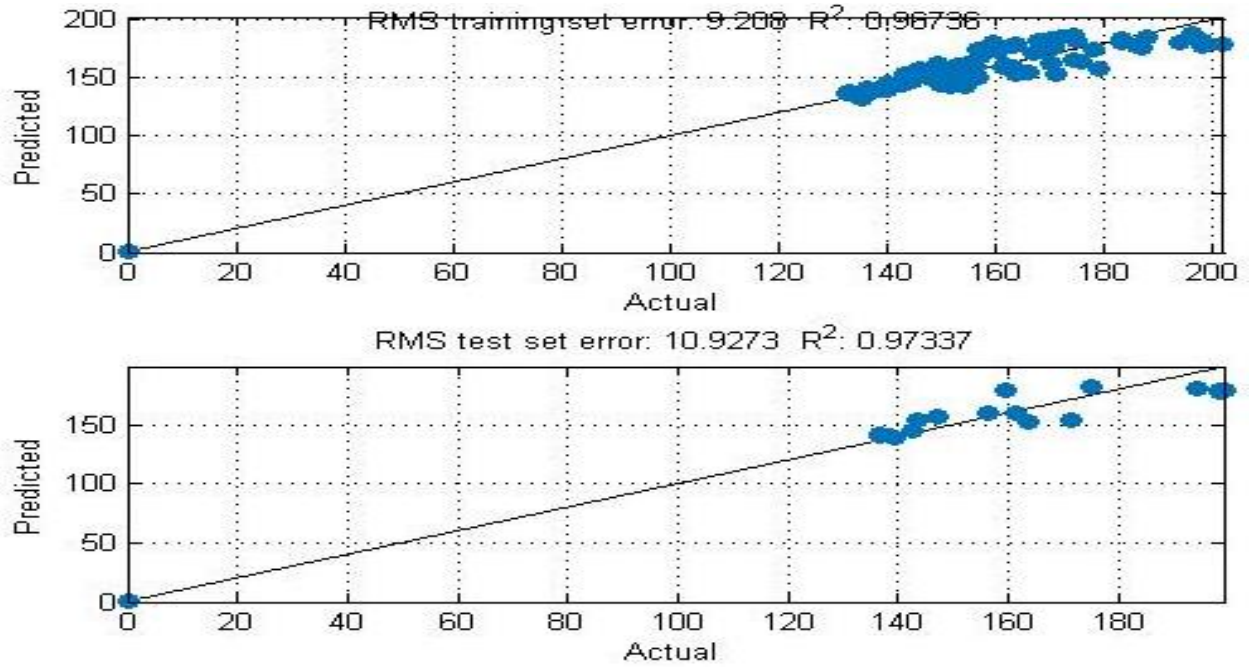

Figure 7.10: Comparison of experimental results and the MGGP model prediction of cutting temperature for (i) training data and (ii) testing data

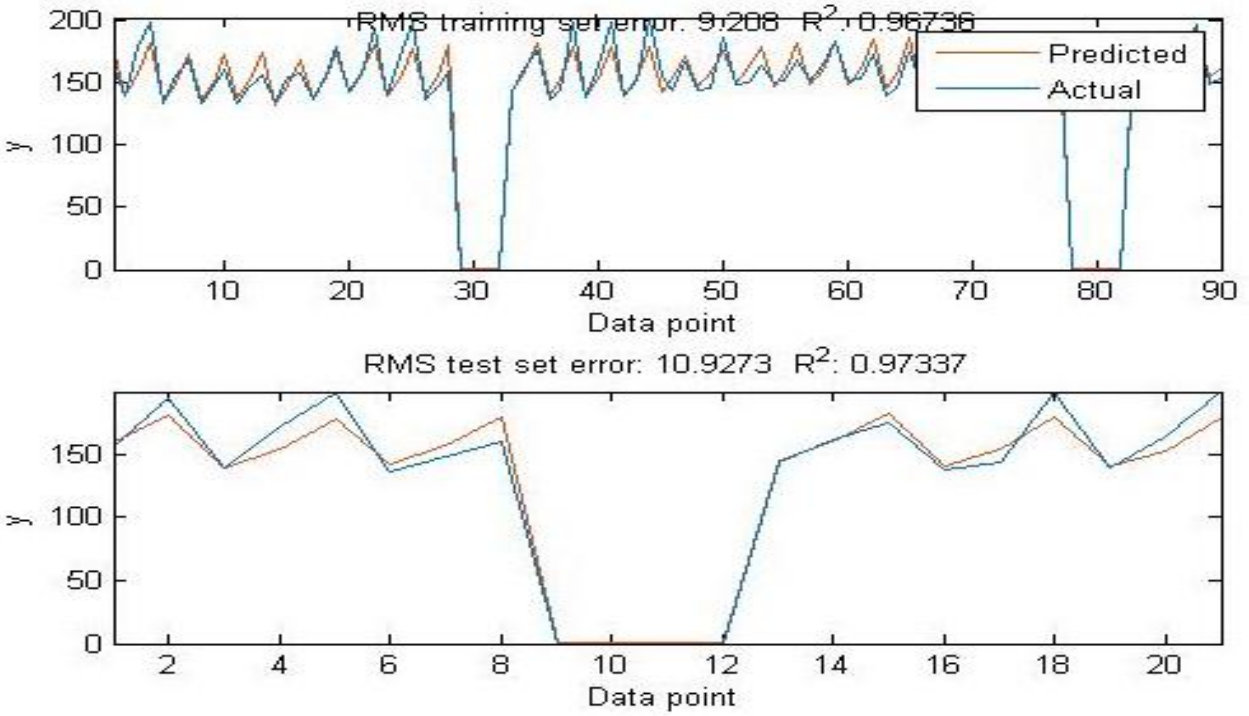

Figure 7.11: Actual versus predicted values of Cutting Temperature (i) training data and (ii) testing data

The error between the calculated values of MGGP model and experimental results of the training and test data are shown in Figure 7.11. The variation explained is 96.73% and 97.33% for the training and testing data

Table: 7.6 Validation of Cutting temperatures

I (Deg)	Speed (m/min)	Feed (mm/min)	Depth of cut (mm)	Temp °C	MGGP Temp °C	% Error
50	24	80	0.6	169.3	159.2201	5.95
50	34	40	0.2	152.8	156.7337	2.57
50	34	40	0.4	154.3	140.2493	9.10
50	34	40	0.6	122.2	115.3905	5.57
50	34	60	0.2	153.2	147.8251	3.50
50	34	60	0.4	142.7	131.3407	7.96
50	34	60	0.6	121.3	112.2899	7.42
50	34	80	0.2	154.5	144.7245	6.32
50	34	80	0.4	136.6	128.2401	6.11

The entire data set of Cutting force, Surface roughness and cutting temperature was divided into three parts as training set, testing set and validation data set. The training and testing sets were directly used for the generation of the regression models. The validation data set is used to validate this evolved regression model by calculating % error.

$$\% \, Error = \left(\frac{V_{MGGP} - V_{Exp}}{V_{Exp}} \right) X100$$

The validation results and % errors were shown in table no. 7.2 to 7.6

Each time the MGGP analysis is conducted, the mat lab code is executed 10times (10 runs mentioned in the parameters for implemented MGGP). For all these runs the R^2 value for testing and training data set is obtained above 0.91, which indicated the acceptability of the evolved regression model. The regression model with best value for training and testing data set is included in the results. The regression model is further validated using another validation dataset. The acceptability of percentage error depends on the application and environmental conditions of machining. In some cases, the measurement may be so difficult that a 10 % to 14% may be acceptable [121].

7.2. Formation of multi objective optimization problem

In this work, three objectives were considered; they were Cutting force, Surface roughness and cutting temperature. Our goal is to minimize the three of them. Thus generation of mono optimal solution will not serve the purpose, as the objectives are contradictory to each other. The simultaneous optimization of Cutting force, Surface roughness and cutting temperature comes into multi objective optimization problem. There cannot be a single optimal solution to a problem

of multi objective optimization. Thus, a set of equally reliable solutions being called as non-dominated or pareto set of optimal solutions were obtained. These optimal solutions are clearly based on the concept of dominance, where it is said that one element dominates another if it is better than the other in at least one objective and not a bad function with respect to all other objectives. The pareto front depicts tradeoffs among challenging objectives and recognizes non dominated solutions. It consists of population members, for whom there is no solution that is better than the Pareto member criteria.

7.2.1. Genetic algorithm for optimal pareto front

MATLAB toolbox for optimization (R2013a) is used to create the Pareto optimal front for Cutting force, Surface Roughness and Cutting Temperature using with 'gamultiobj' function. The initial population for the genetic algorithms generated randomly by default. The elitism process gives emphasis to the best solutions in subsequent generations. The next generation of the population is based on the non-dominated rank. The rank is calculated as crowding distance of individuals in the current pool. The algorithm stops after execution of 100 iterations.

7.2.2. Problem Formulation

In this work, objectives are to minimize the Cutting force, Surface roughness and cutting temperature. These objectives are conflicting in nature. So as to convert two objectives for minimization, it is appropriately modified. The optimization problem is stated as follows:

Objective 1 = Cutting Force Fx, Fy, Fz

Objective 2 = Surface roughness

Objective 3 = Cutting Temperature

Subject to

20>Inclination Angle> 50

14> Cutting Speed > 34

40> Feed > 80

0.2> Depth of cut > 0.6

Where objective 1, 2 and 3 are taken from Equation 7.1, to 7.5, respectively. The Cutting force, Surface roughness and cutting temperature to be minimized were negated in the vector valued fitness function as 'gamultiobj' minimizes all objectives. Ranges of experimental values were used as constraints for the input variables as stated above. In Table 7.2 gives the options and

parameters for the optimization of the genetic algorithm. The algorithm is executed again and again for more number of points in the Pareto optimal front.

Table 7.7: GA Parameters and options

Population type	Double vector type
Population size	100
Function for selection	Tournament
Size of the tournament	2
Reproduction crossover fraction	0.8
Cross over	Scattered function
Mutation	Constrained Dependent Function
Migration factor	0.2
Migration Interval	20
Migration direction	Forward
Distance function	Crowding
Pareto population fraction	0.5

7.2.3. Pareto front and optimal solutions

The change in weighted average of fitness function value was employed as a criterion to stop the algorithm. Pareto fronts after 127 iterations as the best multi objective optimized solutions, which are shown in Figure 7.15 and 7.16. The concave curve in Figures7.15 and 7.16show that, there is no Pareto optimal solution that is better than any other solution since they are all non dominated solutions. The choice of the solution depends on the requirement of the process. The Pareto optimal solutions with corresponding decision variables were given in Table 7.3. Each point on the Pareto front represents a group of decision variables. The choice of set of cutting force, surface roughness and temperature values can be obtained from the table. 5.13And the corresponding decision variables were taken from Table 7.3.

Table: 7.8 Optimal solutions obtianed from NSGA – II

Fx	**Fy**	**Fz**	**Ra**	**Temp**	**Inc. Angle**	**speed**	**feed**	**doc**
895.74	2066.89	500.23	1.97	176.25	25.42	33.99	40.03	0.60
559.44	2995.68	36.30	1.17	138.62	20.03	31.90	79.90	0.20
195.51	1510.90	244.06	1.29	136.50	22.53	33.03	40.04	0.20
1230.71	3503.26	364.73	1.20	137.02	20.14	14.66	78.66	0.20
742.12	1899.89	69.79	1.31	124.33	20.17	14.02	43.34	0.20
201.83	1496.15	255.42	1.27	135.48	20.50	33.71	40.02	0.20
665.05	1871.89	386.66	1.79	155.24	25.22	33.66	40.22	0.44
1115.10	3465.30	324.28	1.19	138.37	20.11	16.93	79.47	0.20
904.07	2081.34	487.71	1.98	175.22	26.12	33.99	40.65	0.59

1273.67	2289.45	377.08	1.72	184.21	37.34	33.76	40.47	0.60
1188.54	3509.63	355.28	1.19	137.83	20.13	15.66	79.40	0.20
466.95	1763.70	313.53	1.59	145.28	25.22	33.58	40.04	0.33
916.27	2860.07	161.90	1.24	134.35	20.32	17.05	65.16	0.20
1135.92	3348.36	310.50	1.21	136.62	20.15	15.64	75.64	0.20
461.26	1794.84	333.95	1.55	143.72	20.61	33.81	40.15	0.33
1109.56	3234.98	284.16	1.22	135.69	20.18	15.49	72.70	0.20
406.33	1810.28	292.26	1.48	141.17	20.74	33.80	41.66	0.29
647.36	2277.83	14.49	1.27	132.34	20.40	19.29	53.27	0.20
603.07	1866.43	365.37	1.73	151.39	24.19	33.75	40.57	0.40
960.52	3115.31	220.67	1.22	136.73	20.46	17.78	71.61	0.20
803.00	2567.17	78.12	1.26	132.86	20.22	17.73	58.77	0.20
862.61	2382.03	53.04	1.27	128.58	20.15	14.69	53.88	0.20
710.31	1889.34	422.89	1.83	158.80	24.18	33.88	40.04	0.47
1015.40	2831.74	179.68	1.25	131.87	20.18	14.59	63.41	0.20
327.59	1660.39	195.23	1.29	132.78	20.42	24.71	41.30	0.20
704.50	1973.52	60.46	1.30	126.73	20.26	15.51	45.18	0.20
372.62	2193.43	117.80	1.24	136.78	20.39	30.80	56.19	0.20
837.79	2000.34	471.19	1.90	169.99	24.21	33.80	40.03	0.56
1233.81	2374.42	370.99	1.78	182.52	35.84	33.50	42.42	0.59
772.01	1961.77	430.20	1.84	163.16	23.32	33.53	40.22	0.51
455.31	1787.09	145.40	1.34	132.60	21.31	21.47	41.81	0.22
936.50	2667.78	132.52	1.26	131.62	20.12	15.54	59.62	0.21
1062.34	3171.73	258.35	1.22	135.65	20.21	16.00	71.72	0.20
296.33	1630.89	282.69	1.38	137.94	20.50	33.71	40.09	0.24
265.56	1603.10	267.57	1.37	137.91	22.03	33.63	40.23	0.23

We consider some values randomly from the table 7.8 and did the validation and find the % error. The % error was in the range of 1.14 to 4.42 for cutting force components, the surface roughness % error is in the range of 3.07 to 4.78 and the Cutting Temperature % error is in the range of 2.81 to 4.94. The same values and validation shown in the tables 7.9 to 7.10

Table: 7.9 Validation of Cutting Force (Fx, Fy and Fz)

Fx		% Error
From Table 7.8	From Eq. 7.1	
895.74	875.32	2.33
665.05	673.41	1.24
916.27	901.37	1.65
803.00	812.32	1.14
372.62	380.54	2.08

Fy		% Error
From Table 7.8	From Eq.7.2	
2066.89	2096.32	1.40
1871.89	1910.56	2.02
2860.07	2785.98	2.65
2567.17	2458.45	4.42
2193.43	2098.52	4.52

Fz		% Error
From Table 7.8	From Eq.7.3	
500.23	488.32	2.43
386.66	398.56	2.98
161.90	169.32	4.38
78.12	75.89	2.93
117.80	110.98	6.14

Table: 7.10 Validation of Surface roughness and cutting temperature

Surface roughness		% Error
From Table 7.8	From Eq. 7.4	
1.97	1.88	4.78
1.79	1.85	3.24
1.24	1.29	3.87
1.26	1.30	3.07
1.34	1.29	3.81

Temperature		% Error
From Table 7.8	From Eq.7.5	
176.25	181.35	2.81
155.24	149.81	3.63
134.35	129.77	3.58
132.86	138.73	4.21
132.60	139.58	4.94

Pareto optimal front:

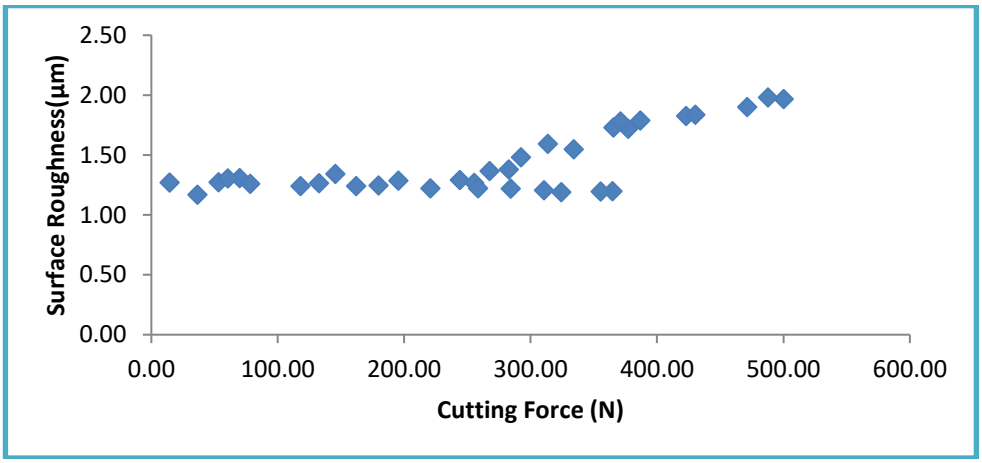

Figure 7.12: Pareto optimal front for Cutting Force and Surface Roughness

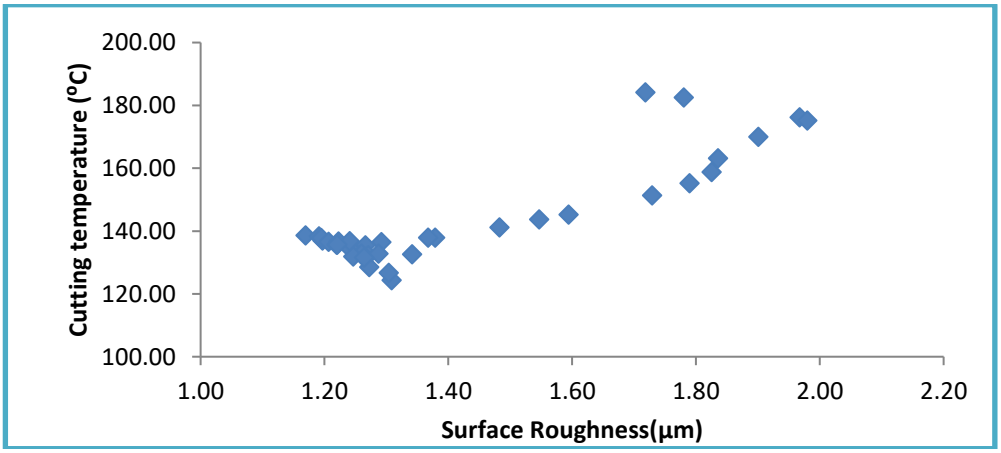

Figure 7.13: Pareto optimal front for Surface Roughness and Cutting Temperature

7.3 Summary

This chapter deals with the generation of regression models for Cutting force (Fx, Fy, Fz), Surface roughness and Cutting temperature using Multi Gene Genetic Programming (MGGP) by considering the experimental data from Chapter V. This chapter also presents the multi-objective optimization of Cutting force (Fx, Fy, Fz), Surface roughness and Cutting temperature using a genetic algorithm. These responses are simultaneously optimized and the optimal levels of the process parameters are determined by the Pareto front.

Empirical models for the chosen performance measures were developed using MGGP. The models obtained were truly reliable and shows very good generalization capability. Higher values of multiple regression coefficients for Cutting force (Fz), Surface roughness and Cutting temperature (i.e.93.68%, 94.84% and 97.33% respectively) reveal that better prediction of physical phenomenon is possible with the developed models. The Pareto-optimal set was found out by using non-dominated sorting genetic algorithm - II and optimal values of Inclination Angle, Cutting Speed, Feed and Depth of cut can be selected for desired value of Cutting force (Fx, Fy, Fz), Surface roughness and Cutting temperature from the Pareto optimal set.

CHAPTER 8

CONCLUSIONS AND FUTURE SCOPE OF WORK

8.1 Conclusions

In the present work, characteristics of rotary face milling process in terms of cutting forces and surface roughness while machining aerospace materials has been discussed. A rotary face milling cutter with provision for different inclination angles to machine Nickel based superalloy Inconel 625 has been designed and fabricated as part of the study of the characteristics of rotary milling process. A detailed investigation is carried out using full factorial experimentation. Optimum process parameters to achieve minimum cutting forces, surface roughness and cutting temperature have also been investigated and reported. A set of experiments were conducted using MQL and Nano coolants. Models for predicting the cutting forces, surface roughness and cutting temperature in rotary milling process have been developed theoretically and also using Multi gene genetic programming (MGGP) and NSGA-II. The developed models were validated with experimental results for estimating the prediction errors.

The major conclusions from this work are presented as below:

1. A conceptual model of the rotary face milling cutter with the facility to carryout machining with different insert inclination angles such as 20°, 30°, 40° and 50° has been designed and developed. The conceptual model has been further developed to accommodate standard rotary insert cartridge. The stress analysis and deflection analysis have been carried out on the cutter model using FEM. The results showed that the cutter designed is safe with factor of safety of 6.28 considering the worst cutting conditions. The rotary face milling cutter has been manufactured at DRDL as per the cutter model. The experimental studies have been carried out with the developed rotary face milling cutter.

2. Experimental results indicated that the cutting forces in rotary milling increased with increase in the feed and depth of cut. The cutting forces decreased with increase in the cutting speed of the cutter which is the case with conventional face milling process. As the inclination angle increased from 30° to 40°, there was a significant increase in cutting forces and this increase was marginal when the inclination angle changed from 40° to 50°. The inclination angle when combined with other process parameters, influence the cutting forces significantly. Hence, rotary face milling cutter can be used for high feed rates during milling of Nickel based superalloys.

3. This investigation reveals that inclination angle of the rotary face milling cutter play a vital role on the surface roughness. For an increase in inclination angle from 30° to 40°, the roughness value R_a has decreased and from 40° to 50° it has increased. Hence, inclination angles between 30° and 40° are suitable for better surface roughness.

4. The experimental investigation reveals that inclination angle of the rotary face milling cutter play a vital role on the cutting temperature. For an increase in inclination angle from 30° to 40°, the cutting temperature has decreased and from 40° to 50° it has increased. Hence, inclination angles between 30° and 40° are suitable for minimum cutting temperature

5. It is noticed that minimum cutting forces are observed for low cutter speeds at high depth of cut values in the case of inclination angle of 30°. As the cutting speed increases, the inclination angle of 40° produces low cutting forces even at high depth of cut values.

Similarly, minimum cutting forces are observed at high inclination angle of 50°for low depth of cut values irrespective of cutting speed and feed values. In the case of 20°inclination angle, the cutting forces obtained does not show usual trend which could be due to no smooth rotation of the insert during cutting. Hence, inclination angles between 30° and 40° are more suitable for machining titanium alloys.

6. Cutting forces of Inconel 625 and SUS304 (AISI 304) are compared and depicted in Table 5.6. The Figure 5.6 shows that the cutting forces in SUS304 (AISI 304) is more when compared to Inconel 625. This is because hardness of Inconel 625 alloys is in the range of 30-42 HRC whereas hardness of SUS304 (AISI 304) is 19 HRC i.e. Inconel 625 alloy have more hardness and Dynamic Shear strength compared to SUS304 (AISI 304)

7. The prediction capabilities of the theoretical model for cutting forces and RSM model for surface roughness have been evaluated. The average percentage deviation in prediction of cutting forces using theoretical model was found to be in the range of 9-20% , 12-18% and 12-20% for F_X, F_Y and F_Z respectively, the average percentage deviation in prediction of surface roughness using RSM model was found to be 9.7%, and the average percentage deviation in prediction of cutting temperature using RSM model was found to be 9.2%.

8. The effect of MQL and Nano coolants are investigated on Inconel 625 in the rotary face milling operation. The average percentage reduction in Cutting force (Fz) is more than 40% and in the average percentage reduction surface roughness is 38% and average percentage reduction in temperature is 50%

9. Predictive models were developed using MATLAB tool box for prediction of cutting force, surface finish and Cutting temperature in rotary milling operation. 80 data sets were used for training the cutting force model, 80 data sets were used for training the surface roughness model, 80 data sets were used for training the temperature model and the prediction capabilities for them were evaluated. The average percentage deviation in prediction of cutting forces using MGGP was found to be 5%, 6% and 7.9% respectively for F_X, F_Y and F_Z. The average percentage deviation in prediction of surface roughness using MGGP model was 6.80%. The average percentage deviation in prediction of Temperature using MGGP model was 5.45%.

8.2 Scope for future work

1. This work can be further extended for machining of other aerospace materials like Nimonic alloys; other Nickel based super alloys, carbon-silicon carbide composites (C-SiC) and structural composite materials etc.

2. The prediction capability of the theoretical model can be improved further if the exact chip cross sectional area in the rotary milling process is determined. Consideration of frictional forces between the tool and work material, spindle and insert rotation uncertainties can also improve the model.

3. This methodology can be applied for rotary milling of other difficult-to-cut aerospace materials if specific cutting pressure K_T for the same material is estimated.

4. The MQL technique will applied with another coolant and also Nano particle vol% combinations will be changed.

References

1. **Koza, J.R.,** Genetic programming: on the programming of computers by means of natural selection. Vol. 1. 1992: MIT press.
2. **Alauddin, M., M.A. El Baradie** and **M.S.J. Hashmi** (1996) Optimization of Surface Finish in End Milling Inconel 718. *Journal of Materials Processing Technology*, Vol. **56**. pp. 54-65.
3. **J. Kwong, D. A. Axinte P.J.Withers, M.C.Hardy**,Minor cutting edge work piece interactions in drilling of an advanced nickel based superalloy International Journal of Machine Tools & Manufacture 49 (2009) 645 – 658
4. **E.O. Ezugwu, J. Bonney, Y. Yamane**,An overview of the Machinability of aero engineering alloys, Journal of material processing technology 134(2003) 233-253.
5. **Durul Ulutan, Tugrul Ozel**,, Machining induced surface integrity in titanium and nickel alloys: Areview, International Journal of Machine Tools & Manufacture 51(2011) 250–280
6. **E.O.Ezugwu a, Z.M.Wang, A.R.Machado**,The machinability of nickel-based alloys: a review Journal of Materials Processing Technology 86 (1999)1–16
7. **Victor M. Cassidy**, Taming the 'Nastalloys' Tips for turning nickel-base Super alloys,Cutting tool engineering magazine, February 2008/volume 60/ number 2.
8. **A. E. I. Elshwain, Norizah Redzuan, Noordin Mohd Yusof**,machinability of Nickel and titanium alloys under of gas-based coolant-lubricants(cls)- a review International Journal of Research in Engineering and Technology, eISSN: 2319-1163 | pISSN: 2321-7308
9. **Melih Cemal Kushan, Sinem Cevik Uzgur, Yagiz Uzunonat and Fehmi Diltemiz** (2012).ALLVAC 718 Plus™ Superalloy for Aircraft Engine Applications, Recent Advances in Aircraft Technology, Dr. Ramesh Agarwal (Ed.), ISBN: 978-953-51-0150-5, InTech
10. Nickel-Based Super Alloys**, INSG** secretariat briefing paper April 2013 – no.20.
11. **Armarego, E.J.A.** and **R.K. Katta** (1997) Predictive Cutting Model for Forces and Power in Self-Propelled Rotary Tool Turning Operations. *Annals of the CIRP*, Vol. **46/1**, pp. 19-24.

12. **Koza, J.R.,** Genetic programming III: Darwinian invention and problem solving. Vol. 3. 1999: Morgan Kaufmann.

13. **Armarego, E.J.A. V. Karri** and **A.J.R. Smith** (1994*b*) Fundamental Studies of Driven and Self-propelled Rotary Tool Cutting Processes-II, Experimental Investigation. *International Journal of Machine tools and Manufacture*, Vol. **34**, No. **6,** pp. 803-815.

14. **Armarego, E.J.A., A. J. R. Smith** and **V. Karri** (1991*a*) Mechanics of Cutting model for Simulated Oblique Rotary Tool Cutting Processes. *Journal of Material Processing Technology*, Vol. **28**, pp. 3-14.

15. **Armarego, E.J.A., A.J.R. Smith** and **V. Karri** (1991*b*) The Development of Cutting model for Simulated Orthogonal Rotary Tool Cutting Processes. *Fifth International Manufacturing Conference in China*, A17-26.

16. **Armarego, E.J.A., V. Karri** and **A.J.R. Smith** (1993) Computer-Aided Predictive Models for Fundamental Rotary Tool Cutting Processes. *Annals of the CIRP*, **42/1**, pp. 49–54.

17. **Armarego, E.J.A., V. Karri** and **A.J.R. Smith** (1994*a*) Fundamental studies of driven and self-propelled rotary tool cutting processes-I, Theoretical investigation. *International Journal of Machine Tools and Manufacturing*, Vol. **34**, No. **6**, pp. 785-801.

18. **Koza, J.R.,** Architecture-Altering Operations for Evolving the Architecture of a Multi-Part Program in Genetic Programming.1994, Stanford University.

19. **Aronovich, G.L.** (1991) Characteristics of Rolling FMinor cutting edge work piece interactions in drilling of an advanced nickel based superalloyriction with Sliding during Rotary Cutting. Wear of Material, *International conf. on Wear of Materials*, Orlando, FL, USA, Apr. 7-11, Vol.**2**, pp. 679-682

20. **Arshinov V., G. Alekseev** Metal Cutting Theory and Cutting tool design, MIR Publications, 1976.

21. **Aykut, S., M. Gölcü, S. Semiz** and **H.S. Ergür** (2007) Modeling of cutting forces as function of cutting parameters for face milling of satellite 6 using an artificial neural network. *Journal of Materials Processing Technology*, Vol. **190**, pp.199-209.

22. **Boothroyd, G., W.A. Knight,** Fundamentals of Machining and Machine Tools, *Marcel Dekker*, NY, 1989.

23. **Chang, X., W. Chen, X. Pang** and **G. J. Zhong** (1995) Selection of Cutting Regime for Self-Propelled Rotary Cutting Tools. Journal of Engineering Manufacture, *Proceedings of Institution of Mechanical Engineers*, Vol. **209**, Part B, pp. 63-66.

24. **Chen, P.** (1992*a*) Cutting Temperature and Forces in Machining of High-Performance Materials with Self-Propelled Rotary Tool. *JSME International Journal series 3*,Vol. **35**, No. **1**, pp. 180-185.

25. **Chen, P.** (1992*b*) High Performance Machining of SiC Whisker-Reinforced Aluminium composite by self-propelled rotary tools. *Annals of the CIRP*, **41/1**, pp. 59-62.

26. **Chen, P. and T. Hoshi** (1990) Tool Wear in Machining of Difficult-to-cut Materials with Rotary Tool. *Proceedings of JSPE Autumn Conference*, Sapporo, Japan, pp. 375-376.

27. **Chen, P.** and **T. Hoshi** (1991) Characteristics of Self-Propelled Rotary Tools in Machining High-Performance Materials. *International Journal of the Japanese Society for Precision Engineering*, Vol. **25**, No. **4**, pp. 267-272.

28. **Dabade, U.A., S.S. Joshi** and **N. Ramakrishnan** (2003) Analysis of surface roughness and chip cross-sectional area while machining with self-propelled round insert milling cutters. *Journal of Materials Processing Technology*, Vol. **132 (1-3)**, pp. 305–312.

29. **Danilov, V.A.** and **N.S. Ivanov** (1979) Rough turning of titanium alloys using self-propelled rotary tools. *Russian Engineering Journal*, Vol**59**, No.**12**, p32-33.

30. **Poli, R.,** A Simple but Theoretically-Motivated Method to Control Bloat in Genetic Programming, in Genetic Programming: 6th European Conference, EuroGP 2003Essex, UK, April 14–16, 2003 Proceedings, C. Ryan, et al., Editors. 2003, Springer Berlin Heidelberg: Berlin, Heidelberg. p. 204-217.

31. **Ezugwu, E.O.** (2007) Improvements in the machining of aero-engine alloys using self-propelled rotary tooling technique. *Journal of Materials Processing Technology*, Vol. **185**, pp. 60-71.

32. **Ezugwu, E.O.** and **Z.M. Wang** (1997), Titanium alloys and their machinability – a review. *Journal of Material Processing Technology*, Vol. **68**, pp. 262-274.

33. **Ezugwu, E.O., K.A. Olajire** and **Z.M. Wang** (2002) Wear evaluation of a self-propelled rotary tool when machining titanium alloy IMI 318. *Journal of Engineering Manufacture, Proceedings of Institution of Mechanical Engineers*, Vol. **216**, Part B, pp. 891- 897

34. **Franco, P., M. Estrems,** and **F. Faura** (2004) Influence of radial and axial runouts on surface roughness in face milling with round insert cutting tools. *International Journal of Machine Tools and Manufacturing*, Vol. **44**, pp. 1555-1565.

35. **Haupt, R.L. and S.E. Haupt,** Practical genetic algorithms. 2004: John Wiley & Sons.

36. **Fu, H. J., R. E. DeVor** and **S. G. Kapoor** (1984) A mechanistic model for prediction of the force system in the face milling operations. *Journal of Engineering for Industry*, Transactions of ASME, Vol. **106**, pp. 81-88.

37. **Goldberg, D.E.,** Genetic Algorithms in Search, Optimization and Machine Learning. 1989: Addison-Wesley Longman Publishing Co., Inc. 372.

38. **Srinivas, N. and K. Deb**, Muiltiobjective Optimization Using Nondominated Sorting in Genetic Algorithms. Evolutionary Computation, 1994. 2(3): p. 221-248.

39. **Fonseca, C.M. and P.J. Fleming**, An Overview of Evolutionary Algorithms in Multiobjective Optimization. Evolutionary Computation, 1995. 3(1): p. 1-16.

40. **Rangaiah, G.P**., Multi-objective optimization: techniques and applications in chemical engineering. Vol. 5. 2016: World Scientific.

41. **Goldberg, D.E. and J.H. Holland**, Genetic algorithms and machine learning. Machine learning, 1988. 3(2): p. 95-99.

42. **Gi Heung Choi** and **David Dornfeld** (1990) Analytical Predictions of Rotary Cutting Processes. *Transactions of NAMRI/SME*, pp.146-153.

43. **Handbook** of data about metals and metal working, ASM METALS REFERENCE BOOK, ASM INTERNATIONAL, 1981.

44. **Hikmet Esen** and **Mustafa Inalli** (2010) ANN and ANFIS models for performance evaluation of a vertical ground source heat pump system. Expert Systems with Applications, Vol. **37**, pp. 8134-8147.

45. **Searson, D.P., D.E. Leahy, and M.J. Willis**. GPTIPS: an open source genetic programming toolbox for multigene symbolic regression. in Proceedings of theInternational multiconference of engineers and computer scientists. 2010. Citeseer.

46. **Hiroyuki Sasahara, Atsushi Kato, Hiroshi Nakajima, Hiromasa Yamamoto, Toshiyuki Muraki** and **Masaomi Tsutsumi** (2008) High-speed rotary cutting of difficult-to-cut materials on multitasking lathe. *International Journal of Machine Tools & Manufacture*, Vol. **48**, pp. 841–850.

47. **Hosokawa, A., T. Ueda, R. Onishi, R. Tanaka** and **T. Furumoto** (2010) Turning of difficult-to-machine materials with actively driven rotary tool. *CIRP Annals - Manufacturing Technology*, Vol. **59**, pp. 89–92.

48. **Garg, A. and K. Tai**. Review of genetic programming in modeling of machining processes. in 2012 Proceedings of International Conference on Modelling, Identification and Control. 2012.

49. **Garg, A. and K. Tai**. Selection of a robust experimental design for the effective modeling of nonlinear systems using Genetic Programming. in 2013 IEEE Symposium onComputational Intelligence and Data Mining (CIDM). 2013.

50. **Garg, A., K. Tai, and M.M. Savalani**, Formulation of bead width model of an SLM prototype using modified multi-gene genetic programming approach. The International Journal of Advanced Manufacturing Technology, 2014. 73(1): p. 375-388.

51. **Garg, A. and K. Tai**, Comparison of statistical and machine learning methods in modelling of data with multicollinearity. International Journal of Modelling, Identification and Control, 2013. 18(4): p. 295-312.

52. **V. Vasu, G Pradeep Kumar Reddy**, "Effect of minimum quantity lubrication with Al_2O_3 nanoparticles on surface roughness, tool wear and temperature dissipation in machining inconel 600 alloy" Publication on 3 oct 2011

53. **Janardhan Reddy, T.A.** and **P.K. Venuvinod** (1979) Optimisation of Tool Setting in Machining with Type II Rotary Tools. *Journal of Institute of Engineers.(India)*, MED, Vol. **59**, Pt ME-4, pp. 205-210

54. **Jim Destefani**, Old tool design takes off, Milling and boring tools with inserts that rotate during cutting promise significant productivity improvements in machining of tough materials. Manufacturing Engineering, Society of Mechanical Engineers, January 2002, Vol. 128 and No. 1.

55. **Joshi, S.S., N. Ramakrishnan, H.E. Nagarwalla,** and **P. Ramakrishnan** (1999) Wear of rotary carbide tools in machining of Al/SiCp composites. *Wear*, Vol. **230**, pp. 124–132.

56. **Kaushikkumar M. Patel** and **Suhas S. Joshi** (2006) Mechanics of machining of face-milling operation performed using a self-propelled round insert milling cutter. *Journal of Materials Processing Technology*, Vol. **171**, pp. 68–76.

57. **Kim, H.S.** and **K.F. Ehmann** (1993) A cutting force model for face milling operations. *International Journal of Machine Tools and Manufacture*, Vol. **33**, pp. 651-673.

58. **Kishawy, H.A.** and **J. Wilcox** (2003) Tool wear and chip formation during hard turning with self-propelled rotary tools. *International Journal of Machine Tools and Manufacture*, Vol. **43**, pp. 433–439.

59. **Kishawy, H.A., C.E. Becze** and **D.G. McIntosh** (2004*b*) Tool performance and attainable surface quality during the machining of aerospace alloys using self-propelled rotary tools. *Journal of Materials Processing Technology*, Vol. **152/3**, pp. 266–271.

60. **Kishawy, H.A., L. Li** and **A.I. EL-Wahab** (2006) Prediction of chip flow direction during machining with self-propelled rotary tools. *International Journal of Machine Tools & Manufacture*, Vol. **46**, pp. 1680–1688.

61. **Li, L.** and **H.A. Kishawy** (2006) A model for cutting forces generated during machining with self-propelled rotary tools, *International Journal of Machine Tools & Manufacture*, Vol. **46**, pp. 1388–1394.

62. Materials Characterization, ASM METALS HANDBOOK, Vol. **10**, ASM INTERNATIONAL.

63. MATLAB User Guide, MathWorks, Inc. USA

64. **Md.Azamathulla, H., Chun Kiat Chang, Aminuddin Ab. Ghani, Junaidah Ariffin, Nor Azazi Zakaria** and **Zorkeflee Abu Hasan** (2009) An ANFIS based approach for

predicting the bed load for moderately sized rivers. *Journal of Hydro-environment Research*, Vol. **3**, pp. 35-44.

65. **N. R. Dhar, M. T. Ahmad, S. Islam,** "An experimental investigation on effect of minimum quantity lubrication in machining AISI 1040 steel" International journal of machine tools and manufacture 47 (2007) 748-753.

66. **Norman, Z.** and **F. Michael** (1973) Procedures and Precautions in Machining Titanium Alloys. *Titanium Science and Technology*, Vol. **1**, pp. 489-504.

67. **Pejman Tahmasebi** and **Ardeshir Hezarkhani** (2010) Application of Adaptive Neuro-Fuzzy Inference System for Grade Estimation. *Australian Journal of Basic and Applied Sciences*, Vol. **4**, No. **3**, pp. 408-420.

68. **Perez H., A. Vizen, J.C. Hernandez** and **M. Guzman** (2007) Estimation of cutting forces in micro milling through the determination of specific cutting pressures. *Journal of Materials Processing Technology*, Vol. **190**, pp. 18-22.

69. **Pradeep Kumar Baro, Suhas S. Joshi** and **S.G. Kapoor** (2005) Modeling of cutting forces in a face-milling operation with self-propelled round insert milling cutter. *International Journal of Machine Tools & Manufacture*, Vol. **45**, pp. 831–839.

70. **Radwan, A.A.** (1979) An Experimental study of chip formation with Self-Propelled Rotary Tools. *North American Manufacturing Research Conference-7*, pp. 262-267.

71. **Radwan, A.A.** and **Y.H. Kabil** (1977) Chip formation in machining with self-propelled rotary cutting tools. *North American Manufacturing Research Conference-5*, pp. 322-326.

72. **Ramaswamy Iyer, N.** and **F. Koenigberger** (1968) Experiments with self-propelled rotary cutting tools. *Proceedings of Ninth IMTDR Conference*, Part 2, pp. 945–959.

73. **Ramesh Kumar K.** (1997) Computer aided predictive performance models for self-propelled rotary tool and circular stationary tool turning. Ph.D. Dissertation, University of Melbourne, Australia.

74. **Ramesh Kumar K., I.K. Kaul** and **B. Maheshwar** (2002) Self-propelled rotary turning: A High performance turning tool for machining Aerospace materials. *NCAAM*, pp. 253-260.

75. Rotary Technology Corporation, USA. http://www.rotarytech.com

76. **Shaw, M.C.** Metal Cutting Principles, Oxford University Press, Oxford, 1983.

77. **Shaw, M.C., P.A. Smith** and **N.H. Cook** (1952) The Rotary Cutting Tool. *Transactions of ASME*, **74**, pp. 1065-1076.

78. **Shuting Lei** and **Wenjie Liu** (2002) High-speed machining of titanium alloys using the driven rotary tools. *International Journal of Machine Tools & Manufacture*, Vol. **42**, pp. 653–661.

79. TOOL ENGINEER'S HAND BOOK, McGraw Hill Co. Ltd. ASTME, 2nd Ed., 1959.

80. **Tsai Kuo-Ming** and **Pie-Jen Wang** (2001) Comparisons of neural network models on material removal rate in electrical discharge machining. *Journal of Material Processing Technology*, Vol. **117**, pp. 111-124.

81. **Venkatesh, V.C., S. Rajesham** and **V. Kamala** (1972) Wear and Surface finish in face-milling with rotary inserts. *Proceedings of fifth All India MTDR conference*, Roorkee, pp. 183-190.

82. **Venuvinod, P.K.** and **P.N. Reddy** (1981*a*) Some Studies on Cutting with Self-Propelled Rotary Tools. *New York ASME*, ASME Paper No. **81-A**/prod -16, pp. 1-11.

83. **Venuvinod, P.K., W.S. Lau** and **P.N. Reddy** (1981*b*) Some Investigations in machining with Driven Rotary tools. *Journal of Engineering for Industrial Manufacturing*, Transactions of ASME, Vol. **103**, pp. 469-477.

84. **Schwefel, H.-P**., Numerical optimization of computer models. 1981: John Wiley & Sons, Inc.

85. **Venuvinod, P.K., W.S. Lau, P.R. Narasimha** and **C. Rubenstein** (1983) On the Formation of a Fluid Film at the Chip Tool Interface in Rotary Machining. *Annals of the CIRP***32**/**1**, pp. 59

86. **Vincent Dessoly, Shreyes N. Melkote** and **Christophe Lescalier** (2004) Modeling and verification of cutting tool temperatures in rotary tool turning of hardened steel. *International Journal of Machine Tools & Manufacture*, Vol. **44**, pp. 1463–1470

87. **Wang, Z.M., E.O. Ezugwu** and **A. Gupta** (1998) Evaluation of a Self-Propelled Rotary Tool in the Machining of Aerospace Materials. *Tribology Transactions*, Vol. **41**, No. **2**, pp. 289-295.

88. **Wangshen Hao, Xunsheng Zhu, Xifeng Li** and **Gelvis Turyagyenda** (2006) Prediction of cutting force for self-propelled rotary tool using artificial neural networks. *Journal of Materials Processing Technology*, Vol. **180**, pp. 23–29.

89. **Zemlyanskii, V.A.** (1966) Self-Induced Rotation of Round Tool Tips. *Russian Engineering Journal*, Vol. XLVI, No. **9**, pp. 68-70.

90. **Fogel, L.J., A.J**. Owens, and M.J. Walsh, Artificial intelligence through simulated evolution. 1966.

91. **Zemlyanskii, V.A.** and **Yu. F. Granin**, (1965) Circular Self-Rotating Tools. *Mashinostroitel*, Vol. **6**, pp. 35-36.

92. **S. A. Sajjadi**, "Effect of temperature on tensile fracture mechanisms of a Ni-base superalloy" Archives of Materials Science and Engineering Volume 28 Issue 1 January 2007 Pages 34-40.

93. **Zhang, Y., J. Wilcox** and **H.A. Kishawy** (2003) An assessment of carbide self-propelled rotary tools during machining hardened steel. *NAMRI/SME 31st North American Manufacturing Research Conference*, Hamilton, Ontario, Canada, pp. 185–192.

94. **Gopala Rao Thellaputta, Pulcharu Subhash Chandra Bose, C.S.P. Rao**, Machinability of Nickel Based Superalloys: A Review, Materials Today: Proceedings 4 (2017) 3712–3721.

95. **Zuprel Uros, Cus Franc** and **Kiker Edi** (2009) Adaptive network based inference system for estimation of flank wear in end-milling. *Journal of Material Processing Technology*, Vol. **209**, pp. 1504-1511.

96. **MaClure, T. F., Adams R., Gugger M.** D., "Comparison of flood Vs.microlubrication on machining performance" (2001).

97. **Baziar, M.H**., et al., Prediction of strain energy-based liquefaction resistance of sand–silt mixtures: An evolutionary approach. Computers & Geosciences, 2011. 37(11): p. 1883-1893.

98. **Laurent Magnier,** Multiobjective Optimization of Building Design Using Artificial Neural Network and Multiobjective Evolutionary Algorithms, A Thesis, at Concordia University, 2008

99. **D. Kondayya and A. Gopala Krishna**, An integrated evolutionary approach for modelling and optimisation of CNC end milling process, International Journal of Computer Integrated Manufacturing Vol. 25, No. 11, November 2012, 1069–1084.

100. **Jung Soo Nam, Pil-Ho Lee and Sang Won Lee,** "A Study on Machining and Environmental Characteristics of Micro-Drilling Process Using Nanofluid Minimum Quantity Lubrication" ASME 2011 International Manufacturing Science and Engineering Conference, Volume 2 Corvallis, Oregon, USA, June 13–17, 2011.

101. **Luke, S. and L. Panait**, Lexicographic parsimony pressure, in Proceedings of the 4th Annual Conference on Genetic and Evolutionary Computation. 2002, Morgan Kaufmann Publishers Inc.: New York City, New York. p. 829-836.

102. **E. O. Ezugwu, D. A. Fadare, J. Bonney, R. B. Da Silva, W. F. Sales**, "Modelling of correlation between cutting and process parameters in high-speed machining of Inconel 718 alloy using an artificial neural network" International journal of machine tools and manufacture 45 (2005) 1375-1385.

103. **K. Weinert**, "Dry machining and minimum quantity lubrication" CIRP Annals - Manufacturing Technology Volume 53, Issue 2, Pages 487-699 (2004).

104. **M. M. A. Khan**, "Effects of minimum quantity lubrication on turning AISI 9310 alloy steel using vegetable oil-based cutting fluid" Journal of Materials Processing Technology 209 (2009) 5573–5583.

105. **Adeel H. Suhail, N. Ismail, S. V. Wong, N. A. Abdul jalil,** "Optimization of cutting parameters based on surface roughness and assistance of workpiece surface temperature inturning process" American J. of engineering and applied sciences 3(1): 102-108,2010.

106. **T. I. EL-Wardany,** "Cutting temperature of ceramic tools in high speed machining of Difficult-To-Cut Materials" International journal of machine tools manufacturing, volume 36, No. 5, Pages 611-634, (1996).

107. **P. Subhash Chandra Bose, C.S.P Rao**, "Modeling and Prediction of SurfaceRoughness, Cutting Force and Temperature" while machining Nimonic-75 and Nicrofer C-263 Super

Alloys using Artificial Neural Network (ANN)" International Journal of MechanicalEngineering and Technology (IJMET), Volume 3, PP 599-613

108. **Kalyanmoy Deb**, A Fast and Elitist Multiobjective Genetic Algorithm:NSGA-II, IEEE transactions on evolutionary computation, vol. 6, no. 2, 2002.

109. **Searson, D**., GPTIPS Genetic Programming & Symbolic Regression for MATLAB User Guide. 2009.

110. **Mohammad Sazzadul Hoque**, "An implementation of intrusion detection system using Genetic Algorithm" International Journal of Network Security & its Applications (Ijnsa), Vol.4, No.2, March 2012.

111. **N. Aslan, Y. Cebeci**, "Application of Box–Behnken design and response surface methodology for modeling of some Turkish coals" Elsevier, Fuel 86 (2007) 90–97.

112. **W. Grzesik,** "Experimental investigation of the cutting temperature when turning with coated indexable inserts" International journal of machine tools and manufacture 39 (1999) 355-369.

113. **Franklin Allen and Risto Karjalainen**, "Using genetic algorithms to find technical trading rules" Elsevier Journal of Financial Economics 51 (1999) 245-271

114. **Edwards D. J. and Mee R. W.,** "Fractional Box-Behnken Designs" Journal of Quality Technology, (2011).

115. **E. O. Ezugwu, A. R. Machado, I. R. Pashby, J. Wallbank**, "The effect of high-pressure coolant supply when machining a heat-resistant nickel-based superalloy" Lubr. Eng. 47 (9) (1991) 751-757.

116. **R. M. Arunachalam, M. A. Mannan, A. C. Spowage**, "Residual stresses and surface roughness when facing age hardened Inconel 718 with CBN and ceramic cutting tools" International journal of machine tools and manufacture 44 (2004) 879-887.

117. **Patrick Reed and Barbara Miniskar**, "Designing a competent simple genetic Algorithmforsearch and optimization" Water Resources Research, Volume 36, No. 12, Pages 3757-3761, December 2010.

118. **Patel, Shailesh J,** "Research and Improvement on structure stability and corrosion resistance of nickel-base super alloy INCONEL alloy 740" Journal of Materials and Design, Volume 27, issue 10 (2006), p. 1120-1127.

119. **N. Aslan, Y. Cebeci,** "Application of Box–Behnken design and response surface methodology for modeling of some Turkish coals" Elsevier, Fuel 86 (2007) 90–97.

120. **Kim, M.-I. and P. Zou**, Modeling of Drilling Forces Based on Twist Drill Point Angles using Multigene Genetic Programming. Mathematical Problems in Engineering, 2016. 2016: p. 9.

121. **Sulaiman, M.A, Che Haron, C.H., Ghani, J.A. and Kasim, M.S.** Optimization of Turning Parametersfor Titanium Alloy Ti-6Al-4V ELI Using theResponse Surface Method (RSM)ISSN: 1985-3157 Vol. 7 No.2 July - December 2013.

PAPERS PUBLISHED ON THE PH.D WORK

1. Machinability of Nickel Based Superalloys: A review, Materials Today Proceedings (Scopus Indexed). Published.

2. Adaptive neuro fuzzy model development for prediction of cutting forces in milling with rotary tools, Materials Today Proceedings (Scopus Indexed). Published

3. Surface Integrity Analysis of Inconel 625 after Rotary milling with Nano Fluid Supplied by MQL Technique (Chinese Journal of Mechanical Engineering) Under Review

4. Effect of cutting parameters on cutting temperature while rotary milling of Inconel 625, Springer conference proceedings (Scopus Indexed). (Reviews over - Under Production Process)

To be communicated

4. Experimental Investigations on the performance of Rotary Face Milling Cutter in Machining of Inconel 625
5. Development of Genetic Programming model for prediction of cutting forces in milling with rotary tools.